Developmental function of *Drosophila* RASSF9 and RASSF10

Jennifer Jasmin Banerjee

University College London

and

Cancer Research UK London Research Institute

PhD Supervisor: Nicolas Tapon

A thesis submitted for the degree of

Doctor of Philosophy

University College London

September 2015

Declaration

I, Jennifer Jasmin Banerjee, confirm that the work presented in this thesis is my own. Where information has been derived from other sources, I confirm that this has been indicated in the thesis.

…….

Abstract

Cell polarity is a fundamental property of most living cells, and its disruption is associated with diseases such as cancer. Members of the N-terminal RASSF protein family have been proposed to function as tumour suppressors and oncogenes, but the underlying mechanisms are not well understood. Proteomic approaches have recently linked the human N-terminal RASSFs to PP1 phosphatases, as well as its regulatory subunit ASPP and two RASSFs - RASSF9 and RASSF10 - showed additional associations to both planar cell polarity (PCP) proteins and the apical-basal polarity determinant Par3/Bazooka.

This thesis investigates the developmental function of RASSF9 and RASSF10 in *Drosophila*. The human interaction network of RASSF9 and RASSF10 is largely conserved in *Drosophila* and additional interactors are revealed. *In vitro* both RASSFs can associate with PCP proteins and the polarity protein Bazooka. In the case of RASSF10 this work suggests a role in establishing cell polarity in the context of asymmetric cell divisions of sensory organ precursors (SOP), the progenitor cells that will give rise to the sensory bristles. Cell biological and genetic approaches provide evidence that RASSF10 functions, together with its interaction partners Dishevelled, Frizzled and Bazooka, in the initial polarisation of SOPs prior to their asymmetric division.

The second part of my thesis investigates the function of the ubiquitin system at the kinetochore in relation to Spc25, which was previously characterised as a novel ubiquitin-binding protein. My data suggest that the ubiquitin-binding properties of Spc25 might be important for the stability of the KMN (Knl1/Mis12/Ndc80) network within the kinetochore complex, also supported by the findings that members of the KMN network, namely Dsn1, Nsl1 and Spc105 are ubiquitylated, giving them the potential to interact with the ubiquitin-binding domain of Spc25. Furthermore, my findings suggest that the ubiquitin system centred on the ubiquitin-binding activity of Spc25 and the KMN network is independent from ubiquitin-mediated degradation.

Acknowledgement

My PhD took me on a journey from yeast to flies and I was able to benefit from the knowledge and experience of not one, but two labs. Nic, thank you for welcoming me into your lab and for being such a fantastic supervisor - it is greatly appreciated and I have learned so much from you. Helle, thank you for giving me the opportunity to join your lab in Clare Hall, and for your guidance and knowledge.

I would like to thank all the people in Helle's lab who accompanied me on the yeast journey. Special thanks to Jo, who was a great teacher. Thank you Magda, Tomio, Liz, Olivier, Laure, Ron, Addie, Chris and John for the support and entertaining coffee breaks in Clare Hall.

The second journey took me into the fly world and I am extremely grateful for all the help and advice I received from Yanxiang, Gaspar, Birgit, Max, Paulo and Yanlan. Tessa, Ieva, John, Anna, Billel and the entire Thompson lab - it is/was great working with you! Thank you Nicola for our wonderful chats and entertaining coffee breaks in LIF.

I also want to thank my secondary supervisors, our collaborators and all the people in the fly facility as well as the facilities in LIF and Clare Hall, and of course, Cancer Research UK, for funding this PhD.

Finally, I would like to thank my parents for always being there, and for their constant support and love. A huge thank-you to my sister, her family and Liz who have all provided me with open arms and a listening ear when needed, as well as to Lal and Anne for looking after me when I first arrived in London. My family and, in particular, my friends in both London and Germany, have made this journey all the more enjoyable.

Tim - there are no words to express my thanks to you for taking this entire PhD journey with me. I dedicate this work to you, as without you it simply would not have been possible.

Table of Contents

Table of Figures

List of Genotypes

Figure 3.13A-B''	*ubi-GFP-RASSF9/+*
Figure 3.13C-D''	*ubi-GFP-RASSF10/+*
Figure 3.13E-E"	*yw, hsFlp; act>y>UAS-lacZ/+; UAS-GFP-RASSF9/+*
Figure 3.13F-F"	*yw, hsFlp; act>y>UAS-lacZ/+; UAS-GFP-RASSF10/+*
Figure 3.14A-A''	*yw, UbxFlp/+; ubi-GFP-RASSF9/+; arm-lacZ, FRT80B/ fz^{P21}, FRT80B*
Figure 3.14B-B''	*yw, UbxFlp/+; ubi-GFP-RASSF10/+; arm-lacZ, FRT80B/ fz^{P21}, FRT80B*
Figure 3.14C-C'''	*yw, hsFlp FRT19A, RFP/ dsh^{3} FRT19A; ubi-GFP-RASSF9/+*
Figure 3.14D-D'''	*yw, hsFlp FRT19A, RFP/ dsh^{3} FRT19A; ubi-GFP-RASSF10/+*
Figure 3.16	*UAS-CD8::GFP/+; tubulin-Gal4/+* (GFP)
	UAS-GFP-RASSF9/+; tubulin-Gal4/+ (GFP-F9)
	UAS-GFP-RASSF10/+; tubulin-Gal4/+ (GFP-F10)
Figure 3.17	*tubulin-Gal4/+* (ctrl)
	UAS-CD8::GFP/+; tubulin-Gal4/+ (GFP)
	UAS-GFP-RASSF9/+; tubulin-Gal4/+ (GFP-F9)
	UAS-GFP-RASSF10/+; tubulin-Gal4/+ (GFP-F10)
Figure 3.23	*yw, hsFlp/+; FRT82B RFP, FRT2A GFP/ FRT82B $RASSF8^{6}$, FRT2A $RASSF9^{128}$, $RASSF10^{B221}$*
Figure 4.1 - 4.4	as written in figure and
	ubi-GFP/+; $RASSF10^{B221}$ and ubi-GFP/+; $RASSF9^{128}$, $RASSF10^{B221}$
	ubi-GFP-F9/+; $RASSF10^{B221}$ and ubi-GFP/+; $RASSF9^{128}$, $RASSF10^{B221}$
	ubi-GFP-F10/+; $RASSF10^{B221}$ and ubi-GFP/+; $RASSF9^{128}$, $RASSF10^{B221}$
Figure 4.5A-D	*RASSF10 control*
Figure 4.5A'-D'	*$RASSF10^{B221}$*
Figure 4.6A-A''	*RASSF10 control*
Figure 4.6B-B''	*$RASSF10^{B221}$*
Figure 4.6D-E''	*RASSF10 control*
Figure 4.6C-C'	*yw, hsFLP/+; FRT80B GFP/ FRT80B $RASSF10^{B221}$*
Figure 4.7A-D'	*RASSF10 control*
Figure 4.7E-F'	*neuralized-Gal4, UAS-tau-GFP/+*
Figure 4.8A-B'''	*baz-GFP/+*
Figure 4.8C-D'''	*arm-fz-GFP/+*
Figure 4.9	*RASSF10 control*

Figure 4.13B-C'''	*RASSF10 control*
Figure 4.15A-A'	*UAS-GFP-RASSF10/+; neuralized-Gal4, UAS-his2B-RFP, RASSF10^{B221}/+*
Figure 4.15B-B'	*UAS-GFP-RASSF9/+; neuralized-Gal4, UAS-his2B-RFP, RASSF10^{B221}/+*
Figure 4.16 - 4.18	*neuralized-Gal4, UAS-pon-GFP/+* (*Wt*) *neuralized-Gal4, UAS-pon-GFP, RASSF10^{B221}/ RASSF10^{B221}* (*RASSF10^{B221}*) *neuralized-Gal4, UAS-pon-GFP, RASSF10^{B221}/+* (*Het* or *RASSF10^{B221}/+*)
Figure 4.19A-A''	*RASSF10 control*
Figure 4.19B-B''	*RASSF10^{B221}*

List of Tables

Abbreviations

aa	amino acids
ACD	Asymmetric cell division
AD	Activation domain
AP-MS	Affinity Purification -Mass-Spectrometry
APF	After puparium formation
aPKC	atypical Protein Kinase C
Arm	Armadillo
ARS	autonomous replication sequence
ASPP	Apoptosis stimulating protein of p53
ATP	Adenosine triphosphate
Baz	Bazooka
BD	DNA binding domain
Ccdc	Coiled-coil domain containing
cDNA	complementary DNA
CK	Casein kinase
Co-IP	co-immunoprecipitation
CRISPR	clustered regularly interspaced short palindromic repeats
Csk	C-terminal Src kinase
DAPI	4', 6-diamidino-2-phenylindole
Dco	Discs overgrown
DEP	Dishevelled, Egl-10, Pleckstrin
Dgo	Diego
DGRC	Drosophila Genomics Resource Center
Dlg	Discs large
DNA	Deoxyribonucleic acid
Ds	Dachsous
Dsh	Dishevelled
DTT	dithiothreitol
DUB	deubiquitylating enzyme
Ecad	E-cadherin
EDTA	Ethylenediaminetetraacetic acid
EGTA	Ethylene glycol tetraacetic acid
EGFR	Epidermal growth factor receptor
Fj	Four-jointed
Flp	Flippase
Fmi	Flamingo
FRT	Flippase recombination target
Ft	Fat
Fz	Frizzled
GFP	Green fluorescent protein
GPCR	G protein-coupled receptor
gRNA	guide RNA
GST	glutathione sulfur transferase
HA	Human influenza hemagglutinin

HECT	homologous to the E6-AP carboxyl terminus
HRP	Horseradish peroxidase
hsFlp	heat-shock promoter driven Flippase
IP	immunoprecipitation
IPTG	isopropyl β-D-1-thiogalactopyranoside
KMN	Knl1, Mis12, Ndc80
LATS	Large tumour suppressor
Lgl	Lethal giant larvae
MIU	motif interacting with ubiquitin
mRNA	messenger RNA
n.s.	not significant
ORF	open reading frame
Par	Partitioning defective
PBS	Phosphate-buffered saline
PCP	Planar cell polarity
PCR	Polymerase chain reaction
PDB	protein data bank
PDZ	PSD95, Dlg, ZO-1
PGK	phosphoglycerate kinase
Pins	Partner of Inscuteable
Pk	Prickle
Pon	Partner of Numb
PP1	Protein phosphatase 1
PP2A	Protein phosphatase 2
RA	Ras association
RASSF	Ras association domain family
RING	really interesting new gene
RNA	Ribonucleic acid
RNAi	RNA interference
SC	synthetic complete
S2	Schneider 2
SH3	Src homology 3
SOP	Sensory organ precursor
Sple	Prickle spiny legs
SPR	surface plasmon resonance
Stbm	Strabismus
Src	Sarcoma
TAZ	Tafazzin
TBS	Tris-buffered saline
TCA	trichloroacetic acid
ts	temperature sensitive
UAS	Upstream activating sequence
UBD	Ubiquitin binding domain
UIM	Ubiquitin-interacting motif
UTR	Untranslated region
UV	ultraviolet
YAP	Yes-associated protein
YPD	yeast peptone glucose medium

Chapter 1 Introduction

In this thesis, I pursued two very different projects and therefore the introduction will cover these separately.

The first project is centred on the developmental function of RASSF9/10 in *Drosophila*. Therefore I will briefly introduce *Drosophila melanogaster* as a model organism. I will then give an overview on the RASSF protein family with the main focus on N-terminal RASSFs. Next, PP1 phosphatases and their connection to N-terminal RASSFs will be explored. I will then provide background to the molecular and functional settings for three potential interactors of RASSF9/10: Wg/Fz canonical signalling and planar cell polarity for Fz/Dsh and the role of Baz in polarity establishment. And lastly, asymmetric cell divisions of sensory organ precursors of the peripheral nervous system will be outlined, in which both planar cell polarity and apical-basal polarity are implicated.

The second project is based on the function of the ubiquitin system associated with Spc25 at the kinetochore in *Saccharomyces cerevisiae*. Firstly, I will briefly introduce *S. cerevisiae* as a model organism and then cover three main topics: the ubiquitin system, the yeast kinetochore, with the main focus on Spc25 and lastly I will introduce Spc25 as a novel ubiquitin-binding protein.

1.1 *Drosophila melanogaster* as a model organism

1.1.1 Advantages and development

Drosophila melanogaster, commonly referred to as the fruit fly, has been studied for over 100 years. Sequencing of the fly genome in the year 2000 (Adams et al., 2000) and genomic comparative analysis revealed that about 70% of human disease genes have homologous sequences in the *Drosophila* genome (Reiter et al., 2001). Consequently, *Drosophila* represents an ideal model organism to study functions of genes in disease as well as developmental processes. Moreover, *Drosophila* has only four chromosomes (one sex chromosome and 3 autosomes), making genetic manipulations relatively straightforward. The genetic toolkit for *Drosophila* has vastly expanded over the years

and there are multiple strategies to generate transgenic flies, harbouring for example gene deletions or genomic insertions (see Material and Methods) (del Valle Rodriguez et al., 2012, St Johnston, 2013). There are many different resources available, such as RNAi collections for knock-down of genes of interest or tagged transgenes. Besides the genetic advantages, the maintenance of flies is cheap and simple. Another major benefit is the short life cycle: it takes just 10 days for the development of a fertilised egg to the adult fly when kept at 25 °C.

The life cycle comprises four stages, namely the embryo, larva, pupa and adult. The embryo develops within one day after fertilisation and hatches as a first instar larva, which then grows over the next four to five days, increasing its weight about 200 times (from first to second to third larval instar) (Stocker and Gallant, 2008). The third instar larva pupariates and after four to five days the adult fly emerges. During metamorphosis in the pupal stage, adult tissues are formed and most larval tissues are removed. The adult structures such as eyes, wing, legs and thorax develop from larval epithelial structures - the so-called imaginal discs. The different stages and tissues provide a variety of model systems to choose from to analyse different processes such as proliferation, cell death and differentiation.

1.1.2 The development of the wing imaginal disc

In this thesis I have primarily worked with wing imaginal discs, as well as pupal or adult wing and notum. Therefore I will briefly introduce their development. Imaginal discs are epithelial structures, which derive from the embryonic epithelium (Bate and Arias, 1991). During larval development they grow exponentially - the wing imaginal disc starts from 30 cells and consist of approximately 50.000 cells when reaching the pupal stage (Milán et al., 1996). With the onset of metamorphosis the wing imaginal disc undergoes morphological changes and gives rise to the wing (hinge and blade) as well as part of the notum (the other part is contributed by the leg disc (Zeitlinger and Bohmann, 1999)) (Figure 1.1) (Stocker and Gallant, 2008). The differential expression of several organisers, such as Hedgehog, Engrailed, Wingless and Dpp (Decapentaplegic), defines the growth and patterning of the distinct compartments (Gomez-Skarmeta et al., 2003).

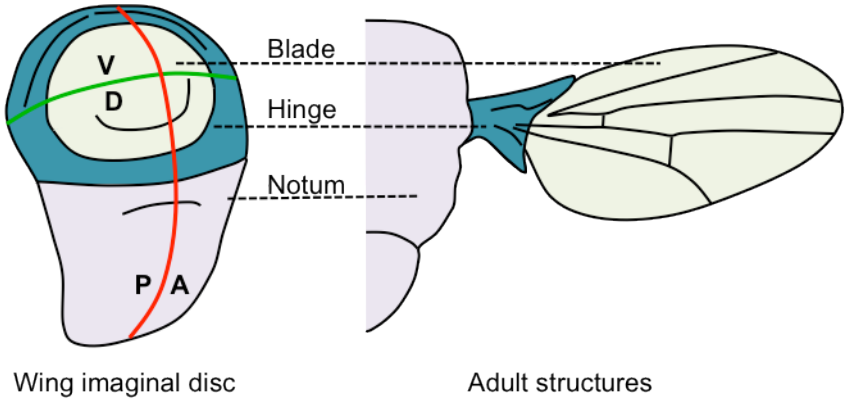

Figure 1.1 - The wing imaginal disc and corresponding adult structures.
The adult wing (hinge and blade) and part of the adult notum are formed from the wing imaginal disc (on the left). Dpp (red) is expressed along the anterior-posterior boundary and Wg (green) along the dorsal-ventral boundary.

1.2 N-terminal RASSFs

1.2.1 The Ras association domain family

The Ras association domain family (RASSF) comprises a group of proteins that share a conserved domain - the Ras association (RA) domain. According to the position of RA domain, RASSFs are classified into classical RASSFs (RA domain at C-terminus) and N-terminal RASSFs (RA-domain at N-terminus) (Sherwood et al., 2010). In humans there are 6 different classical RASSFs (RASSF1-6) and 4 N-terminal RASSFs (RASSF7-10) (Figure 1.2). None of these contain any known enzymatic domains and they therefore appear to be scaffold proteins. Besides their RA domain, classical RASSFs have a Salvador/RASSF/Hippo (SARAH) domain at their C-terminus, which gives them the potential to homo-dimerise or hetero-dimerise with other SARAH domain proteins, such as Mst1/2 (Mammalian Sterile 20-like, *Drosophila* Hippo) (Chan et al., 2013, Scheel and Hofmann, 2003). N-terminal RASSFs lack the SARAH domain, but have predicted coiled-coil regions towards their C-termini. The name of the RA domain implies that RASSFs interact with Ras GTPases. Many of them can indeed bind to Ras or other small GTPases *in vitro* (Rodriguez-Viciana et al., 2004), but for example RASSF8 and RASSF10 lack this ability, and the RA domain of these proteins are likely

to bind other ligands (Chan et al., 2013). Indeed, the functional relevance of binding to small GTPases still needs to be established in most RASSF family members (Sherwood et al., 2010). Strikingly, RASSFs are misregulated in various forms of cancer, making them of high interest for research (Sherwood et al., 2010, Volodko et al., 2014, Richter et al., 2009).

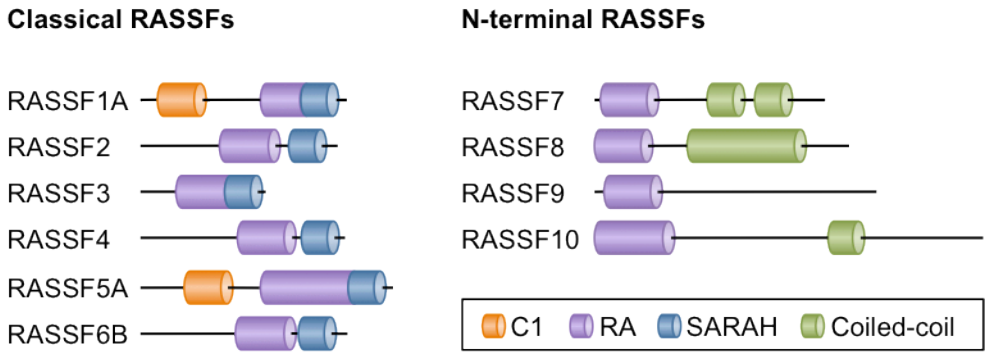

Figure 1.2 - Domain structure of the human RASSF family.

The human RASSF family consists of classical RASSFs (RASSF1-6) and N-terminal RASSFs (RASSF7-10) (figure adapted from (Sherwood et al., 2010)). N-terminal RASSFs contain an N-terminal RA domain (purple) and predicted coiled-coil regions (green). Besides their RA domains, classical RASSFs also have SARAH domain (blue) at the C-terminus, which enables them to form homo- and heterodimers. RASSF1 and RASSF5 also contain cysteine rich C1 domains (orange).

1.2.2 Human N-terminal RASSFs are associated with various cancers

In the following sections, I will present what is known about the human N-terminal RASSFs and then introduce the *Drosophila* homologues in the next subchapters.

RASSF7 is a candidate oncogene, as RASSF7 expression is found to be upregulated in various cancers (Sherwood et al., 2010). Consistent with this, its expression can be induced by hypoxia (Recino et al., 2010), which often occurs in tumours. Studies in *Xenopus* embryos and human cell culture demonstrated that it is required for normal mitosis, as knockdown of RASSF7 prevents spindle formation and induces growth

arrest (Recino et al., 2010, Sherwood et al., 2008). Indeed, RASSF7 localises to the centrosomes (Recino et al., 2010, Sherwood et al., 2008) and is thought to promote tubulin growth (Recino et al., 2010). Another study suggested that RASSF7 has an additional function in negatively regulating the pro-apoptotic function of JNK signalling by interacting with the small GTPase N-Ras and the Map kinase MKK7, thus preventing MKK from activating JNK (Takahashi et al., 2011).

In contrast to RASSF7, RASSF8 seems to act as a tumour suppressor. RASSF8 mRNA expression is downregulated in lung cancer tissue and ectopic expression can inhibit colony formation of lung cancer cell lines (Falvella et al., 2006). These findings were further supported by a more recent study, which showed that RASSF8 depletion increases colony formation and tumour growth in mouse xenograft experiments (Lock et al., 2010). Importantly, this study showed that RASSF8 localises to the cell junctions, and upon reduction of RASSF8 levels, junction formation is inhibited, as indicated by mislocalisation of the junctional components β-catenin and E-cadherin. As a mechanism for the tumour formation upon RASSF8 depletion, it has been proposed that the destabilisation of junctions firstly increases cytoplasmic β-catenin levels, thus promoting Wnt/β-catenin signalling (Wg/Fz signalling, see 1.4.1) and secondly increases anti-apoptotic NF-κB signalling (Lock et al., 2010).

RASSF9, formerly known as P-CIP1 (PAM C-terminal interactor protein-1), was suggested to function in the endosomal trafficking of peptidylglycine α-amidating monooxygenase (PAM) (Chen et al., 1998). However, this hypothesis is based on the *in vitro* interaction between PAM and RASSF9, as well as the subcellular localisation of ectopically expressed RASSF9 (which was found enriched in endosomes), thus further research would be necessary to validate this proposed function. More recently, the function of RASSF9 was revisited. In mice and rats RASSF9 mRNA is widely expressed with strong expression in heart, lung, kidney and skin (Lee et al., 2011, Chen et al., 1998). In the skin, RASSF9 is specifically expressed in the epidermal keratinocytes and is important for normal epidermal homeostasis, as loss of *RASSF9* leads to hyperproliferation and impaired differentiation of keratinocytes in mice (Lee et al., 2011). Interestingly, mice mutant for *RASSF9* are also reduced in size and life span (Lee et al., 2011). The underlying mechanisms of the function of RASSF9 still need to

be resolved. Moreover, there are contradicting reports about whether or not RASSF9 is able to bind to Ras GTPases *in vitro* (Rodriguez-Viciana et al., 2004, Chan et al., 2013).

RASSF10 is considered to be a potential tumour suppressor based on the finding that it is epigenetically silenced by promoter methylation in a variety of cancers, such as gastric cancer, prostate cancer, glioblastomas, pancreatic cancer, childhood leukaemia and thyroid cancer (Dansranjavin et al., 2012, Hill et al., 2011, Schagdarsurengin et al., 2009, Wei et al., 2013, Hesson et al., 2009, Richter et al., 2012). In addition, RASSF10 overexpression inhibits colony formation of cancer cell lines (Wei et al., 2013, Hill et al., 2011) and reduces tumour growth in mouse xenograft experiments (Wei et al., 2013, Guo et al., 2015), while reduction of RASSF10 levels induces colony formation (Hill et al., 2011). So far two different models have been suggested how RASSF10 acts as a tumour suppressor based on changes in expression profiles. Firstly, it has been proposed that RASSF10 activates p53 by inhibition of the p53 inhibitor Mdm2 and thus promotes the expression of pro-apoptotic genes (Guo et al., 2015). Secondly, RASSF10 was suggested to inhibit growth by supressing Wnt/β-catenin signalling (Wei et al., 2013). However, the mechanism(s) of how RASSF10 functions in either pathway still needs to be resolved. Interestingly, RASSF10 was found to be cytoplasmic and localises to the spindle poles during mitosis in cell lines (Hill et al., 2011), similar to RASSF7, suggesting a potential additional mitotic role.

1.2.3 N-terminal RASSFs in *Drosophila*

In *Drosophila*, the RASSF family contains four members: one classical RASSF (see 1.3.2) and three N-terminal RASSFs (RASSF8-10). RASSF8 is the homologue of human RASSF7 and RASSF8 and the *Drosophila* genes *CG13875* and *CG32150* are believed to encode the homologues of mammalian RASSF9 and RASSF10 (Sherwood et al., 2010). I will subsequently refer to *CG13875* as *RASSF9* and to *CG32150* as *RASSF10*, as this nomenclature has already been introduced (Sherwood et al., 2010).

The function of RASSF8 has been extensively studied in our lab and it was shown that RASSF8 is an important factor for junctional integrity (similar to human RASSF8), together with its binding partner ASPP (see following subchapter).

In contrast, the function of RASSF9 and RASSF10 in *Drosophila* has not been analysed in detail. There have been no reports about RASSF9. Although the function of

RASSF10 has so far not directly been addressed, it has been recovered in different high-throughput approaches. Firstly, in a genome-wide RNAi screen, RASSF10 was found to negatively regulate Hedgehog signalling (Nybakken et al., 2005). Strikingly, in microarray screens, *RASSF10* mRNA was shown to be highly and specifically expressed in sensory organ precursors of the peripheral nervous system in wing imaginal discs and the pupal notum (Reeves and Posakony, 2005, Buffin and Gho, 2010). Furthermore, the mRNA expression seems to be regulated by the proneural Achaete-Scute complex (Reeves and Posakony, 2005). Interestingly, in *Xenopus* tadpoles *RASSF10* mRNA is prominently expressed in the brain, suggesting a potential role for RASSF10 in neurogenesis (Hill et al., 2011).

1.2.4 RASSF8 and ASPP

Drosophila RASSF8, similar to human RASSF8, is important for the junctional remodelling in the developing retina, which undergoes drastic morphological changes. During the development of the retina, excess cells are removed by apoptosis and new junctions are formed to give rise to the perfectly patterned compound eye. Our lab has shown that RASSF8 acts together in this process with another scaffold protein - ASPP (apoptosis stimulating protein of p53, or Ankyrin-repeat, SH3-domain and proline-rich-region containing protein). RASSF8 can directly bind to ASPP and both proteins require each other for their specific localisation at the adherens junctions (Langton et al., 2009). Loss of either of the proteins leads to gaps in the adherens junction belts as well as mis-arrangements of the cells, causing a rough eye phenotype (Langton et al., 2009, Langton et al., 2007). How do RASSF8 and ASPP regulate the junctional remodelling? Our lab found that ASPP is required for the activity of the C-terminal Src kinase (Csk) at the junctions, where it normally inhibits the activity of Src kinase and thus prevents Src from disassembling the junctions (Langton et al., 2009, Langton et al., 2007). Recently it has been shown that the localisation of the ASPP-RASSF8 complex in interommatidial cells is dependent on the scaffold protein Magi, which seems to position them at the adherens junctions, most likely by direct binding to RASSF8 (Zaessinger et al., 2015). Furthermore this study proposed an additional mechanism: Magi together with the ASPP-RASSF8 complex recruits the polarity determinant Bazooka (Baz, vertebrate Par3) to the developing junctions (Zaessinger et al., 2015),

which in turn could promote the deposition of new junctional material (see 1.5). Further investigations are necessary to test whether and how the Csk/Src and Baz-mediated mechanisms are connected.

Flies mutant for either *ASPP* or *RASSF8* are overgrown, suggesting that they both act as tumour suppressors (Langton et al., 2009, Langton et al., 2007). However, the phenotypes of *ASPP* or *RASSF8* mutants are not completely identical, suggesting that they also have independent functions. For instance, loss of *RASSF8* induces a wing rounding phenotype that is not observed in *ASPP* mutants (Langton et al., 2009), probably due to a defect in proximal-distal axis elongation.

While *Drosophila* has a single ASPP protein, there are three different mammalian ASPP isoforms - ASPP1, ASPP2 and iASPP (inhibitor of ASPP). ASPP proteins are dysregulated in many cancers and can act as tumour suppressors (ASPP1/2) and oncogenes (iASPP) (Sullivan and Lu, 2007). As the name suggests mammalian ASPPs can bind to p53 (Bergamaschi et al., 2004, Bergamaschi et al., 2003). While ASPP1/2 promote the activity of p53 in activating the transcription of pro-apoptotic genes (e.g. *Bax*, *Pig3*) (Samuels-Lev et al., 2001, Bergamaschi et al., 2004), iASPP inhibits p53 (Bergamaschi et al., 2003). *Drosophila* ASPP is considered the homologue of ASPP1/2, but in contrast does not appear to regulate the activity of p53, as *ASPP* mutants do not phenocopy *Drosophila* p53 mutant (failure of radiation-induced cell death) and the ASPP1/2 contact residues on p53 are not conserved in flies (Langton et al., 2007).

In addition to its nuclear function in promoting p53 activity, ASPP2, like *Drosophila* ASPP, localises to the tight junctions (in *Drosophila* to the adherens junctions) in mammalian epithelial cells and is required for junctional integrity (Cong et al., 2010). ASPP2 associates with Par3 and recruits it to the junctions, thus promoting their formation as well as polarity establishment (Sottocornola et al., 2010, Cong et al., 2010). Considering that in *Drosophila* ASPP acts together with RASSF8 (and Magi) to recruit Baz (Zaessinger et al., 2015) it would be interesting to see whether RASSF8 is also implicated in Par3 recruitment in mammalian systems, especially since human RASSF8 is also required for the integrity of cell junctions (Lock et al., 2010) and can bind to ASPP1/2 (Langton et al., 2009).

In addition to the described characteristics and potential functions of the mammalian N-terminal RASSFs (1.2.2) and ASPP isoforms, they all interact with the catalytic

subunits of PP1 serine/threonine phosphatases and especially ASPP is a well-described regulatory subunit with identified ASPP/PP1 substrates (see following subchapter).

1.3 Serine/threonine phosphatases - connections to RASSF and ASPP protein families

Protein phosphorylation is an important post-translational modification. Kinases catalyse the transfer of the γ phosphate from ATP to certain amino acid residues, mostly serine, threonine or tyrosine residues. Protein phosphorylation is crucial for a variety of cellular functions, for instance allowing specific interactions between proteins, defining their subcellular localisation, targeting proteins for degradation or changing the activity of enzymes. Importantly, protein phosphorylation is reversible, since phosphates can be removed by phosphatases. The regulation of proteins by the opposing interplay of kinases and phosphatases allows modulating different cellular functions and signalling events.

1.3.1 PP1, a protein serine/threonine phosphatase

Phosphoprotein phosphatases (PPP) form one of the four described phosphatase superfamilies, and specifically dephosphorylate serine and threonine residues (Boens et al., 2013). Members of the PPP superfamily - namely PP1, PP2A, PP2B (PP3 or Calcineurin), PP4, PP5, PP6 and PP7 - have highly similar catalytic domains, which require binding of metal ions (Mg^{2+} or Mn^{2+}) (Shi, 2009). Catalytic subunits exhibit little intrinsic substrate specificity - therefore they associate with regulatory subunits, which allow specific binding of substrates, often define the subcellular localisation of the catalytic subunit, and sometimes restrict access to the catalytic site.

PP2A holoenzymes are heterotrimeric complexes and consist of a catalytic subunit C, a scaffold subunit A (C and A exist as a heterodimer) and a regulatory subunit B, which specifies the substrate. PP1 holoenzymes are composed of a catalytic subunit, and one of a large array of regulatory subunits (around 200 candidates have been identified so far) (Boens et al., 2013). In humans there are four different catalytic subunits: PP1α, PP1β/δ, and the two splice variants, PP1γ_1 and PP1γ_2 (Peti et al., 2013). *Drosophila* also

has four different catalytic subunits, but these are encoded by separate loci. PP1α96A, PP1α87B and PP1α13C, which represent homologues of human PP1α and PP1γ, and PP1β9C, which is related to human PP1β/δ (Kirchner et al., 2007). PP1 catalytic subunits share a high level of sequence identity, thus it is not surprising that most regulatory subunits can bind to all subunits, however, some regulatory subunits can discriminate between catalytic subunits. For example, *Drosophila* MYPT-75D (myosin phosphatase targeting subunit, homologue of human MYPT1) associates solely with the PP1β9C subunit (Kirchner et al., 2007). Most, but not all, of the regulatory subunits interact with the PP1 catalytic subunits through conserved motifs. So far 10 different motifs were described (Boens et al., 2013), such as the highly common RVxF motif, the SILK motif, the MyPhoNE (myosin phosphatase N-terminal element) motif and the RARL motif to name a few (Hendrickx et al., 2009, Wakula et al., 2003).

Besides the substrate-specifying regulatory subunits, catalytic subunits can bind to inhibitory subunits (e.g. Inhibitor-1, Inhibitor-2, CPI-17), which suppress the activity of the catalytic subunit by sterically obstructing the catalytic domain (Boens et al., 2013), as seen for example in the crystal structure of Inhibitor-2 and PP1 (Hurley et al., 2007). Interestingly, in some instances, the regulatory and inhibitory subunits form trimeric complexes with the catalytic domain, e.g. the Spinophilin/Inhibitor-2/PP1 complex. Structural analysis showed that, in the trimeric complex, Inhibitor-2 binds to PP1 through its SILK motif instead of the RVxF motif, leaving the RVxF binding surface free for the regulatory subunit Spinophilin (Dancheck et al., 2011). Although there are no reports for the simultaneous binding of two regulatory subunits, it is possible that trimeric complexes could also exist through differential binding to the PP1 surface. Importantly, structural data obtained so far suggest that neither binding of regulatory nor inhibitory subunits changes the confirmation of the catalytic subunit (Peti et al., 2013).

In the following section I will give an overview of the connections between PPP and classical RASSFs, the ASPP protein family and N-terminal RASSFs.

1.3.2 *Drosophila* RASSF functions with PP2A as a negative regulator of Hippo signalling

In *Drosophila* there is solely one classical RASSF, which has been shown to bind to the serine/threonine kinase Hippo to suppress the Hippo signalling pathway, a major growth control pathway (Polesello et al., 2006). The conserved Hippo pathway promotes inhibition of cell proliferation as well as induction of apoptosis (Yu and Guan, 2013). Briefly, activation of Hippo (mammalian Mst1/2) results in the phosphorylation by the downstream kinase Warts (mammalian LATS) of the transcriptional co-activator Yorkie (mammalian YAP and TAZ), which is thereby retained in the cytoplasm and cannot activate its pro-growth transcriptional programme in concert with transcription factors such as Scalloped (Yu and Guan, 2013).

Another study provided the underlying mechanism by which RASSF regulates Hippo signalling: RASSF is part of the STRIPAK (Striatin-interacting phosphatase and kinase) PP2A phosphatase complex, which inhibits Hippo by dephosphorylating sites required for its activity (Ribeiro et al., 2010). Although all human classical RASSFs can bind to Mst1/2, RASSF3 is the only one interacting with the STRIPAK complex (Hauri et al., 2013), suggesting that not all classical RASSFs inhibit Mst1/2 similarly to *Drosophila* RASSF. This is also consistent with previous findings that some of the human classical RASSFs promote Mst1/2 activity, for example RASSF1A prevents PP2A from dephosphorylating and thus inhibiting Mst1/2 (Guo et al., 2011). It will be interesting to test whether RASSF3, like *Drosophila* RASSF, acts together with PP2A to inhibit Hippo signalling.

1.3.3 ASPP is a PP1 substrate specificity subunit

The three mammalian ASPP isoforms can all bind to PP1 catalytic subunits (Llanos et al., 2011, Skene-Arnold et al., 2013). Moreover, ASPP1 and ASPP2 interact with PP1 catalytic subunits via the RVxF motif, while iASPP, which lacks the RVxF motif binds to PP1 through a RARL motif (Llanos et al., 2011, Skene-Arnold et al., 2013). ASPP family proteins may therefore act as specificity subunits for PP1 complexes. Indeed, different studies provided evidence for functional ASPP/PP1 complexes.

Phosphorylation of the mammalian Hippo pathway transcriptional co-activators YAP and TAZ (the mammalian Yorkie homologues) prevents their nuclear localisation therefore shutting down their transcriptional activity (Yu and Guan, 2013). Both YAP and TAZ have been shown to be dephosphorylated by PP1 *in vitro* (Wang et al., 2011, Liu et al., 2011) and also that they can bind to ASPP2 (Hauri et al., 2013, Liu et al., 2011). Furthermore, expression of ASPP2 decreases phospho-YAP (Royer et al., 2014) or TAZ (Liu et al., 2011) levels in HEK293 cells, while PP1-binding mutants of ASPP2 (affecting the RVxF motif) have no such effect. In agreement with this, ASPP1/2 expression increases YAP/TAZ transcriptional activity, while its depletion has the opposite effect (Royer et al., 2014, Liu et al., 2011, Hauri et al., 2013). Interestingly, in the case of YAP, ASPP2 functions at junctions to recruit PP1 and to specifically dephosphorylate junctional YAP (Royer et al., 2014). Thus, the ASPP2/PP1 complex promotes the nuclear localisation of YAP/TAZ. It is interesting to note that this pro-growth function contrasts with ASPP1/2 tumour-suppressive role in promoting p53 activity (see 1.2.4), suggesting that ASPP's role in in different types of cancer may be determined by its sub-cellular localisation.

Recently another substrate was identified for the ASPP/PP1 complex - the centrosome linker protein C-Nap1, which promotes the assembly of centrosomes (Zhang et al., 2015). Phosphorylation of C-Nap1 by the kinase NEK2A prior to mitosis is thought to promote centrosome linker disassembly, thus facilitating centrosome duplication and formation of a bipolar spindle, while PP1 counteracts C-Nap1 phosphorylation (Meraldi and Nigg, 2001). C-Nap1 interacts with both ASPP1 and ASPP2, which bridge its interaction with PP1 (Zhang et al., 2015), and PP1 can dephosphorylate the NEK2A phosphorylation sites *in vitro* (Helps et al., 2000). Importantly, overexpression of either ASPP1 or ASPP2, but not of PP1-binding mutants reduces the phosphorylation levels of C-Nap1 (Zhang et al., 2015). Lastly, simultaneous knockdown of ASPP1 and ASPP2 causes defects in centrosome assembly in late telophase, suggesting that they act redundantly (Zhang et al., 2015). In conclusion these studies provide evidence that mammalian ASPP1/2 act as regulatory subunits of PP1 providing specificity for several substrates and directing the localisation of PP1.

1.3.4 N-terminal RASSFs in the PP1 network

A recent study revealed potential novel functions for human N-terminal RASSFs. Hauri *et al.* established an interaction network for N-terminal RASSFs by performing mass spectrometry on affinity purifications of different bait proteins (Hauri et al., 2013). Strikingly, all of the N-terminal RASSFs interacted with PP1 catalytic subunits (PP1α, PP1β/δ and PP1γ) as well as ASPP family proteins, ASPP1 and ASPP2 (see Figure 1.3).

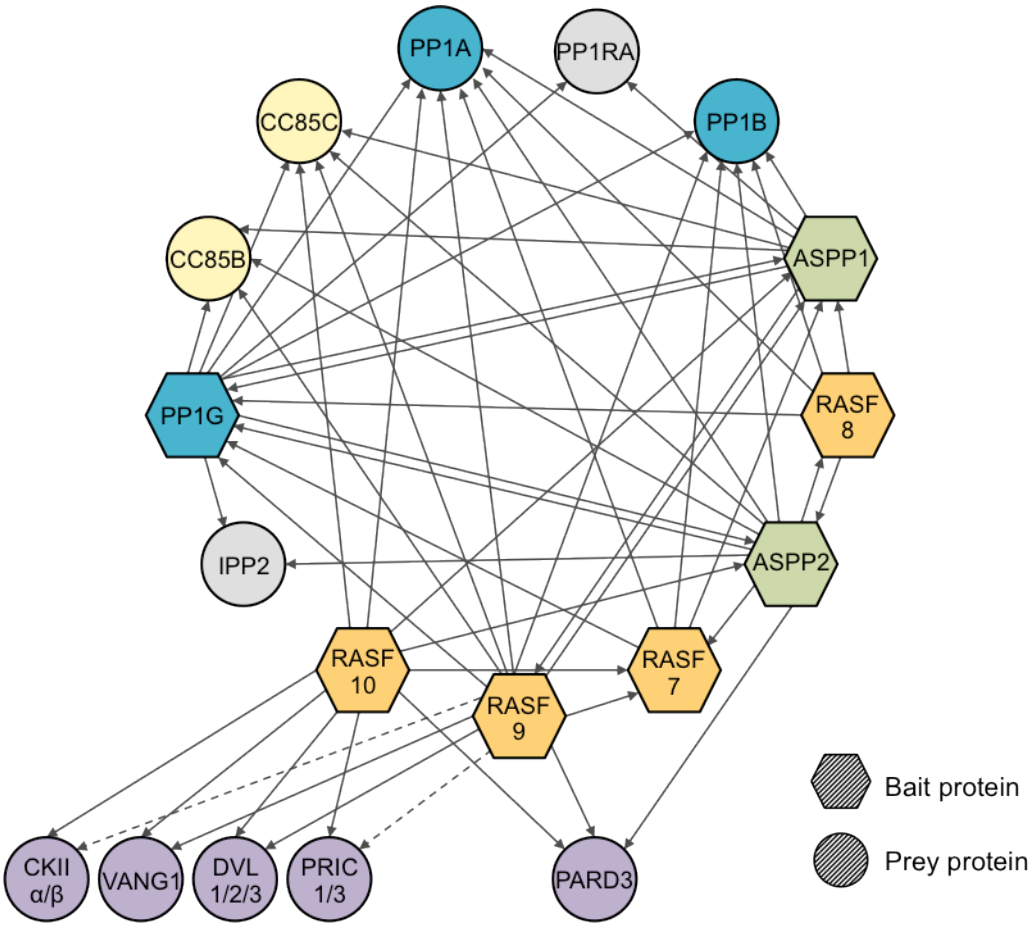

Figure 1.3 - Interaction network of N-terminal RASSFs, ASPP and PP1.
Affinity purification of bait proteins (hexagons) was followed by mass spectrometry to allow identification of interactors (prey proteins, circles). Arrows indicate the direction of the affinity purification. Interaction network between PP1 catalytic subunits (blue), known PP1 regulatory subunits (grey), ASPP family proteins (green), N-terminal RASSFs (orange), Ccdc85 family proteins (yellow) and potential substrates (purple) (adapted from (Hauri et al., 2013)). Dashed lines indicate that there is just an interaction with one of the subunits/isoforms.

These results suggested that N-terminal RASSFs could be part of the previously described ASPP/PP1 complexes and thus be additional substrate-specifying regulatory subunits.

In addition, this study revealed novel and specific interactors for human RASSF9 and RASSF10, as they were found to co-purify several core planar cell polarity proteins - Dishevelled, Prickle and Vang - as well as the polarity determinant Par3, which could be potential substrates of N-terminal RASSF/ASPP/PP1 complexes (see Figure 1.3) (Hauri et al., 2013). Importantly, PP1 was previously shown to dephosphorylate Par3 at several residues important for its subcellular localisation *in vitro* (Traweger et al., 2008), however the regulatory subunit(s) involved are unknown. In the case of ASPP and RASSF8 this could explain how they might influence the junctional integrity via Par3, which has been reported to promote the recruitment of E-cadherin clusters to remodelling junctions (McGill et al., 2009, McKinley et al., 2012). Thus, the data presented by Hauri *et al.*, opens the possibility that the N-terminal RASSFs function in the context of cell polarity as part of PP1 phosphatase complexes. In the following subchapters I will therefore introduce the functions and regulation of core planar cell polarity proteins and the polarity determinant Baz/Par3 in *Drosophila*.

1.4 Canonical Wg/Fz signalling and planar cell polarity

The canonical Wg/Fz signalling pathway and the planar cell polarity (PCP) pathway share two common components: the seven-pass transmembrane receptor Frizzled (Fz) and its effector Dishevelled (Dsh in flies, Dvl in mammals). Both pathways were first described in *Drosophila*, however mammalian homologues have been identified and were demonstrated to be conserved and essential in vertebrates. Though both pathways function through Fz and Dsh, their mechanisms and outputs are very different. While canonical Wg/Fz signalling results in activation of transcriptional expression of target genes via Armadillo (Arm, β-catenin in vertebrates), the PCP pathway establishes the polarisation of cells along a tissue axis visible by the asymmetric distribution of its core components and subsequently of its effectors (Strutt, 2003).

Wg (Wingless) was the first of the seven Wnt genes to be identified in *Drosophila* and is the ligand/signal that activates the canonical cascade. Analysis of different

mutant alleles of *wg* and other pathway members demonstrated the importance of Wg/Fz signalling in *Drosophila* development. Loss of canonical Wg/Fz signalling at the embryonic stage is lethal and leads to segmentation and multiple patterning defects in embryos (Patel et al., 1989, Lawrence et al., 1995, Immergluck et al., 1990). During larval stages Wg/Fz signalling is required for a number of processes, such as wing growth and patterning (Sharma and Chopra, 1976, Johnston and Sanders, 2003, Giraldez and Cohen, 2003, Neumann and Cohen, 1996, Martinez Arias, 2003) and patterning for the development of the peripheral nervous system (Phillips and Whittle, 1993, Couso et al., 1994). Dsh was early on demonstrated to be essential for Wg/Fz signalling, as complete loss of Dsh function resulted in *wg*-like phenotypes (Perrimon and Mahowald, 1987). Strikingly, Frizzled was not discovered as the Wg/Wnt receptor until almost 10 years later (Bhanot et al., 1996), due to the redundancy between the two *frizzled* genes *fz* and *fz2*. Loss of function of neither *fz* nor *fz2* caused *wg*-like phenotypes on their own, however Wg/Fz signalling was disrupted upon loss of both (Chen and Struhl, 1999), finally demonstrating the absolute requirement for Fz receptors in transducing the Wg signal. In vertebrates, canonical signalling is essential for normal development and its disruption causes diverse diseases including cancer (reviewed in (Clevers and Nusse, 2012, Clevers, 2006)), making the canonical Wg/Fz signalling pathway a field of great therapeutic interest.

The Arm/β-catenin-independent functions of Fz and Dsh were discovered early on, since viable mutant alleles caused defects in the planar polarisation of trichomes and sensory bristles on the adult fly (Theisen et al., 1994, Adler et al., 1987), distinct to Wg or Arm loss of function. Mutational analysis, followed by genetic interaction studies in *Drosophila* revealed other genes that were required for establishing the polarity within the plane of the tissue/epithelium leading to the definition of the PCP pathway. In the following sections, I will firstly introduce the canonical Wg/Fz signalling pathway and the PCP pathway. I will then highlight the different requirements for Fz and Dsh in both pathways and lastly look at post-translational modifications of Fz/Dsh.

1.4.1 The canonical Wg/Fz signalling pathway

Over 30 years of research in multiple model systems including *Drosophila*, *Xenopus* and mammals has led to the following model of the signalling cascade. In the canonical

Wg/Fz pathway, Frizzled functions as the receptor for Wg/Wnt ligands and the signalling cascade ultimately leads to Armadillo (Arm, β-catenin in vertebrates) dependent activation of the expression of multiple target genes, leading to a variety of cellular responses. In the absence of Wg/Wnt, cytoplasmic Arm/β-catenin is associated with GSK3 (glycogen synthase kinase 3, Shaggy in flies), Axin and APC (adenomatous polyposis coli) (Hamada et al., 1999, Yu et al., 1999, Itoh et al., 1998), which promotes phosphorylation of Arm/β-catenin by GSK3 and Casein Kinase I (CKI) (Yanagawa et al., 2002, Pai et al., 1997). Phosphorylated Arm/β-catenin is targeted for ubiquitylation and subsequent proteasomal degradation via the $SCF^{\beta\text{-}TrCP}$ complex (Jiang and Struhl, 1998, Aberle et al., 1997, Winston et al., 1999), thus limiting its cytoplasmic accumulation. In the nucleus, the Wg/Wnt signalling responsive transcription factor TCF (T cell factor) is bound to the co-repressor Groucho, and supresses the expression of Wg/Wnt target genes in the absence of a ligand (Cavallo et al., 1998, Lawrence et al., 2000).

The pathway is activated by the presence of Wg/Wnt ligands. Secreted Wg/Wnt binds to the extracellular cysteine-rich region of the N-terminus of Frizzled receptors, which then associate with their co-receptor Arrow (mammalian LPR5/6) (Tolwinski et al., 2003, Wehrli et al., 2000, Tamai et al., 2000). The signal is transmitted via Dsh binding to the intracellular domains of Fz (Wong et al., 2003) and “activated” Dsh protects Arm/β-catenin from degradation (see below). The cytoplasmic stabilised Arm/β-catenin translocates to the nucleus where it associates with TCF (van de Wetering et al., 1997) and together with the other co-activators Pygopus and Legless (mammalian BCL9) (Thompson et al., 2002, Kramps et al., 2002), activates the expression of various Wg/Wnt target genes.

The role of Dsh and how exactly Arm/β-catenin is stabilised are still not clear. Upon activation of the signalling cascade Axin was shown to be recruited and to interact with LPR5 at the membrane (Mao et al., 2001), subsequently disassembling the GSK3-Axin-APC destruction complex. One suggested role for Dsh is the recruitment of Axin to the membrane (Cliffe et al., 2003, Kishida et al., 1999), and both proteins were shown to directly bind to each other (Fiedler et al., 2011). Interestingly, the phosphorylation state of Axin appears to be important for the maintenance of the destruction complex. Phosphorylation of Axin by CKI promotes its binding to GSK3, whereas

dephosphorylation by PP1 destabilises the destruction complex in cell culture experiments (Luo et al., 2007, Kim et al., 2013). Moreover, cell culture overexpression experiments suggest that the association of Axin and LPR5/6 depends on GSK3 and CKI-mediated phosphorylation of the co-receptor itself (Zeng et al., 2005), which requires both Fz and Dsh (Zeng et al., 2008).

The published work suggested a model in which Arm/β-catenin stabilisation is achieved via inactivation/disassembly of the destruction complex. However, a contrasting model was recently proposed (Li et al., 2012). In this study the authors found by looking at endogenous protein levels in HEK293 cells that activation of the signalling cascade does not interfere with the assembly of the destruction complex, but instead appears to block ubiquitylation of phosphorylated β-catenin, which then stays associated with the destruction complex (which is still recruited to Dsh-LPR5/6) and unbound, unphosphorylated β-catenin is then free transfer to the nucleus. In another recent study an additional mechanism of Arm/β-catenin stabilisation via endocytosis was proposed, since inhibition of endocytosis decreased Arm/β-catenin levels independently of the GSK3-Axin-APC destruction complex in *Drosophila* (Gagliardi et al., 2014). Further research will be necessary to elucidate the mechanism(s) by which Arm/β-catenin is stabilised upon activation by Wg/Wnt and especially how Dsh, which is essential for this process, contributes to the signalling cascade.

1.4.2 Planar cell polarity

There are two types of polarity in most epithelial cells: apical-basal polarity (see 1.5) and PCP. PCP is required for correct tissue morphogenesis and disruption of the pathway elicits visible phenotypes on all cuticular epithelial structures of the adult fly - making *Drosophila* an ideal model to study PCP. In *Drosophila* the components of the core PCP pathway are: Fz, Dsh, the cytoplasmic proteins Diego (Dgo) and Prickle (Pk), the four-pass transmembrane protein Strabismus (Stbm, or Van Gogh, Vang) and the seven-pass transmembrane protocadherin Flamingo (Fmi, or Starry night/Stan). Loss of any of the core components leads to typical PCP defects, such as swirly trichomes (hairs) on the wing and body, random orientation of sensory bristles (except for Dgo (Feiguin et al., 2001)) and of ommatidia in the eye (Adler et al., 1987, Theisen et al., 1994, Usui et al., 1999, Feiguin et al., 2001, Wolff and Rubin, 1998, Taylor et al., 1998,

Gubb and Garcia-Bellido, 1982). All components are conserved in vertebrates, and PCP has been shown to be involved in many different processes (in epithelia as well as non-epithelial tissues), such as hair orientation, neural tube closure and gastrulation in mice (Singh and Mlodzik, 2012). However, the analysis of PCP in vertebrates is more complex compared to *Drosophila* due to redundancy between the homologues of the core components. Hence, *Drosophila* remains the preferred model system for elucidating the mechanisms involved in establishing PCP.

The core PCP pathway operates in parallel to a second molecular system - the Fat/Dachsous/Four-jointed (Ft/Ds/Fj) system, which is composed of the atypical cadherins Ft and Ds and the Golgi-localised kinase Fj (which modulates Ft and Ds by phosphorylation) (see 1.4.5 and (Goodrich and Strutt, 2011)). Like the core PCP pathway, the Ft/Ds/Fj group is required to establish the polarity along tissue axes. Loss of Ft or Ds activity results in classical PCP defects (Casal et al., 2002, Adler et al., 1998, Yang et al., 2002). In addition the Ft/Ds/Fj system is required for proximo-distal (P-D) axis elongation, for instance in the wing by promoting oriented cell divisions along the P-D axis and orienting cell flows during pupal development (Mao et al., 2011, Aigouy et al., 2010, Baena-Lopez et al., 2005).

The epithelial cuticular structures of the adult fly display the outcome of PCP: the epithelial cells of the wing have one trichome localised on the distal side of each cell, the trichomes of the thorax and abdomen are on the posterior side, and all hairs/bristles and external sensory bristles are aligned along the tissue axis. Thousands of cells of the various epithelial tissues need to be polarised along the appropriate axis. Thus it is thought that planar polarisation requires firstly a directional input, which initiates the direction of polarisation, secondly interpretation of the cue leading to intracellular polarisation and lastly intercellular cell-cell communication to propagate the asymmetry locally.

1.4.3 Asymmetric localisation of PCP components

During pupal wing development, just before prehair formation, Fz, Dsh and Dgo become highly enriched at the distal apical cell cortex (Axelrod, 2001, Strutt, 2001, Feiguin et al., 2001), whereas Stbm and Pk are at the posterior apical cell cortex of wing epithelial cells (Figure 1.4) (Bastock et al., 2003, Tree et al., 2002). Fmi is planar

polarised on the distal and proximal side and homophilically interacts with Fmi on adjacent cells (Figure 1.4) (Usui et al., 1999). In sensory organ precursors (SOPs), that will eventually give rise to the sensory bristles, Fz/Dsh are found on the posterior cell cortex and Stbm/Pk on the anterior cell cortex (pupal notum SOPs) (Segalen et al., 2010, Bellaiche et al., 2004) while Flamingo is uniformly localised (Lu et al., 1999). Asymmetric localisation of Fz/Dsh/Dgo and Stbm/Pk is also observed at specific stages in the R3/R4 photoreceptor precursors in the developing eye imaginal disc (Das et al., 2004, Strutt et al., 2002).

The asymmetry of the core components is important for their downstream effectors, which interpret the PCP signal. Effectors differ for each PCP tissue: In the wing the formation of a single trichome on the distal side of each cell is dependent on the interplay of the downstream effectors Fuzzy, Fritz and Inturned, which localise to the proximal side (reading the Stbm/Pk signal) and promote the distal localisation of Multiple Wing Hairs, thus restricting hair formation to the distal side (Strutt and Warrington, 2008). In SOP cells, the asymmetric localisation of the core components is required for spindle orientation (see 1.7.2). In the R3 photoreceptor, Fz and Dsh positively regulate the transcription of the Notch ligand Delta (Dl), thus allowing Notch-mediated cell fate specification of the R3 and R4 photoreceptors (Fanto and Mlodzik, 1999, Strutt et al., 2002). These examples demonstrate the importance of the asymmetric localisation of the core components and moreover the diverse outputs of PCP.

Over the last decades several studies have addressed how the asymmetric localisation is maintained within the cell and how neighbouring cells communicate the polarity, by performing genetic interactions, subcellular localisation, clonal analysis and co-immunoprecipitation experiments. Firstly, loss-of-function experiments revealed that the asymmetric distribution is dependent on the presence of all of the core components (Strutt, 2002). Moreover, Fmi is absolutely required for initiating the apical localisation of the other components since for all, the membrane localisation is abolished in loss-of-function clones of *fmi* (Tree et al., 2002, Bastock et al., 2003, Shimada et al., 2001, Feiguin et al., 2001, Strutt, 2001). Based on similar loss-of-function experiments, the next molecules in this apparent hierarchy are Fz and Stbm, which are required to re-localise the cytoplasmic components to the membrane. Fz recruits Dsh (Axelrod et al.,

1998) and Dgo binds to Dsh (Jenny et al., 2005), whereas Stbm recruits Pk to the opposite side (Jenny et al., 2003, Bastock et al., 2003). Loss or overexpression of Dsh, Pk and Dgo does not affect the membrane localisation of the receptors, but their asymmetric distribution (Shimada et al., 2001, Strutt, 2001, Feiguin et al., 2001, Tree et al., 2002, Bastock et al., 2003). Thus, the cytoplasmic components are required to maintain, but not to establish the initial asymmetry and moreover their levels need to be regulated.

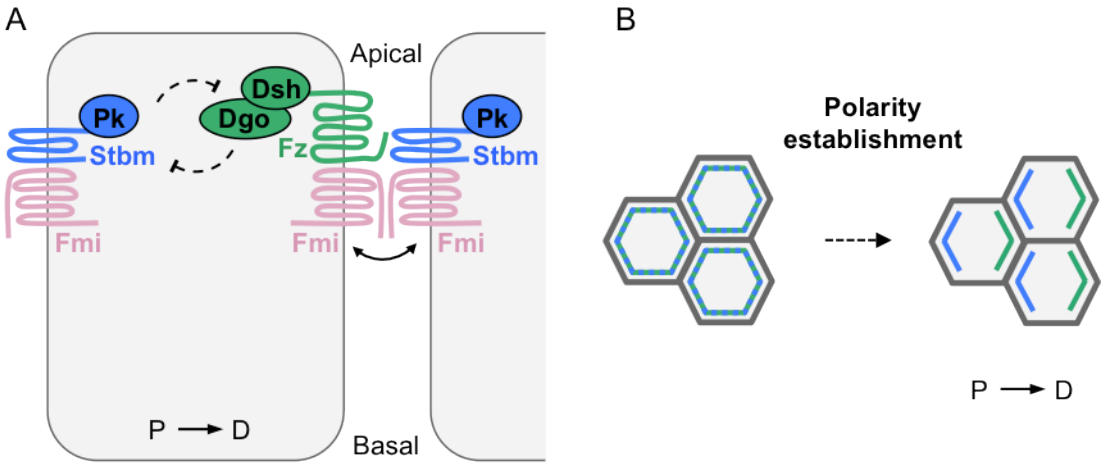

Figure 1.4 - Asymmetric distribution of core PCP components.
(A) Outline of a planar polarised cell showing the asymmetric distribution and interactions of core polarity components. Stbm/Fmi complexes localise apically to the proximal side opposite Fz/Fmi complexes at the distal side. Fz recruits Dsh and Dgo, whereas Stbm recruits Pk. Mutual antagonism between Pk and Dgo contribute to the asymmetry, as well as intercellular interactions between neighbouring Fz/Fmi and Stbm/Fmi complexes based on homophilic Fmi interactions and preferential clustering of Fz/Fmi and Stbm/Fmi. (B) PCP components show initially no planar polarisation in epithelial cells of the pupal wing and are uniformly spread around the cell cortex. During development they become planar polarised along the proximal-distal axis, due to an unknown polarity cue. Fz/Dsh/Dgo (green) localise distally, whereas Stbm/Pk (blue) localise to the proximal side.

Positive feedback loops and mutual antagonism involving the core components are thought to promote the asymmetry. Dgo promotes Dsh binding to Fz, whereas Pk can

compete with Dgo for Dsh binding and thus inhibits Dsh/Fz activity (Figure 1.4) (Tree et al., 2002, Jenny et al., 2005). In addition, clustering of Fz/Fmi complexes into concentrated puncta (promoted by Dsh) at the distal side and Stbm/Fmi complexes (promoted by Pk) on the adjacent membrane of the neighbouring cell results in highly stable complexes and thus provides positive feedback (Figure 1.4) (Strutt et al., 2011, Aigouy et al., 2010).

Besides the feedback regulation of the main components, other mechanisms contribute to maintain the asymmetry. Fz and Dsh are transported in vesicles along non-centrosomal microtubules to the distal side of the cell (Shimada et al., 2006). Moreover the ubiquitin system regulates the levels of the cytoplasmic components, as ubiquitylation contributes to keep Pk (via the Cullin1/SkpA/Supernumerary limbs ubiquitin ligase complex) and Dsh (via the Cullin-3/Diablo/Kelch ubiquitin ligase complex) at the right level at the apical junctions (Strutt et al., 2013a, Strutt et al., 2013b, Cho et al., 2015). Regulation of the core components via ubiquitin-mediated degradation seems to be a general mechanism as in mice, levels of the Pk homologue Prickle1 are regulated by Smurf ubiquitin ligases (Narimatsu et al., 2009).

1.4.4 Intercellular communication

Between two neighbouring cells, distal Fz/Fmi complexes of one cell interact with proximal Stbm/Fmi complexes of the adjacent cell. The intercellular association seems to be facilitated by homophilic Fmi interactions (Usui et al., 1999) and interactions between the extracellular domains of Fz and Stbm (Wu and Mlodzik, 2008, Chen et al., 2008). The communication of polarity information between cells became first obvious in the non-autonomous effects seen for *fz* loss-of-function clones in the developing pupal wing. Neighbouring wild type cells re-orient their polarity (hair) towards the mutant tissue (Adler et al., 1997). Loss-of-function clones of *stbm* cause the opposite phenotype, with the hair pointing away from the clonal area (Taylor et al., 1998). In *fz* mutant clones, solely Stbm/Fmi complexes are present, which then recruit the Fz/Fmi complexes of the neighbouring wild type cell to the adjacent membrane, thus altering the polarity of the surrounding cells. Conversely, Fz/Fmi complexes of *stbm* mutant cells associate with Stbm/Fmi complexes of wild type cells. Although loss of *fmi* does not cause non-autonomous effects on its own, double mutant clones for either *fz/fmi* or

stbm/fmi do not alter the polarity of adjacent wild type tissue, demonstrating that Fmi is required for intercellular communication (Strutt and Strutt, 2007). Taken together, the intercellular connection between Fz/Fmi and Stbm/Fmi complexes allows the communication of polarity from cell to cell. Interestingly, the *Drosophila* Selectin Furrowed has recently been shown to promote and stabilise the intercellular interactions between Fz and Stbm together with Fmi (Chin and Mlodzik, 2013).

The intercellular communication does not require the cytoplasmic components Dsh, Pk and Dgo, as none of them cause non-autonomous defects when clonally inactivated. Moreover, unlike *fmi*, they do not supress the non-autonomous *fz* or *stbm* phenotypes (Strutt and Strutt, 2007). However, Dsh and Pk participate in concentrating the clusters of the intercellular Fz-Fmi and Stbm-Fmi complexes into stable puncta (Strutt et al., 2011).

Importantly mutant clones of *fz* or *stbm* only affect the polarity of surrounding wild type cells in close proximity, but not the overall polarity of the wing, suggesting that most of the cells orient towards the stronger upstream cue. Intra- and intercellular interactions explain how asymmetry is maintained and communicated between cells. But what is the directional input that initially defines the polarity axis?

1.4.5 Directional inputs for PCP

The Ft/Ds/Fj system is proposed to provide directional inputs for the asymmetry of the core components (Ma et al., 2003, Yang et al., 2002). The ligand of Ft, Ds, and Ft form heterophilic complexes in *trans* across neighbouring cells (Matakatsu and Blair, 2006) and are planar polarised (Ambegaonkar et al., 2012, Bosveld et al., 2012, Brittle et al., 2012), with Ft localising proximally and Ds distally in the developing wing (Brittle et al., 2012, Sagner et al., 2012). The planar polarisation is the result of, firstly, opposing expression gradients of Ds and Fj (Ds is high proximally and Fj is high distally) (Yang et al., 2002). Secondly, Fj modulates the affinity of the Ft-Ds interaction by phosphorylation, such that phosphorylation of Ft enhances the interaction whereas phosphorylation of Ds decreases it (Simon et al., 2010, Ishikawa et al., 2008, Brittle et al., 2010). The opposing expression gradients of Ds and Fj and the modulation of the Ft-Ds affinity by Fj thus provide an axis for polarity direction, which leads to asymmetric distribution of Ft and Ds within the cell (Hale et al., 2015).

The global polarity axis created by the Ft/Ds/Fj system is therefore an attractive candidate to provide directional input for the polarity of the core PCP system. Indeed, it was recently demonstrated that the Ft/Ds/Fj group orients apical non-centrosomal microtubules along the P-D axis (plus ends are enriched distally), thereby facilitating the directed vesicular transport of Fz and Dsh to the distal cortex of the wing and thus orienting the polarity of the core components at least in the proximal and central wing regions (Matis et al., 2014, Olofsson et al., 2014, Shimada et al., 2006, Harumoto et al., 2010). In the study from Matis *et al*., the authors point out that the P-D orientation of the microtubules in the distal wing margin is independent of the Ft/Ds/Fj system and suggest that a different signal must operate to polarise them in distal regions. It is worth pointing out that, after many years of controversy relating to how core PCP and Ft/Ds/Fj PCP are functionally connected, three recent studies showed that they are indeed linked via one of the two Pk isoforms (Spiny-legs), although these studies suggest different mechanisms (Ayukawa et al., 2014, Merkel et al., 2014, Olofsson et al., 2014).

In canonical Wg/Fz signalling, Wg/Wnts are the ligands for Frizzled receptors (see 1.4.1). Several studies have suggested that Wnts might be the directional input for PCP in different vertebrate systems (Gao et al., 2011, Gros et al., 2009). In *Drosophila* a study from the Mlodzik lab suggests that Wg and Wnt4, which are both expressed at the wing margin, act redundantly (explaining why this function was not previously identified) as polarity cues in the wing (Wu et al., 2013). This study shows that mis-expression and loss-of-function of Wg/Wnt4 affects polarity similarly to the effects of core components and independently of canonical Wg/Fz signalling. Furthermore, the authors suggest a mechanism in which the Wg/Wnt4 gradient emanating from the wing margin modulates the affinity of the Fz/Stbm intercellular interactions, thus providing directional input (Wu et al., 2013). Interestingly, the previously mentioned study from the Axelrod lab suggests an alternative role for Wnt4 in the orientation of non-centrosomal microtubules, as mis-expression of Wnt4 (but not Wg) disturbs their alignment along the P-D axis (Matis et al., 2014).

Moreover, morphogenetic movements during development from the wing imaginal disc to the pupal wing are also thought to provide directional input (Sagner et al., 2012, Aigouy et al., 2010). Taken together, the examples detailed above demonstrate that

there is likely more than one directional input for the PCP system. It is therefore possible that these inputs act redundantly, providing robustness to PCP establishment.

1.4.6 Different requirements for Fz and Dsh in the canonical and PCP pathways

The canonical Wg/Fz and the PCP pathway both signal through Fz and Dsh, however the downstream effectors are distinct and specific for each pathway. Specificity seems to be achieved by different engagements and requirements for Fz and Dsh. Frizzled receptors belong to the superfamily of G-protein-coupled receptors (GPCRs) and comprise an N-terminal extracellular domain (containing the CRD domain for Wg/Wnt binding), a seven-pass transmembrane domain and a C-terminal intracellular domain (Wang et al., 2006). In *Drosophila* the two different Frizzled receptors Fz and Fz2 act redundantly in Wg/Fz signalling (Chen and Struhl, 1999). Fz2 seems to be the main receptor and was shown to have the higher affinity for Wg/Wnt binding (Strapps and Tomlinson, 2001, Rulifson et al., 2000). Conversely, the PCP pathway seems to function solely through Fz, as firstly expression of Fz2 does not rescue the PCP phenotype in *fz* and *fz2* double mutants (Chen and Struhl, 1999) and secondly overexpression of Fz2 results in Wg-specific defects (and no PCP defects) (Rulifson et al., 2000). A further difference is that the apical localisation of Fz is not essential for canonical Wg/Fz signalling, as endogenous and ectopically expressed Fz2 localise along the entire apical-basal membrane (Wu et al., 2004). The intracellular C-terminal tail is critical for the subcellular localisation, as transgenic Fz2 chimeras containing the Fz C-terminus are able to localise apically (Wu et al., 2004).

The cytoplasmic protein Dsh/Dvl contains three conserved domains: an N-terminal DIX (Dishevelled and Axin) domain, a PDZ (PSD95, Dlg, ZO-1) domain and a C-terminal DEP (Dishevelled, Egl-10, Pleckstrin) domain (Boutros et al., 1998). Several studies in *Drosophila* and *Xenopus* used Dsh/Dvl truncation approaches combined with rescue experiments and binding studies with Fz receptors to decipher the different requirements for the Wg/Fz and core PCP pathway. PCP signalling requires the PDZ domain and the DEP domain, while canonical Wg/Fz engages the DIX domain, the PDZ domain and to a lesser degree the DEP domain (Axelrod et al., 1998, Boutros et al., 1998, Penton et al., 2002). Dsh/Dvl supposedly binds through the DEP domain

(Axelrod, 2001) to the intracellular C-terminal tail and the three intracellular loop (ICL1-3) of Frizzled receptors (Tauriello et al., 2012). Moreover, a conserved motif within the C-terminal tail of Fz - the KTxxxW motif (*Drosophila* Fz: aa 557–561) - is critical for Dsh/Dvl binding (Strutt et al., 2012, Wu et al., 2008), which was shown to also weakly interact with the PDZ domain of Dsh/Dvl (Wong et al., 2003). Interestingly, the stable localisation of Dsh at the membrane, which is essential for PCP, is apparently not required for canonical Wg/Fz signaling (Axelrod, 2001, Wu et al., 2004).

A recent study tried to dissect the different requirements of Fz in more detail by large-scale mutagenesis (Strutt et al., 2012). While several residues were found to be essential for both pathways, the analysis also revealed mutations (in the ICL and the KTxxxW motif) that caused PCP-specific defects. The authors propose a model in which Fz receptors might undergo conformational changes upon PCP activation, thus allowing specific Dsh interactions (Strutt et al., 2012). However, it is as yet unclear for either pathway exactly how Fz gets activated. Activation of Dsh is believed to depend on the phosphorylation state of Dsh, which will be explored in the next subchapter.

1.4.7 Regulation of Dsh and Fz by post-translational modifications

Dsh/Dvl is a known phosphoprotein (Yanagawa et al., 1995) and contains about 14% of serine and threonine residues, as well as several tyrosine residues. Endogenous Dsh is hyperphosphorylated (in fly embryos, larvae and pupae) and phosphorylation of Dsh can be induced in cell culture upon co-expression of Wg, Fz, Fz2 and Dgo (Yanfeng et al., 2011, Yanagawa et al., 1995, Jenny et al., 2005). This strongly suggests that Dsh is activated by phosphorylation for both the Wg/Fz and PCP pathway. Several kinases, such as CKI, CKII and Par1, were shown to bind to and phosphorylate Dsh (Sun et al., 2001, Willert et al., 1997, Song et al., 2000, Klein et al., 2006, Strutt et al., 2006). However, the functional relevance of the phosphorylation is not well understood. In *Drosophila*, CKIε (Dco, Discs overgrown) promotes Dsh asymmetric distribution in pupal wings (Strutt et al., 2006). Loss of *CKIε* reduces the phosphorylation level of endogenous Dsh and causes mild PCP defects, although no specific phosphorylation sites were identified (Strutt et al., 2006). Similarly, loss of the non-receptor tyrosine kinase Abelson (Abl) elicits PCP defects, and Abl phosphorylates Dsh on a conserved residue (Tyr473) within the DEP domain in *Drosophila* (Singh et al., 2010).

Furthermore, *dsh (Y473F)* mutant flies show strong PCP defects (but no canonical Fz/Wg defects) and the mutant protein fails to localise at the membrane, thus demonstrating the importance of phosphorylation *in vivo* (Singh et al., 2010).

The two examples above highlight the positive effects of Dsh phosphorylation. However, phosphorylation of Dsh/Dvl can also target it for degradation. Phosphorylated Dvl was shown to be ubiquitylated by the E3 ubiquitin ligase Itch and subsequently degraded in HEK293 cells (Wei et al., 2012). Strikingly, Dvl can be partially dephosphorylated by PP1c *in vitro* upon association with the kinase Hipk2, which protects Dvl from Itch-mediated degradation (Shimizu et al., 2014). As mentioned above, *Drosophila* Dsh is ubiquitylated by the Cullin-3/Diablo/Kelch ubiquitin ligase complex, which appears to specifically target the hyperphosphorylated form of Dsh (Strutt et al., 2013a). Phosphorylation-dependent degradation of Dsh/Dvl could therefore be a conserved mechanism to maintain the appropriate levels of Dsh. Interestingly, although several conserved serine and threonine residues are found phosphorylated in endogenous Dsh, mutation of these residues does not cause canonical Wg/Fz or PCP defects (Yanfeng et al., 2011). This could mean that Dsh activity might require phosphorylation of multiple residues. Thus, phosphorylation and dephosphorylation of Dsh can regulate its activity in both canonical Wg/Fz and PCP signalling. The underlying mechanisms, especially how activation of the pathways promotes or activates the kinases and phosphatases, remain elusive.

As well as Dsh/Dvl activity, phosphorylation has also been reported to regulate Fz activity. Fz receptors have predicted protein kinase A (PKA), protein kinase C (PKC) and casein kinase II (CKII) phosphorylation sites (Wang et al., 2006). Indeed, two serine residues (Ser554 and Ser560, just before and within the KTxxxW motif) in the C-terminal tail of *Drosophila* Fz can be phosphorylated *in vitro* by aPKC (Djiane et al., 2005). This study further showed that phosphorylation by aPKC inhibits Fz PCP activity in the developing eye through an unknown mechanism independent of Dsh recruitment (Djiane et al., 2005). Similarly, inhibitory effects in connection with phosphorylation were reported for the *Xenopus* Fz3 receptor (Yanfeng et al., 2006). Ectopically expressed Fz3 in *Xenopus* embryos was found to be phosphorylated on Ser576 (70 aa after the KTxxxW motif) and other C-terminal residues, which was dependent on the presence of co-expressed Dvl. Expression of Ser576 non-

phosphorylatable mutants increased the induction of neural crest markers, indicating that phosphorylation might have an inhibitory effect on Fz signalling activity (Yanfeng et al., 2006). Phosphorylation of Fz could lead to its destabilisation or internalisation/degradation (Djiane et al., 2005). Indeed, Fz receptors have recently been reported to be regulated by ubiquitylation. *Drosophila* Fz2 and mammalian Fz4 are stabilised by the deubiquitylation enzyme UBPY (USP8), which therefore promotes canonical Wg/Fz signalling (Mukai et al., 2010). Conversely, two related transmembrane E3 ubiquitin ligases, RNF43 and ZNRF3, have been shown to inhibit Fz activity by targeting it to the lysosome in different vertebrate systems (Hao et al., 2012, Koo et al., 2012).

1.5 The polarity determinant Bazooka

Polarity of cells as described for PCP is achieved by asymmetric distribution of polarity determinants. Epithelial cells are not only polarised along the tissue axis (as described above), but also along the apical-basal axis. Polarisation of cells along a certain axis is essential for many different cellular functions, such as determination of cell fate of daughter cells, migration, cell shape or orientation of cell divisions.

The PDZ domain-containing scaffold protein Bazooka (Baz, Par3 in vertebrates) is a crucial polarity determinant for many different cell types. Together with other polarity determinants Baz/Par3 is, for example, essential for establishing the anterior-posterior axis in *Drosophila* oocytes and *C. elegans* embryos, apical-basal polarity in epithelial cells and the asymmetry of cell fate determinants in the developing nervous system of *Drosophila* (Goldstein and Macara, 2007). In the following section, I will outline the functions of Baz as a polarity determinant, its interactors and its regulation in epithelial cells and non-epithelial cells in *Drosophila*.

In *Drosophila* oocytes, neuroblasts (neuronal stem cells) and SOPs (the precursors of the external sensory organs, see 1.7), Baz localises asymmetrically on one side of the cell, together with the serine/threonine kinase aPKC and its binding partner Par6 (Segalen and Bellaiche, 2009, St Johnston and Ahringer, 2010). Baz can bind to both aPKC (Wodarz et al., 2000) and Par6 (Petronczki and Knoblich, 2001), which also associate independently of Baz (Hutterer et al., 2004). In oocytes, the serine/threonine

kinase Par1 and Lethal giant larvae (Lgl) localise posteriorly, opposite the Baz-aPKC-Par6 complex and this asymmetry defines the A-P axis (St Johnston and Ahringer, 2010). The asymmetric localisation is maintained by mutual antagonism and positive feedback between the two complexes. Par1 can phosphorylate Baz on and Ser151 and Ser1085, which induces 14-3-3 binding to Baz, thereby excluding it from the posterior cortex (Benton and St Johnston, 2003b). On the other hand, aPKC can phosphorylate Par1 and Lgl, and non-phosphorylatable mutants of which are no longer restricted to the posterior domain of the oocyte cortex (Doerflinger et al., 2010, Tian and Deng, 2008). Thus, phosphorylation of Par1 and Lgl by aPKC removes the former from anterior/lateral regions. In dividing neuroblasts, the Baz-aPKC-Par6 complex localises together with the other polarity determinants Inscuteable and Partner of Inscuteable (Pins) at the apical cortex to establish the basal asymmetric enrichment of cell fate determinants required for producing daughter cells of distinct fates through asymmetric cell division (ACD) (Knoblich, 2008). The apical-basal asymmetry is, as in oocytes, maintained by mutual inhibition of apical and basal polarity determinants: Baz is excluded from the basal cortex by Par1 phosphorylation and aPKC-mediated phosphorylation of Lgl removes it apically (Betschinger et al., 2003, Wirtz-Peitz et al., 2008).

In epithelial cells, the interactions and regulation of Baz are more complex, due to the presence of different domains along the apical-basal axis defined by distinct polarity determinants. Epithelial cells can be divided into the apical domain (containing the tight junctions in mammals), the adherens junction, the lateral domain (containing the septate junctions in *Drosophila*) and the basal domain (Figure 1.5) (St Johnston and Ahringer, 2010). Apical-basal polarity is crucial to epithelial cell function, as it is required to form stable cell-cell junctions and hence act as a barrier that allows directed transport of different ions and molecules (Tepass, 2012). In this section, I will focus on *Drosophila* apical-basal polarity.

Besides Baz, aPKC and Par6, two other conserved groups of proteins are involved in polarity determination - the Crumbs (Crb) complex and the Scribble group (St Johnston and Ahringer, 2010). The Crb complex is composed of the transmembrane protein Crb with the cytoplasmic proteins Stardust (Sdt) and PatJ. Like the Baz-aPKC-Par6 complex, the Crb complex localises apically (Figure 1.5). The Scribble group is composed of

Scribble, Lgl and Dlg and defines the basolateral region (Figure 1.5), where Par1 also localises (Benton and St Johnston, 2003b). aPKC/Par6 and Baz are also localised apically, however, unlike in oocytes and neuroblasts, the localisation of Baz and aPKC/Par6 only partially overlaps (Figure 1.5). For instance, in the epithelial cells of the *Drosophila* embryonic epidermis and in the photoreceptors, aPKC and Par6 co-localise with the Crb complex, whereas Baz is found more basally at the adherens junctions (Walther and Pichaud, 2010, Morais-de-Sa et al., 2010, Harris and Peifer, 2005).

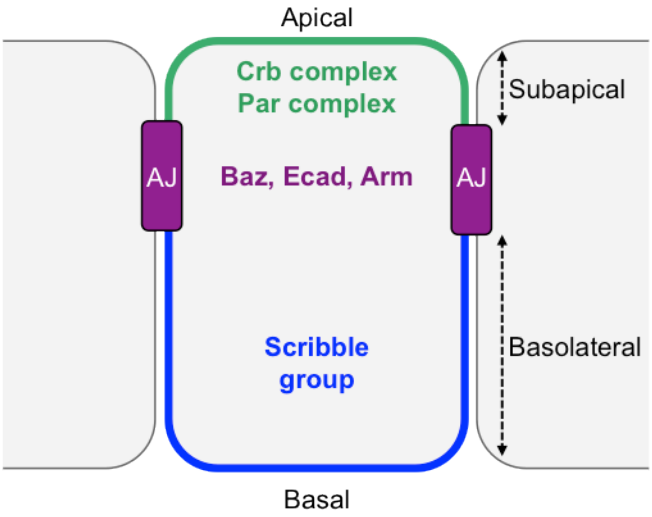

Figure 1.5 - Apical-basal polarity determinants in *Drosophila* epithelial cells.
Outline of a *Drosophila* epithelial cell showing the localisation of important polarity components along the apical-basal axis. Apical polarity determinants (Crb complex, Par complex) define the apical and subapical region (green). The adherens junctions (AJ, purple) contain the junctional components E-cadherin, Arm and also the polarity determinant Baz. The Scribble group proteins are found at the basal and basolateral region (blue), which contain the septate junctions.

The apical and basal polarity determinants prevent each other from spreading into the opposite domains, thus maintaining the apical-basal polarity (Bilder et al., 2003, Johnson and Wodarz, 2003, Tanentzapf and Tepass, 2003), though the exact mechanisms are still not fully understood and several factors appear to be involved

(Tepass, 2012). As in oocytes and neuroblasts, the different inhibitory phosphorylations contribute to the polarisation: phosphorylation of Baz by Par1 and 14-3-3 binding removes it from the basolateral domain and phosphorylation of Par1 and Lgl by aPKC removes them apically (Benton and St Johnston, 2003b, Betschinger et al., 2003). In addition, Crb self-recruitment through its extracellular domain is thought to reinforce the apical domain (Fletcher et al., 2012).

Baz has several functions in the establishment of the apical domain. Firstly, Baz is required for the recruitment of aPKC/Par6 to the apical cortex, which is also dependent on Cdc42 (Harris and Peifer, 2005, Hutterer et al., 2004). It was recently shown that Baz also recruits Sdt, thus promoting the formation of the Crb complex apically (Krahn et al., 2010a). Taken together this promotes interactions between aPKC/Par6 and the Crb complex (Sotillos et al., 2004, Kempkens et al., 2006), which are required to define the apical domain. Another important function of Baz is its role in the positioning and assembly of the adherens junctions (Harris and Peifer, 2005, McGill et al., 2009), which is independent of aPKC/Par6. All these functions require the apical cortical localisation of Baz, which is facilitated by the following characteristics: Baz can bind directly through a polybasic C-terminal region to phosphoinositides of the cortical membrane, which can be disrupted by Rho-kinase mediated phosphorylation (Krahn et al., 2010b, Simoes Sde et al., 2010). Additionally, Baz interacts via its PDZ domains with the adherens junction components Arm and Echinoid (Wei et al., 2005b). Moreover oligomerisation of Baz via its N-terminus promotes its cortical localisation (Benton and St Johnston, 2003a).

The apical exclusion of Baz and its restriction to adherens junctions, which requires the dissociation of Baz from aPKC/Par6 is important for the apical polarity in epithelial cells (Laprise and Tepass, 2011). This is achieved by two different means: firstly, aPKC phosphorylates Baz on Ser980, which weakens the interaction between Baz and aPKC and secondly, Crb competes with Baz for Par6 binding (Morais-de-Sa et al., 2010, Walther and Pichaud, 2010). The importance of the competition between Crb and Baz for Baz apical exclusion is further strengthened by the finding that phosphorylated Baz is still part of the aPKC/Par6 complex in oocytes and neuroblasts - both of which lack the Crb complex (Morais-de-Sa et al., 2010, Hong et al., 2001). Thus phosphorylation of Baz on Ser890 is not sufficient to disrupt the Baz-aPKC-Par6 complex and is not

essential for polarity in oocytes or neuroblasts. As mentioned above, phosphorylation by Par1 removes Baz from the basolateral cortex, thus further restricting its localisation to the adherens junctions.

Lastly, phosphorylation of Baz can be reversed by dephosphorylation. In *Drosophila* neuroblasts the Par1 site Ser1085 of Baz can be dephosphorylated by PP2A phosphatase complexes (Krahn et al., 2009). Inhibition of PP2A reverses apical-basal polarity in the neuroblasts, thus suggesting that it is important to maintain certain levels of phosphorylated and dephosphorylated Baz (Krahn et al., 2009). Interestingly, PP1 can dephosphorylate mammalian Par3 *in vitro* (corresponding sites in Baz: the Par1 site Ser151 and the aPKC site Ser980), and inhibition of PP1 delays the formation of tight junctions (adherens junctions in *Drosophila*) in cell culture experiments (Traweger et al., 2008). In conclusion, the interplay between kinases and phosphatases gives rise to dynamic regulation of apical-basal polarity, which is important when cells are remodelled during development.

1.6 Cross talk between PCP and polarity determinants

Several studies link core PCP components to apical-basal polarity determinants. Mammalian Dishevelled can bind aPKC *in vitro* and regulate its activity in the context of axonal differentiation (Zhang et al., 2007). In addition, Dishevelled was reported to regulate the basal localisation of Lgl in *Xenopus* ectoderm and *Drosophila* follicular cells (Dollar et al., 2005). In developing *Drosophila* photoreceptors, it was proposed that Fz activity in non-PCP dependent photoreceptors is inhibited through phosphorylation by aPKC, most likely mediated by PatJ binding to Fz, whereas Baz binding to aPKC suppresses the inhibitory function in planar-polarised photoreceptors (Djiane et al., 2005). Moreover, Scribble functions in PCP in *Drosophila* and vertebrates (Montcouquiol et al., 2003, Courbard et al., 2009). Loss-of-function of Scribble in *Drosophila* causes PCP defects in eye and wing and Scribble might function as an effector of Stbm, supported by the finding that they can bind to each other across species (Courbard et al., 2009, Kallay et al., 2006). Lastly, Baz can bind to one of the two Fmi splice variants and Baz overexpression can cause mild PCP defects in the wing, however, the physiological relevance of this finding could not be established

(Wasserscheid et al., 2007). Most relevant to this thesis, apical-basal polarity determinants and PCP components are functionally linked in the asymmetric cell divisions of sensory organ precursors (SOP), which will be introduced in following section.

1.7 Asymmetric cell divisions of sensory organ precursors

Sensory organ precursor (SOP) cells are the progenitors of the external sensory organs in *Drosophila*. External sensory organs (often referred to as bristles) are part of the peripheral nervous system and allow sensing of mechanical (via mechanoreceptors) and chemical (via chemoreceptors) stimuli (Jarman, 2002, Stocker, 1994). Mechanoreceptors, such as microchaetes and macrochaetes on the notum or abdomen, or the margin bristles of the wing are composed of an external hair, socket, sheath and neuron and appear in regularly spaced stereotypical positions (Huang et al., 1991, Hartenstein and Posakony, 1989). They are the result of asymmetric cell divisions starting from a single SOP cell.

1.7.1 Development of external sensory organs

With onset of the metamorphosis, one epithelial cell within the single-layered epithelial tissue is selected to become the SOP. The selection requires the expression of proneural genes in a group of cells (the proneural cluster). Proneural genes, such as the Achaete-Scute complex, encode basic helix-loop-helix (bHLH) transcription factors (Calleja et al., 2002). Their expression in imaginal disks is in turn regulated by different patterning genes, such as Iroquois, Pannier and Wg, which define the localisation of the proneural cluster (Simpson, 2007). One cell of the proneural cluster will express the highest level of proneural genes and will subsequently become the SOP. The selection is based on Notch-mediated lateral inhibition (Simpson, 1990). Proneural proteins together with other bHLH transcription factors (e.g. Daughterless (Murre et al., 1989)) activate specific genetic programmes required for SOP fate (Reeves and Posakony, 2005).

Once the SOP cell is selected, it will divide asymmetrically in the plane of the epithelium and along the tissue axis into two daughter cells of different fate: pIIa and

pIIb (Figure 1.6C) (Roegiers et al., 2001b, Hartenstein and Posakony, 1989). The pIIa cell will undergo another asymmetric division in the plane of the epithelium, giving rise to the hair and socket cells (Figure 1.6). The pIIb cell is of neural fate and will asymmetrically divide along the apical-basal axis (like neuroblasts) to give rise to the glial cell (with undergoes apoptosis) and the pIIIb cell which itself divides asymmetrically into the neuron and the sheath cell (Figure 1.6A, B) (Hartenstein and Posakony, 1989, Gho et al., 1999). The different cell fates in the SOP lineage are dependent on the presence of the cell fate determinants Numb and Neuralized, which are asymmetrically localised during each of the divisions and hence unequally distributed into the two daughter cells (Figure 1.6A, C) (Le Borgne and Schweisguth, 2003, Rhyu et al., 1994). The different cell fates of the daughter cells are achieved and maintained via Notch-mediated lateral inhibition, and the presence of Numb and Neuralized inhibits Notch signalling in the pIIb cell, whereas Notch signalling is active in the pIIa sibling (Le Borgne and Schweisguth, 2003, Rhyu et al., 1994, Schweisguth, 2015). The asymmetry of cell fate determinants within the SOP is dependent on different apical-basal polarity determinants, while PCP is required to orient the division.

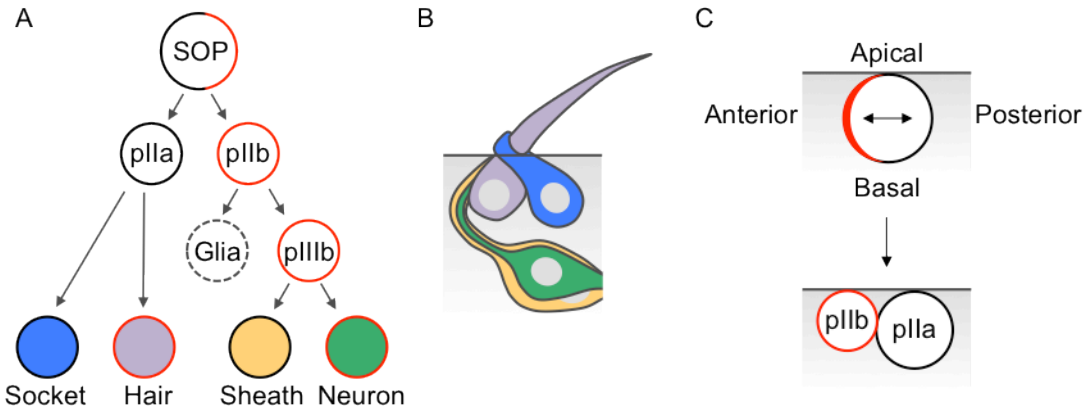

Figure 1.6 - Cell lineage of the SOP divisions and composition of mechanosensory bristles. (A) Cell fate lineage of the SOP cell. The SOP cell divides asymmetrically into pIIa and pIIb cell, by unequal distribution of cell fate determinants (red). Asymmetric division of pIIa gives rise to socket (blue) and hair cell (purple). The pIIb lineage consists of two follow up asymmetric divisions producing sheath cell (orange) and neuron (green). (B) Composition of an adult mechanosensory bristle (colours correspond to A). (C) The first asymmetric division of the SOP is within the plane of the epithelium and along the tissue axis (here anterior-posterior).

1.7.2 PCP and apical-basal polarity determinants are required to establish asymmetry in SOPs

The SOPs of the pupal notum divide along the anterior-posterior (A-P) axis and cell fate determinants localise to the anterior cortex, thus giving rise to an anterior pIIb and a posterior pIIa cell (Roegiers et al., 2001b, Le Borgne and Schweisguth, 2003). The core PCP proteins, the apical-basal polarity determinants Baz, aPKC, Par6, Dlg, as well as Pins (Partner of Inscuteable) and the G-protein subunit $G\alpha_i$ establish SOP asymmetry (Segalen and Bellaiche, 2009).

In epithelial cells, the Baz-aPKC-Par6 complex is found at the apical cell cortex, whereas Dlg localises basolaterally around the cortex (St Johnston and Ahringer, 2010). However, in premitotic SOP cells, the polarity determinants are found asymmetrically localised with the Baz-aPKC-Par6 complex at the posterior apical cortex, while Pins, Dlg and $G\alpha_i$ form a complex (Pins can bind to both Dlg and $G\alpha_i$) at the anterior lateral cortex (Schaefer et al., 2001, Bellaiche et al., 2001b). Consequently, in SOPs the localisation of the apical-basal polarity determinants needs to be remodelled and PCP provides the initial polarity cue, as epithelial cells and SOPs are planar polarised along the A-P axis with Fz/Dsh on the posterior side and Stbm/Pk on the anterior side (Bellaiche et al., 2004, Segalen et al., 2010). Fz/Dsh recruits the Baz-aPKC-Par6 complex to the posterior apical cortex (though it is unclear how), while Stbm/Pk promotes the anterior localisation of the Dlg-Pins-$G\alpha_i$ complex, probably by direct binding between Stbm and Dlg, at least at the apical-most part of the cortex (Figure 1.7) (Bellaiche et al., 2004).

The asymmetric localisation of the polarity determinants then directs the cell fate determinants to the anterior cortex upon entry of mitosis (Figure 1.7). As mentioned above, Neuralized localises asymmetrically, however the mechanism for its anterior positioning is unknown (Schweisguth, 2015). Numb is excluded from the posterior cortex through an inhibitory phosphorylation by aPKC (Wirtz-Peitz et al., 2008). In this study it was suggested that, in interphase, aPKC/Par6 is bound to Lgl, which inhibits the activity of aPKC. Upon entry into mitosis, the mitotic kinase Aurora A activates aPKC by phosphorylation of Par6, leading to Lgl phosphorylation by aPKC, removing Lgl from the complex. Lgl displacement allows binding of Baz, which then recruits Numb to aPKC/Par6. However, the inhibitory role of Lgl does not appear to be essential for

SOP ACD, because *lgl* mutants show a normal, albeit delayed, asymmetry of Baz and cell fate determinants (Langevin et al., 2005a, Wirtz-Peitz et al., 2008, Justice et al., 2003).

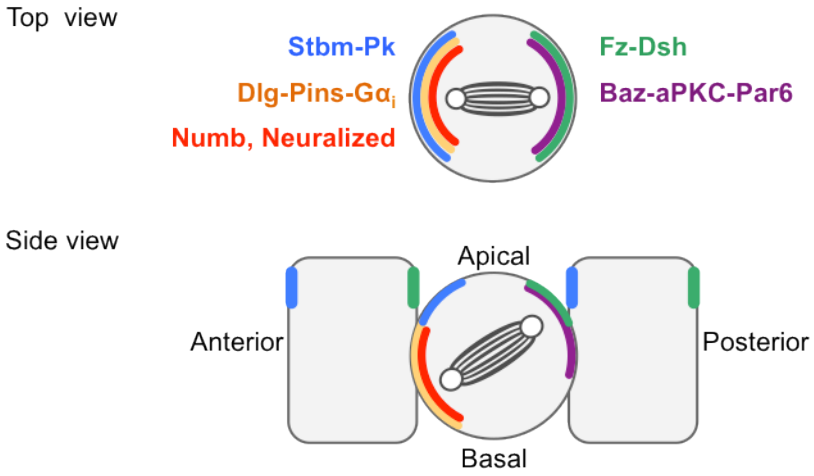

Figure 1.7 - Asymmetry in dividing SOP cells and spindle orientation.
The PCP components are planar polarised along the anterior-posterior axis and promote the planar localisation of polarity determinants (side view). Fz/Dsh position the Baz-aPKC-Par6 complex at the anterior cell cortex, whereas Stbm/Pk promote the localisation of the Dlg-Pins-$G\alpha_i$ complex at the posterior side. Both polarity determinant complexes direct the localisation of cell fate determinants to the posterior cell cortex. Fz/Dsh align the spindle along the anterior-posterior axis due to direct interactions of Dsh with Mud/NuMA (top view) and Pins with Mud/NuMA (side view), ensuring in-plane divisions.

None of the core PCP proteins are essential for the asymmetric localisation of the polarity determinants in mitosis and therefore for the asymmetric localisation of cell fate determinants. In PCP mutants, the polarity complexes still localise opposite each other (albeit uncoupled from the A-P axis), due to the so-called mitotic rescue, most likely mediated by Pins (Bellaiche et al., 2004, Bellaiche et al., 2001b). Interestingly, in contrast, at interphase the PCP components are essential for the asymmetric localisation of the Baz-aPKC-Par6 complex. Moreover, the polarity seems independent of the Dlg-Pins-$G\alpha_i$ complex, thus suggesting that the initial polarity is indeed provided by PCP

(Besson et al., 2015). It is unclear how Fz/Dsh promote the posterior apical enrichment of Baz-aPKC-Par6, though mammalian Dvl has been shown to associate with aPKC (Zhang et al., 2007). In epithelial cells, Baz and aPKC/Par6 localisation only partially overlaps, due to phosphorylation of Baz by aPKC and competition between Baz and Crb for aPKC/Par6 binding. In SOP cells, which remain connected to the neighbouring epithelial cells, a special mechanism must operate which allows the strong Fz/Dsh dependent apical enrichment of Baz-aPKC-Par6 complexes at interphase. It is not known whether the differential phosphorylations of Baz (by aPKC or Par1) are important for its localisation in SOPs.

1.7.3 Spindle orientation in ACD

As mentioned before, SOPs in the pupal notum divide along the A-P axis and in the plane of the epithelium (Figure 1.6C and Figure 1.7). Strikingly, unlike in symmetric divisions of epithelial cells, Fz and Dsh are required to localise the spindle along the A-P axis. In *fz* or *dsh* mutants ACD of SOPs exhibit a randomised division angle (Gomes et al., 2009, Bellaiche et al., 2001a, Bellaiche et al., 2004), whereas SOPs mutant for *baz* or *pins* divide along the A-P axis (Bellaiche et al., 2001b). Indeed, Dsh binds via its DEP domain to the C-terminus of Mushroom body defective (Mud, the homologue of mammalian Nuclear Mitotic Apparatus, NuMA), which in turn orients the spindle along the A-P axis via binding to the dynein complex (Segalen et al., 2010). As Fz and Dsh localise to the apical posterior cortex, this would result in an out-of-plane spindle orientation along the apical-basal axis. The anterior localised Pins, which can also bind to Mud-Dynein (Bowman et al., 2006), is thought to oppose this effect by positioning the spindle more towards the plane of the epithelium (Figure 1.7) (Segalen et al., 2010).

Interestingly, PCP proteins are neither required for spindle orientation nor cell fate determinant asymmetry in the subsequent ACDs of the pIIa and pIIb cells, whereas Baz is essential (Roegiers et al., 2001a, Roegiers et al., 2001b). Moreover, the pIIb and pIIIb divisions resemble neuroblast asymmetric divisions along the apical-basal axis, where the Baz-aPKC-Par6 complex localises together with Inscuteable (not expressed in SOPs or pIIa) apically and positions cell fate determinants basally (e.g. Miranda, Prospero, Numb) (Roegiers et al., 2001a, Roegiers et al., 2001b). In neuroblasts Inscuteable recruits Pins and $G\alpha_i$ to the apical cortex, which, together with Mud-NuMA, align the

spindle along the apical-basal axis (Bowman et al., 2006, Mapelli and Gonzalez, 2012). It is not clear which factors (except for Baz) are required for the pIIa ACD, but it seems neither Fz/PCP nor Inscuteable are involved, suggesting a different, as yet unknown mechanism (Roegiers et al., 2001a, Roegiers et al., 2001b).

1.8 An introduction to *Saccharomyces cerevisiae*

The second part of my thesis uses *Saccharomyces cerevisiae*, also known as budding yeast, as a model organism. The yeast genome was the first eukaryotic genome to be fully sequenced in 1996 and although yeast is a fungus, about 31% of the proteins have clearly identifiable human homologues (Botstein et al., 1997). Yeast cells can either be haploid or diploid. Haploid cells undergo mitosis in asymmetric cell divisions (budding) and two haploid cells of different mating type (*MAT*a and *MAT*α) can form diploid cells. Diploid cells can either mitotically divide, or under nitrogen limiting conditions undergo meiosis to form four haploid spores. Genetic manipulation in yeast is very effective, due to its high homologous recombination efficiency and the fact that cells can be easily transformed. This allows besides ectopic expression of plasmids, also the stable and exact integration of foreign DNA sequences into the genome. Moreover, genes can therefore easily be deleted or tagged using PCR-based methods and site-specific mutations introduced (see Material and Methods). The tool-kits to manipulate the yeast genome are well established and collections of tagged genes are available, making yeast an ideal organism to work with.

1.9 Ubiquitin and ubiquitin-binding domains

1.9.1 Ubiquitylation of proteins

Ubiquitylation is an important post-translational modification, within which the minute 8 kDa ubiquitin is conjugated to a lysine residue on the modified protein. Three different enzymes are involved in this process - namely, an ubiquitin-activating enzyme (E1), an ubiquitin-conjugating enzyme (E2) and an ubiquitin ligase (E3) (Figure 1.1A) (Finley et al., 2012). Firstly, the E1 activates ubiquitin by forming a thioester bond with the glycine residue of ubiquitin, under ATP consumption. Activated ubiquitin is then

transferred onto the E2, forming another thioester bond. Lastly, the E3s help in the final step of covalently binding the C-terminus of ubiquitin to the ε-amino group of a lysine residue on the target protein. This leads to the monoubiquitylation of a protein. However, there are a number of different ubiquitin signals, as one protein can be monoubiquitylated several times and repeated conjugation of another ubiquitin molecule to a lysine residue on an already-bound ubiquitin results in the formation of polyubiquitin chains (Figure 1.1B) (reviewed in (Ikeda and Dikic, 2008, Behrends and Harper, 2011). Ubiquitin has seven lysine residues and, for all of them polyubiquitin chains have been described (lysine 6, 11, 27, 29, 33, 48, or 63), as well as linear ubiquitin chains via linkage of the N-terminal methionine. Furthermore, ubiquitylation is a reversible modification as deubiquitylation enzymes (DUBs) have the capacity to remove ubiquitin signals, by catalysing the hydrolysis of the isopeptide bond between ubiquitin and the target (Finley et al., 2012).

The different ubiquitin signals are then specifically recognised by ubiquitin receptor proteins, which can be ubiquitin-binding adaptors for targeting to the proteasome or other effector proteins unrelated to proteolysis. Consequently, ubiquitin signalling can be found in a vastly wide-ranging number of different cellular processes for example, endocytosis, DNA repair, cell cycle control, apoptosis, stress response, transcription regulation and of course ubiquitin-mediated proteolysis to name but a few (reviewed in (Grabbe et al., 2011, Hammond-Martel et al., 2012, Chen and Sun, 2009, Broemer and Meier, 2009, Hochstrasser, 1996)). The degradation of proteins via the 26S proteasome requires the action of multiple ubiquitin receptors, as well as DUBs (Finley et al., 2012). The proteasome consists of two components, the 20S core particle (CR) and the 19S regulatory particle (RP). The CR provides the proteolytic activity, whereas the RP contains the ubiquitin receptors Rpn10 and Rpn13 to recognise ubiquitylated substrates and DUBs to recycle ubiquitin. Ubiquitylated proteins are transported to the RP by shuttling ubiquitin receptors Rad23, Ddi1 and Dsk1 (Finley et al., 2012).

Mass spectrometry analysis of the human and yeast proteome has revealed over 10,000 potential ubiquitylation sites for 4,273 human proteins and 870 sites for 438 yeast proteins (Wagner et al., 2011, Starita et al., 2012). This presents us with the possibility of revealing yet unknown functions of ubiquitin signalling.

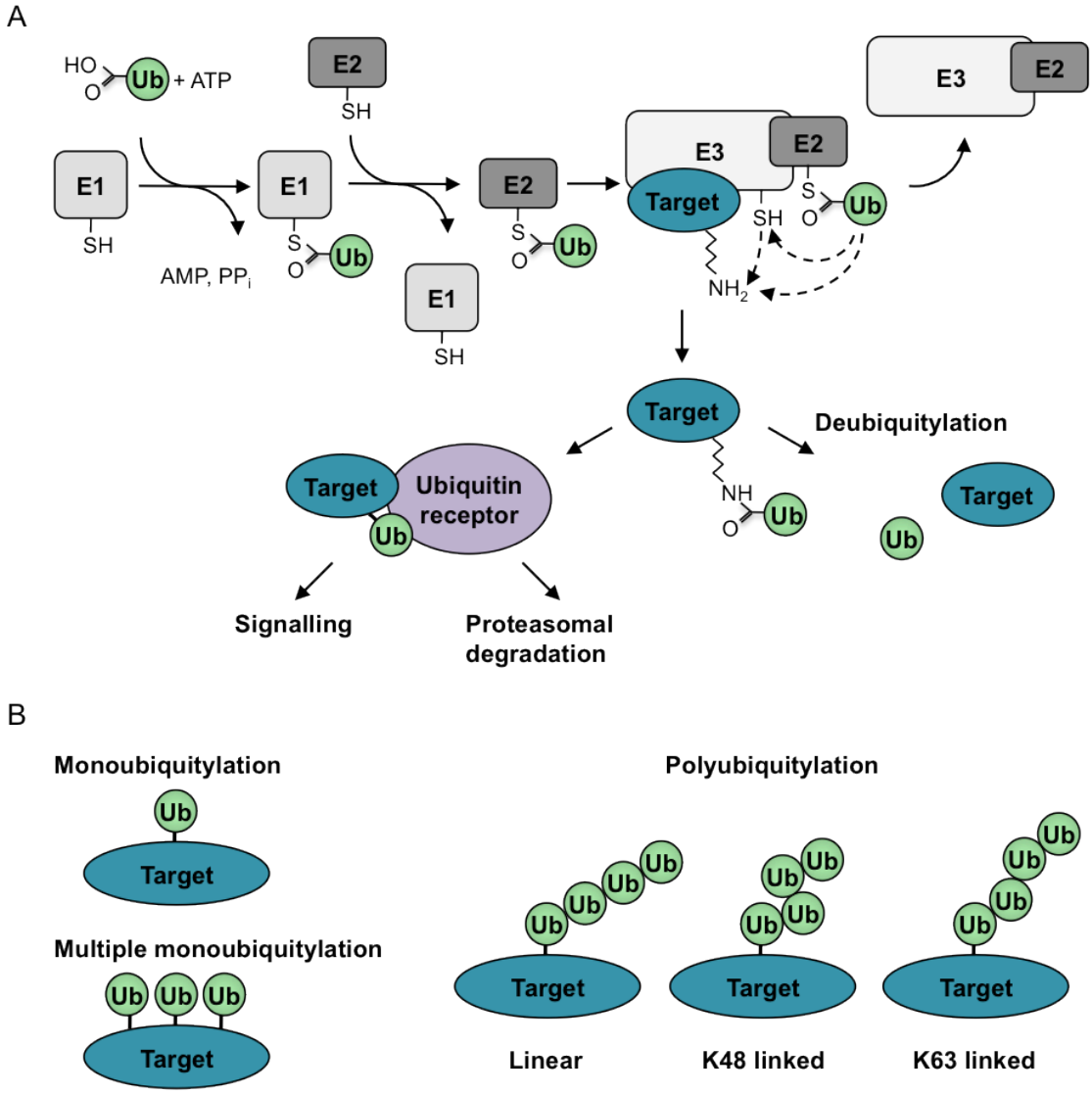

Figure 1.8 - Model of the ubiquitylation cascade and downstream processes, as well as different ubiquitin signals.

(A) The ubiquitylation cascade involves the three different enzymes E1, E2 and E3, which conjugate ubiquitin to the lysine residue of a target protein. Ubiquitin can be removed by deubiquitylation mediated by DUBs. (B) Examples for the different ubiquitylation signals. The cascade can lead to monoubiquitylation, multiple monoubiquitylation or polyubiquitylation of target proteins. Linear, lysine 48 and lysine 63 linked chains are shown as examples for polyubiquitylation.

1.9.2 Ubiquitin conjugating factors

In yeast there is just one ubiquitin-activating enzyme E1 - Uba1, which is consequently absolutely essential (McGrath et al., 1991). Conversely, there are 11 different ubiquitin-conjugating enzymes E2 and strikingly over 50 different E3 ubiquitin ligases (Hicke et al., 2005). E2s can cooperate with several different E3s, which recognise the substrate and thus provide the substrate specificity. For example, the E2 Rad6 (Ubc2) can function together with the E3 Ubr2 to ubiquitylate Rpn4 (transcription factor of proteasomal genes), which leads to its degradation (Wang et al., 2004) or with the E3 Rad18 to ubiquitylate PCNA, important for the DNA damage tolerance pathway (Hoege et al., 2002). Moreover, Rad6 works together with the E3 Ubr1 in the N-end rule pathway, in which substrates with destabilised N-terminal residues are specifically recognised by Ubr1 and subsequent ubiquitylation targets them for proteasomal degradation (Sriram et al., 2011).

Ubiquitin ligases are classified according to their domain into HECT (homologous to the E6-AP carboxyl terminus) domain and RING (really interesting new gene) domain E3s. While HECT domain E3s form a thioester with ubiquitin before transferring it to the target protein, RING domain E3s do not and instead facilitate the ubiquitylation by positioning target and E2 in close proximity (Figure 1.1A) (Finley et al., 2012). RING domain E3s can either bind to the target protein themselves (e.g. Rad18) or associate with subunits that specify the substrate specificity, as seen for example for SCF complexes or the multi-subunit APC/C (Anaphase promoting complex/cyclosome) complexes (Deshaies and Joazeiro, 2009).

1.9.3 Ubiquitin-binding domains

The various ubiquitin signals on modified proteins as well as free ubiquitin are recognised by ubiquitin-binding proteins (also known as ubiquitin receptors). These contain ubiquitin-binding domains (UBD) over which the interaction with ubiquitin takes place. Interaction with the target protein itself increases the specificity of recognition. To date, about 20 different UBDs have been described (see Figure 1.9 for examples, reviewed in (Husnjak and Dikic, 2012, Hurley et al., 2006, Dikic et al., 2009)). They have been classified according to their structure, e.g. α-helical UBDs, zinc

finger (ZnF) and plekstrin homology domain. Besides their structural variation, ubiquitin-binding domains also differ, even within one group of UBDs, with regards to their affinity for ubiquitin, the interaction surface on ubiquitin and - perhaps most importantly - their specificity for certain ubiquitin linkages. Therefore, the following section aims to highlight the complexity of ubiquitin recognition by ubiquitin-binding domains using a series of examples.

In order to determine the affinity of UBDs for ubiquitin (in form of the dissociation constant K_D) several biophysical methods, such as isothermal titration calorimetry (ITC), surface plasmon resonance (SPR) experiments, NMR and also electrospray ionisation-mass spectrometry (ESI-MS), can be used. The affinity for ubiquitin ranges between 1 μM and 1 mM for different UBDs (Hicke et al., 2005). The α-helical UIM (ubiquitin-interacting motif) domain, for example, of the human Eps15 protein binds to monoubiquitin relatively weakly with 900 μM, while the UIM-1 domain of Vps27 has been shown to have a higher affinity with 250 μM (Fisher et al., 2003). In addition to the interaction between the UBD and ubiquitin, ubiquitin receptors interact in most cases with the ubiquitylation target itself. The combination of two weak affinities facilitates the high specificity for the modified target, as too high affinities for ubiquitin binding would lead to unspecific interactions. The affinity variation among different UBDs can, in some cases, be explained by the fact that many ubiquitin receptors contain more than one UBD and sometimes even different kinds of UBDs. Many of the UBDs interact with ubiquitin via the hydrophobic patch (formed by isoleucine 44, valine 70, leucine 8) on ubiquitin. Some UBDs, however, bind to a completely different region on ubiquitin. The human protein Rabex-5 contains besides an α-helical MIU (motif interacting with ubiquitin), the structurally different zinc-finger domain (ZnF A20). Both of them have been shown to interact with ubiquitin (Lee et al., 2006, Penengo et al., 2006). The crystal structure of Rabex-5 and ubiquitin demonstrates that the MIU domain interacts with the isoleucine 44 hydrophobic patch on ubiquitin with a K_D of ~ 28 μM, while the ZnF A20 domain binds to a different region on ubiquitin centred around aspartate 58 and with a higher affinity (~ 12 μM) (Penengo et al., 2006) (Figure 1.9B). The presence of both domains increases the affinity to about 6 μM.

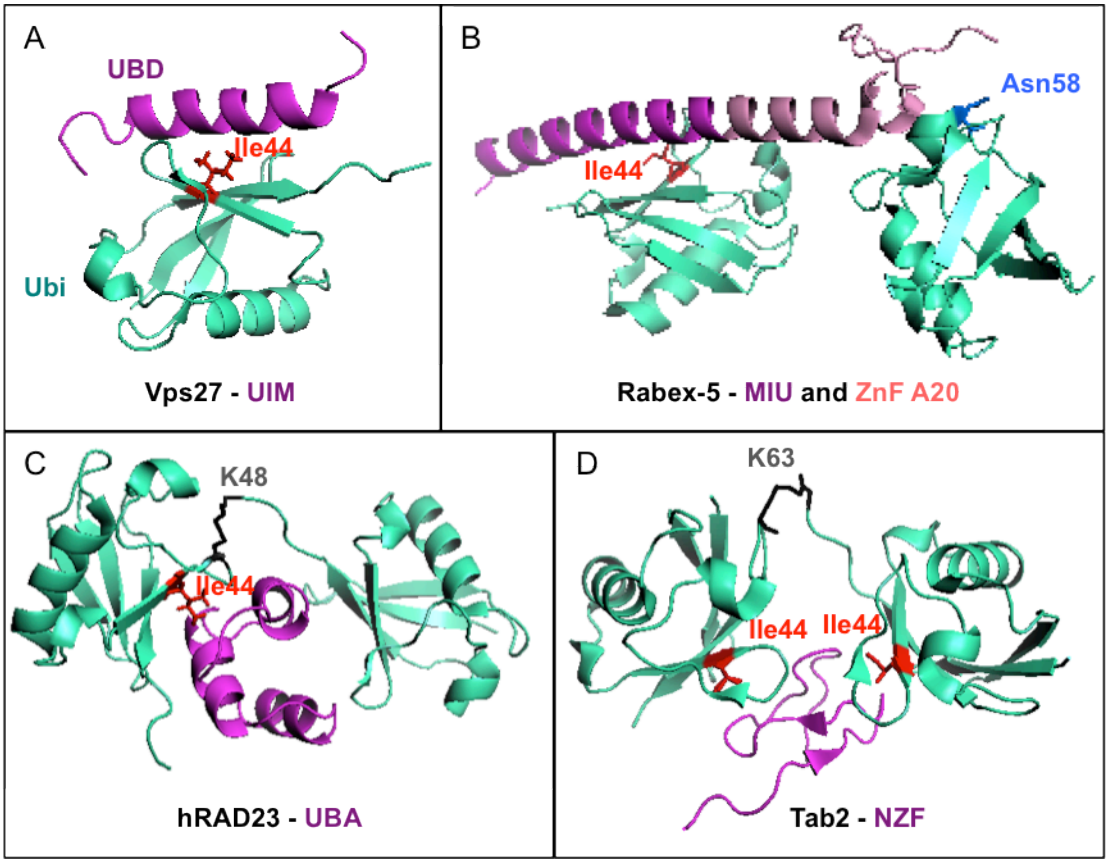

Figure 1.9 - Modes of ubiquitin binding by different ubiquitin-binding domains.
(A) Crystal structure of the UIM domain of Vps27 and monoubiquitin (PDB access code: 1Q0W). The UIM domain contacts ubiquitin via its hydrophobic patch, centred around Ile44 (red). (B) Crystal structure of the MIU and ZnF A20 domain of Rabex-5 and ubiquitin (PDB access code: 2FIF). While the MIU domain binds to the hydrophobic patch of ubiquitin, the ZnF20 A20 domain contacts a different region (around aspartate 58, in blue) of ubiquitin. (C) Crystal structure of the UBA domain of human RAD23A and lysine 48-linked diubiquitin (PDB access code: 1ZO6). The UBA domain binds specifically to lysine 48-linked ubiquitin chains. (D) Crystal structure of the NZF domain of Tab2 and lysine 63-linked diubiquitin (PDB access code: 2WWZ). The UBA domain binds specifically to lysine 63-linked ubiquitin chains.

Remarkably, ubiquitin receptors can distinguish between different ubiquitin signals and possess, in some cases, a high affinity for a certain ubiquitin signal. In a recent study the affinities of different UBDs to various ubiquitin linkages were compared using ESI-MS (Sokratous et al., 2012). While the previously described MIU domain of Rabex-5 had no certain linkage specificity (interacts with monoubiquitin), the three-α-helical UBA (ubiquitin-associated) domain of human RAD23A (Figure 1.9C) was

highly specific for lysine 48-linked polyubiquitin chains, when compared to the other linkages (lysine 11, 27 or 63) or monoubiquitin. Crystal structures of the UBD with ubiquitin help us understand how high affinities for certain linkages can be explained. For instance, the zinc finger containing NZF (Npl4 associated zinc finger) domain of the human protein Tab2 has a preference for binding to lysine 63-linked polyubiquitin chains. Crystallisation of Tab2 with lysine 63-linked diubiquitin revealed that there are two interaction sites within the NZF domain (Figure 1.9D) (Kulathu et al., 2009). In this context, the two ubiquitins contact one interface each, while monoubiquitin and linear chains are sterically not able to bind both interfaces.

Recognition of ubiquitin signals by UBDs is, as seen in the examples above, a very complex procedure that can be achieved in various ways. Crystal structures of ubiquitin-binding proteins and ubiquitin, as well as the characterisation of the interaction between them help in understanding how individual UBDs of certain proteins function. The kinetochore protein Spc25 has previously been revealed as a novel ubiquitin-binding protein in *S. cerevisiae* (Shengkai Zhao, unpublished result). The ubiquitin-binding domain was so far not identified and sequence comparison with known UBDs showed no similarity, indicating that Spc25 has an as yet unknown strategy of binding ubiquitin.

1.10 The yeast kinetochore

The kinetochore is a multi-protein complex that connects the plus-ends of microtubules to the centromeres and governs chromosome segregation in both meiosis and mitosis. In yeast, solely one kinetochore binds to each point centromere of 125 bp (comprised of DNA-elements CDI, CDII, CDIII), however, in vertebrates it is rather more complicated as one kinetochore complex attaches up to 20 microtubules to regional centromeres, which can be several mega bp long (Westermann et al., 2007). The many proteins, more than 60 in yeast (over 100 in mammalians), that build the kinetochore are mainly organised in subcomplexes - Cbf3, Ctf19, Ndc80, Mtw1, Spc105, Ipl1 and Dam1 complex (Figure 1.10A). According to their position within the kinetochore, they have been classified as inner (centromere binding), central (linking the inner to the outer kinetochore) or outer kinetochore (binding to the plus-ends of the microtubule) proteins

(reviewed in (Cheeseman et al., 2002, Westermann et al., 2007)). A variety of different approaches, such as loss-of-function studies, interaction studies, co-purifications, subcellular localisation and structural analysis, have contributed in dissecting the organisation of the kinetochore.

Inner kinetochore components are the Cbf3 complex (Cep3, Ctf13, Ndc10 and Skp1), which binds directly to the CDIII element of the centromere (Espelin et al., 1997) and the H3 histone variant Cse4, which is part of the nucleosome exclusively at centromeres (Furuyama and Biggins, 2007). Mif2 is another inner kinetochore protein and requires both, Cbf3 and Cse4 for centromere attachment. In addition, Mif2 associates with the Mtw1 (Mtw1, Dsn1, Nsl1, Nnf1) complex, thus acting as a link between inner and central components (Westermann et al., 2003). Central components are besides the Mtw1 complex, the Spc105 complex (Spc105, YDR532), the Ndc80 complex (Ndc80, Nuf2, Spc24, Spc25) and the Ctf19 complex (COMA complex and several other proteins) (Joglekar et al., 2009, Westermann et al., 2007). The Mtw1, Spc105 and Ndc80 subcomplexes are closely interacting with each other and form the KMN (Knl1/ Mis12/Ndc80) network (see 1.10.1). Lastly, the Ipl1 complex and the *S. cerevisiae* specific Dam1 complex as well as Stu2 are positioned at the microtubules and are grouped as outer kinetochore components (Westermann et al., 2007). The kinase Ipl1 (yeast homologue of Aurora B) of the Ipl1 complex regulates correct kinetochore-microtubule attachment by phosphorylation (see 1.10.2) (Pinsky et al., 2006b). The Dam1 complex is crucial for the chromosome segregation, as it moves with the depolymerising microtubules towards the spindle poles and thus provides the necessary pulling force (Westermann et al., 2006).

1.10.1 The Ndc80 complex and the KMN network

The Ndc80 complex, which is crucial for the chromosome segregation, belongs to the central kinetochore and connects microtubules and inner kinetochore proteins. The conserved four-protein complex consists of the Ndc80-Nsl1 heterodimer and the Spc25-Spc24 heterodimer and all four proteins are required for proper chromosome segregation (Janke et al., 2001, Wigge and Kilmartin, 2001, Wei et al., 2005a). Spc25 and Spc24 have C-terminal globular domains, and N-terminal coiled-coil regions, while Ndc80 (yeast homologue of human Hec1) and Nuf2 have N-terminal globular domains

with the coiled-coil regions located at the C-terminus (Figure 1.10D) (reviewed in (Tooley and Stukenberg, 2011)). The two heterodimers bind to each other, via the coiled-coil regions, producing the dumbbell-shaped Ndc80 complex. Regarding the overall structural organisation, the Ndc80 complex consists of two globular domains (formed by the globular domains of either Spc24 and Spc25 or Ndc80 and Nuf2) separated by a long coiled-coil region. This was first revealed by rotary shadowing electron microscopy (EM) (Wei et al., 2005a). The structure of Ndc80 complex was later confirmed in another study with the crystal structure of a "bonsai" version of the human Ndc80 complex, in which large proportions of the coiled-coil regions of all four proteins were removed (as they might have been too flexible) and Spc25 was fused to Ndc80 and Spc24 to Nuf2 (see Figure 1.10D) (Ciferri et al., 2008). The comparison of the human complex to the crystal structure of the globular domains of yeast Spc25 and Spc24 show how highly conserved the structures are from yeast to humans (Figure 1.10C) (Wei et al., 2006).

Figure 1.10B illustrates the interactions of the Ndc80 complex. The Ndc80 complex binds to the microtubule interface directly via the Ndc80-Nuf2 heterodimer (Wei et al., 2005a). Dam1, of the 10-protein Dam1 complex, interacts with the Ndc80 complex and was shown to be required for the binding of Ndc80 to the microtubules *in vitro* (Lampert et al., 2010, Tien et al., 2010). Phosphorylation of the N-terminus of *C. elegans* Ndc80 by Aurora B kinase inhibits binding to the microtubules *in vitro* and in mammalian cell culture (Cheeseman et al., 2006, DeLuca et al., 2006). However, a more recent study has shown that phosphorylation of Ndc80 by Ipl1, is not essential for intact chromosome segregation in yeast *in vivo* (Akiyoshi et al., 2009).

The Ndc80 complex is a member of the KMN network, which includes, besides the Ndc80 complex, the Mtw1 complex (also MIND or MIS12 complex) and the Spc105 complex (also Knl1 complex) (Nekrasov et al., 2003, Cheeseman et al., 2006, Petrovic et al., 2010). The Mtw1 complex consists of the four proteins Mtw1, Nnf1, Dsn1 and Nsl1, in which Mtw1 and Nnf1, as well as Dsn1 and Nsl1 form stable heterodimers (Maskell et al., 2010). Thus far, the following interactions were reported for the KMN network: Ndc80 interacts, via the globular domain of the Spc25-Spc24 dimer, with the Mtw1 complex, as seen in Figure 1.10B (Maskell et al., 2010, Hornung et al., 2010).

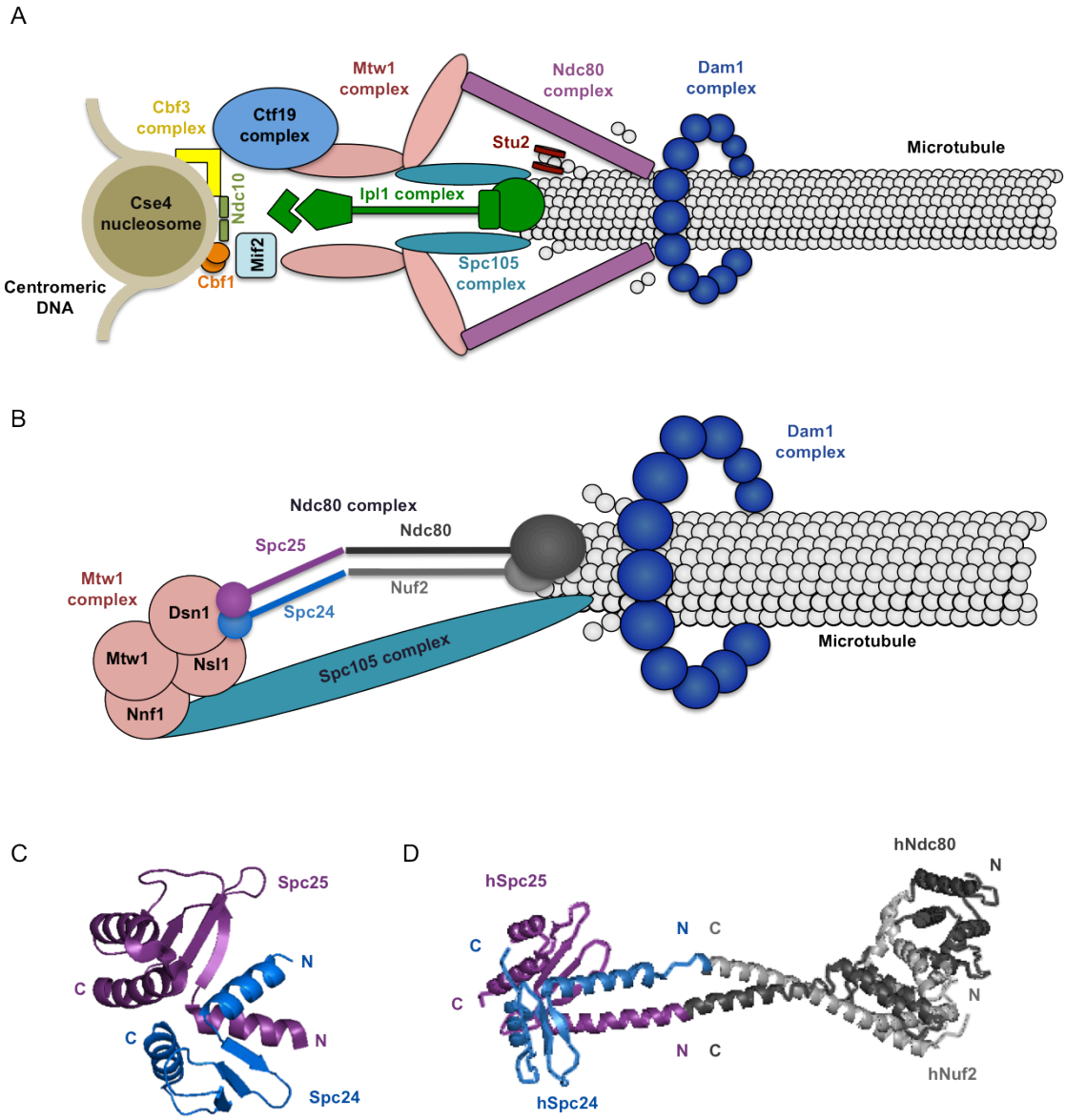

Figure 1.10 - Organisation of the yeast kinetochore and of the Ndc80 complex.

(A) Model of the architecture of the yeast kinetochore. The main complexes of the kinetochore are highlighted in different colours (figure adapted from (Westermann et al., 2007)). (B) Model of the interactions of the Ndc80 complex. The Ndc80 complex interacts via the Ndc80-Nuf2 heterodimer with the microtubules directly and binds to the Mtw1 complex via the Spc25-Spc24 heterodimer. (C) Structure of the globular domains of yeast Spc25 and Spc24 (PDB access code: 2FV4)(Wei et al., 2006). (D) Structure of the bonsai version of the human Ndc80 complex (PDB access code: 2VE7). In this "bonsai" version a large proportion of the coiled-coil region of the human Ndc80 complex was removed, Spc25 (118-224) was fused to Ndc80 (80-286) and Spc24 (122-197) to Nuf2 (1-169) in order to gain the crystal structure (Ciferri et al., 2008).

Most interestingly, *in vitro* interaction studies have shown that the interaction of the full Ndc80 complex with the Mtw1 complex was stronger than interaction with the Spc25-Spc24 dimer, indicating that the entire Ndc80 complex is required for increased binding and also that the Dsn1-Nsl1 heterodimer alone is not sufficient for binding to the Ndc80 complex (Hornung et al., 2010). A further study with human proteins has revealed that the interaction takes place between Spc24 and the C-terminus of Nsl1 and that Knl1 (yeast Spc105) also binds to the Mtw1 complex via Nsl1 (Petrovic et al., 2010). In addition, Spc105 (human Knl1) binds the Mtw1 complex in yeast and humans via its C-terminus, while the N-terminus interacts with the microtubules (Cheeseman et al., 2006, Kiyomitsu et al., 2007, Maskell et al., 2010). Nonetheless a more detailed insight into the interactions within the KMN network is still to be discovered.

The Mtw1 complex has the important role of connecting the Ndc80 complex to the inner kinetochore (via binding to Mif2). In addition, the Ndc80 complex is attached to the inner kinetochore by direct binding to the recently identified centromere associated Cnn1 complex (Cnn1 and Wip1) (Schleiffer et al., 2012, Malvezzi et al., 2013). The association of Spc24/Spc25 with Cnn1 (CENP-T) is dependent on its phosphorylation status and Cnn1 competes with the Mtw1 complex for binding to Spc24/Spc25 (Malvezzi et al., 2013).

1.10.2 Post-translational modifications of kinetochore components

Post-translational modifications of kinetochore components play a crucial role to control the correct chromosome segregation. I will use a few examples to illustrate the importance. Ipl1 (Aurora B) phosphorylates several of the kinetochore components, for example Dam1, Ndc80 and Dsn1. Ipl1-mediated phosphorylation of Ndc80 and Dam1 has supposedly inhibitory functions for their microtubule attachment (Cheeseman et al., 2006, DeLuca et al., 2006, Gestaut et al., 2008), while Dsn1 phosphorylation is important for proper assembly of the kinetochore (Akiyoshi et al., 2013a). As a counterbalance PP1 phosphatases can oppose the activity of Ipl1 (Pinsky et al., 2006a, Francisco et al., 1994). Ipl1 activates (most likely by causing microtubule-kinetochore detachment) the spindle checkpoint, which stalls the cell cycle until kinetochores are properly attached to the microtubules (Pinsky et al., 2006b, Biggins, 2013). In addition, the spindle checkpoint can be activated by phosphorylation of Spc105 by Mps1 (while

PP1 counteracts), which leads to the recruitment of spindle checkpoint proteins to the kinetochore (Biggins, 2013, London et al., 2012). Besides regulation of kinetochore components by phosphorylation/dephosphorylation, several kinetochore components have been shown to be modified by SUMOylation and ubiquitylation. For example, the modification of Ndc10 with small ubiquitin-like modifier (SUMO) is required for its localisation at the spindle (Montpetit et al., 2006). Conversely, SUMOylation of the mammalian inner kinetochore component CENP-I leads to its degradation (Mukhopadhyay et al., 2010).

1.10.3 The ubiquitin system at the kinetochore

To date, there have been a few reports about ubiquitin signalling at the kinetochore, with most of them being associated with ubiquitin-mediated degradation. One instance is the ubiquitin-mediated degradation of Cse4. Cse4 is a histone variant of H3, which can is only found at centromeric nucleosomes (see Figure 1.10A). The exclusive location of Cse4 at the centromere was demonstrated to be achieved by ubiquitin-mediated degradation of Cse4, with Psh1 as the E3 ubiquitin ligase in yeast (Hewawasam et al., 2010, Ranjitkar et al., 2010). The proposed mechanism behind this is that the Scm3-bound Cse4 is incorporated into the centromeric nucleosome and protected from ubiquitylation and degradation, while free Cse4 is degraded, which consequently prevents the mislocation into euchromatin (Hewawasam and Gerton, 2011). Furthermore, CID, the Cse4 homolog in *Drosophila melanogaster* was also shown to be regulated via proteolysis, indicating a conserved mechanism for the localisation of Cse4 (Moreno-Moreno et al., 2006). Another case where ubiquitin-mediated degradation plays a role within the kinetochore comes within the regulation of the spindle-checkpoint by means of controlling the Aurora B kinase (Aurora2) in humans (Biggins et al., 1999, Honda et al., 2000). In addition, a recent study revealed that Dsn1 levels were regulated by ubiquitin-mediated degradation through the E3 ubiquitin ligase Ubr2 (Akiyoshi et al., 2013b). Ubr2 binding to Dsn1 requires the Ubr2 adaptor Mub1. Interestingly, Ubr2/Mub1 targeted prominently a mutated version of Dsn1, which cannot be phosphorylated by Ipl1 (Aurora B), suggesting that the function of Ubr2/Mub1 might be to ensure the correct integrity of the kinetochore (Akiyoshi et

al., 2013b). These few chosen examples illustrate, that ubiquitin-mediated degradation of kinetochore components plays an important role for kinetochore function.

However, the first report of ubiquitin signalling independent from ubiquitin-mediated proteolysis was the regulation of Dam1 methylation (by Set1) via ubiquitylation of the histone H2BK123, as missing ubiquitylation prevented the methylation of Dam1 (Latham et al., 2011). However, it is not clear how the regulation between these two post-translational modifications is carried out.

1.10.4 Yeast Spc25 is a novel ubiquitin-binding protein

In his PhD thesis Shengkai Zhao introduced Spc25 as a novel ubiquitin-binding protein (Zhao, 2010). Zhao characterised the ubiquitin-binding properties of Spc25 using different biochemical, as well as physical, approaches and furthermore, tried to reveal the function of the ubiquitin binding of Spc25 within the kinetochore. The following section will focus on his main findings.

Spc25 was discovered as a novel ubiquitin-binding protein in a yeast two-hybrid screen. The 221 amino acid long Spc25 consists of a N-terminal coiled-coil region (1-106), a flexible linker (107-132) and a C-terminal globular domain (133-221), as illustrated in Figure 1.11. Bioinformatical analysis showed that the protein sequence of Spc25 shares no similarity to any previously described ubiquitin-binding domains. Hence, Spc25 binds to ubiquitin via an unknown UBD. In order to reveal the minimum region of Spc25 required for the interaction with ubiquitin, yeast two-hybrid experiments with different truncations of Spc25 were performed. This elucidated that Spc25 binds to ubiquitin via its flexible linker region as well as the C-terminal globular domain. Furthermore, mutation of a number of moderately conserved hydrophobic residues within Spc25 showed that the leucine 109 residue within the linker region is critical to the ubiquitin binding, as the interaction with ubiquitin was abolished in the two-hybrid system. As with many ubiquitin-binding proteins, Spc25 interacts with the hydrophobic patch on ubiquitin (formed by leucine 8, isoleucine 44 and valine 70), which was shown by *in vitro* pull-down experiments. The dissociation constant, K_D, for the interaction between monoubiquitin and a truncated version of the Spc25-Spc24 complex was determined with the surface plasmon resonance based BIACORE system. The result showed that ubiquitin binds to the Spc25-Spc24 complex with a high affinity

(14.2 μM). As previously mentioned, Spc25 forms a heterodimer with Spc24 within the Ndc80 complex and crystallisation has revealed that the globular domains of both Spc25 and Spc24 are combined in a single globular domain within the Ndc80 complex in both yeast (Figure 1.10C) and humans (Figure 1.10D) (Wei et al., 2006, Ciferri et al., 2008). Although Spc24 was negative for interaction with ubiquitin in the yeast two-hybrid system, it cannot be ruled out that Spc24 contributes to the ubiquitin binding.

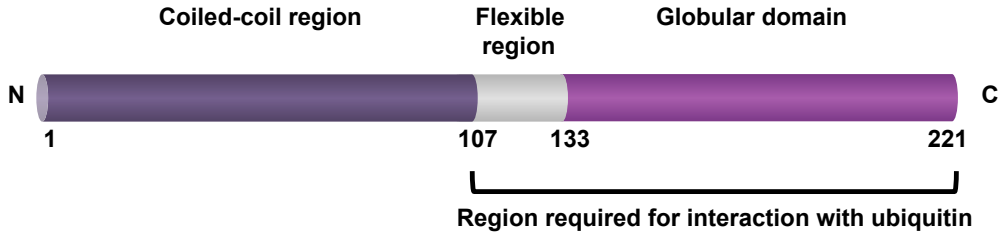

Figure 1.11 - Model of the organization of yeast Spc25.
Spc25 contains a N-terminal coiled-coil region, a flexible linker and a C-terminal globular domain. Interaction with ubiquitin requires the flexible region as well as the globular domain.

Several approaches were then taken to uncover the biological function of the ubiquitin binding of Spc25. First of all, cells harbouring the ubiquitin-binding deficient L109A mutation of *SPC25* were analysed regarding their phenotype. However, no obvious defects were found, as *spc25 (L109A)* mutants were viable and possessed normal growth compared to wild type cells. As it is known that Spc25 is required for chromosome segregation and a normal spindle checkpoint (Janke et al., 2001), it was then tested whether ubiquitin binding was involved in these functions. Treatment with the microtubule toxin benomyl did not affect the spindle checkpoint in *spc25 (L109A)* mutants. Furthermore, the mutation did not result in an increased plasmid loss in a plasmid loss assay, indicating that chromosome segregation is not grossly disturbed. In conclusion, the L109A mutation of Spc25 did not interfere with chromosome segregation, or with the spindle checkpoint. However, it is possible that the L109A

mutation of Spc25 does not completely suppress its binding to ubiquitin and therefore did not bring about an obvious phenotype.

Despite the fact that the ubiquitin-binding deficiency of Spc25 did not noticeably affect cells *in vivo*, this study did reveal useful synthetic interactions of the *spc25 (L109A)* mutant. Firstly, it was discovered that *spc25 (L109A)* cells exhibited a growth defect when combined with GFP-tagged Mcm21 of the Ctf19 complex. Furthermore, *spc25 (L109A)* increased the temperature sensitivities for mutant alleles of *DSN1* (*dsn1-7* and *dsn1-8* respectively). These synthetic interactions have given rise to the theory that the ubiquitin binding of Spc25 might be required for maintaining the stability of the kinetochore complex.

Ubiquitin signalling is based on specific interactions of the ubiquitin-binding protein with both ubiquitin and the ubiquitylated target itself. In order to find the ubiquitylated target that interacts with the ubiquitin-binding domain of Spc25, 16 kinetochore proteins were screened for *in vivo* ubiquitylation. Tested candidates were kinetochore proteins in close proximity to Spc25 as well as spindle checkpoint proteins (MAD proteins). A large proportion of the proteins were found to be modified. Most strikingly, from the synthetic interaction experiments, Dsn1 and Mcm21 were both ubiquitylated.

1.11 Aims of this thesis

Members of the N-terminal RASSF family are associated with several cancers and are considered to be tumour suppressors and oncogenes (1.2.2). Little is known about the function of two of its members - RASSF9 and RASSF10 - which have homologues in *Drosophila*. This thesis aims to characterise the developmental function of RASSF9 and RASSF10 using *Drosophila* as a model organism. A recent study from our collaborator Matthias Gstaiger revealed, that all members of the human N-terminal RASSFs are found in an interaction network with PP1 catalytic subunits and ASPP family members (Figure 1.3) (Hauri et al., 2013). In humans ASPP can act as a regulatory subunit of PP1 (1.3.3) and *Drosophila* RASSF8 and ASPP function together (Langton et al., 2009). Taken together, this led us to speculate that N-terminal RASSFs in general might act as specificity subunits for ASPP/PP1 phosphatase complexes. RASSF9 and RASSF10 were also found to interact with several members of the planar cell polarity pathway, as

well as the apical-basal polarity determinant Par3/Baz, suggesting a connection to cell polarity (Hauri et al., 2013). This thesis aims to establish whether *Drosophila* RASSF9 and RASSF10 could potentially act as specificity subunits for ASPP/PP1 phosphatase complexes, and especially whether and how these two N-terminal RASSFs are connected to planar cell polarity.

In Chapter 3 of this thesis, I will describe the interaction network for *Drosophila* RASSF9 and RASSF10 and the *in vivo* approaches taken to address their developmental function. Based on these findings Chapter 4 investigates the specific role of RASSF10 in the polarity establishment of SOPs of the peripheral nervous system.

In Chapter 5, I will present the separate project I worked on in Helle Ulrich's lab (London Research Institute, Clare Hall laboratories). The kinetochore component Spc25 was previously characterised as a ubiquitin-binding protein, raising the possibility that this ubiquitin-binding property might be important for the stability of the kinetochore (1.10.4). Therefore this project aimed at further elucidating the function of the ubiquitin system around Spc25 at the kinetochore.

Chapter 2 Materials and Methods

2.1 General bacterial methods

2.1.1 Transformation of chemically competent cells

For bacterial transformations, chemically competent *E. coli* were first thawed on ice. The plasmid was added and the cells carefully mixed. This was followed by incubation on ice for 30 minutes and heat shock for 50 seconds at 42 °C. Cells transformed with plasmids possessing an ampicillin resistance could be plated directly onto LB plates containing ampicillin. For plasmids encoding for a kanamycin or zeocin resistance, LB medium without antibiotics was added to the cells first. Cells were then recovered for one hour at 37 °C before being plated on LB plates with the appropriate antibiotic. Double transformations, with both ampicillin and kanamycin resistance, were treated the same as those with kanamycin alone and grown on LB plates containing both antibiotics. For a full list of bacterial strains used in this thesis, please refer to the Appendix, Table 7.2.

2.1.2 Isolation of plasmid DNA

To isolate plasmids from transformed bacterial cells, single colonies were picked with the tip of a pipette and inoculated in 3 mL fresh LB medium containing the appropriate antibiotic(s). Cultures were grown overnight at 37 °C and plasmids were purified with the QIAprep Spin Miniprep Kit (Qiagen, Tapon lab) or the GeneJET Plasmid Miniprep Kit (Thermo scientific, Ulrich lab) according to the manufacturer's instructions. Alternatively, for larger quantities of plasmid DNA, midipreps were performed using the GenElute HP plasmid midi kit (Sigma-Aldrich). The concentration of plasmids was then determined by measuring the absorbance at 260 nm with a NanoDrop ND-1000 Spectrophotometer (Thermo Scientific), using 1.5 µL of plasmid solution.

2.2 General molecular biology methods

2.2.1 PCR - Polymerase chain reaction

Standard PCRs were performed with the Taq PCR Master Mix (Qiagen) in 20 µL reactions, containing 0.8 µL of both sense and antisense primer (10 µM) and 1 µL DNA. The standard PCR programme was:

1. 94 °C, 3 minutes
2. 94 °C, 30 seconds
3. X °C, 30 seconds (X= specific annealing temperature for primer pair)
4. 72 °C, 1 min/1000 bp Repeat steps 2-4, 34 times
5. 72 °C, 10 minutes

Inserts for cloning (restriction and Gateway) were amplified with the PWO Master Mix (Roche) in 20 µL reactions containing 0.8 µL of both sense and antisense primer (10 µM) and 1 µL DNA, using the following programme:

1. 94 °C, 2 minutes
2. 94 °C, 30 seconds
3. X °C, 30 seconds
4. 72 °C, 1 min/1000 bp Repeat steps 2-4, 34 times
5. 72 °C, 5 minutes

Alternatively, the Phusion high fidelity DNA polymerase (Finnzymes) was used for insert amplification. A 50 µL reaction was set up with 10 µL 5x Phusion HF buffer, 0.4 µL dNTPs (25 mM), 2.5 µL of both sense and antisense primer (10 µM), 0.5 µL Phusion polymerase and 1 µL DNA. Cycling conditions were as follows:

1. 98 °C, 30 seconds
2. 98 °C, 10 seconds
3. X °C, 30 seconds
4. 72 °C, 30 seconds/1000 bp Repeat steps 2-4, 29 times
5. 72 °C, 10 minutes

In Helle Ulrich's lab, standard PCRs were performed using the Simple Red Taq DNA polymerase (Thermo Scientific). A 25 µL reaction contained 2.5 µL 10x buffer with 15 mM $MgCl_2$, 0.8 µL dNTPs (25 mM), 1.25 µL of both sense and antisense primer (10 µM), 0.25 µL Simple Red polymerase and 1 µL DNA. The standard PCR programme was:

1. 94 °C, 2 minutes
2. 94 °C, 20 seconds
3. X °C, 30 seconds
4. 72 °C, 1 min/1000 bp Repeat steps 2-4, 34 times
5. 72 °C, 5 minutes

For all PCRs a Peltier Thermal Cycler (MJ Research) was used. After the amplification, the PCR products were checked for their sizes by gel electrophoresis.

2.2.2 Agarose gel electrophoresis

Agarose gels generally contained 1% agarose (Life Technologies), which was dissolved in 0.5x TAE buffer (1x TAE in Helle Ulrich's lab). To visualize the DNA, ethidium bromide (Sigma-Aldrich) or SYBR® Safe (1:10000, Life Technologies) was mixed into the melted agarose. Ready gels were placed in a TAE (0.5x or 1x) buffer-filled, horizontal gel electrophoresis unit (Advance Scientific or Jencons). DNA samples were mixed with 6x or 10x DNA loading buffer and loaded onto the gel. As a sizing standard, the 1 kbp plus ladder (Life Technologies), was run with the samples. Electrophoresis was carried out at 100-135 V for 20 to 45 minutes (depending on the size of the product). The DNA was visualised with the UV transilluminator BioDoc-It™ system (UVP) and gel pictures were printed using a video graphic printer (SONY). To cut out bands of gels, DNA was visualised with a transilluminator (Syngene).

2.2.3 Restriction enzyme based cloning

For cloning, plasmids and PCR products were digested with the appropriate restriction enzymes (New England Biolabs) according to the manufacturer's recommendations. A typical 50 µL digestion contained 1 µg of DNA, 5 µL 10x buffer (supplied with the

restriction enzymes), 10-20 units of enzyme and, if required, 100 µg/mL BSA. It was then incubated for 1-2 hours at 37 °C. Before the ligation, vector and insert were purified using either the QIAEX II Gel Extraction Kit (Qiagen) or the GeneJET Gel Extraction Kit (Thermo Scientific, Ulrich lab) following the manufacturer's instructions. For the ligation of the digested, purified insert and vector, the Quick-Stick ligase from BIOLINE was used. Vector and insert were mixed in a 1:3 ratio, and 0.5 µL Quick-Stick ligase and 2.5 µL 4x QS buffer were added (final volume of 10 µL). The reaction was mixed thoroughly by pipetting and incubated for 10 minutes at room temperature to allow ligation. The ligation was either used directly in the transformation of *E. coli* (2.1.1) or stored at −20 °C until further usage.

2.2.4 Gateway system

Expression plasmids for S2 cells, and plasmids for injection of fly embryos, were all made with the Gateway system (Life Technologies), which does not require restriction enzymes and is based on the site-specific recombination system of bacteriophage λ. The BP clonase mix facilitates the site-specific recombination between attB and attP sequences, creating attL and attR sites. The LR clonase mix promotes the recombination of attL and attR sites (creating attB and attP sites). Inserts flanked by attB sites are, in the first step, recombined into a pDONR vector (BP clonase reaction). Inserts in the pDONR vectors are flanked by attL sequences and can then be recombined into a destination vector with attR sites (LR clonase reaction).

Inserts were amplified from existing plasmids, or cDNA from DGRC with appropriate primers to allow recombination into pDONR Zeo vectors. Forward primers were designed the following way: They contained the attB1 sequence, the Kozak sequence, the start codon and the insert-specific sequence. The reverse primers were comprised of the insert specific sequence, in case of N-terminal tags, followed by a stop codon and the attB2 sequence. Inserts were PCR amplified, analysed by agarose gel electrophoresis and purified with the QIAEX II Gel Extraction Kit (Qiagen). For the 5 µL BP-reaction, 100 ng of insert and 100 ng of pDONR Zeo were incubated with 1 µL BP clonase mix for approximately 2-3 hours, at room temperature. The BP-reaction was then transformed in *E. coli* (2.1.1) (Zeocin selection) and plasmids checked by PCR and sequencing. Inserts from pDONR vectors were then transferred into destination vectors

in the LR reaction. The 5 µL reaction contained 1 µL of the destination vector, 0.5 µL of pDONR and 1 µL LR clonase mix. After 2-3 hours incubation at room temperature, bacteria were transformed with the reaction and plasmids were then checked by PCR and sequencing. Destination vectors for expression of tagged proteins in S2 cells all derived from the *Drosophila* Gateway™ Vector Collection.

2.2.5 Sequencing

Sequencing was carried out in order check the correctness of plasmids and the presence of mutations. 150 ng of plasmid DNA or x ng of PCR products (x = length of PCR product times 0.02, purified beforehand by Gel Extraction) were used for the sequencing reaction. Furthermore, the 20 µL reaction contained 7.5 µL Big Dye sequencing buffer (Applied Biosystems), 0.5 µL Big Dye terminator v3.1 ready mix and 3.2 pmol primer. The reaction took place in a Peltier Thermal Cycler (MJ Research) with a PCR programme approved by Applied Biosystems. Sequence products were cleaned with the DyeEx 2.0 Spin Kit (Qiagen). The Sequencing was then carried out by the CRUK sequence facility. Sequences were analysed using the SeqMan programme (DNAStar Inc.).

2.3 General protein methods

2.3.1 SDS-PAGE

For the SDS-PAGE, ready-made NuPAGE 4-12% Bis-Tris gradient gels (Life Technologies) were used. These were run with the manufacturer's NuPAGE MOPS SDS Running Buffer in the XCell SureLock® mini-cell (Life Technologies). Samples were mixed using the NuPAGE sample buffer with reducing agent as recommended by Life Technologies and heated for 10 minutes at 75 °C. As a sizing standard, the Amersham Rainbow Marker (GE Healthcare) was loaded next to the protein samples and all gels were run at 150 to 200 V for between 1 and 2 hours, depending on the molecular weight of the proteins. After SDS-PAGE, gels were analysed by Coomassie staining or western blot.

In Helle Ulrich's lab, besides the ready-made gels, Tris-glycine gels were prepared according to Lämmli (Laemmli, 1970) using the Mini-PROTEAN system (Bio-Rad). The stacking gel had an acrylamide concentration of 5%, while the acrylamide concentration for the separating gel ranged from 7.5% to 15%, according to the size of the protein of interest. Samples were mixed with 5x Lämmli loading buffer (5 minutes at 95 °C) or HU buffer for yeast protein extracts (10 minutes at 65 °C) and PageRuler^{TM} pre-stained protein ladder (Fermentas) was used as a sizing standard.

2.3.2 Coomassie staining

To detect proteins directly on the gel, protein gels were stained with the Coomassie-based solution, Simple Blue Safe Stain (Life Technologies) or InstantBlue (Expedeon). Gels were incubated in the solution, with gentle agitation for up to an hour, then washed extensively with water to remove excess dye. For documentation, gels with visualised proteins were scanned.

2.3.3 Western Blots

Western blot analysis was performed to detect proteins using specific antibodies after SDS-PAGE. Proteins were transferred from the polyacrylamide gels onto a PVDF membrane (Amersham Hybond from GE Healthcare) using the Mini-PROTEAN Tetra cell system (Bio-Rad). Firstly, the membrane was activated with methanol and then rinsed with water. Western blotting filter paper (Thermo Scientific) and sponges were soaked in cold transfer buffer. The set-up in the cassette from the positive anode to the negative cathode was as follows: 1 sponge, 1 filter paper, the activated membrane, the gel, 1 filter paper and 1 sponge. The transfer took place at 4 °C for 1.5 hours at 100 V. Afterwards, the membrane was blocked in PBS with 5% milk for 1 hour, at room temperature. Incubation - with the appropriate dilution of the primary antibody in PBS with 5% milk - was either carried out overnight at 4 °C, or for 2 hours at room temperature. To remove any unbound antibody, the membranes were washed three times for 10 minutes in TBS-T and then incubated with the appropriate dilution of secondary antibody in PBS with 5% milk for 1 hour at room temperature. As before, three 10-minute wash steps in TBS-T removed the excess antibody. Antibodies, and

their dilutions used for western blot analysis, can be found in Table 2.3. The HRP-labelled proteins were detected with the Pierce ECL 2 Western Blotting Substrate (Thermo Scientific). The membrane was then exposed for different time periods to films (Amersham Hyperfilm ECL from GE Healthcare), which were developed in an automatic X-ray film processor JP-33 (Jungwon Precision Industry).

If the membrane was to be used for detection with another antibody, it was first washed for 20 minutes in TBS-T and then stripped by incubation for 10 minutes in 0.5 M NaOH. The membrane was subsequently washed for 20 minutes in TBS-T and could then be used for antibody detection, as before.

In Helle Ulrich's lab, a semi-dry blotting apparatus (Roth) with a three-buffer system was used for transfers. The set-up in the semi-dry blotting apparatus from the positive anode to the negative cathode was as follows: 1 layer of filter paper (Whatman® gel blotting paper from Fisher Scientific) soaked in western blot buffer I, 1 layer of filter paper in western blot buffer II, the activated membrane (Immobilon®-P transfer membrane from Millipore), the gel and finally two layers of filter paper in western blot buffer III. The transfer was carried out at 60 mA for 1 hour (1.5 hours for proteins over 70 kDa). Blocking (PBS-T with 5% milk), antibody incubations (in PBS-T with 5% milk) and washing (in PBS-T) steps were carried out as previously described. The different antibodies and working dilutions are listed in Table 2.5. In the Ulrich lab, the HRP-catalysed Western Lightning Plus system (PerkinElmer) and CL-XPosure™ films (Thermo Scientific) were used for developing.

2.3.4 Determining protein concentrations

In order to determine the protein concentration, the Bio-Rad protein assay was used. This colorimetric assay is based on Bradford. The Bio-Rad protein assay dye reagent was diluted 1:5 in water and 1 mL was added to a cuvette, mixed with 1 µL protein sample and the absorbance at 595 nm was measured in a Biophotometer (Eppendorf). Protein concentrations in mg/mL were calculated by comparing the measured absorbance at 595 nm to a BSA standard curve, which was created beforehand with defined concentrations of BSA.

In some cases, the concentration of purified proteins was determined with the absorbance at 280 nm, using the NanoDrop ND-1000 Spectrophotometer (Thermo

scientific). The molar extinction coefficient (ε) of proteins was estimated with the following formula:

ε = (no. of tyrosines) x 1490 + (no. of tryptophans) x 5500 + (no. of cysteines) x 125

Concentrations of the proteins could then be calculated with Lambert-Beer's law (with a path length of 1):

Concentration = Absorbance at 280 nm / (ε x path length)

2.4 Methods for *Drosophila melanogaster* experiments

2.4.1 Fly husbandry and stock maintenance

Flies were kept in plastic vials, or bottles, with fly food and at 25 °C.

Balancer chromosomes have two characteristics - recessive lethal or sterile mutations and multiple inversion breakpoints - which allow the maintenance of genetic loci, e.g. mutations or inserted transgenes. This keeps the occurrence of meiotic recombination between the balancer and the genetic locus of interest to a minimum. Therefore, stable stocks of mutants or transgenes can be kept (and are not lost over generations), as viable progeny and will either be heterozygous for the balancer and the mutation/transgene, or homozygous for the mutation/transgene if viable. Additionally, balancer chromosomes have visible markers allowing them to be recognised and making them essential for cross schemes. Balancer chromosomes used for the X (homozygous sterile) chromosome were FM6 and FM7c (B^1 as visible marker), for the second chromosome, CyO (Cy^1 as visible marker) and, for the third chromosome, TM6b ($Antp^{Hu}$ and Tb^1 as visible marker), TM3 Sb (Sb^1 as visible marker) and TM3 Ser (Ser^1 as visible marker).

2.4.2 Gene disruption by imprecise P-element excision

Mutant flies for *RASSF9* were generated by imprecise P-element excision. The following cross scheme was used:

F0: ♂♂ *Δ2-3; Dr/TM3* × ♀♀ *P(EP)G18523/TM6b*

F1: ♂♂ *Δ2-3/+; P(EP)G18523/TM3* × ♀♀ *TM3/TM6b*

F2: single ♂ *P(EP)G18523/TM3* or *TM6b* × ♀♀ *TM3/TM6b*

Flies harbouring the P-element *P(EP)G18523* in the first intron of the *RASSF9* locus were crossed to a *Δ2-3* transposase-expressing stock (F0). As P-elements are transposons, they can be mobilised by their cognate transposase. Both the P-element and the transposase carried the *mini-white* gene as a visible marker, causing red eyes. Males heterozygous for the P-element and the transposase were crossed to a balancer stock (F1). In these males (and their germline) the transposase was active, mobilising the P-element. Therefore, males of the next generation (F2) with white eyes had the P-element excised and were negative for the transposase, as the *mini-white* marker was absent. Single white-eyed males were crossed to a balancer stock and, after 3 days, genotyped by PCR for the presence of an imprecise excision, where part of the neighbouring sequences are deleted along with the transposon. DNA was extracted from single males with the DNeasy Blood and Tissue kit (Qiagen) (see 2.4.9). As part of the P-element could still be present, a long-range DNA polymerase, the LA Taq (Takara), was used for the screening. A 20 µL reaction contained 0.2 µL LA Taq, 2 µL 10X LA PCR Buffer II, 3.2 µL of dNTP (2.5 mM), 0.2 µL DMSO, 0.4 µL of each primer (10 µM) and the following programme was used:

1. 94 °C, 1 minute
2. 94 °C, 30 seconds
3. 54 °C, 30 seconds
4. 72 °C, 12 minutes Repeat steps 2-4, 34 times
5. 72 °C, 10 minutes

The progeny of males positive for a deletion in *RASSF9* were used to establish the stock.

2.4.3 Gene disruption using CRISPR/Cas9

RASSF10 mutant flies were made with the CRISPR/Cas9 system. This system is based on the bacterial CRISPR associated nuclease (Cas) that causes double strand breaks in specific genomic sites, which are complementary to a CRISPR RNA. CRISPR (clustered regularly interspaced short palindromic repeats) and Cas nucleases form an immune system in bacteria to protect the bacterial genome from the exogenous DNA of viruses or plasmids. The CRISPR/Cas9 system has been successfully modified for site-specific genome engineering (e.g. deletions or tagging of genes) in flies (Gratz et al.,

2013, Port et al., 2014). The CRISPR RNA was shortened to the minimum-required region for the direction and binding of Cas9 and is referred to as guide RNA (gRNA). gRNAs contain a 20-nucleotide region complementary (spacer) to the chosen cleavage site in the fly genome and a transactivating RNA for binding to Cas9 (already present in the expression plasmids). The only requirement for a potential target site of Cas9 is the presence of the 3 bp protospacer adjacent motif (PAM, NGG) at the 3' end of the cleavage site. Expression plasmids for the gRNA just have to be injected into transgenic flies expressing the Cas9 nuclease (various different lines are available) and the progeny can then be screened for desired modifications.

To generate deletion mutants of *RASSF10,* gRNA pairs - causing two double strand breaks and, therefore, potentially leading to deletions excising part of *RASSF10* - were used. Maxine Holder in the Tapon lab designed the oligonucleotides (see Table 2.8) for the gRNAs using the Perrimon lab's website (http://www.flyrnai.org/crispr/). The two gRNA pairs used for the injection, the sequence of the respective genomic target site and the respective oligonucleotides, are listed in Table 2.1. gRNA pair B should target Cas9 to cut in the intron before exon 2 (gRNA B1) and 260 bp into exon 4 (gRNA B2), potentially creating a deletion of 1546 bp. Cas9 directed by gRNA pair C should cut before exon 1 and 335 bp into exon 1, potentially causing a 822 bp deletion.

Table 2.1 - *RASSF10* gRNA pairs for injection in flies with genomic target site

	gRNA	**Target site 5' to 3' (PAM and cut site▼)**	**Oligonucleotides**
gRNA pair B	gRNA B1	CCTCTT▼AATCGATCTACATACTC	gRNA B1 fw and rv
	gRNA B2	CCAACT▼GTATAGGGGTACCGAAA	gRNA B2 fw and rv
gRNA pair C	gRNA C1	GGCCCACAGGGGCCGTG▼AAATGG Intron before exon 1	gRNA C1 fw and rv
	gRNA C2	CCTCTA▼TGGCGTTAATAGCACTG	gRNA C2 fw and rv

My colleague, Maxine Holder cloned the gRNA expression plasmids for the injection in flies, as follows: For the phosphorylation and annealing of the ordered oligonucleotides following reaction was set up: 6.5 µL water, 1 µL of both sense and

antisense oligo (100 µM) and 0.5 µL T4 PNK (New England Biolabs). The following programme was used for the thermo cycler:
37 °C, 30 minutes
95 °C, 5 minutes
Ramp down to 25 °C at 0.1 °C per second

The pCFD3-dU6:3gRNA plasmid (Simon Bullock) was digested with BbsI restriction enzyme (New England Biolabs) and the insert ligated. For the ligation, a 15 µL reaction contained: 50 ng of linearised plasmid, 1 µL annealed and phosphorylated oligonucleotides (diluted 1/200, 1.5 µL of 10X T4 DNA ligase buffer and 1 µL of T4 DNA ligase (New England Biolabs). After incubation for 30 minutes at room temperature, 3 µL of the ligation was used for the transformation of competent bacteria. Plasmids were confirmed for correctness by sequencing and sent, for embryo injections, to the Fly Facility (Department of Genetics) at the University of Cambridge. The gRNA expression plasmid pairs (250 ng/µL of each plasmid for pair B and pair C) were injected into embryos of a germ-line restricted nos-Cas9 line (*y*^{1}*, M(nos-Cas9.P)ZH-2A, w*). Surviving founders were crossed to a balancer stock (*y;;Dr/TM3)*.

As the activity of Cas9 is not uniform within the germ line, one founder produces progeny of which only a proportion will be positive for deletions (or cuts). Additionally, the cut sites (and therefore deletions) can differ between individuals. Hence, the following screening strategy was used to identify positive founders: a pool of the female progeny of the founders was genotyped for the presence of deletions. In parallel, the male progeny was crossed to a *RASSF10* deficiency line (*Df(3L)BSC575*/*TM6b*) to identify mutants by phenotype. Five of the female progeny of each founder were pooled and total DNA was extracted with fly DNA buffer (see 2.4.9). For the genotyping PCR 2 µL of DNA and the Taq PCR Master Mix (Qiagen) was used (see Table 2.8 for genotyping primers). 10 white-eyed (negative for Cas9) males of the progeny (2nd founder) from each positive founder were individually crossed to females of the deficiency line and, after 3 days, genotyped for deletions in *RASSF10*. Progeny heterozygous for the deficiency and the deletion mutant could then be checked for phenotypic changes. A single male of the progeny of several 2nd founders, heterozygous for a *RASSF10* deletion and the balancer *TM6b*, was then crossed to females of a

balancer stock (*w;;TM3/TM6b*) to establish stable lines balanced over *TM6b*. From these lines, DNA was extracted and the *RASSF10* locus sequenced to characterise the deletion.

To obtain a control stock with an identical genetic background, exactly the same crosses were made, starting with a non-injected male of the *nos-Cas9* line.

2.4.4 Recombination of genetic loci

The combination of genetic loci located on the same chromosome was achieved by meiotic recombination in females. Flies harbouring one or other of the two loci of interest were crossed. Virgin females of the next generation heterozygous for both loci, allowing meiotic crossover, were collected. The females (F1) were then crossed with males of a suitable balancer stock and the progeny (F2) screened for positive recombinants. The method of screening was dependent on the loci.

Screening for combinations of mutant alleles was done by genotyping. Single males were first crossed to females of a balancer stock. The DNA of males was extracted with fly DNA buffer after 3 days (see 2.4.9) and 2 µL of DNA were used for the genotyping PCRs with PWO Master Mix (Roche) or Taq PCR Master Mix (Qiagen). Genotyping primers are listed in Table 2.8. Progeny of males positive for both mutations were used to establish a stable stock. Recombination of three mutant alleles was achieved in two steps. First, double mutants were generated and then double mutants were combined to generate triple mutants and genotyped.

The recombination of an FRT chromosome with a mutant allele (see 2.4.7) was monitored depending on the FRT chromosome used. In the case of FRT chromosomes (FRT82B) with neomycin resistance, G418 food allowed pre-selection solely of progeny harbouring the FRT. G418- resistant males were crossed with a balancer stock and then genotyped for the presence of the mutation. For FRT chromosomes without neomycin resistance, males had to be screened by genotyping PCRs for the presence of both the mutant allele and the FRT.

Recombinants of *GAL4* drivers and UAS fluorophore-tagged transgenes were identified by the presence of fluorophore signal with the pE-300^{white} illumination system (CoolLED). The recombination of GAL4 drivers with UAS transgenes whose expression caused an obvious defect was detected by phenotype.

2.4.5 PhiC31 integrase-mediated transgenesis

To express GFP-tagged transgenes in flies, the PhiC31 integrase-mediated system was used. The bacteriophage-derived PhiC31 integrase facilitates the site specific and stable recombination between two sequences, the bacterial attachment site, attB, and phage attachment site, attP. Plasmids containing attB sites can therefore be integrated site specifically into attP sites inserted in the fly genome. Fly lines with different attP sites were made by P-element insertion, and injection of plasmids with attB site and transgene allows the insertion of the transgenes into the genome. The expression vectors used in this thesis - pKC26w_GW and pKC26_UAS_GW - also contain the *mini-white* gene as a visible marker, which allows the identification of positive transformants by the orange-red eye colour. pKC26w_GW (Yanxiang Zhou) contains the *ubiquitin* promoter, that allows ubiquitous expression of transgenes with an N-terminal GFP-tag. In this study, the pKC26_UAS_GW vector was made by replacing the *ubiquitin* promoter with UAS sequences. Hence, UAS-transgenes with an N-terminal GFP-tag can be inserted into the genome and their expression can then be controlled with Gal4 drivers (see 2.4.6). Plasmids were sent to BestGene Inc for injection in embryos and selection of positive transformants. Table 2.2 lists all the plasmids, genomic insertion sites and the genotype of the fly line used to make transgenic flies.

Table 2.2 - Plasmids, insertion sites and fly lines used for injections

Plasmid name	Plasmid backbone	Insertion site	Genotype
UAS-GFP-RASSF10 UAS-GFP-RASSF9	pKC26w_UAS_GW	2L 28E7	PBac(yellow[+]-attP-3B)VK00002
Ubi-GFP-RASSF10 Ubi-GFP-RASSF9 Ubi-GFP-RASSF8 Ubi-GFP	pKC26w_GW	2L 28E7	PBac(yellow[+]-attP-3B)VK00002
UAS-GFP-RASSF10 UAS-GFP-RASSF9	pKC26w_UAS_GW	3R 89E11	PBac(yellow[+]-attP-9A)VK00027

2.4.6 Gal4/UAS system

The Gal4/UAS system allows pattern-specific expression of transgenes in flies. It is based on a bipartite expression system in which the *S. cerevisiae* transcription factor

Gal4 binds to upstream activating sequences (UAS) from where it then activates gene expression. In flies, Gal4 driver lines enable Gal4 expression in the distinct pattern of a driver gene where a transposon encoding the Gal4 gene is inserted. The UAS sequence can be fused to transgenes of interest (tagged or native genes and RNAi constructs) and inserted into the fly genome. Crossing a Gal4 driver line to one that harbours the UAS-transgene will lead to transgene expression in the pattern of the Gal4-driver expression. In this study, the ubiquitously-driving *tubulin-Gal4* and *actin-Gal4*, the wing pouch driving *nubbin-Gal4* and *MS1096-Gal4,* the dorsal wing compartment driving *apterous-Gal4* and the sensory organ precursor specific *Neuralized-Gal4* lines were used for targeted expression of either transgenes (tagged or untagged) or RNAi lines for gene silencing.

2.4.7 The FRT/FLP system

Mutant clones in fly tissues were made with the FRT/FLP system. This system is based on the yeast FLP recombinase (FLPase) that mediates site-specific recombination between two FLPase recombination target (FRT) sites on homologous chromosomes. Transgenic flies were generated with FRT sites located close to the centromere for each chromosome arm. To generate mutant clones, the respective FRT chromosomes were recombined with the mutant allele of interest (2.4.4). These flies were then crossed to a stock harbouring the FLPase and the same FRT chromosome recombined with a constitutively expressed marker (e.g. *GFP*, *RFP* or *lacZ*). In larval tissue of the progeny where the FLPase was active, mitotic recombination between the two FRT sites occurred, giving rise to daughter cells homozygous for the mutant allele (negative for the marker), homozygous for the marker (twin spot) or heterozygous for mutant allele and marker. The activity of the FLPase is thereby restricted by its promoter. In this thesis, two different FLPases were used to generate mutant clones. Firstly, *UbxFLP* was used, in which the FLPase activity is limited to the wing imaginal disc (also leg and haltere) in early larval stages. Clones were also made with *hsFLP*, in which a heat-shock inducible promoter drives the FLPase activity. To induce the expression of FLPase, larvae were heat-shocked twice - 48 and 72 hours after egg laying - for 1 hour at 37 °C.

2.4.8 The FLPout system

The FLPout system is a combination of the FLP/FRT and the Gal4/UAS systems. It allows the clonal *Gal4* driven expression of transgenes. A line harbouring both *hsFLP* and the *UAS-GFP*-transgene was crossed with a line with a FLPout construct. The progeny was heat-shocked for 8 minutes at 37 °C, 96 hours after egg laying. The FLPout construct contained the ubiquitously active *actin* promoter separated from the Gal4 transcription factor by two FRT sequences flanking a transcriptional termination signal. In this state, *actin* driven *Gal4* expression is repressed. When heat-shocked, the FRT sites are recombined out in a small number of cells, removing the termination signal. In this way, *Gal4* activity is restricted to the mitotic clones, facilitating the expression of the UAS-transgenes.

2.4.9 Isolation of genomic DNA from fly tissue

Fly DNA was usually extracted from a single fly using the DNeasy Blood and Tissue kit (Qiagen). Flies were homogenised in 180 µL PBS with a pipette tip and DNA extraction carried out according to the manufacturer's protocol. DNA was eluted in 100 µL of the supplied elution buffer. The DNA was stored at 4 °C and, for PCRs, 1 µL of extracted DNA was used. Alternatively, for the genotyping (except for *RASSF9* P-element excision) a single fly was homogenised in 50 µL fly DNA buffer (with Proteinase K). The mixture was incubated for 30 minutes at 37 °C to allow digestion with Proteinase K, which was inactivated by a 2-minute incubation at 95 °C. 2 µL of this solution containing DNA was used for PCRs.

2.4.10 Isolation of RNA from fly tissue and RT-PCR

RNA from adult flies, embryos or pupae was extracted with the RNeasy Kit (Qiagen). Between 10 and 30 adult flies or embryos (collected from one apple juice plate and washed twice in PBS) were homogenised in 600 µL of RLT buffer, supplemented with β-mercaptoethanol (1 in 100) with a pellet pestle mixer (Sigma-Aldrich). RNA was extracted according to the manufacturer's protocol. RNA concentrations were determined by measuring the absorbance at 260 nm with the NanoDrop ND-1000

Spectrophotometer (Thermo Scientific). Before the RNA could be used for reverse transcription PCR (RT-PCR), DNA was removed from the preparation by DNase treatment. For the 10 µL reaction, 1 µL of 10x DNase buffer (Promega) and 1 µL of DNase (Promega) were incubated with 1 µg of RNA for 30 minutes at 37 °C. The digestion was stopped by adding 1 µL of DNase Stop Solution (Promega) and 10 minutes heat inactivation at 65 °C. DNase treated and untreated RNA was stored at −80 °C.

RT-PCR was carried out with the First Strand cDNA Synthesis Kit (Roche) according to the manufacturer's protocol, using 8.2 µL of the DNase-treated RNA and random primers. 2 µL of synthesised cDNA was used for PCR reactions with PWO (see 2.2.1).

2.5 Immunofluorescence and imaging

2.5.1 Dissection and staining protocols for different fly tissues

For dissection and staining of imaginal discs, L3 larvae or white prepupae were collected and dissected in cold PBS with sharp forceps (#5, Dumont). Larvae were halved and the anterior part turned inside out. The carcasses were fixed in 4% paraformaldehyde (PFA, Taab) in PBS for 20 minutes at room temperature. All incubation steps were carried out with mild agitation in a light protected chamber at room temperature (except primary antibody incubation). Samples were washed four times for 5 minutes in cold PBT and then permeabilised with PBT-0.3 for half an hour. After another 5-minute wash in PBT, blocking was performed in 10% normal goat serum (NGS, MP Biomedicals) for 1 hour. Primary antibody incubation in 10% NGS in PBT took place overnight at 4 °C and excess antibody was removed in five wash steps for 5 minutes in PBT. Secondary antibody incubation was for 1 hour in 10% NGS in PBT, followed by five 5-minute wash steps in PBT. Imaginal discs were dissected in PBS and mounted in Vectashield anti-fade mounting medium (with or without DAPI, Vector laboratories) on glass slides (Thermo Scientific) for imaging.

For pupal wing stainings, white prepupae were aged for 30 hours (30 hours APF). Pupae were then pulled out (from the anterior side) of the opened pupal cases and punctured to allow the fixative to enter. Fixation was carried out in 4% PFA in PBS at

4 °C overnight and protected from light. The next day pupal carcasses were rinsed with PBS. In PBT-0.3, pupal wings were carefully pulled out of the cuticle pocket. The following steps were then carried out at room temperature, slightly shaking in a light protected chamber: Wings were permeabilised for 40 minutes in PBT-0.3 and blocked with 0.15% BSA in PBT-0.3. Antibody incubations were in 0.15% BSA in PBT-0.3 (overnight at 4 °C for primary and 1 hour at room temperature for secondary antibodies). Wings were then washed with PBT-0.3, for 4x10 minutes after primary antibody incubation and for 3x20 minutes after secondary antibody. Pupal wings were mounted in Vectashield.

For pupal nota stainings, white prepupae were collected and aged for 15 hours (15 hours APF). Pupae were attached with the posterior side to a rubber pad with fine needles, covered in PBS and the pupal case removed. Pupal nota were carefully cut out with micro scissors and fixed for 20 minutes in 4% PFA in PBS. After rinsing the tissue three times with PBT, nota were permeabilised for one hour in PBT and then blocked for 1 hour in 10% NGS in PBT. Primary antibodies were added for 2 hours and nota were washed for 3x10 minutes with PBT. Secondary antibody incubation was for 1 hour in 10% NGS in PBT and nota were washed three times in PBT. All staining steps were performed, without shaking, at room temperature under exclusion of light. To allow straightening of the tissue, nota were incubated in PBS 50% glycerol overnight at 4 °C. Finally, nota were mounted in Vectashield with the apical side facing up.
All primary antibodies, fluorophore-labelled secondary antibodies, and their working dilutions used for immunofluorescence, are listed in Table 2.4.

2.5.2 Mounting of adult wings

For analysis of wing roundness and wing size, adult female flies were transferred into 70% ethanol. In isopropanol, wings were removed from the flies with forceps and placed onto a glass slide. Wings were mounted in Euparal (ALS) with a cover slip placed upon them. Samples were then dried at 65 °C overnight in an SM30 incubator from Grant Boekel.

2.5.3 Microscopy and imaging

Fluorophore-labelled samples prepared, as specified in 2.5.1, were imaged on an SP5 laser scanning confocal (Leica) with 20x or 40x objectives. Generally, Z-stacks were acquired in order to cover the entire apical signal with a Z-stack size of 0.5 µm. Images were then processed with ImageJ 1.46r and Photoshop CS5.1.

Images of adult wings (preparation see 2.5.2) were taken with an Axioplan2 microscope from Zeiss and a Leica camera.

Images of the notum and abdomen of adult flies (in 70% ethanol) were acquired with a Leica MZ7.5 dissection microscope and a Leica camera.

2.5.4 Preparation and live imaging of pupal nota

To image asymmetric cell divisions of sensory organ precursors in the pupal notum, pupae expressing fluorophore-tagged proteins were dissected at 15 hours APF. A single pupa was stuck (apical side facing up) onto a glass slide with double-sided tape. The pupal case was carefully removed from head and notum with forceps. Two stacks of 18x18 mm cover slides (each stack contained 4 slides glued together with nail polish) were positioned in front and behind the pupa, forming a chamber. A thin layer of Voltalef Oil 10S (VWR) was spread evenly onto a 20x50 cover slide. The cover slide was placed carefully - with the oil side facing the pupa - onto the stacks and pupa, and sealed with nail polish.

Live imaging was performed with an SP5 laser scanning confocal (Leica) with a 40x objective. Images (apical Z-stack, Z-stack size of 0.5 µm) were acquired for about 2 hours. For the Pon-GFP analysis, apical Z-projections contained 10 stacks and images were acquired every 51.62 seconds. Movies were processed and analysed with ImageJ 1.46r.

2.6 Analysis and quantifications

2.6.1 Quantification of wing size and roundness

To quantify wing roundness, mounted wings (see 2.5.2) were analysed as follows: The length of the wing was measured by drawing a line along the L3 vein from the proximal

to the distal and the width by drawing a line from the anterior to the posterior passing through the posterior cross-vein (Figure 3.17). Wing roundness was then calculated as the ratio of length to width.

As wing size is very sensitive to the supply of food (which, in turn, is dependent on the amount of larvae in one vial), flies of different genotypes had to develop under the same food conditions in density-controlled crosses. For density-controlled crosses, flies were kept for egg-laying on apple juice plates in cages overnight. The next day, 50 first instar larvae were carefully picked and transferred into a normal food vial. Wings of density-controlled adult flies were mounted and imaged, and the wing size determined with ImageJ 1.46r. Therefore an outline around the entire wing was drawn and the area measured.

2.6.2 Quantification of mechanoreceptor defects

Duplications of stout bristles of adult wings were quantified for 100 wings (the left and right wing for each of 50 flies, see Figure 4.2) of each genotype on a Leica dissection microscope. The same flies were also analysed for missing or additional thoracic macrochaetes (see Figure 4.3).

2.6.3 Analysis and quantification of SOP divisions

The Pon-GFP distribution from the mother SOP cell into daughter cells was measured in ImageJ 1.46r as follows: the Pon-GFP signal's Grey value was measured for both daughter cells (pII_{min} and pII_{max}) after the cells had fully divided (five time points after elongation onset). The Pon segregation was then calculated by dividing the smaller Grey value (intensity pII_{min}) by the bigger Grey value (intensity pII_{max}). In case of a Pon mis-segregation, pII_{min} and pII_{max} intensities will have similar values and the ratio will therefore be approaching 1.

The division angle relative to the anterior-posterior body axis (A-P-axis: 0°) was also measured for each division (4 time points after elongation onset) in ImageJ 1.46r and as illustrated in Figure 4.18. Clockwise divisions were given positive values (0 to 180 °), and counter clockwise divisions ascribed negative values (0 to -180 °).

The analysis for the polarity of the Pon crescent was carried out with ImageJ 1.46r. First, a freehand tool was used to draw a perfect outline of each SOP cell (line width 3 pixels) just before the start of division. This line was then straightened and a Plot Profile for the Pon-GFP signal was created (distance in microns over Grey value). The Grey values were then used to determine the polarity of the Pon crescent. We used a fast Fourier transformation to calculate the polarisation coefficient, using the following equation:

$$|P| = \sqrt{a^2 + b^2}$$

a and b being defined as:

$$a = \frac{1}{N}\sum_{k=1}^{N} I_k \cos\left(\frac{k2\pi}{N}\right)$$

$$b = \frac{1}{N}\sum_{k=1}^{N} I_k \sin\left(\frac{k2\pi}{N}\right)$$

N: Number of observations

$$I_k = \frac{\text{Grey value k}}{\text{Mean of Grey values}}$$

The normalisation to mean intensity was in order to control for different baseline signal intensities across the different video-micrographs. We are grateful to Xavier Tapon for providing a Python programme to help with the analysis.

2.6.4 Statistical analysis

Statistical analysis was performed with the Prism 6 software, using either an unpaired nonparametric t-test (Mann-Whitney test) or in case of multiple comparisons a one-way ANOVA (Bonferroni's correction multiple comparisons test) to test whether mean values differed significantly. In case of the bristle (margin and thoracic) analysis the distributions of bristle defect categories between different genotypes were tested for significant differences using the Fisher's exact test (Freeman-Halton extension) (Freeman and Halton, 1951) with the SPSS 21 software. The extended Fisher's exact test was used to calculate the P-values as the Chi square test was invalid for most of the

calculations, due to small numbers and the presence of 0 counts. In all figures error bars represent the mean ± the standard deviation.

2.7 S2 cell culture and protein methods

Drosophila S2 cells were maintained at 25 °C in 75 cm^2 flasks (Corning) containing 12 ml of S2 medium (Gibco). Once a week, cells were transferred into a flask (ratio 1:10) with fresh medium. To avoid contaminations, the handling of S2 cells took place in a safety cabinet (BioMAT2).

2.7.1 Transient transfection of S2 cells

To express tagged proteins in S2 cells, the cells were transiently transfected using the Effectene Transfection Reagent (Qiagen). First, $3x10^6$ cells (in 1.5 mL medium) were seeded in the well of a 6-well plate (Corning) and left to settle for approximately 30 minutes. In the meantime, plasmids (50-500 µg, depending on the expression level) were prepared for the transfection, according to the manufacturer's instructions. 180 µL EC buffer, 8 µL enhancer and 25 mL Effectene Transfection Reagent were used per transfection. Cells were then incubated for 48 hours before being lysed. All plasmids used for transfections are listed in Table 2.6 of section 2.14.1.

2.7.2 Isolation of total protein extracts from S2 cells

Transfected cells from 2.7.1 were collected from each well of the 6-well plates 48 hours after transfection. Cells were then harvested by centrifugation at 10000 rpm for 1 minute at 4 °C and washed in 1 mL ice-cold PBS. For the cell lysis, cell pellets were resuspended in 200 µL of freshly-prepared NP40 lysis buffer and then incubated for 10 minutes on ice. This was followed by centrifugation at 13200 rpm for 20 minutes at 4 °C. The protein extract with soluble proteins in the supernatant was then used either directly for western blot analysis, for co-IP experiments, or stored at −80 °C.

2.7.3 Co-immunoprecipitation

For co-immunoprecipitation (co-IP) experiments 80 µL of the cell lysates (prepared as described in 2.7.2) was added to 220 µL of NP40 lysis buffer containing 10 µL of Anti-FLAG M2 Affinity Gel (Sigma-Aldrich, in NP40 lysis buffer pre-equilibrated). The lysate-gel mix was then incubated under rotation for 1.5 hours at 4 °C to allow binding of FLAG-tagged proteins (and their binding partners) to the affinity gel. Beads were washed with NP40 lysis buffer for 4x5 minutes to remove unspecific binding. After the last wash, 10 µL of 4xNuPAGE sample buffer, 6 µL of Np40 lysis buffer and 4 µL 10xNuPAGE reducing agent were added to the dried beads, and samples were then denatured for 10 minutes at 75 °C. Input samples for co-IPs contained 5 µL of total lysate, 5 µL of 4xNuPAGE sample buffer, 2 µL of 10xNuPAGE reducing agent and 8 µL of NP40 lysis buffer. 20 µL of co-IP and input samples were then analysed via SDS-PAGE and western blot.

2.8 RASSF10 antibody generation

To generate an antibody against RASSF10, the following expression and purification strategy was used. A short fragment of ^{GST}RASSF10 (375-468) with an N-terminal GST-tag was expressed from pGEX-4-T1 (GE Healthcare) in the *E. coli* strain BL21 Codon^{2+}. A pre-culture was grown overnight at 37 °C in an LB medium containing ampicillin (100 µg/mL). The following day, the overnight culture was used to set up the main culture with a starting OD_{600} of 0.1 to 0.2 in LB with the respective antibiotics. The main culture was grown at 37 °C until an OD_{600} of 0.5 to 0.8 was reached. At this point, protein expression was induced by adding 0.5 mM IPTG and the culture then kept at 18 °C overnight. The cells were pelleted the next morning by centrifugation at 4000xg for 20 minutes. For the cell lysis, cells were resuspended in ice-cold GST lysis buffer and opened by sonication (SANYO sonifier) on ice using 4 one-minute bursts with a one-minute interval in between each burst. From this point on, all subsequent steps were carried out on either on ice, or at 4 °C. Cell debris was removed by centrifugation at 30000xg for 30 minutes (Beckman). Purification of the GST-tagged protein was carried out as follows. The soluble lysate was incubated with Glutathione Sepharose 4B (GE Healthcare) (pre-equilibrated in GST wash buffer) under rotation for

one hour at 4 °C to allow the binding of GST-tagged proteins. The medium was collected by centrifugation at 500xg for one minute and the supernatant was removed. Next, the medium was washed six times with GST wash buffer (followed each time by medium sedimentation at 500xg). The GST-tagged RASSF10 fragment was eluted from the Glutathione Sepharose 4B by adding GST elution buffer. The medium was sedimentated by centrifugation at 500xg, and the GST-RASSF10 containing supernatant could be collected. Fractions from wash and elution steps were then analysed by SDS-PAGE and Coomassie staining as well as by anti-GST western blot. To remove the glutathione from the purified protein, the eluate was dialysed against PBS with 10% glycerol at 4 °C overnight.

The purified RASSF10 (375-468) fragment (4.2 mg) was then sent to Eurogentec for antibody production (3-month immunisation programme in rabbits) and antibody purification.

2.9 Methods for yeast experiments

2.9.1 Yeast cultivation and strains

Yeast cells were grown under standard conditions in YPD medium at 30 °C. Temperature-sensitive mutants were instead grown at their permissive temperature of 25 °C and normally shifted to higher temperatures for the experiments. Strains that carried episomal plasmids, integrated cassettes or integrative plasmids were grown on SC (synthetic complete) medium lacking the amino acid of the respective marker. All media contained 2% glucose as the carbon source.

All the yeast strains used in this thesis are listed in Table 7.1 in the Appendix. Strains created by myself were made either by crossings, PCR-based epitope tagging or disruption of genes, or by integration of plasmids. YIp128 vectors were linearised by EcoRV digestion and integrated into the LEU2 locus. In order to introduce the L109A mutation of Spc25 in the wild type allele, the YIp211-P-SPC25-T (L109A) vector was digested with PstI and integrated in the URA3 locus. Growth on 5-FOA (5-fluoroorotic acid) plates allowed for the selection of clones that had lost the integrated plasmid and colonies that were positive for the L109A mutation in the *SPC25* allele (due to recombination) were identified via sequencing.

2.9.2 Yeast mating and tetrad dissection

In order to create mutant strains, haploid cells of different genotypes were first mated. The haploid strains were grown overnight in 3 mL YPD at 30 °C and, for temperature-sensitive mutants, at 25 °C. The next day, 5 µL of each culture was directly pipetted on top of each other onto a YPD plate and incubated for 4 to 6 hours at 25/30 °C (until zygotes were detected under the microscope). Zygotes were then picked and separated on the plate using a MSM micromanipulator (Singer) and grown for 2 to 3 days in the incubator. Diploids were scraped off the plate and mixed into 1 mL of 1% KOAc to allow sporulation. After 2 to 3 days 5 µL of the spores were mixed with 5 µL Z0.5 solution and incubated for 15 minutes at room temperature in order to digest the ascus wall. 5 µL of the solution was then dropped and distributed in a line on an YPD plate and the tetrads were dissected with the micromanipulator. After growth for 3 to 5 days at 25/30 °C, tetrads were replica-plated and analysed by growth on restrictive media or temperature shift to 37 °C for temperature-sensitive alleles or PCR/sequencing.

2.9.3 Spot assay for temperature sensitivity

Yeast cultures were grown in YPD overnight at the permissive temperature of 25 °C. The next day a dilution series was set up with the culture starting from an OD_{600} of 0.2 and then further diluted by the factor 1/10 to an OD_{600} of $2x10^{-4}$. For every culture 3.3 µL of the four dilutions were spotted on YPD plates (one for every temperature). Plates were incubated for 3 days at the different temperatures (25-35 °C) and scanned at day 2 and day 3.

2.9.4 Yeast transformation

In order to tag alleles, delete genes, integrate plasmids in the yeast genome or for expression from episomal plasmids, yeast cells were transformed with the respective DNA in the following way. First, the relevant strain was grown overnight at 30 °C (or at 25 °C for temperature-sensitive mutants), diluted with fresh medium in the morning and grown until an OD_{600} of 1 to 2 was reached. Cells were then harvested by centrifugation for 3 minutes at 800xg and the pellet resuspended in 100 µL LIT. Following this, DNA

was mixed with 10 µL herring sperm DNA and then added to the cells. For transformations, 5 µL PCR product was used for PCR-based epitope tagging or gene disruption, whereas for linearised or circular plasmids 0.5 to 1 µg and for episomal plasmids 100 ng were used respectively. 500 µL PEG/LIT was mixed into the cell-DNA suspension by vortexing. The cells were then incubated for 15 to 30 minutes under rotation. 50 µL of DMSO were added just before the heat shock at 42 °C for 15 minutes or 10 minutes for temperature-sensitive strains. Cells were harvested at 800xg for 30 seconds and resuspended in 100 µL sterile water. Cells were plated on selective medium according to the selection marker used. In the case of the KanMX auxotrophic marker, cells were not plated directly but recovered for 4 hours in YPD medium before plating them on G418 plates. Colonies were analysed after 3 days incubation at 25 or 30 °C by colony PCR and where applicable by SDS-PAGE/western blot.

2.9.5 Isolation of genomic DNA

In order to extract genomic DNA from yeast cells, the MasterPure^{TM} yeast DNA purification kit from Epicentre was used. Therefore, 1 mL cells of an overnight culture (OD_{600} of 8 to 10) were harvested and DNA was isolated according to the manufacturer's instructions.

2.9.6 Colony PCR for yeast

For the yeast colony PCR a small fraction of the colony was picked with the tip of a pipette and resuspended in 50 µL zymolyase mix. After 10 minutes incubation spherobalsted cells were pelleted for 5 minutes at 4500xg and the supernatant was sucked off. After the pellet was dried for 5 minutes at 95 °C, 25 µL PCR mix (Simple Red polymerase from Thermo Scientific) was added directly. Following PCR programme was applied:

1. 94 °C for 3 minutes
2. 94 °C for 45 seconds
3. 54 °C for 30 seconds
4. 72 °C for 1 minute Repeat step 2-4 for 34 times
5. 72 °C for 7 minutes

2.9.7 PCR-based gene disruption and epitope tagging

In order to epitope tag the C-terminus of alleles (Knop et al., 1999) or delete them (Longtine et al., 1998), a PCR-based technique was applied. Therefore, special plasmids containing tagging cassettes (6HA-, 9myc etc.) for selection with different auxotrophic markers (Knop et al., 1999, Funakoshi and Hochstrasser, 2009), or plasmids with knockout cassettes (Wach et al., 1994) were used. In both cases specific primer pairs had to be designed according to (Longtine et al., 1998, Knop et al., 1999, Funakoshi and Hochstrasser, 2009). For epitope tagging, sense primers contained the last 50 bp upstream of the stop codon from the respective gene, while reverse primers contained 50 bp after the stop codon. Both of them ended in 3' with specific sequences flanking the tagging cassette. The gene disruption primers also consisted in 3' of sequences complementary to the knockout cassette, but the gene specific 5' region contained 50 bp upstream of the start codon for forward primers and 50 bp upstream of the stop codon for reverse primers.

Tagging or disruption cassettes were then amplified with the relevant primers from the plasmids in a 100 µL Simple Red polymerase reaction (see 2.2.1). PCR products were ethanol precipitated, resuspended in 15 µL sterile water and analysed by agarose gel electrophoresis. The strains of interest were transformed with 5 µL of the PCR product as described in 2.9.4 and grown on SC− plates for 3 days. Following this, colonies were analysed via PCR for the presence of the tag and, in case of deletions for the absence of the gene, using primers within the open reading frame. Furthermore, the expression of the tagged proteins was tested by SDS-PAGE and western blot with antibodies according to the tagging.

2.9.8 Site-directed mutagenesis

In order to create single amino acid substitutions in proteins (Spc25 (L109A), Rabex-5 (A58G)), mutations were introduced in the integrative yeast plasmids by site-directed mutagenesis. Site-directed mutagenesis was carried out as specified by the QuickChange® Site-Directed Mutagenesis Kit manual from Stratagene, using the PfuTurbo DNA polymerase.

2.9.9 Isolation of total protein extract from yeast

To test the expression of proteins, total protein extract from yeast cells was obtained in the following way. Cells were grown overnight in YPD at 30 °C (or 25 °C for temperature-sensitive strains) and diluted 1:10 for the main culture. At an OD_{600} of 2 the cells were harvested and kept on dry ice. Pellets were resuspended in 500 µL sterile water and mixed with 75 µL of 1.85 M NaOH and 7.5% β-mercaptoethanol. After incubation for 15 minutes on ice 75 µL of 55% (w/v) TCA was added, followed by another 10 minutes incubation on ice to allow the precipitation of proteins. After centrifugation for 10 minutes at 16000xg, the supernatant was carefully removed so that no liquid remained. The protein-containing pellets were then resuspended in 40 µL HU buffer, denatured for 10 minutes at 65 °C and samples were then ready to be analysed via SDS-PAGE and western blot.

2.9.10 Pull-downs to test *in vivo* ubiquitylation

To test the *in vivo* ubiquitylation of kinetochore components, Ni-NTA pull-downs under denaturing conditions were performed (Ulrich and Davies, 2009). For this purpose, strains harbouring TAP-, 6xHA-, or 9xmyc-tagged alleles of different kinetochore proteins were first transformed with an episomal vector for the copper inducible expression of 6xHis-tagged ubiquitin. Cultures were then grown overnight in 3 mL YPD at 30 °C in the presence of 0.1 mM $CuSO_4$ to allow His-ubiquitin expression. The next day, the overnight cultures were used to set up 50 mL main cultures in YPD and 0.1 mM $CuSO_4$, which were grown at 30 °C until an OD_{600} between 1 and 2 was reached. For the pull-downs, 50 OD_{600} cells were used. Cells were harvested by centrifugation for 5 minutes at 800xg and pellets were kept on dry ice. They were then resuspended in 5 mL of cooled water and, at this point, 50 µL of the suspension was used to prepare the input samples as described in section 2.9.9. To open the cells, 0.8 mL of 1.85 M NaOH and 7.5% β mercaptoethanol were added to the remaining cell solution, strongly vortexed and incubated for 20 minutes on ice. Next, 0.8 mL of 55% (w/v) TCA were mixed in and after another 20 minutes on ice, proteins were pelleted by centrifugation with 16000xg at 4 °C for 20 minutes. The supernatant was then carefully removed and the protein-pellet dissolved for approximately 1 hour in 1.5 mL buffer A

at room temperature. The insoluble fraction was removed by centrifugation at 10000xg for 15 minutes. Total ubiquitin conjugates were isolated by adding 20 µL of in buffer A pre-equilibrated Ni-NTA resin (Qiagen). Imidazole and Tween 20 were also added, so that the binding buffer contained 15 mM imidazole and 0.15% Tween 20. Binding of His-tagged ubiquitin conjugates was carried out overnight under rotation at room temperature. Unspecific binding to the resin was then removed by extensive washing of the beads - twice with buffer A and three times with buffer C. After the final wash step, all the liquid was removed from the beads and they were boiled in 40 µL NuPAGE sample buffer (Life Technologies, prepared according to the manufacturer) for 3 minutes at 100 °C. Pull-down and input samples (1:8 dilution) were loaded directly on NuPAGE 4-12% Bis-Tris gels (Life Technologies) and analysed by western blot with an antibody against the respective tag.

To test the effect of inhibition of the proteasome on the ubiquitylation of proteins, the respective alleles were tagged in a *PDR5* deletion strain to enable the efficient uptake of the inhibitor MG132 (Calbiochem). Strains were then transformed with the episomal plasmid for copper inducible His-ubiquitin expression. Cell cultures were grown as described above, with the difference that 50 µM MG132 was added to the main culture at an OD_{600} of 1 and then grown for a further 2 hours before the cells were harvested. Pull-downs were performed as before and analysed by SDS-PAGE/western blot.

2.9.11 Cycloheximide chase assay

In order to test the stability of tagged (TAP, 9xmyc, 6xHA) proteins, a cycloheximide chase assay was carried out. Therefore, strains harbouring the tagged alleles were grown overnight in 3 mL YPD at 30 °C. The next day, the cultures were diluted in 30 mL YPD and further grown until an OD_{600} of approximately 1 was reached. Protein *de novo* synthesis was then inhibited by adding cycloheximide to a final concentration of 100 µg/mL and the cells' protein amount was monitored by taking 1 mL aliquots at several time points. The cells were harvested and pellets were kept on dry ice. Total protein extracts were prepared as described in section 2.9.9 and analysed by SDS-PAGE and western blot using the appropriate antibodies.

2.10 Protein purification and protein interaction studies

2.10.1 Purification of the Spc25 (107-221)-Spc24 (154-213) complex and ubiquitin for crystallisation trials

For the crystallisation of the Spc25 (107-221)-Spc24 (154-213) complex with ubiquitin, the following expression systems and purification strategies were applied. Spc25 (107-221) was expressed from pET15b (Novagen) and ^{His}Spc24 (154-213) from pEHisTeva (derived from pET30a) with a N-terminal TEV protease cleavable His-tag. Spc25 (107-221) and ^{His}Spc24 (154-213) were co-expressed in the *E. coli* strain BL21 Codon^{2+}. A pre-culture was grown overnight at 37 °C in LB medium containing ampicillin (100 µg/mL) and kanamycin (50 µg/mL). The following day the overnight culture was used to set up the main culture with a starting OD_{600} from 0.1 to 0.2 in LB with the respective antibiotics. The main culture was grown at 37 °C until an OD_{600} of 0.5 to 0.8 was reached. At this point protein expression was induced by adding 0.2 mM IPTG and the culture was kept at 37 °C for a further 5 hours. The cells were then pelleted by centrifugation at 7700xg for 20 minutes. Cell pellets were either stored at −80 °C or put on ice for further processing. Cell pellets were resuspended in ice-cold Ni-NTA lysis/wash buffer and the cells were opened by sonication (BRANSON sonifier) on ice using 5 bursts for 1 minute (40% input) with a one-minute interval in between. From this point on, all subsequent steps were carried out on either ice or at 4 °C. Cell debris was removed by two centrifugation steps, first at 10000xg for 30 minutes followed by ultracentrifugation of the soluble fraction (Beckmann Ultracentrifuge) at 100000xg for 30 minutes. The soluble lysate was then incubated with in Ni-NTA lysis/wash buffer pre-equilibrated Ni-NTA resin (Qiagen) under rotation for 1 hour at 4 °C to allow the binding of His-tagged proteins and then loaded onto a column. The flow through was collected and the resin was extensively washed with Ni-NTA lysis/wash buffer (at least 6 times). This was done to minimize unspecific binding before the Spc25 (107-221)-^{His}Spc24 (154-213) complex was eluted from the Ni-NTA resin with imidazole containing Ni-NTA elution buffer. At this stage, the His-tag of Spc24 was removed using TEV protease. Therefore, TEV protease was added in an OD_{280} ratio of 1:20 to the sample. Cleavage was carried out overnight at 4 °C and under dialysis in Ni-NTA dialysis buffer to remove the imidazole of the sample. In order to expunge the His-

tagged TEV protease from the sample another Ni-NTA affinity chromatography was carried out the next day. The procedure was as described above, but differed in that the Ni-NTA wash buffer II, which contains a lower concentration of imidazole, was used for washing. The Spc25-Spc24 complex with the cleaved His-tagged was collected from the flow-through and wash fractions. Cleavage with TEV protease and reverse Ni-NTA affinity chromatography was repeated because there was still His-tagged Spc24 present (tested via anti-His western blot and Coomassie staining of the gel).

After the initial Ni-NTA purification there were still various other proteins present, so three more purification steps with different columns on an ÄKTA protein purification system (GE Healthcare) were performed. After testing different purification strategies the following one turned out to be the most efficient in obtaining a very pure Spc25 (107-221)-Spc24 (154-213) complex: First of all, the probe was run over a HiTrap Q HP anion exchange column (GE Healthcare), taking advantage of the very poor binding ability of the Spc25-Spc24 complex to a strong anion exchanger. Therefore, the protein sample was dialysed against HiTrap Q buffer I overnight and loaded onto the in HiTrap Q buffer I pre-equilibrated anion exchange column. This buffer contained 100 mM salt and, under those conditions, the Spc25-Spc24 complex did not bind to the column but most of the contamination proteins did. These were eluted in a salt gradient from 100 mM to 1 M NaCl (10 to 100% HiTrap Q elution buffer I) and discarded. In the next step, the wash fractions with the Spc25-Spc24 were pooled and dialysed against HiTrap Q buffer II and loaded onto an in HiTrap Q buffer II pre-equilibrated HiTrap Q column. With no salt present in the buffer the Spc25-Spc24 complex bound to the column and was eluted by using a 0 to 200 mM salt gradient (0 to 20% HiTrap Q elution buffer II). The remaining proteins on the column were eluted via a 200 mM to 1 M salt gradient. The already very pure Spc25-Spc24 protein sample was then concentrated in the centrifuge (5000 MCWO, Vivaspin) and loaded on a Superdex 75 16/60GL gel filtration column (GE Healthcare) (pre-equilibrated with gel filtration buffer for crystallisation). The fractions were analysed by SDS-PAGE followed by Coomassie staining.

Ubiquitin (bovine, Sigma-Aldrich) was dissolved in PBS with 10% glycerol and also loaded on the Superdex 75 16/60 column under the same conditions as described above.

2.10.2 Crystallisation trials

The purified Spc25-Spc24 complex and ubiquitin (see 2.10.1) were sent to our collaborator, Martin Singleton, for crystallisation trials. Silva Zakian, a postdoc in Martin Singleton's lab, set up crystallisation screens. Ubiquitin and the Spc25-Spc24 complex were concentrated to 8 mg/mL and 14 mg/mL, respectively, and then mixed at a ratio of 1.2 to 1 (ubiquitin to complex). The sitting drop vapor diffusion technique was used. Different standard screens were set up and approximately 1000 different conditions were tested.

2.10.3 Co-elution of Spc25-Spc24 and ubiquitin in a sizing column

The interaction between the Spc25-Spc24 complex and ubiquitin was also tested for co-elution in a sizing column. Proteins that bind to each other shift the elution profile when loaded together to a higher molecular weight. Spc25 (107-221) was expressed from pET15b (Novagen) and ^{His}Spc24 (154-213) from pEHisTeva (derived from pET30a). Expression of the Spc25-^{His}Spc24 complex, cell lysis, Ni-NTA affinity chromatography (without His-tag cleavage) was carried out as described in 2.10.1. Samples were then dialysed overnight (using gel filtration buffer for the sizing column) and concentrated, before being loaded onto a Superdex 75 16/60 gel filtration column (GE Healthcare). Ubiquitin (bovine, Sigma-Aldrich) in PBS with 10% glycerol was loaded onto the Superdex 75 16/60 column under the same conditions.

To test whether Spc25-24 and ubiquitin co-elute, the purified Spc25-^{His}Spc24 complex (0.39 mg) was first loaded alone onto the Superdex 75 16/60 column and the elution profile acquired. Next, ubiquitin (0.29 mg) and the complex (0.39 mg) were mixed in a molar ratio of 2:1 and loaded onto the sizing column to generate the second elution profile. An overlay of both elution profiles allowed for a direct comparison.

2.10.4 Purification of His-tagged Spc25 and Spc24 for BIACORE

^{His}Spc25 (107-221) and ^{His}Spc25 (L109A)(107-221) were expressed from pET28a (Novagen) and ^{His}Spc24 (154-213) from pET15b (Novagen). ^{His}Spc25 (107-221) and ^{His}Spc25 (L109A)(107-221) were both co-expressed with ^{His}Spc24 (154-213) in BL21

Codon^{2+} under the same conditions as described in 2.10.1. Cell lysis and the Ni-NTA affinity chromatography were also done as in 2.10.1 expect that the His-tag was not cleaved afterwards. The concentrated samples (5000 MCWO, Vivaspin) were loaded directly on a Superdex 75 16/60 gel filtration column (GE Healthcare) (pre-equilibrated with gel filtration buffer for BIACORE). Fractions were analysed by SDS-PAGE and Coomassie staining as well as anti-His western blot.

2.10.5 BIACORE analysis

The interaction studies between the Spc25-Spc24 complex and ubiquitin using surface plasmon resonance technology were performed on a BIACORE X instrument (GE Healthcare). All steps were carried out with a flow rate of 5 µL/min at 25 °C and all the buffers and reagents were from GE Healthcare. Before the CM5 sensor chip was used, it was left at room temperature for half an hour to avoid condensation. The BIACORE instrument was prepared with HBS buffer and the chip was then inserted and docked. For activation of the sensor chip surface 30 µL of a NHS/EDC mix (1:1 ratio) was injected. 35 µL of diluted anti-GST antibody (30 µg/mL) was captured on the surface (9000 RU) and the chip was deactivated with 35 µL ethanolamine. Next, equimolar amounts of GST (662 RU) and GST-tagged ubiquitin (895 RU) were captured on two separate flow cells. Increasing concentrations of ^{His}Spc25(107-221)-^{His}Spc24(154-213) (1-40 µM) or ^{His}Spc25(L109A)(107-221)-^{His}Spc24(154-213) (10-400 µM) were injected and SPR signals (in RU) of both cells were measured for 300 seconds. The GST background SPR signal was subtracted from the GST-ubiquitin signal and, for the calculation of the dissociation constants, the BIAevaluation (version 3) software was used. Finally, SPR signals at the equilibrium state were plotted against the sample concentration in order to obtain the steady state K_D.

2.10.6 Yeast two-hybrid

The interaction between human Spc25 and different ubiquitin constructs was monitored with the yeast two-hybrid system. Human Spc25 and ubiquitin constructs were already available fused to either the Gal4 activation domain (pGAD vector) or the Gal4 DNA binding domain (pGBT vector). Hence it was possible to test the interaction from both

sides, once for the fusion of Spc25 to the activation domain and the fusion of ubiquitin to the binding domain and vice versa. The yeast two-hybrid strain PJ69-4A was transformed (see 2.9.4) with the individual pGAD constructs and, at the same time, with the corresponding pGBT constructs, using 1.5 µL of each plasmid. Empty pGAD and pGBT vectors served as negative controls. Human Spc24 was co-expressed for the two-hybrid analysis. Therefore, it was cloned in the YEplac195-ADH/T vector (pHU 2167) for episomal expression and then transformed into the different strains already harboring the pGAD and pGBT constructs (the empty expression vector was also transformed as a control). Transformants containing all three vectors were selected on plates lacking the respective markers. For the two-hybrid experiment 5 colonies were picked and resuspended in 500 µL of sterile water for each transformation. 3.3 µL of the cells were then spotted onto three different selective plates. Selective plates for the expression of the three plasmids served as a positive control. Plates additionally lacking histidine were used to monitor weak interactions, while plates without histidine and adenine were used to reveal stronger interactions. The plates were incubated at 30 °C for 3 days and scanned after 2 and 3 days.

2.11 Media

2.11.1 *E. coli*

Luria Broth (LB) medium, LB agar and LB plates with 100 µg/mL ampicillin, 50 µg/mL kanamycin and 50 µg/mL Zeocin were provided by the media production team of CRUK. Bacteria cultures were grown in LB medium containing 100 µg/mL ampicillin, 50 µg/mL kanamycin or both. LB medium with added antibiotics was stored at 4 °C.

Ampicillin: 100 mg/mL in sterile water, filter sterilised (22 µm)

Kanamycin: 50 mg/mL in sterile water, filter sterilised (22 µm)

Zeocin: 50 mg/mL in sterile water, filter sterilised (22 µm)

2.11.2 *Drosophila melanogaster*

Fly food: 360 g agar, 3600 g maize, 3600 g malt, 1200 mL molasses, 440 g soya, 732 g yeast extract, 280 mL of acid mix (500 mL propionic and 32 mL orthophosphoric acid) and water to make 50 L total (provided by the fly facility)

Fly food with G418: 300 µL of 25 mg/mL Geneticin solution (Gibco) were added to one vial of pre-perforated food.

Apple juice plates: 36 g agar, 1600 mL distilled water, 500 mL apple juice, 25 g sucrose, 4 g nipagin, 20 mL ethanol (provided by the fly facility)

S2 medium: Schneider's Drosophila Medium (Gibco) with 10% Fetal Bovine Serum (Sigma-Aldrich) and 100 unit/mL penicillin and 100 mg/mL streptomycin (Gibco).

2.11.3 Yeast

Yeast peptone glucose (YPD) medium, YPD agar, 4% w/v bacto agar, 20% glucose was provided by CRUK's media production team.

Dropout powder stock: 2 g of p-aminobenzoic acid and 20 g each of alanine, arginine, asparagine, aspartic acid, cysteine, glutamine, glutamic acid, glycine, inositol, isoleucine, lysine, methionine, phenylalanine, proline, serine, threonine, tyrosine and valine were weighed out and mixed overnight under rotation.

SC (synthetic complete) powder: 36.7 g dropout powder was mixed with the following components 2 g histidine, 4 g leucine, 2 g uracil, 2 g tryptophan, 0.5 g adenine, leaving any of these amino acids out as required.

2.5x SC medium: 5 g SC powder (specific), 4.25 g of yeast nitrogen base (without amino acids and ammonium sulfate) and 12.5g ammonium sulfate were dissolved in 1 l water and stirred for at least half an hour. Aliquots of 200 mL were autoclaved.

SC medium: 200 mL 2.5x SC medium, 50 mL 20% w/v glucose, 250 mL water

SC plates: 200 mL 2.5x SC medium and 50 mL 20% w/v glucose were mixed with 250 mL melted 4% w/v Bacto agar.

G418 plates: Geneticin 50 mg/mL (Gibco), 1:10 diluted in melted YPD agar (cooled down to 50 °C)

5-FOA plates: 500 mg of 5-fluoroorotic acid was dissolved in 200 mL 2.5x SC medium, 8 mL uracil (2mg/mL) and 8 mL adenine (2mg/mL), 50 mL 20% w/v glucose and then mixed with 250 mL melted 4% w/v Bacto agar.

2.12 Buffers and solutions

2.12.1 General

CRUK's media production facility provided following standard solutions: 0.5 M EDTA pH 8.0, 1 M $MgCl_2$, 5 M NaCl, 1x and 10x PBS, 50x TAE buffer, TE buffer pH 8, 1 M Tris-HCl pH 7.5 and pH 8, 10x TBS.

2.12.2 Tapon lab

PBT: PBS with 0.1% (v/v) Triton X-100 (Fisher Scientific)

PBT-0.3: PBS with 0.3% (v/v) Triton X-100 (Fisher Scientific)

TBST: TBS with 0.1% (v/v) Tween 20 (Fisher Scientific)

Transfer buffer: 25 mM Tris base, 192 mM glycine, 20% (v/v) methanol

NP40 lysis buffer: 50 mM Tris HCl pH 8, 150 mM NaCl, 1% (v/v) IGEPAL (CA-630) (Sigma-Aldrich), 1 mM EGTA, 100 µL/ml NaF, 10 µL/ml phosphatase inhibitor cocktail 2 (Sigma-Aldrich), 10 µL/ml phosphatase inhibitor cocktail 3 (Sigma-Aldrich), protease inhibitor cocktail (Roche)

Fly DNA buffer: 10 mM Tris-HCl pH8, 1mM EDTA, 25 mM NaCl, 1 µL Proteinase K (Roche) per 50 µL buffer

10x DNA loading buffer: 25 mL 10x TAE, 25 mL glycerol and 0.175 g Orange G (Sigma-Aldrich)

GST lysis buffer: PBS, 0.1% (v/v) IGEPAL (CA-630) (Sigma-Aldrich), protease inhibitor cocktail (Roche)

GST wash buffer: PBS, 0.1% (v/v) IGEPAL (CA-630) (Sigma-Aldrich)

GST elution buffer: 50 mM Tris-HCl, 10 mM reduced glutathione, pH 8

2.12.3 Ulrich lab

1% KOAc: potassium acetate in sterile water, filter sterilised (22 µm)

Z0.5 solution: 37 µL STE buffer, 2 µL 1 M DTT, 1 µL zymolyase 20T (20 mg/mL)

STE buffer: 1.2 M sorbitol, 25 mM Tris HCl pH 8, 25 mM EDTA pH 8

Zymolyase 20T: 20 mg/mL in sterile water from (Seikagaku Biobusiness)

DTT 1M: dithiothreitol 154.2 mg/mL in sterile water (Melford)

LIT: 100 mM lithium acetate, 10 mM Tris pH 7.4, autoclaved

PEG/LIT: 100 g PEG 3350 dissolved in 100 mL LIT, autoclaved

Herring sperm DNA: 10 mg/mL in TE buffer, sonicated and boiled for 5 minutes at 95 °C (Sigma-Aldrich)

HU buffer: 8 M urea, 5% SDS, 200 mM Tris-HCl pH 6.8, 1 mM EDTA, 0.1% bromophenol blue, before usage 1.5% DTT

Zymolyase mix: 1 mg/mL Z20 zymolyase and 50 mM DTT in sterile water

6x DNA loading buffer: 50% w/v sucrose, 0.1% w/v bromophenol blue, 0.1% w/v xylene cyanol F, dissolved in TE buffer

TAE buffer: 40 mM Tris base, 40 mM glacial acetic acid, 1 mM EDTA pH 8

5x Lämmli loading buffer: 250 mM Tris-HCl pH 6.8, 500 mM, 10% w/v SDS, 0.1% w/v bromophenol blue, 10% v/v glycerol

5x Lämmli running buffer: 125 mM Tris base, 1.25 M glycine, 0.5% v/v SDS

PBS-T: 1x PBS with 0.05% Tween 20

Western blot buffer I: 300 mM Tris-HCl pH 10.4, 15% v/v methanol

Western blot buffer II: 30 mM Tris-HCl pH 10.4, 15% v/v methanol

Western blot buffer III: 25 mM Tris-HCl pH 9.4, 40 mM ε-aminocaproic acid, 15% v/v methanol

Buffer A: 6 M guanidine hydrochloride, 100 mM phosphate buffer pH 8, 10 mM Tris-HCl pH 8

Buffer C: 8 M urea, 100 mM phosphate buffer pH 6.3, 10 mM Tris-HCl pH 6.3

Phosphate buffer 0.1 M: mix 0.1 M Na_2HPO_4 and 0.1 M NaH_2PO_4 to the required pH

Ni-NTA lysis/wash buffer: 30 mM imidazole, 100 mM NaCl, 50 mM NaH_2PO_4, pH 8

Ni-NTA elution buffer: 250 mM imidazole, 100 mM NaCl, 50 mM NaH_2PO_4, pH 8

Ni-NTA dialysis buffer: 100 mM NaCl, 50 mM NaH_2PO_4, 10% Glycerol, pH 8

Ni-NTA wash buffer II: 20 mM imidazole, 100 mM NaCl, 50 mM NaH_2PO_4, pH 8

HiTrap Q buffer I: 10% glycerol, 1 mM EDTA, 1 mM DTT, 50 mM Tris-HCl pH 8, 100 mM NaCl

HiTrap Q elution buffer I: 10% glycerol, 1 mM EDTA, 1 mM DTT, 50 mM Tris-HCl pH 8, 1 M NaCl

HiTrap Q buffer II: 5% glycerol, 1 mM EDTA, 1 mM DTT, 10 mM Tris-HCl pH 7.8

HiTrap Q elution buffer II: 5% glycerol, 1 mM EDTA, 1 mM DTT, 10 mM Tris-HCl pH 7.8, 1 M NaCl

Gel filtration buffer for crystallisation: 10 mM DTT, 100 mM NaCl, 50 mM Tris-HCl pH 7.5

Gel filtration buffer for sizing column: 100 mM NaCl, 50 mM Tris-HCl pH 7.5, 10% glycerol

Gel filtration buffer for BIACORE: 10 mM Hepes pH 7.4, 150 mM NaCl, 3 mM EDTA

HBS buffer: 10 mM Hepes pH 7.4, 150 mM NaCl, 3 mM EDTA, 0.005% (v/v) surfactant P20

2.13 Antibodies

2.13.1 Tapon lab

Table 2.3 - List of antibodies used for western blotting in Nicolas Tapon's lab

Primary antibody	Source	Species	Dilution
FLAG (M2)	Sigma-Aldrich	Mouse	1:1000
FLAG	Sigma-Aldrich	Rabbit	1:5000
GST (sc-138)	Santa Cruz	Mouse	1:5000
HA (3F10)	Roche	Rat	1:1000
HA (12CA5)	CRUK	Mouse	1:5000
Myc (sc-40)	Santa Cruz	Mouse	1:1000
Myc (sc-798)	Santa Cruz	Rabbit	1:1000
Tubulin (E7)	DSHB	Mouse	1:2000
Secondary antibody	**Source**	**Species**	**Dilution**
HRP anti-mouse	GE Healthcare	Sheep	1:5000
HRP anti-rabbit	GE Healthcare	Donkey	1:5000
HRP anti-rat	GE Healthcare	Goat	1:5000

Table 2.4 - List of antibodies used for immunofluorescence in Nicolas Tapon's lab

Primary antibody	Source	Species	Dilution
Arm (N2 7A1)	DSHB	Mouse	1:10
ASPP	Nicolas Tapon/Eurogentec	Rat	1:500
Baz	Franck Pichaud	Rabbit	1:500
Baz	Andreas Wodarz	Rat	1:500
β-gal	Promega	Mouse	1:500
β-gal	MP Biomedicals	Rabbit	1:500
Ci (2A1)	DSHB	Rat	1:100
Dsh (CA)	Tadashi Uemura	Rat	1:1000
Ecad (DCAD2)	DSHB	Rat	1:20
Fmi (74)	DSHB	Mouse	1:10

Hnt (1G9)	DSHB	Mouse	1:20
Rab11	Akira Nakamura	Rabbit	1:8000
RASSF10	This study/Eurogentec	Rabbit	1:500
Stbm	David Strutt	Rat	1:1000
Secondary antibody	**Source**	**Species**	**Dilution**
Alexa Fluor 488 anti-mouse	Life Technologies	Goat	1:500
Alexa Fluor 633 anti-mouse	Life Technologies	Goat	1:500
Rhodamine Red X anti-mouse	Jackson ImmunoResearch	Donkey	1:500
Alexa Fluor 488 anti-rabbit	Life Technologies	Goat	1:500
Alexa Fluor 546 anti-rabbit	Life Technologies	Goat	1:500
Alexa Fluor 633 anti-rabbit	Life Technologies	Goat	1:500
Cyanine Cy5 anti-rabbit	Jackson ImmunoResearch	Donkey	1:500
Cyanine Cy5 anti-rat	Jackson ImmunoResearch	Donkey	1:500
Rhodamine Red X anti-rat	Jackson ImmunoResearch	Donkey	1:500

2.13.2 Ulrich lab

Table 2.5 - List of antibodies used in Helle Ulrich's lab

Primary antibody	**Source**	**Species**	**Dilution**
FLAG (M2)	Sigma-Aldrich	Mouse	1:3000
GST (sc-138)	Santa Cruz	Mouse	1:5000
HA (12CA5)	CRUK	Mouse	1:5000
His (H1029)	Sigma-Aldrich	Mouse	1:5000
Myc (9E19)	CRUK	Mouse	1:5000
PGK (A6457)	Life Technologies	Mouse	1:5000
TAP (CAB1001)	Cambio	Rabbit	1:5000
Ubiquitin (P4D1)	Cell Signaling Technology	Mouse	1:5000
Secondary antibody	**Source**	**Species**	**Dilution**
HRP anti-mouse (P0447)	Dako	Goat	1:5000
HRP anti-rabbit (P0399)	Dako	Swine	1:5000

2.14 Plasmids

2.14.1 Tapon lab

Table 2.6 lists all the plasmids used in Nicolas Tapon's lab. For plasmids made in this study the construction is described, for plasmids derived from other people the source is stated.

Table 2.6 - List of plasmids used in Nicolas Tapon's lab

Name	Construction or source
Entry vector for Gateway cloning	
RASSF9 pDONR stop	PCR amplify RASSF9 from plasmid with primers 47/48, BP reaction into pDONR Zeo
RASSF10 pDONR stop	PCR amplify RASSF10 from plasmid with primers 49/50, BP reaction into pDONR Zeo
Pk pDONR	PCR amplify Pk from plasmid with primers 44/46, BP reaction into pDONR Zeo
Sple pDONR	PCR amplify Sple from plasmid with primers 45/46, BP reaction into pDONR Zeo
Stbm pDONR	PCR amplify Stbm from RE54419 (DGRC) with primers 1/2, BP reaction into pDONR Zeo
Fz pDONR	PCR amplify Fz from plasmid LD32066 (DGRC) with primers 72/73, BP reaction into pDONR Zeo
3stop-HA pDONR	PCR amplify 3stop-HA from plasmid GFP pAHW with primers 135/136, BP reaction into pDONR Zeo
RASSF8 stop dTOPO	Nicolas Tapon/Yanxiang Zhou
Site specific integration and expression via the UAS or Ubi promoter in flies	
pKC26_UAS_GW	PCR amplify UAS from plasmid pTGW with primers 39/40, MIuI/NotI digestion and clone into pKC26w_GW vector.
UAS-GFP-RASSSF9	LR reaction of RASSF9 pDONR stop with pKC26w_UAS_GW
UAS-GFP-RASSSF10	LR reaction of RASSF10 pDONR stop with pKC26w_UAS_GW
pKC26w_GW	Pedro Gaspar/Yanxiang Zhou
Ubi-GFP-RASSF9	LR reaction of RASSF9 pDONR stop with pKC26w_GW
Ubi-GFP-RASSF10	LR reaction of RASSF10 pDONR stop with pKC26w_GW
Ubi-GFP	LR reaction of 3stop-HA pDONR with pKC26w_GW
Ubi-GFP-RASSF8	LR reaction of RASSF8 stop dTOPO with pKC26w_GW
Expression in flies, CRISPR	
pCFD3-dU6:3gRNA	Simon Bullock

Expression of RASSF10 (375-468) in *E. coli* for antibody generation	
pGEX-RASSF10 (375-468)	PCR amplify dRASSF10 fragment from plasmid with primers 90/91, EcoRI/XhoI digestion and clone into pGEX-4T-1
Expression in S2 cells	
ASPP pAMW	Nicolas Tapon/ Paul Langton
Baz pAFW	Andreas Wodarz
CKIα pAWF	Nicolas Tapon/ Paulo Ribeiro
CKIIα pAWF	Nicolas Tapon
Dco pAFW	Nicolas Tapon/ Paulo Ribeiro
Dsh pAWM	Nicolas Tapon/ Lennart Kester
Fz pAWM	LR reaction of Fz pDONR with pAWM
Gish I pAFW	Nicolas Tapon/ Paulo Ribeiro
Gish F pAFW	Nicolas Tapon/ Paulo Ribeiro
GFP pAFW	Nicolas Tapon
GFP pAHW	Nicolas Tapon
GFP pAMW	Nicolas Tapon
PP1α13C pAFW	Nicolas Tapon/ Yanxiang Zhou
PP1α87B pAFW	Nicolas Tapon/ Yanxiang Zhou
PP1α96A pAFW	Nicolas Tapon/ Yanxiang Zhou
PP1β9C pAFW	Nicolas Tapon/ Yanxiang Zhou
Prickle Pk pAWM	LR reaction of Pk pDONR with pAWM
Prickle Sple pAWM	LR reaction of Sple pDONR with pAWM
RASSF8 pAWF	Nicolas Tapon/ Eunice Chan
RASSF8 pAWH	Nicolas Tapon/ Eunice Chan
RASSF9 pAWF	Nicolas Tapon/ Lennart Kester
RASSF9 pAWH	Nicolas Tapon/ Lennart Kester
RASSF10 pAWF	Nicolas Tapon/ Lennart Kester
RASSF10 pAWH	Nicolas Tapon/ Lennart Kester
Sec15 pAFW	Nicolas Tapon/ Eunice Chan
Stbm pAWM	LR reaction of Stbm pDONR with pAWM
WAVE pAWF	Nicolas Tapon/ Eunice Chan

2.14.2 Ulrich lab

Table 2.7 lists all the plasmids used in Helle Ulrich's lab. For plasmids made in this study the construction is described, for plasmids derived from other people the source is stated.

Table 2.7 - List of plasmids used in Helle Ulrich's lab

pHU	Name	Construction or source
Yeast episomal expression vector		
73	YEplac195-G/T	Helle Ulrich
308	YEplac181	(Gietz and Sugino, 1988)
386	YEplac112	(Gietz and Sugino, 1988)
654	YEp181-ADH/T	Helle Ulrich
2167	YEplac195-ADH/T	Cloning of ADH-promoter (pHU 654) as EcoRI/HindIII fragment in pHU73 YEplac195-G/T
2187	YEplac195-ADH-hSPC24	PCR amplify hSpc24 from human cDNA with primers oHU1478/1479, BamHI digestion and clone into YEplac195-ADH/T vector
818	YEp-His-UBI	Helle Ulrich
821	YEp181-CUP1-His-Ubi	Helle Ulrich
Yeast expression		
147	YIplac128-G/T	Helle Ulrich
2246	Ylplac204-Pdsn1-Dsn1_a	GENEART
2247	Ylplac204-Pdsn1-Dsn1_b	GENEART
2248	Ylplac204-Pdsn1-Dsn1_c	GENEART
2249	Ylplac204-Pdsn1-Dsn1_d	GENEART
2283	Ylplac128-Pdsn1-Dsn1_a	pHU2246 cut with EcoRI and SalI and fragment cloned into pHU147
2284	Ylplac128-Pdsn1-Dsn1_b	pHU2247 cut with EcoRI and SalI and fragment cloned into pHU147
2285	Ylplac128-Pdsn1-Dsn1_c	pHU2248 cut with EcoRI and SalI and fragment cloned into pHU147
2286	Ylplac128-Pdsn1-Dsn1_d	pHU2249 cut with EcoRI and SalI and fragment cloned into pHU147
2287	Ylplac128-Pdsn1-Dsn1_wt	pHU2286 cut with EcoRV and NsiI and fragment cloned into pHU2283

Yeast two hybrid		
82	pGBT9	Clontech
145	pGAD424	Clontech
1035	pGAD-Ubi3RΔGG	Helle Ulrich
1036	pGBT-Ubi3RΔGG	Helle Ulrich
1529	pGAD-Ubi4(3R,HT)	Helle Ulrich
1530	pGBT-Ubi4(3R,HT)	Helle Ulrich
1531	pGBT-Ubi4(3R,linker)	Helle Ulrich
1532	pGAD-Ubi4(3R,linker)	Helle Ulrich
1684	pGBT-SPC25	Helle Ulrich
1700	pGAD-SPC25	Helle Ulrich
1721	pGBT-hSPC25	Helle Ulrich
1722	pGAD-hSPC25	Helle Ulrich
Tagging or gene disruption		
233	pFA-HIS3	(Wach et al., 1994)
245	pGEX-Ubi	Helle Ulrich
228	pYM3	(Knop et al., 1999)
229	pYM6	(Knop et al., 1999)
1724	YIp211-P-SPC25-T (L109A)	Helle Ulrich
2152	pFA6a-6xGLY-3xFLAG-HIS3MX6	(Funakoshi and Hochstrasser, 2009)
2258	pFA6a-6xlinker-Vps27 UIM-1 (256-278)-6xGLY-3xFLAG	PCR amplify Vps27 (256-278) from yeast gDNA with primers oHU2212/2213, PacI and BamHI digestion and clone into pHU2152
2259	pFA6a-6xlinker-Rabex 5 MIU-1 (48-74)-6xGLY-3xFLAG	PCR amplify Rabex-5 (48-74) from human cDNA with primers oHU2214/2215, PacI and BamHI digestion and clone into pHU2152
2233	pFA6a-6xlinker-Rabex 5 MIU-1 (A58G)-6xGLY-3xFLAG	Site directed mutagenesis of plasmid pHU 2259 with primers oHU2232/2233
Expression in *E. coli*		
839	pet15b	Merck
1717	pET28a-Spc25 (107-221)	Helle Ulrich
1720	pET15b-SPC24 (154-213)	Helle Ulrich

1985	pEHisTeva	(Liu and Naismith, 2009)
2120	pET15b-Spc25 (107-221)	PCR amplify Spc25 (107-221) from plasmid pHU1717 with primers oHU1848/1164, NcoI/BamHI digestion and clone into pET15b vector
2121	pEHisTeva-Spc24 (154-213)	PCR amplify Spc24 (154-213) from plasmid pHU1720 with primers oHU1847/1228, NcoI/BamHI digestion and clone into pEHisTeva vector
2122	pET28a-Spc25 L109A (107-221)	Site directed mutagenesis of plasmid pHU1717 with primers oHU1700/1881

2.15 DNA Oligonucleotides

DNA Oligonucleotides were ordered from Sigma-Aldrich.

2.15.1 Tapon lab

Table 2.8 - List of oligonucleotides used in Nicolas Tapon's lab

#	Name	Sequence
Gateway		
1	Stbm attB1	GGGGACAAGTTTGTACAAAAAAGCAGGCTTCACC ATGGAAAACGAATCCGTCAAGTCGGAACAC
2	Stbm attB2 ns	GGGGACCACTTTGTACAAGAAAGCTGGGTGTACG GATGTTTCGGAGTTCAACTTAAGAACAAATTTGTT GC
44	Prickle Pk attB1	GGGGACAAGTTTGTACAAAAAAGCAGGCTTCACC ATGGATACCCCAAATCAAATGCCTGTTGAGC
45	Prickle Sple attB1	GGGGACAAGTTTGTACAAAAAAGCAGGCTTCACC ATGAGCAGCCTGTCAACCGGTGG
46	Prickle attB2 ns	GGGGACCACTTTGTACAAGAAAGCTGGGTGCGAG ATGATGCAGTTCTTGTCCTTGTCGC
47	dF9 attB1	GGGGACAAGTTTGTACAAAAAAGCAGGCTTCACC ATGCAGAGCCTACCACTACCAGGAGAT
48	dF9 attB2 stop	GGGGACCACTTTGTACAAGAAAGCTGGGTGTTAAA CAAGGGTGCCGAGGTGTTGAATATCC
49	dF10 attB1	GGGGACAAGTTTGTACAAAAAAGCAGGCTTCACC ATGGCGCCCCAACAACAGAACTC
50	dF10 attB2 stop	GGGGACCACTTTGTACAAGAAAGCTGGGTGTTACA CCAGCATACTGGCATTATTATCGCAAAACTC
72	Fz attB1	GGGGACAAGTTTGTACAAAAAAGCAGGCTTCACC ATGTGGCGTCAAATCCTGTTTATTTTACCCACC

73	Fz attB2 ns	GGGGACCACTTTGTACAAGAAAGCTGGGTGGACG TACGCCTGCGCCCGG
123	F10 attB1 252-end	GGGGACAAGTTTGTACAAAAAAGCAGGCTTCACC ATGTACAAGTGGCTCAAGAAGCTATTGCATCTGAA
126	F10 attB1 405-end	GGGGACAAGTTTGTACAAAAAAGCAGGCTTCACC ATGTCGGAAATGTGCCGACTGTACCG
135	stop-HA attB1	GGGGACAAGTTTGTACAAAAAAGCAGGCTTCACCT GACGTAAGCTAGATGGATCTCCACCGC
136	HA attB2	GGGGACCACTTTGTACAAGAAAGCTGGGTGTCATC CGCCATGAGCAGCGTAATCTG
Cloning		
39	UASt fw	CGACGCGTGCATGCCTGCAGGTCGGA
40	UASt rv	TAATGCGGCCGCCATAGTGACTGGAT
90	dF10 375-468 fw	CGAATTCTTGCGAAATAGTGTACGATATAAGTTG
91	dF10 375-468 rv	CGCTCGAGCAGACGCTTTAAGT
Reverse transcriptase PCR		
	RpL32 fw	TGTCCTTCCAGCTTCAAGATGACCATC
	RpL32 rv	CTTGGGCTTGCGCCATTTGTG
	F10 5' UTR fw	TGCAGTGTGAACCAGTGAAGA
	F10 ex1 rv	TTCATCCACCAAACGCTCCT
	F10 ex2 fw	CGGAGTGACGAACAAGACGA
	F10 ex4 rv	ACATCGAAAATCCCGTGGCT
Genotyping		
	RASSF8 fw	AGGAGAAGCAGAAGCAGAAGAGGAG
	RASSF8 rv	GTTGTGGCTGCTATGCTGATCGTAGTC
	RASSF9 fw	ATAATATGGCAATGCTCGCA
	RASSF9 rv	GTGGGTTTTAGTTACTAATCCAC
	RASSF10 (B) fw	GCCCCAACAACAGAACTCCAC
	RASSF10 (B) rv	CCTTTCGCCTCCTTATGCAG
	RASSF10 (C) fw	GTTCCTTCGCTGCATTTTCC
	RASSF10 (C) rv	TTCAGTGGAAATGCTGGCG
	Neo2 f	AGAGGCGCTTCGTCTACGGAGCGACA
	hsp70_FRT r	CGGCAAGCAGGCATCGCCATGGGTC
	FRT(hs) fw	AGGTGAGGTTCTCGGCTAGT
	FRT(hs) rv	AACTCTGAATAGGTCGATAGCGT

CRISPR oligonucleotides for gRNA	
gRNA B1 fw	GTCGAGTATGTAGATCGATTAAG
gRNA B1 rv	AAACCTTAATCGATCTACATACT
gRNA B2 fw	GTCGTTTCGGTACCCCTATACAGT
gRNA B2 rv	AAACACTGTATAGGGGTACCGAAA
gRNA C1 fw	GTCGGCCCACAGGGGCCGTGAAA
gRNA C1 rv	AAACTTTCACGGCCCCTGTGGGC
gRNA C2 fw	GTCGCAGTGCTATTAACGCCATAG
gRNA C2 rv	AAACCTATGGCGTTAATAGCACTG

2.15.2 Ulrich lab

Table 2.9 - List of oligonucleotides used in Helle Ulrich's lab

oHU	Name	Sequence
Deletion of genes and test for deletion		
108	UBR2 tag up	GCTAATTTCGTAGCAATTTTGAATGACTAGACAT TTGTTGGATAAATCGATGAATTCGAGCTCG
109	UBR2 ko down	AGGTAAGATTCGTTAACTAAATTAATAGCTACTT AACAAGCACGCCGTACGCTGCAGGTCGAC
1149	PDR5 ko test	GTGCCACAACATTTTCAGATT
1984	Ubr2 UTR test down	ATAATCAACGCATTCATACTT
1985	Ubr2 ORF test down	CTATAACCAATATAAGAGAT
1986	Ubr2 ORF test up	CACTTTAGCAACATAAGAATG
C-terminal tagging of genes and test for tagging		
1570	Dsn1 C terminal tagging down	AACAGCTGTTGAAGGGATTAAGTTTATCTTTCAG TAAAAAACTGGATTTACGTACGCTGCAGGTCGAC
1571	Dsn1 C terminal tagging up	ATGTTACATATGCAGAAGTATCCGATTTTTTTTTG ATTTTTTCTTTTATTATCGATGAATTCGAGCTCG
1572	Dsn1 test	GCAGATGTTGAGACAAAG
1976	Spc105 C terminal tagging down	TGGAGTTCTTCCTTCATTTACGAAAAGTAGAATA CATTTAGAGTTTACGCGTACGCTGCAGGTCGAC
1977	Spc105 C terminal tagging up	AAAAAAAGTGATGAGATATTACTAGTCATCGTTG TCCTATTATAAACACTATCGATGAATTCGAGCTC G
1978	Spc105 test	GAAGCGCTTTTGCAGTTCAA
1980	Tag test	AGATCTATATTACCCTGTTATCCCTAGCGG

2206	Spc25 tag down	ACCTCGCGGCATTTTTAGTCGTGGCCCGCGATAT GCTTCTGGCATCTTTAGGGGGAGGCGGGGGTGGA
2207	Spc25 tag up	TCATCTAAATCATAGGCCCAGAATAAACTGAACA GATGCGTATAAAGGCGATCGATGAATTCGAGCTC G
2208	Spc24 tag down	ACCTCAGCGATTTCTATAAGACCAAATACATCTG GGAAAGATTAGGAAAGGGGGGAGGCGGGGGTGG A
2209	Spc24 tag up	GCTCATTGAATATGTATGCCACTGTAGTATTTTAT TAATGATCTCAATTTATCGATGAATTCGAGCTCG
2210	Spc25 UBD tag down	ACCTCGCGGCATTTTTAGTCGTGGCCCGCGATAT GCTTCTGGCATCTTTAGCTTCAGGATCTGGAGCA
2211	Spc24 UBD tag down	ACCTCAGCGATTTCTATAAGACCAAATACATCTG GGAAAGATTAGGAAAGGCTTCAGGATCTGGAGC A
Sequencing		
1163	Spc25 down	CGCGGATCCGAATGGCCAGCATAGACGCATT
1267	ADH seq down	CGTCATTGTTCTCGTTCCC
Cloning		
1164	Spc25 up	CGCGGATCCTTATAAAGATGCCAGAAGCATA
1227	Spc24 154 down	CCGCTCGAGGAAGCAAACGAAAATATTCT
1228	Spc24 up	CGGGATCCTCACTTTCCTAATCTTTCCC
1321	SPC25 117 down	CGGAATTCGGTAAAGAGTGTGTCCAA
1478	hSPC24 down	CGCGGATCCCGATGGCCGCCTTCCGCG
1479	hSPC24 up	CGCGGATCCCTACCACTCGGTGTCCA
1847	Spc24 (154) n down	CCGCCATGGAAGCAAACGAAAATATTCT
1848	Spc25 (107) n down	CGCCATGGCGCGCGAGCTGGACTCGCTGCT
1849	Spc25 (107) x up	GCGCTCGAGTTATAAAGATGCCAGAAGCATATCG C
2059	DSN1 promoter down	CGGAATTCAAGAGCGCAGAACCAAACCAAA
2060	DSN1 promoter up	CCGGGATCCCCTCTACCTAAATAAAGAAAA
2212	Vps27 UIM-1 (256-274) down	CGCGGATCCGCTTCAGGATCTGGAGCACCTGAGG ATGAAGAAGAGCTGATAAGGAAA
2213	Vps27 UIM-1 (256-278) up	GCGTTAATTAAAGCGCTATTTCTAGATTCTTT
2214	Rabex-5 MIU (48-74) down	CGCGGATCCGCTTCAGGATCTGGAGCACAGAAGC AGATTCAGGAGGACTGGGAGCTG
2215	Rabex-5 MIU (48-74) up	GCGTTAATTAAGCTCTGACTGCTGGCAAAGGC

Chapter 3 Interaction network and characterisation of *Drosophila* RASSF9 and RASSF10

When I started working on this project, the mammalian affinity purification-mass spectrometry (AP-MS) results from our collaborator, Matthias Gstaiger, had shown that human N-terminal RASSFs are found in an interaction network with different PP1 catalytic subunits and ASPP1/2 (Hauri et al., 2013). The substrate specificity of serine/threonine protein phosphatase 1 (PP1) catalytic subunits is achieved through association with different regulatory subunits, which not only allow substrate selection, but also define PP1 localisation within the cell. Human ASPP1/2 and iASPP were shown to bind to all of the PP1 catalytic subunits and are considered to be regulatory subunits for PP1s (Llanos et al., 2011, Skene-Arnold et al., 2013). At the time of my arrival in the Tapon lab, Yanxiang Zhou, a graduate student, was investigating the ASPP/PP1 complex in *Drosophila*. In his thesis, he was able to show that the ASPP/PP1 holoenzyme associates with RASSF8, which in turn allows the recruitment of potential substrates, such as the polarity protein Baz (Zhou, 2014). Thus, RASSF8 functions as a specificity subunit of the ASPP/PP1 complex. Taken together, the mammalian AP-MS results and Yanxiang Zhou's findings allow us to hypothesise that *Drosophila* RASSF9 and RASSF10 could also be substrate-specifying subunits of alternative ASPP/PP1 complexes (see Figure 3.1). Most interestingly, the Gstaiger lab discovered that human RASSF9 and RASSF10 also interact with a different set of proteins compared with RASSF7/8 - components of the PCP signalling pathway (Hauri et al., 2013).

This chapter aims to characterise RASSF9 and RASSF10, two members of the N-terminal RASSF family in *Drosophila* by looking at their interaction network, subcellular localisation and the gain- and loss-of-function phenotypes. In the following subchapters, I will first explore whether RASSF9 and RASSF10 are part of the ASPP/PP1 complex, share interaction partners with RASSF8 and test whether they function in planar cell polarity. Finally, I will present deletion mutants of *RASSF9* and *RASSF10* in flies, and lastly address a potential redundancy between N-terminal RASSFs.

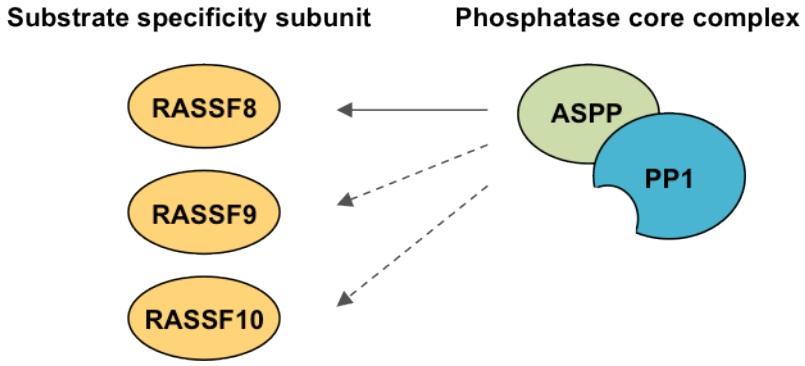

Figure 3.1 - N-terminal RASSFs as potential specificity subunits of ASPP/PP1 complexes. RASSF8 is part of ASPP/PP1 phosphatase complexes and recruits their substrates. RASSF9 and RASSF10 could also act as specificity subunits for ASPP/PP1 complexes.

3.1 *Drosophila* RASSF9 and RASSF10

RASSF9/CG13875 encodes for a 486 aa protein and *RASSF10/CG32150* for a 524 aa (*CG32150-RA/RC*) protein. An alternatively spliced variant of *RASSF10* (*CG32150-RD*) translates into a shorter 118 aa version, containing the N-terminus (see 3.5.2 for transcripts). Analysis of the protein sequences with InterProScan (Jones et al., 2014) revealed that RASSF9 (CG13875-PA/PB) and RASSF10 (CG32150-PA/PC) both contain an RA-like domain at the N-terminus, and have, like other RASSFs, predicted coiled-coil domains at the C-terminus (Figure 3.2). With either *Drosophila* sequence, NCBI BLAST searches return homologues of RASSF9 and RASSF10 across species. However, the alignment of RASSF9 and RASSF10 with their potential human homologues shows that they share relatively little sequence identity (23-31%) with the highest similarity displayed between their RA domains (Figure 3.2). In conclusion, although RASSF9 and RASSF10 are thought to represent the homologues of human RASSF9 and RASSF10, the human and fly proteins share limited sequence homology, begging the question whether their interaction partners are conserved across species.

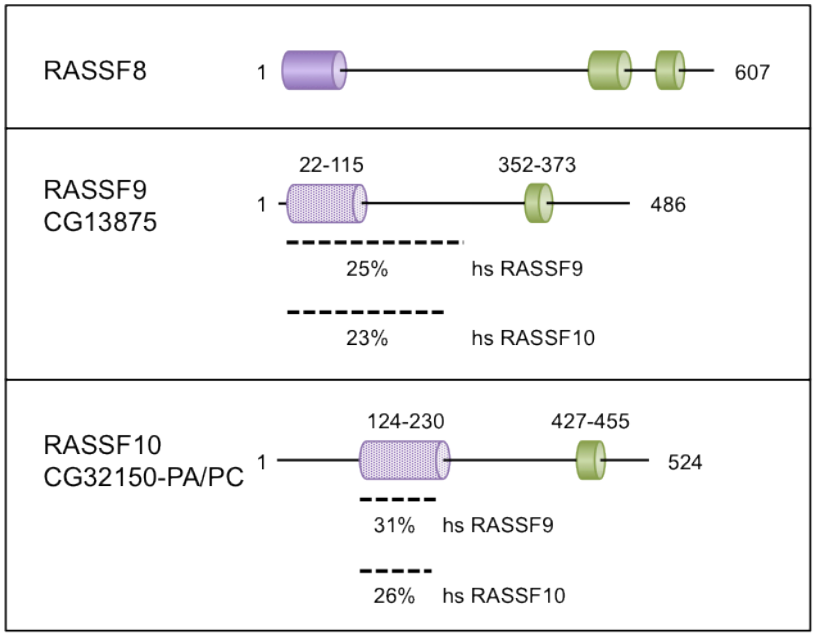

Figure 3.2 - Predicted domain structure of N-terminal RASSFs in *Drosophila*.
Protein domains were predicted using InterProScan and sequence identities with human RASSF9/10 were acquired using NCBI BLAST. RASSF9 and RASSF10 both contain a N-terminal RA-like domain (highlighted in purple) and coiled-coil regions (highlighted in green). Coverage of the alignment with human RASSF9/10 is indicated by a dashed line and percentage sequence identities given below.

3.2 N-terminal RASSFs as potential PP1 regulatory subunits

3.2.1 *Drosophila* RASSF9 and RASSF10 bind to ASPP

In *Drosophila*, ASPP and RASSF8 are well-established binding partners (Langton et al., 2009). The mammalian AP-MS results from the Gstaiger laboratory showed that human RASSF9 and RASSF10 bind to the human ASPP isoforms, ASPP1 and ASPP2, as does human RASSF8. To test whether the interaction with ASPP was conserved in *Drosophila,* I performed co-immunoprecipitation (co-IP) experiments from lysates of transfected S2 cells (Figure 3.3). This revealed that ASPP co-immunoprecipitated with RASSF8, RASSF9 and - to a lesser degree - with RASSF10.

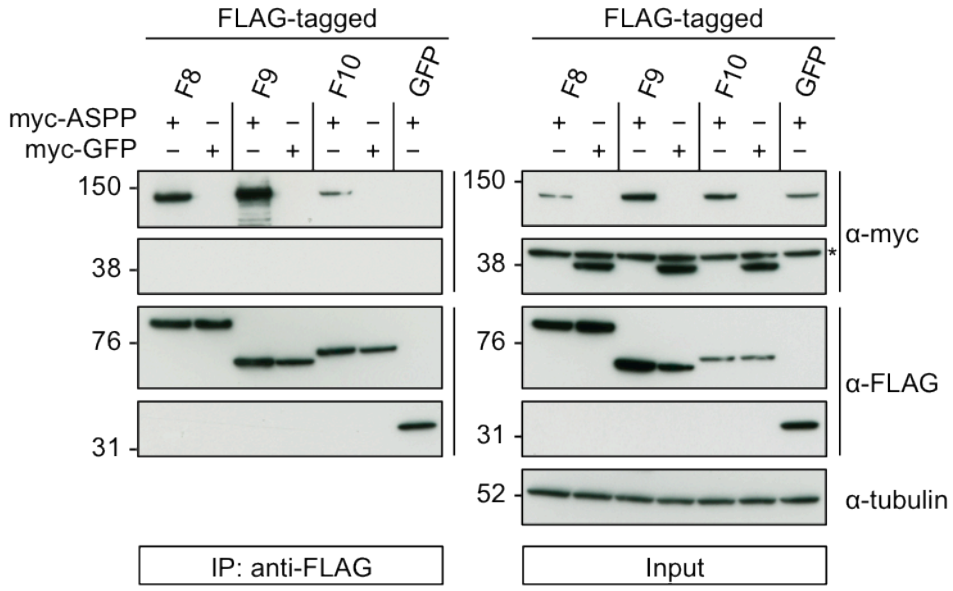

Figure 3.3 - ASPP binds to each of the N-terminal RASSFs.

S2 cells were transfected with the indicated tagged constructs and co-IP experiments were performed with cell lysates using anti-FLAG affinity gel. Immunoprecipitates (IP) and input samples were analysed by western blotting using the appropriate antibodies. Tubulin was used as a loading control. Cross-reacting, non-specific bands are labelled with an asterisk. ASPP co-immunoprecipitates with each of the N-terminal RASSFs. Representative western blot of two independent co-IP experiments.

3.2.2 *Drosophila* N-terminal RASSFs form a trimeric complex with ASPP-PP1α96A

After confirming that the interaction of RASSF9 and RASSF10 with ASPP was indeed conserved in *Drosophila*, I performed co-IP experiments to test whether RASSF9/10 can form a trimeric complex with ASPP/PP1. Yanxiang Zhou had already shown that ASPP bridges the association between RASSF8 and PP1 (Zhou, 2014). *Drosophila* has four different PP1 catalytic subunits, namely PP1α96A, PP1α87B, PP1α13C, and PP1β9C. I decided to use PP1α96A for this experiment, as this subunit had previously shown the strongest interaction with ASPP in co-IP experiments (Zhou, 2014). I pulled down FLAG-tagged PP1α96A and tested whether myc-tagged ASPP and HA-tagged RASSFs were present (Figure 3.4). In parallel, RASSFs were analysed for their ability

to bind to PP1α96A in the absence of transfected ASPP. As expected, immunoprecipitation of RASSF8 with PP1α96A only occurred in the presence of ASPP (Figure 3.4). RASSF9 and RASSF10 were also able to bind to ASPP/PP1 but, interestingly, they also immunoprecipitated with PP1α96A in the absence of ASPP. In contrast, N-terminal RASSFs were not recovered in control (FLAG-GFP) immunoprecipitates. Thus, *Drosophila* RASSF9 and RASSF10 associate with PP1α96A, but, unlike RASSF8, this interaction is not dependent on ASPP. RASSF9 appears to be stabilised in the presence of ASPP in the input samples (Figure 3.3 and Figure 3.4). However, in order to ascertain whether the stabilisation observed in transfected S2 cells has a biological relevance, this should be tested *in vivo*, for example *ASPP* loss-of-function clones.

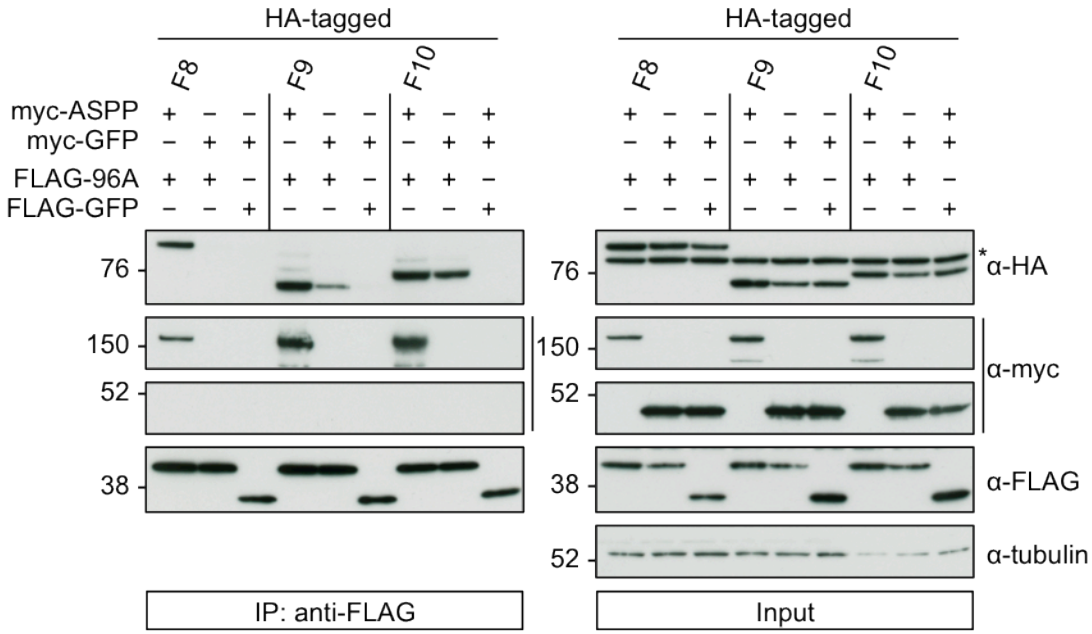

Figure 3.4 - N-terminal RASSFs can form a trimeric complex with ASPP and PP1α96A.
S2 cells were transfected with the indicated tagged constructs and co-IP experiments were performed from cell lysates using anti-FLAG affinity gel. IP and input samples were analysed by western blotting using the appropriate antibodies. Tubulin was used as a loading control. Cross-reacting, unspecific bands are labelled with an asterisk. ASPP and RASSF8 co-immunoprecipitate with PP1α96A (96A). RASSF9 and RASSF10 co-immunoprecipitate with PP1α96A in, the presence or absence of ASPP. Representative western blot of two different co-IP experiments.

3.2.3 RASSF9 and RASSF10 bind to all PP1 catalytic subunits

Next, I investigated the binding of RASSF9 and RASSF10 to the four different PP1 catalytic subunits, PP1α96A, PP1α87B, PP1α13C, and PP1β9C. In co-IP experiments with lysates of transfected S2 cells, pulling down the different FLAG-tagged PP1 subunits, RASSF9-HA (Figure 3.5A) and RASSF10-HA (Figure 3.5B) were detectable for all four, but not in the FLAG-GFP controls.

As RASSF9 and RASSF10 were found to bind to each of the PP1 catalytic subunits, I proceeded to analyse their protein sequence using ScanProsite (de Castro et al., 2006) for the presence of known PP1-binding elements, namely the RVXF, SILK, MyPhoNE and RARL motif (Hendrickx et al., 2009, Wakula et al., 2003). However, neither protein contained any of the motifs. This suggests that RASSF9 and RASSF10 contain an as yet unknown PP1-binding motif.

In his PhD thesis, Yanxiang Zhou demonstrated that the preferential binding of *Drosophila* ASPP to PP1α96A and PP1β9C is facilitated by their extended C-terminus, which is not present in PP1α87B and PP1α13C (Zhou, 2014). However, RASSF9 and RASSF10 exhibited no preference for PP1α96A and PP1β9C over PP1α87B and PP1α13C (Figure 3.5), suggesting that the extended C-termini of PP1α96A and PP1β9C do not contribute to the interaction. This is in agreement with the fact that, unlike RASSF8, RASSF9 and RASSF10 do not require ASPP to associate with PP1 catalytic subunits.

In conclusion, the presence of ASPP is not required for the interaction of PP1 with RASSF9/10, allowing us to consider two different scenarios: either RASSF9 and RASSF10 could function as regulatory subunits themselves, or a different regulatory subunit - one which is endogenously expressed in S2 cells - mediates the binding to PP1s.

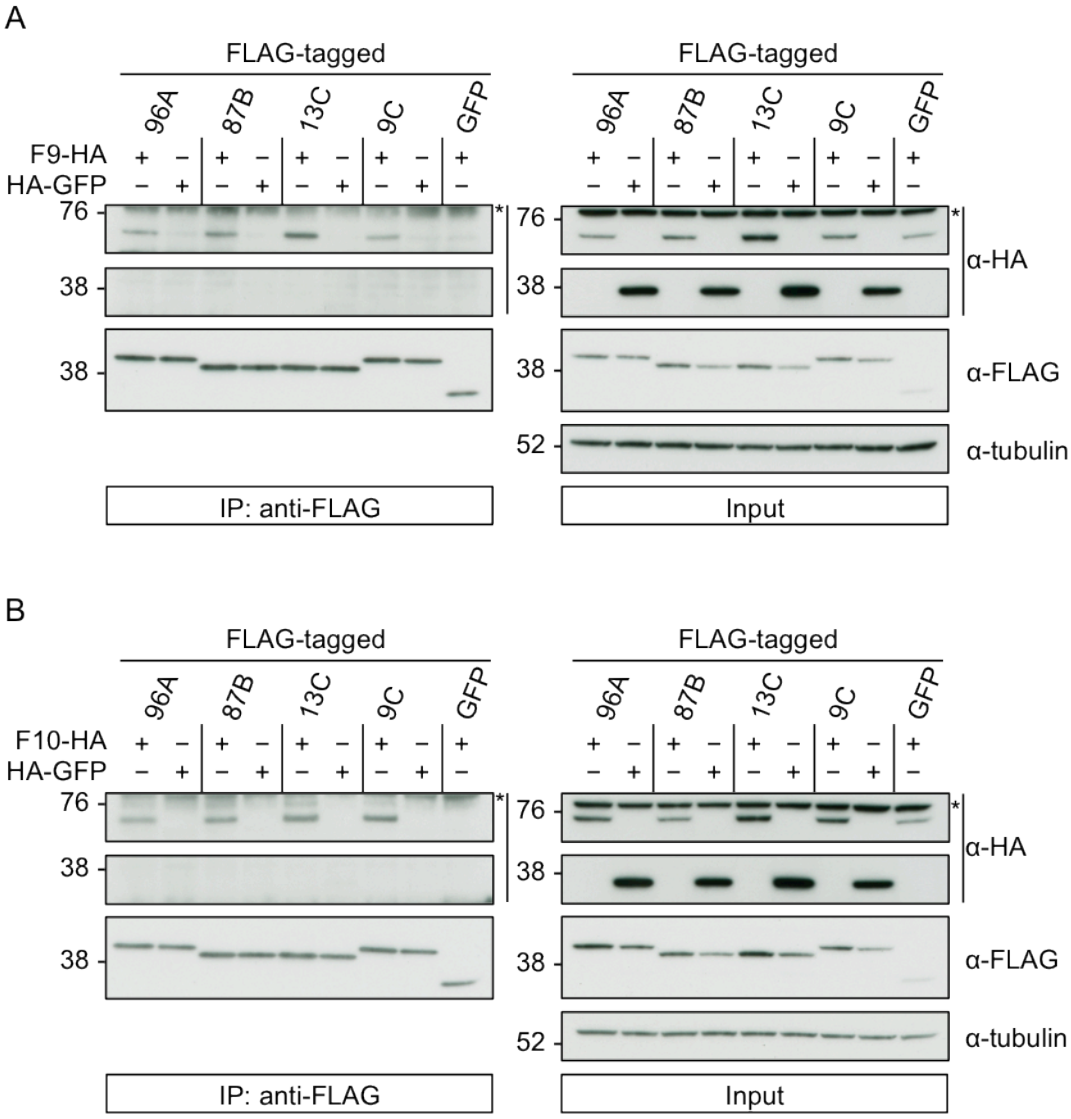

Figure 3.5 - RASSF9 and RASSF10 can bind to all PP1 catalytic subunits in *Drosophila*.
S2 cells were transfected with the indicated tagged constructs and co-IP experiments were performed from cell lysates using anti-FLAG affinity gel. IP and input samples were analysed by western blotting using the appropriate antibodies. Tubulin was used as a loading control. Cross-reacting, unspecific bands are labelled with an asterisk. RASSF9-HA (A) and RASSF10-HA (B) co-immunoprecipitate with each of the PP1 catalytic subunits (96A: PP1α96A, 87B: PP1α87B, 13C: PP1α13C, 9C: PP1β9C). Representative western blot of two different co-IP experiments.

3.3 RASSF9 and RASSF10 bind to several RASSF8 interactors

In this section, I will explore the association of RASSF9 and RASSF10 with validated RASSF8 binding partners (Baz, Sec15 and SCAR/WAVE), which we identified using a yeast two-hybrid approach (Eunice Chan, unpublished results). Like RASSF8, these proteins are involved in cell-cell junction remodelling (Langevin et al., 2005b, McGill et al., 2009, McKinley et al., 2012, Walther and Pichaud, 2010), and we consider them as putative targets of the ASPP/PP1 complex.

First, I tested whether RASSF9 and RASSF10 could associate with the polarity determinant Baz - the *Drosophila* homologue of human Par3. The binding to Baz was of particular interest, as Yanxiang Zhou showed in his thesis that Baz can bind, via RASSF8, to the ASPP/PP1 complex and, like Par3 (Traweger et al., 2008) can be dephosphorylated by PP1 *in vitro*, making it a likely *in vivo* substrate of the ASPP/PP1 complex. Furthermore, Par3 was recovered in human RASSF9 and RASSF10 AP-MS experiments by the Gstaiger lab (Hauri et al., 2013). Indeed HA-RASSF9 and HA-RASSF10 were recovered in FLAG-Baz immunoprecipitates (Figure 3.6). Note that expression of Flag-tagged Baz in S2 cells did not yield in a single band, but a ladder of bands, which represent degradation products of Baz, as has been previously reported (Krahn et al., 2009). Nonetheless, degraded Baz fragments were still able to co-immunoprecipitate the N-terminal RASSFs.

Next, I tested whether RASSF9 and RASSF10 could bind to Sec15, a member of the exocyst complex, and SCAR, an activator of actin filament polymerisation *via* the Arp2/3 complex (Zallen et al., 2002). I found that RASSF9 and RASSF10, but not the FLAG-GFP controls, both also bind to Sec15 (Figure 3.7A) and SCAR (Figure 3.7B).

Interestingly, the input levels of all N-terminal RASSFs seem higher when coexpressed with Baz compared to the GFP control (Figure 3.6). Similarly, RASSF8 (but not RASSF9/10) input levels increase upon coexpression of Sec15 (Figure 3.7A) or SCAR (Figure 3.7B). As mentioned before the biological relevance of these observations would have to be addressed in *in vivo* experiments.

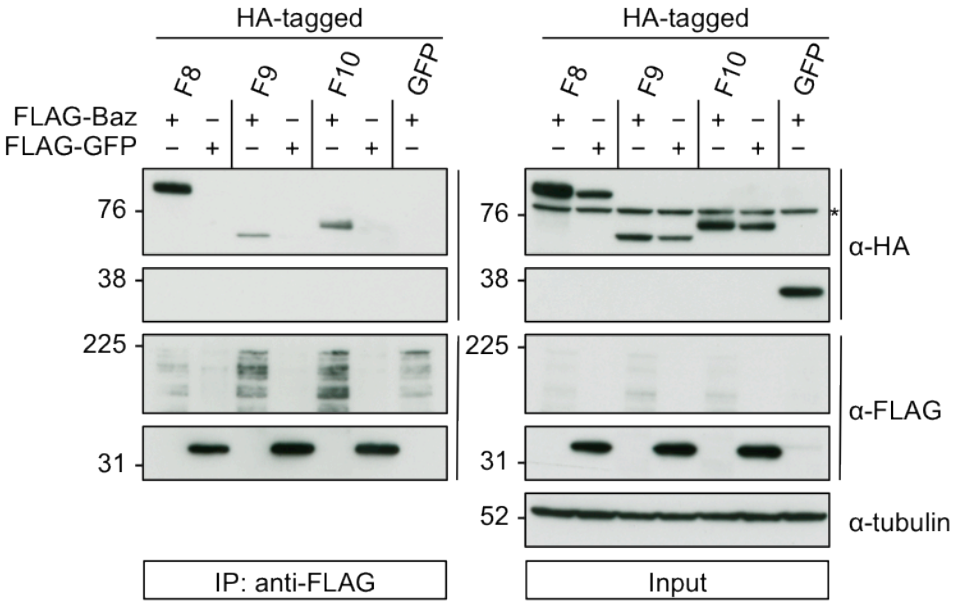

Figure 3.6 - RASSF8, RASSF9 and RASSF10 associate with Baz.

S2 cells were transfected with the indicated tagged constructs and co-IP experiments were performed from cell lysates using anti-FLAG affinity gel. IP and input samples were analysed by western blot using the appropriate antibodies. Tubulin was used as a loading control. Cross-reacting, unspecific bands are labelled with an asterisk. Representative western blot of two different co-IP experiments.

In conclusion, despite the limited sequence homology between these proteins *Drosophila* RASSF9 and RASSF10 have the potential to physically interact with several known RASSF8 interactors. This could indicate that N-terminal RASSFs share certain functions and might therefore be at least partially redundant. The potential redundancy will be addressed in section 3.6. In the following section I will focus on the specific interactors of RASSF9 and RASSF10.

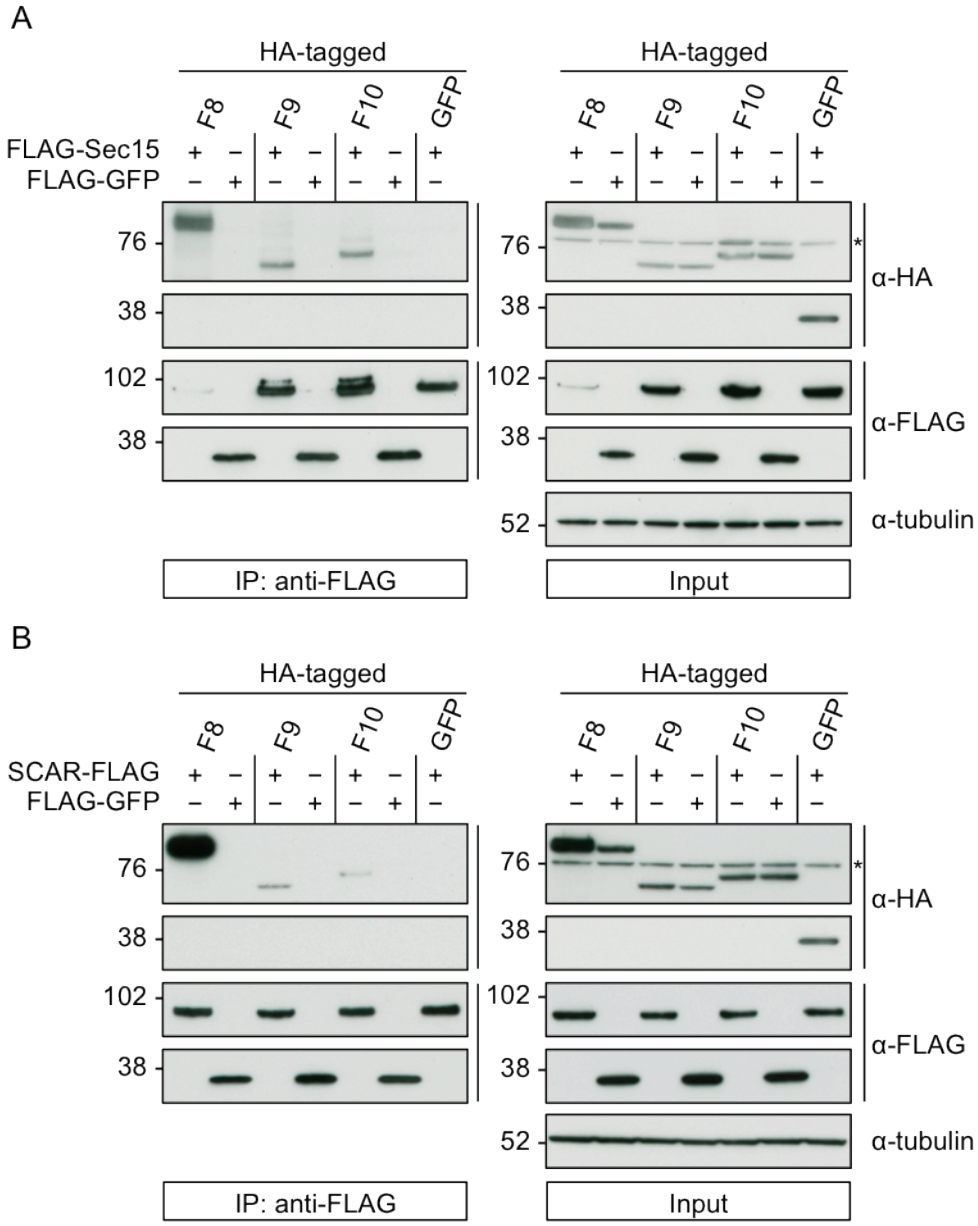

Figure 3.7 - RASSF8, RASSF9 and RASSF10 associate with Sec15 and SCAR.

S2 cells were transfected with the indicated tagged constructs and co-IP experiments were performed from cell lysates using anti-FLAG affinity gel. IP and input samples were analysed by western blot using the appropriate antibodies. Tubulin was used as a loading control. Cross-reacting, unspecific bands are labelled with an asterisk. (A) N-terminal RASSFs co-immunoprecipitate with the exocyst subunit Sec15. (B) N-terminal RASSFs co-immunoprecipitate with Arp2/3 activator SCAR. Representative western blot of two different co-IP experiments.

3.4 Interactions with PCP components

The results of the mammalian AP-MS analysis from our collaborator Matthias Gstaiger showed that human RASSF9 and RASSF10 bind to several proteins of the core planar cell polarity (PCP) pathway. Different isoforms of the human homologues of *Drosophila* Dishevelled, Strabismus, Prickle and Casein kinase subunits CKIIα and CKIIβ were found to interact with RASSF9 and RASSF10, but not with RASSF7 and RASSF8 (Hauri et al., 2013). Thus suggesting that these might be RASSF9 and RASSF10-specific interactors.

Planar cell polarity is required for the polarity within the plane of an epithelium and is established by the asymmetric distribution of its core components: the seven-pass transmembrane receptor Fz, Dsh and Dgo localise on one side of the cell (distal/posterior) whereas the four-pass transmembrane protein Stbm and Pk are found on the other side (proximal/ anterior), while Fmi localises on both sides, as described in the introduction (see 1.4.3). Besides their function in PCP, Fz and Dsh are also key players in canonical Wg/Fz signalling, where Fz functions as the receptor for Wg/Wnt family ligands and transduces the signal via its effector Dsh (see 1.4.1). In order to explore whether RASSF9 and RASSF10 are involved in PCP and/or canonical Wg/Fz signalling, I tested whether the mammalian interactions were conserved in *Drosophila*.

3.4.1 Interaction with Dishevelled

Firstly, I checked the interaction of N-terminal RASSFs with the phosphoprotein Dsh (mammalian Dvl). *Drosophila* RASSF10 has previously been reported to interact with Dsh in a genome-wide yeast-two hybrid screen (Formstecher et al., 2005). Dsh robustly co-immunoprecipitated with RASSF9 and RASSF10, while no binding was observed to RASSF8 or the GFP controls (Figure 3.8). Interestingly, in input samples in which Dsh was co-expressed with the N-terminal RASSFs, Dsh was present as a double band, with a faint higher molecular weight band. A mobility shift representing phosphorylated Dsh, can be induced by co-expression of Dgo in HEK293 cells (Jenny et al., 2005) or Fz in S2 cells and HEK293 cells (Yanfeng et al., 2011). The form of Dsh co-immunoprecipitated with RASSF9 and RASSF10 appears to run at a higher molecular weight (at 102 kDa) compared to the lower molecular weight band in the input samples

(below 102 kDa), indicating that RASSF9 and RASSF10 both preferentially bind to a post-translational modified - most likely phosphorylated - form of Dsh. This should be verified in the future with phosphatase treatment.

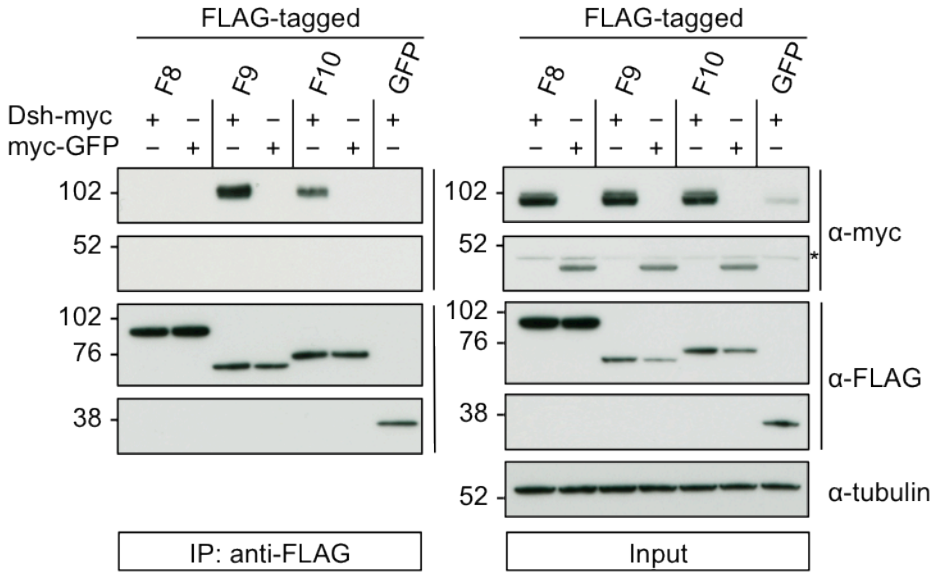

Figure 3.8 - RASSF9/10, but not RASSF8 bind to Dsh.

S2 cells were transfected with the indicated tagged constructs and co-IP experiments were performed from cell lysates using anti-FLAG affinity gel. IP and input samples were analysed by western blotting using the appropriate antibodies. Tubulin was used as a loading control. Cross-reacting, unspecific bands are labelled with an asterisk. Dsh interacts with RASSF9 and with RASSF10. Representative western blot of two different co-IP experiments.

3.4.2 Interaction with Prickle and Strabismus

Next, I explored the interaction between the N-terminal RASSFs and Pk (Prickle). In *Drosophila*, two of the three Pk isoforms are known to be involved in PCP, and cause distinct phenotypes (Gubb et al., 1999, Lin and Gubb, 2009). Pk^{Pk} (Prickle) and Pk^{Sple} (Spiny-legs) derive from alternative splicing and only differ in the length of their N-terminal extensions: 13 aa in the case of Pk^{Pk}, 346 aa for Pk^{Sple} (Gubb et al., 1999, Lin and Gubb, 2009). Both Pk^{Pk} (Figure 3.9A) and Pk^{Sple} (Figure 3.9B) weakly associated with RASSF9, and not at all to RASSF10. However, the binding between RASSF9 and Pk isoforms was not consistent in different IP-experiments - sometimes a faint band was present and at other times no interaction was detectable.

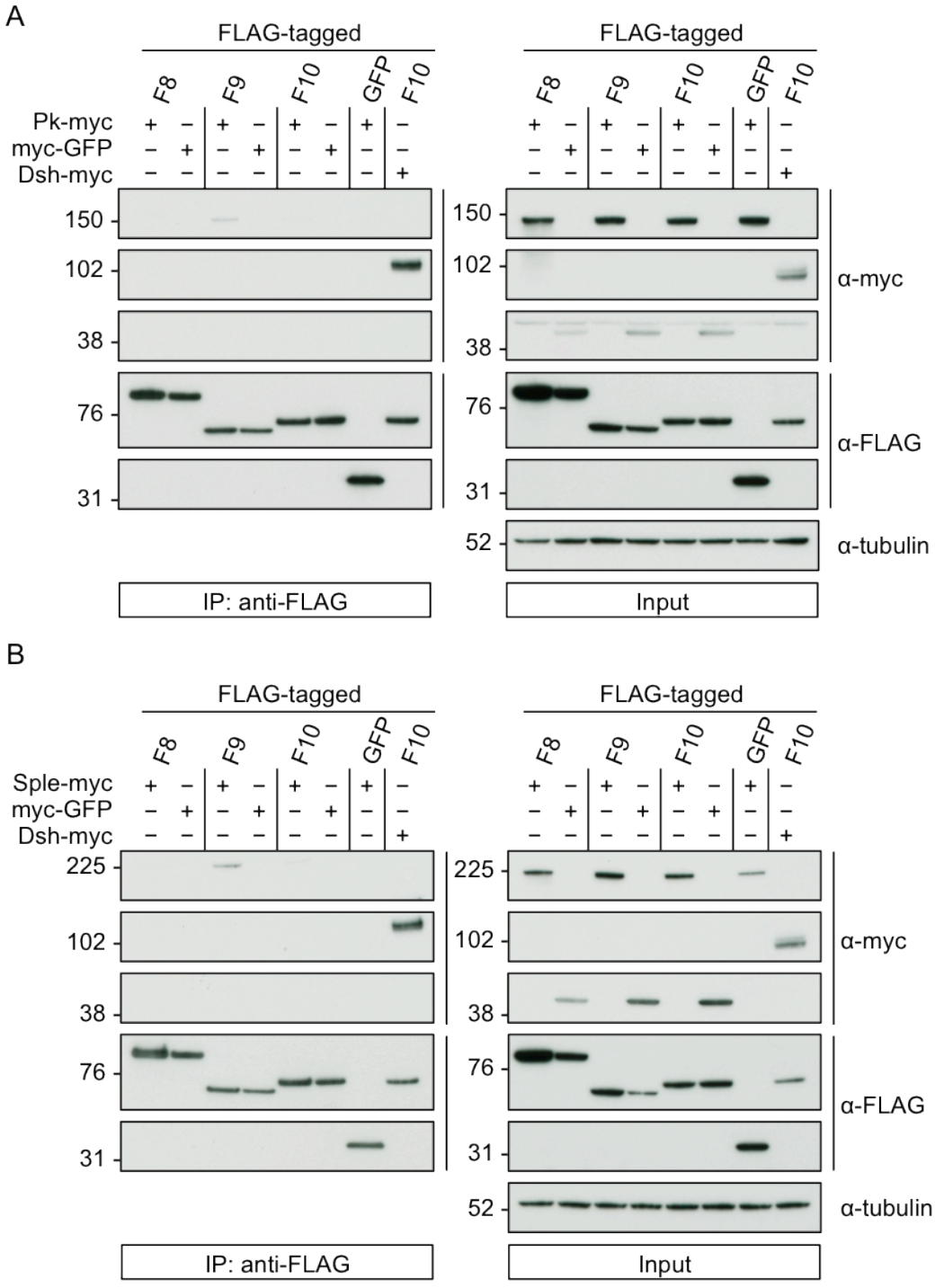

Figure 3.9 - RASSF9, but not RASSF10 can bind weakly to both Prickle isoforms.

S2 cells were transfected with the indicated tagged constructs and co-IP experiments were performed from cell lysates using anti-FLAG affinity gel. IP and input samples were analysed by western blot using the appropriate antibodies. Tubulin was used as a loading control. Both Prickle isoforms (Pk: Prickle; Sple: Spiny-legs) weakly co-immunoprecipitate with RASSF9 (not observed in two other co-IP experiments) and cannot be detected in RASSF8 or RASSF10 precipitates. The co-IP between Dsh and RASSF10 was used as a positive control.

It is probable that the weak binding between RASSF9 and Pk isoforms is indirect and could be mediated by the endogenously expressed Dsh in S2 cells, as Pk and Dsh have been shown to bind to each other (Tree et al., 2002, Jenny et al., 2005). A similar scenario was observed for the four-pass transmembrane protein Stbm (Strabismus, also known as Van Gogh or Vang), which weakly and inconsistently interacted with RASSF9 (Figure 3.10). As for Pk, it is likely that the interaction with Stbm is indirect and could be bridged by endogenous Dsh, which can physically interact with Stbm (Bastock et al., 2003).

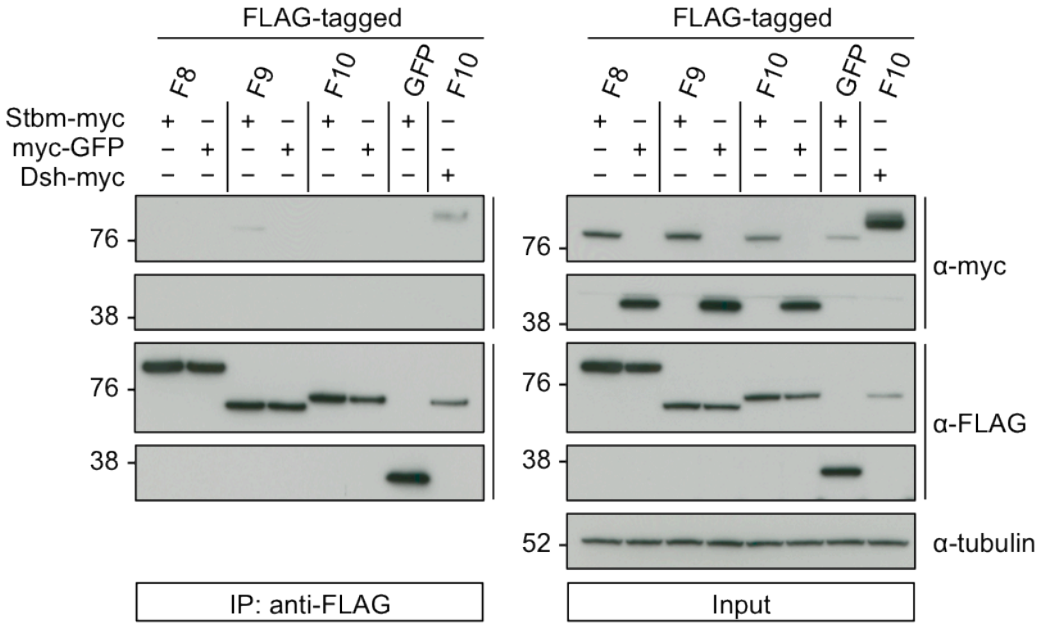

Figure 3.10 - RASSF9 binds weakly to Strabismus.

S2 cells were transfected with the indicated tagged constructs and co-IP experiments were performed from cell lysates using anti-FLAG affinity gel. IP and input samples were analysed by western blot using the appropriate antibodies. Tubulin was used as a loading control. Stbm weakly co-immunoprecipitates with RASSF9 (not observed in two other co-IP experiments) and cannot be detected in RASSF8 or RASSF10 precipitates. The co-IP between Dsh and RASSF10 was used as a positive control.

3.4.3 Interaction with Frizzled

In addition to the hits from the mammalian AP-MS results, I also checked whether any of the N-terminal RASSFs in *Drosophila* could bind to the seven-pass transmembrane

receptor Fz, which is essential for both canonical Wg/Fz-signalling and PCP and whose cytoplasmic tail binds Dsh (Strutt, 2003, Singh and Mlodzik, 2012). Fz co-immunoprecipitated with RASSF10 and was not detectable for RASSF8, RASSF9 or the FLAG-GFP control (Figure 3.11). I repeated the pull-downs in both directions but could never detect any binding between Fz and RASSF9, whereas the interaction with RASSF10 was robust. The interaction of Fz and RASSF10 might not be conserved in humans, as Fz was not present in the AP-MS results for human RASSF9 and RASSF10 (Hauri et al., 2013), and the HEK293 cells used in the analysis have been reported to express mRNA of several Fz receptors (Atwood et al., 2011).

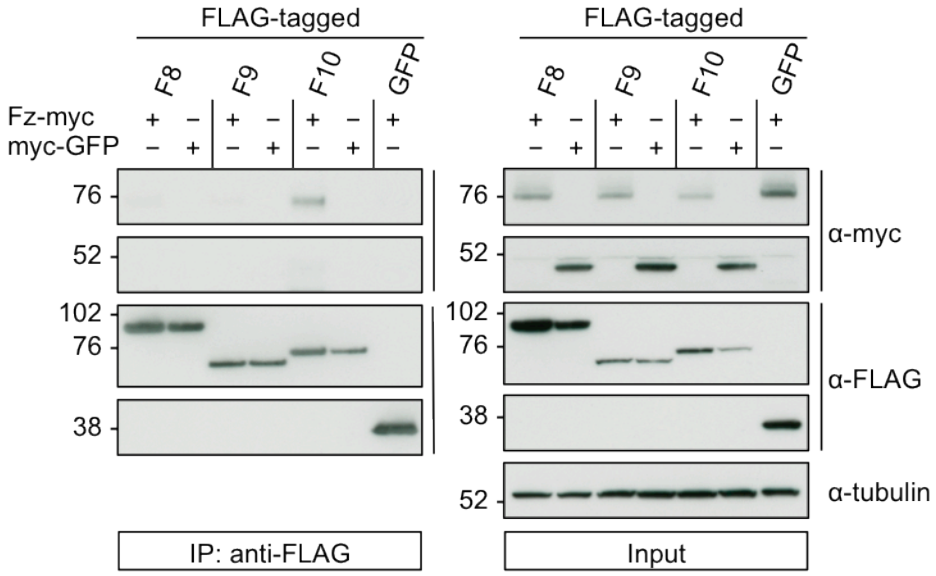

Figure 3.11 - RASSF10 binds to Frizzled.

S2 cells were transfected with the indicated tagged constructs and co-IP experiments were performed from cell lysates using anti-FLAG affinity gel. IP and input samples were analysed by western blot using the appropriate antibodies. Tubulin was used as a loading control. RASSF10, but not RASSF9 and RASSF8 can interact with Fz. Representative western blot of at least two independent co-IP experiments.

3.4.4 Interaction with CKI and CKII family members

Lastly, having examined interactions with core PCP components, I tested the interaction between casein kinases and N-terminal RASSFs. CKII and several CKI isoforms have

been associated with canonical Wg/Fz and PCP signalling. CKII, which comprises two catalytic α subunits and two regulatory β subunits, was shown to bind and phosphorylate Dsh in *Drosophila* (Willert et al., 1997, Song et al., 2000) and in mammary epithelial cells (Song et al., 2000). Moreover, several studies have shown the requirement of different CKI isoforms: CKIα (Strutt et al., 2006), CKIε (Dco, Discs Overgrown) (Strutt et al., 2006, Klein et al., 2006), CKIγ (Gish, Gilgamesh) (Zhang et al., 2006) for either canonical Wg/Fz or PCP, or both signalling pathways.

Both RASSF9 and RASSF10 but not the GFP control or RASSF8 immunoprecipitated with CKIIα (Figure 3.12A). I then tested the interactions with CKI isoforms α, ε and γ and found that RASSF9 and RASSF10 bound to all of them, while RASSF8 was only positive (and much weaker compared to RASSF9/10) for interaction with CKIα (see Figure 3.12B for summary of interactions). Overexpression of CKII or CKI isoforms did not cause a mobility shift in any of the RASSFs in the input samples, suggesting that they may not be substrates of these kinases. Thus, RASSF9 and RASSF10 can associate with not only PP1s, but also several protein kinases.

A

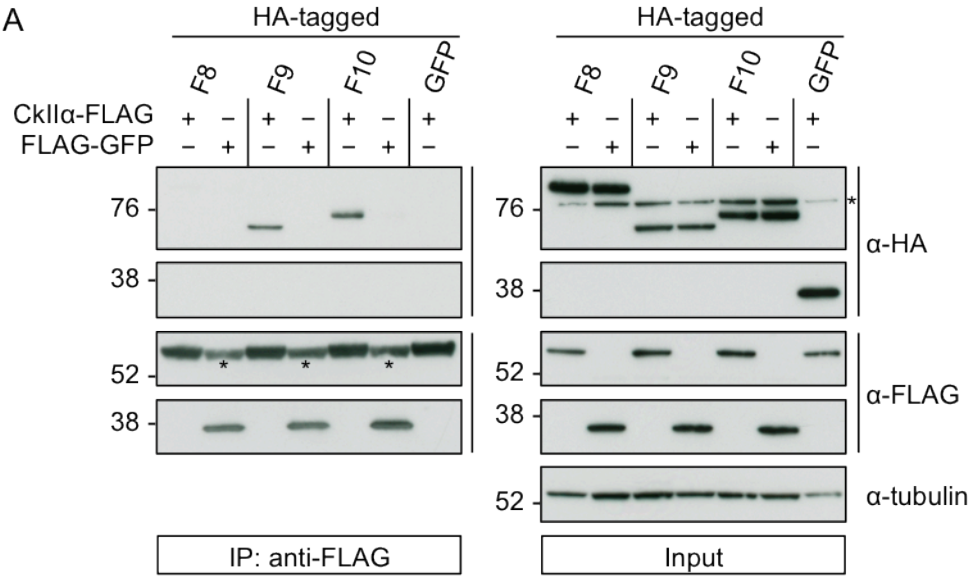

B

Interaction	CKIα	Dco (CKIε)	Gish (CKIγ)
RASSF8	+	–	–
RASSF9	+	+	+
RASSF10	+	+	+

Figure 3.12 - Description see following page.

Figure 3.12 - RASSF9 and RASSF10 bind to CKIIα and several CKI family members.
S2 cells were transfected with the indicated tagged constructs and co-IP experiments were performed from cell lysates using anti-FLAG affinity gel. IP and input samples were analysed by western blot using the appropriate antibodies. Tubulin was used as a loading control. Cross-reacting, unspecific bands are labelled with an asterisk. (A) RASSF9 and RASSF10, but not RASSF8 co-immunoprecipitate with CKIIα. Representative western blot of two independent co-IP experiments. (B) Table of the tested interactions between N-terminal RASSFs and CKI family members. RASSF9/10 also interact with CKIα, CKIε and CKIγ, whereas RASSF8 is only able to bind to CKIα.

3.4.5 Localisation of GFP-tagged RASSF9 and RASSF10

A distinct feature of the core PCP proteins is their planar polarisation within the tissue. In epithelial cells of pupal wings, the seven-pass transmembrane cadherin Fmi localises asymmetrically to the distal and the proximal side of the cell (Usui et al., 1999). The seven-pass transmembrane receptor Fz and the cytoplasmic proteins Dsh and Dgo are found on the distal side (Axelrod, 2001, Strutt, 2001, Feiguin et al., 2001), whereas the four-pass transmembrane protein Stbm and the cytoplasmic protein Pk are located on the proximal side (Bastock et al., 2003, Tree et al., 2002). Since my interaction studies in S2 cells suggested a robust interaction between RASSF9/RASSF10 and Dsh, I examined their subcellular localisation *in vivo*.

As no commercial antibodies were available against the endogenous proteins, I initially generated constructs to express GFP-tagged versions of RASSF9 or RASSF10 under control of the *ubiquitin 63E* (*ubi*) promoter, as well as UAS constructs for expression under the UAS/Gal4 system. Transgenic flies were inserted on 2L (cytological location 28E7) (Ubi-lines and UAS-lines) or 3R (cytological location 89E11) (UAS-lines) using the PhiC31 integrase system.

I first looked at the localisation in wing imaginal discs of L3 larvae. Ubiquitously-expressed N-terminal GFP-tagged RASSF9 and RASSF10 both localised in the same plane as E-cadherin at the adherens junctions in wing disc epithelial cells, as seen in planar (XY) and transverse (Z) confocal sections in Figure 3.13 (A-B'' for RASSF9 and C-D'' for RASSF10). Moreover, the localisation of RASSF10 appeared to be polarised proximo-distally in the wing disc (Figure 3.13C-C'').

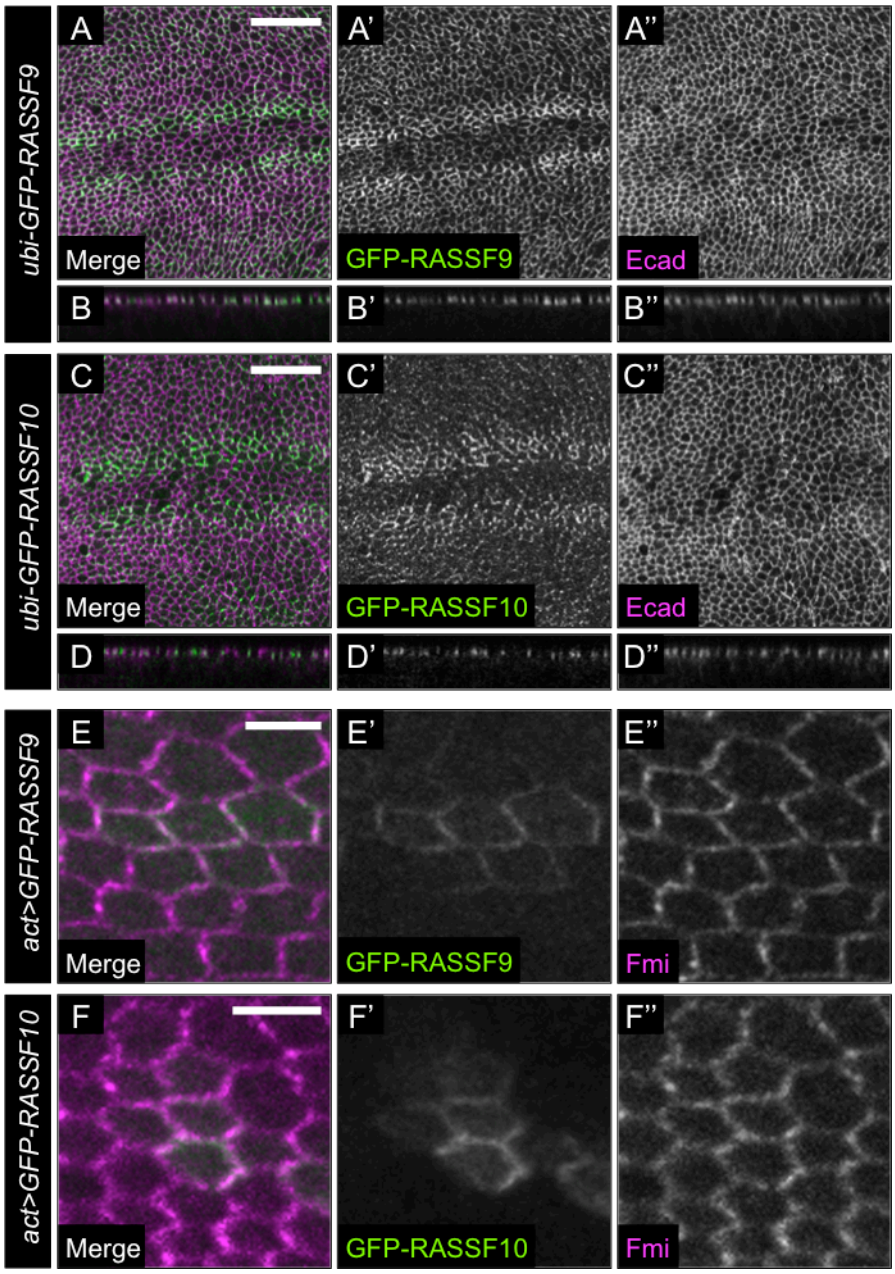

Figure 3.13 - Localisation of GFP-RASSF9 and GFP-RASSF10 in L3 wing imaginal discs and pupal wings.

Planar (A-A'', C-C'') and transverse confocal sections (B-B'', D-D'') of wing imaginal discs stained for Ecad. *GFP-RASSF9* and *GFP-RASSF10* were expressed under the *ubi* promoter. GFP-RASSF9 (A-B'') and GFP-RASSF10 (C-D'') co-localise with E-cadherin at the adherens junctions. Posterior is to the left and anterior to the right. Scale bar = 20 μm. Planar confocal sections of pupal wings at 30 hours APF stained for Fmi (E-F''). FLPout clones expressing GFP-RASSF9 or GFP-RASSF10 under control of *actin-Gal4* were induced with *hsFLP*. GFP-RASSF9 (E-E'') and GFP-RASSF10 (F-F'') are planar polarized and localize in the same plane as Fmi. Proximal is to the left, distal to the right (E-F''). Scale bar = 5 μm.

Since RASSF10 appeared planar-polarised in L3 wing discs, I examined its localisation in pupal wings. Using the FLPout system, mitotic clones expressing GFP-RASSF9 or GFP-RASSF10 under control of *actin-Gal4* were induced with *hsFLP*. RASSF9 and RASSF10 were localised in the same plane as Fmi in pupal wings 30 hours APF (after pupa formation) (Figure 3.13E-F''). Moreover, at the clonal border of GFP-RASSF9 and GFP-RASSF10 expressing cells, both appeared to localise to the distal side of the cell. This indicates a similar localisation to Dsh and Fz, further supporting the connection between RASSF9/10 and the Fz/Dsh complex.

3.4.6 Localisation of RASSF10, but not RASSF9 is dependent on Frizzled and Dishevelled

Since distal PCP proteins are dependent on Fz for their cortical localisation, I tested whether RASSF9 and RASSF10 localisation is affected by loss of Fz or Dsh. Therefore, I combined the ubi-GFP-RASSF9/10 lines with *fz* and *dsh* mutants on FRT chromosomes. fz^{P21} is a planar polarity specific allele encoding for a truncated version of Fz (Jones et al., 1996). dsh^{3} is a lethal allele for Dsh, affecting both planar cell polarity and Wg-signalling (Yanagawa et al., 1995, Strutt et al., 2006). Mitotic clones mutant for either *fz* or *dsh* had no visible effect on the subcellular localisation of GFP-RASSF9 in L3 wing imaginal discs (Figure 3.14A-A'', C-C''). Strikingly, GFP-RASSF10 was barely detectable in both *fz* and *dsh* mutant clones, while E-cadherin was unaffected (Figure 3.14B-B'', D-D'').

In late larval wing imaginal discs Dsh is mainly cytoplasmic, but also shows a weak symmetric membrane localisation, which has been shown to be independent of Fz whereas, from the pupal stages on, localisation of Dsh at the membrane requires Fz (Axelrod, 2001). Though Fz has been shown to lose its asymmetric localisation in *dsh* clones, it remains localised to the membrane, at least in pupal wings (Strutt, 2001). These findings suggest that, in the case of larval wing imaginal discs, Dsh will still be at the membrane in *fz* clones and Fz will be present in *dsh* clones. The loss of RASSF10 localisation in *dsh* and in *fz* clones therefore implies that RASSF10 stability and its localisation at the membrane in wing imaginal discs most likely requires the presence of both Dsh and Fz simultaneously. Interestingly, GFP-RASSF10 localised in a clear border at the edge of *fz* mutant clones in wing imaginal discs (Figure 3.14B-B''). This

observation resembles the effect seen for the localisation of, for example, Fz, Fmi and Pk in cells neighbouring *fz* mutant clones in pupal wings, where a loss of *fz* affects the polarity of bordering wild type cells due to its non-autonomous effect (Tree et al., 2002, Strutt, 2001, Usui et al., 1999).

Additionally to the effect on RASSF10 levels in *fz* and *dsh* mutant clones described above, I observed that Fz and Dsh also affected RASSF10 levels in S2 cells (Figure 3.15). Co-expression of Fz with RASSF10 caused an increase in RASSF10 levels, compared to the GFP-myc control, while expression of Dsh had no noticeable effect on RASSF10 levels. Co-expression of Dsh and Fz led to hyper-phosphorylation of Dsh, visible by the appearance of strong additional bands at higher molecular weight as previously described (Yanfeng et al., 2011). RASSF10 can also induce a mobility shift of Dsh (Figure 3.8), however this effect is much weaker compared to the one induced by Fz (Figure 3.15). Interestingly, co-expression of all three proteins not only greatly stabilised RASSF10, but also led to an increase in Fz and Dsh levels.

In conclusion, I showed that RASSF9 stability and localisation is independent of Fz and Dsh in wing imaginal discs. This suggests that RASSF9 is associated with different proteins at the adherens junctions. Conversely, I found that the stability and localisation of RASSF10 required the presence of both Fz and Dsh. In S2 cells, Fz co-expression leads to Dsh phosphorylation and RASSF10 stabilisation and all three proteins are greatly stabilised when co-expressed. However, the molecular mechanism of this stabilisation remains unclear.

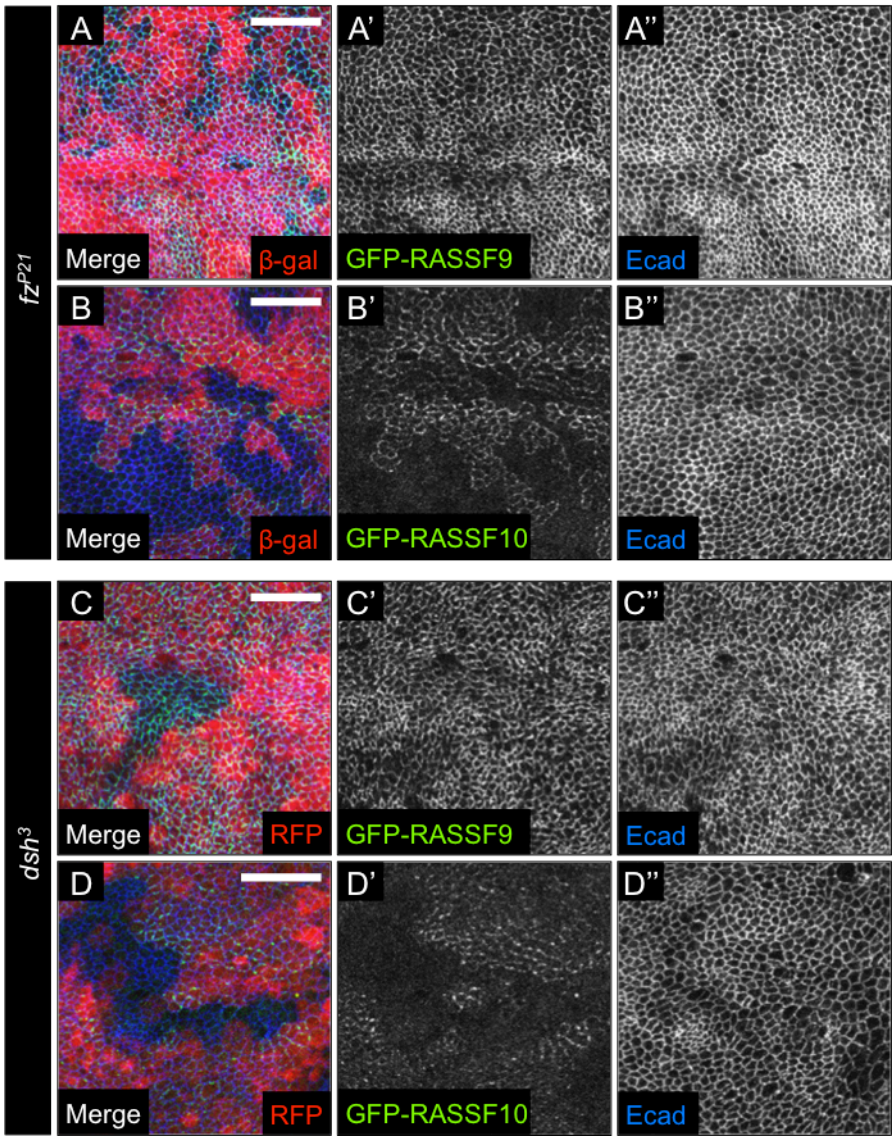

Figure 3.14 - Loss of Frizzled and Dishevelled affects RASSF10, but not RASSF9 localisation in wing imaginal discs.

Planar confocal sections of wing imaginal discs stained for E-cad (A-D''). Mitotic clones were induced with *UbxFlp* for fz^{P21} and *hsFlp* for dsh^{3}. Wild type tissue is lacZ (stained with β-gal) or RFP positive, mutant tissue lacZ/RFP negative. *GFP-RASSF9* and *GFP-RASSF10* were expressed under the *ubi* promoter. GFP-RASSF9 (A-A''', C-C''') and E-cad localisation are not affected, whereas GFP-RASSF10 (B-B''', D-D''') disappears in fz^{P21} and dsh^{3} clones. Posterior is to the left and anterior to the right. Scale bar = 20 µm.

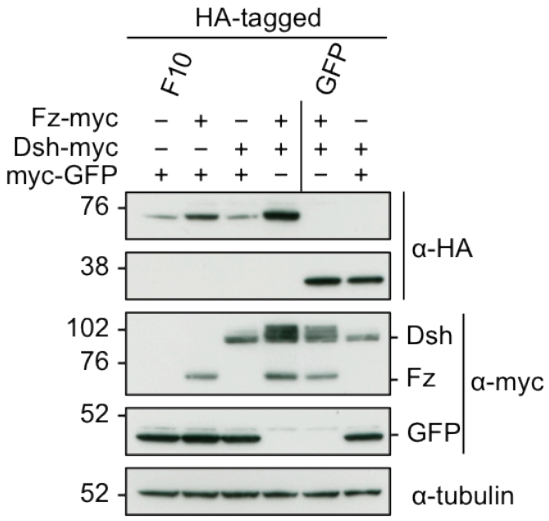

Figure 3.15 - RASSF10 is stabilised by the presence of Dsh and Fz in S2 cell lysates.
S2 cells were transfected with the indicated tagged constructs and cell lysates were analysed by western blot using the appropriate antibodies. Tubulin was used as a loading control. Co-expression of Fz and Dsh leads to stabilisation of RASSF10. Representative western blot of two different transfections.

3.4.7 Gain-of-function phenotypes of RASSF9 and RASSF10

The association with planar cell polarity proteins in S2 cells, the localisation of GFP-tagged RASSF9/10 and RASSF10's stability dependence upon the presence of Dsh and Fz all suggested a potential involvement in planar cell polarity. Ectopic expression of core PCP proteins causes loss of planar cell polarity, which is visible in adult flies in the form of, for example, eye roughness, random orientation of thoracic or abdominal bristles and trichome swirls on the wing. To test whether ectopic expression of RASSF9 and RASSF10 would lead to similar phenotypes, I expressed *UAS-GFP-RASSF9/10* lines with a set of different drivers (*actin-Gal4*, *apterous-Gal4*, *engrailed-Gal4*, *nubbin-Gal4*, *MS1096-Gal4*, *patched-Gal4*, *scabrous-Gal4*, *tubulin-Gal4*). For RASSF9 misexpression, I could not see a PCP phenotype with any driver. Strong expression of GFP-RASSF10 with *tubulin-Gal4* and *apterous-Gal4* elicited a small swirly trichome patch on the wing around the L4 vein (Figure 3.16A, D, G), whereas *UAS-GFP-RASSF9* expression (Figure 3.16C, F) behaved like the *UAS-CD8::GFP* control (Figure 3.16B, E).

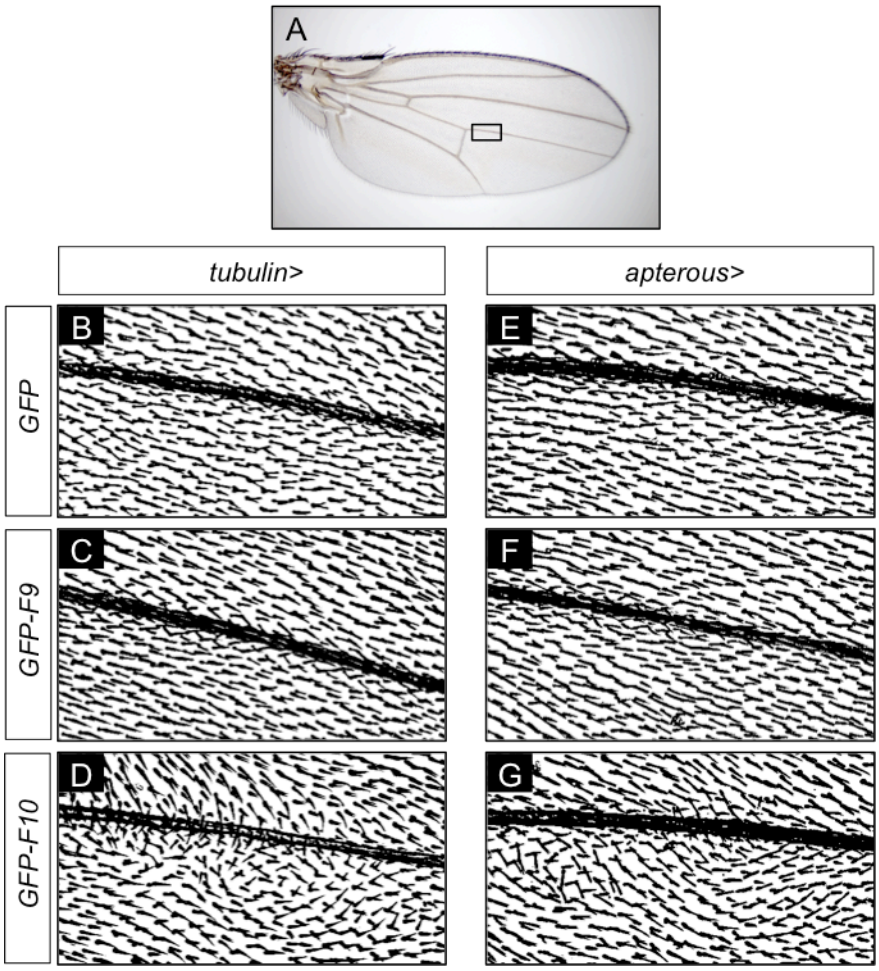

Figure 3.16 - Ectopic expression of RASSF10 causes a small trichome swirl.
(A) Adult wing outlining the position of the trichome swirl. (B-G) Close up of adult wings as outlined in (A). Ectopic expression of *CD8::GFP* (B, E) and *GFP-RASSF9* (C, F) with *tubulin-Gal4* or *apterous-Gal4* does not lead to trichome swirls, whereas expression of *GFP-RASSF10* (D, G) causes small swirls with both drivers.

In conclusion, ectopic expression of RASSF10 only caused a very mild PCP defect with the strong drivers, *tubulin* and *apterous-Gal4*. However, the biological relevance of this gain-of-function phenotype is questionable as none of the other drivers tested caused an obvious defect.

Tubulin-Gal4-driven expression of RASSF9 and RASSF10 also mildly affected wing shape in opposing ways (Figure 3.17A-C). While expression of *GFP-RASSF10* caused significantly longer wings compared to expression of the *GFP* control, *GFP-RASSF9* expression caused rounder wings. Though there was a mild effect on wing shape for the

ectopic expression of RASSF9 and RASSF10, the results should be treated with caution as even expression of GFP elongated the wing compared with *tubulin-Gal4/+* flies.

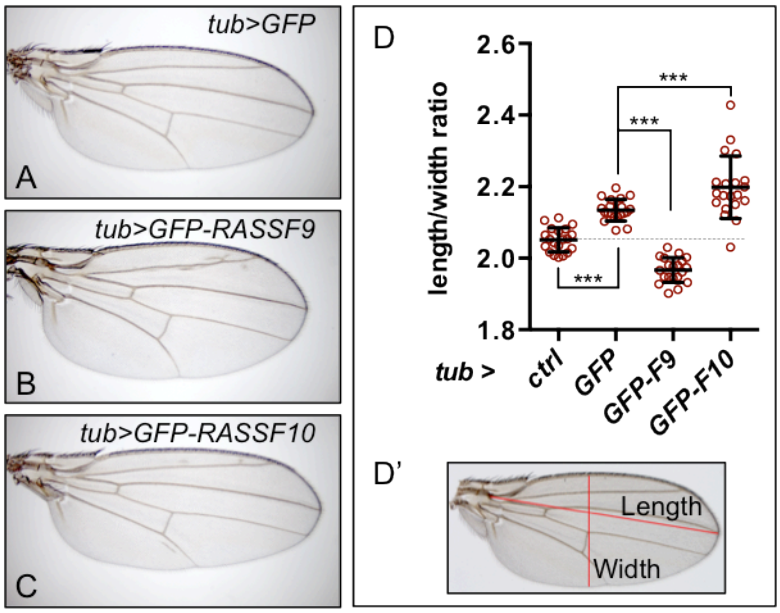

Figure 3.17 - Ectopic expression of RASSF9 and RASSF10 mildly affects wing shape. Adult wings of flies expressing *CD8::GFP* (A), *GFP-RASSF9* (B) or *GFP-RASSF10* (C) with the *tubulin-Gal4* driver. (D) Quantification of the wing roundness. The wing roundness was measured by dividing the length of the wing along the L3 vein by the width of the wing from the anterior to the posterior passing through the cross-vein as seen in (D'). 20 wings were measured for each genotype and error bars represent the mean ± standard deviation. Wing roundness differed significantly between the *tubulin-Gal4/+* control and the *tubulin-Gal4* driven *CD8::GFP* control. Expression of *CD8::GFP* or *GFP-RASSF10* led to elongated wings, with *GFP-RASSF10* being significantly longer than *CD8::GFP* expressing wings. Expression of *GFP-RASSF9* caused significantly rounder wings compared to *CD8::GFP*. (One-way ANOVA with Bonferroni's correction: ***P<0.001).

3.5 RASSF9 and RASSF10 loss of function

Thus far, I have shown that *Drosophila* RASSF9 and RASSF10 can bind to ASPP and PP1 subunits and therefore have the potential to be part of a phosphatase complex with or without ASPP. Interestingly, they are also able to bind to several known RASSF8

interactors, hinting at a potential redundancy between N-terminal RASSFs. Furthermore, I was able to demonstrate that the binding of RASSF9 and RASSF10 to Dsh is conserved in *Drosophila* and to discover the interaction of RASSF10 with Fz. The stability and localisation of ectopic expressed RASSF10, but not RASSF9, is dependent on the Fz receptor and its effector Dsh.

In order to gain insight into RASSF9 and RASSF10 *in vivo* function, I examined their loss-of-function phenotypes. In the following section, I will describe the generation and characterisation of mutant alleles of *RASSF9* and *RASSF10*.

3.5.1 Generation and characterisation of a *RASSF9* mutant

At the beginning of this thesis, *RASSF9/CG13875* was an uncharacterised gene with no available mutant alleles. In order to generate flies mutant for *RASSF9*, I performed imprecise P-element excisions using *P(EP)G18523*, which is inserted in the first intron before the 5' UTR of the *RA* transcript, as illustrated in Figure 3.18A. The P-element was mobilised by crossing to a transposase source, as described in the Material and Methods section (2.4.2). Putative excision males were identified by the absence of the *mini-white* marker in the P-element and individually crossed to a balancer stock, then genotyped by PCR to identify imprecise excisions.

In total, 176 males were screened for a genomic deletion. Out of those, only one male (number 128) was positive for an obvious genomic deletion of approximately 1.7 kbp, and the allele was named $RASSF9^{128}$ (Figure 3.18B). I also recovered one of the precise excisions to use as a control stock in subsequent experiments.

To characterise the alleles, mutant and control *RASSF9* loci were sequenced. This showed that the $RASSF9^{128}$ allele has 1783 bp excised, removing the 5' UTR of transcript *RA*, exon1-3 and 374 bp of exon 4. Furthermore, it contains an additional 30 bp insertion (originating from the P-element) upstream of the remaining exon 4. The *RASSF9* locus of the precise excision had no changes compared to the wild type, except for an additional 58 bp (remains of the P-element) upstream of the 5' UTR (RA).

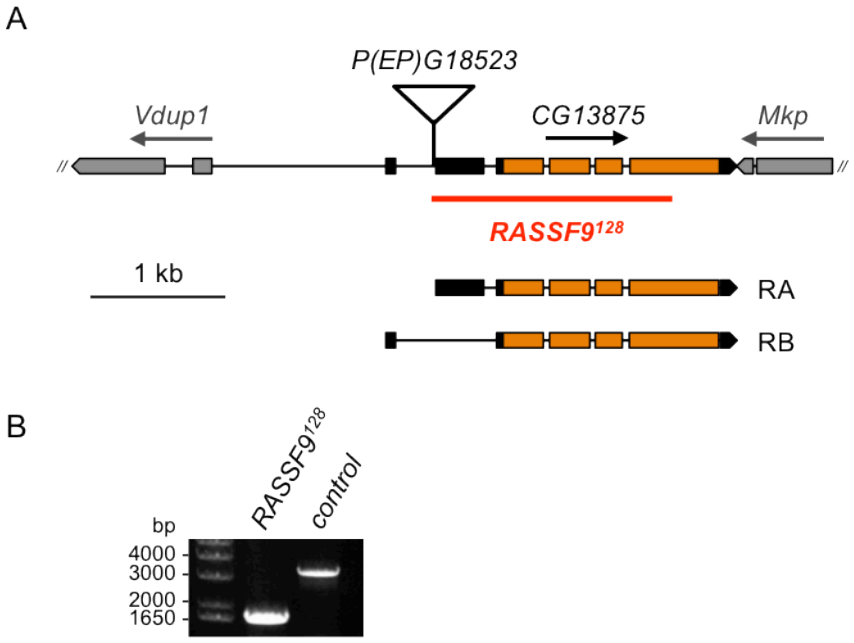

Figure 3.18 - Disruption of *RASSF9/CG13875* by imprecise P-element excision.
(A) Genomic map of the *RASSF9* (*CG13875*) locus, showing the position of the P-element *P(EP)G18523* and the two predicted *RASSF9* transcripts (RA and RB). *RASSF9* exons are highlighted in orange, untranslated regions in black. Neighbouring genes, *Vdup1* and *Mkp*, are highlighted in grey. The generated imprecise excision $RASSF9^{128}$ (marked in red) has the P-element and most of *RASSF9* deleted. (B) PCR with primers flanking the *RASSF9* locus on DNA from $RASSF9^{128}$ or control (precise P-element excision) flies confirming the 1783 bp excision.

$RASSF9^{128}$ mutants were homozygous viable and could be kept as a healthy and stable homozygous stock. I could not detect any visible phenotype, either in the homozygotes, or in *trans* with a deficiency line for *RASSF9 (Df(3L)ED201*). I was unable to detect *RASSF9* transcript by reverse transcriptase PCR (RT-PCR) from fly tissues, presumably because of low expression level, therefore I could not confirm the absence of transcript in the mutant. Nevertheless, since $RASSF9^{128}$ removes all RASSF9 conserved regions, including the entire RA domain, this allele is likely to represent a null.

Given the interaction partners and subcellular localisation of GFP-RASSF9, I examined the RASSF9 mutants for PCP-like phenotypes or phenotypes similar to loss

of ASPP or RASSF8. Mutants in genes involved in PCP usually display misorientation of sensory bristles (mechanoreceptors) and trichomes on the wings and body (see 1.4.2). I examined the *RASSF9*^{128} mutant flies carefully for bristle orientation, but could not detect any abnormalities.

Flies mutant for *ASPP* or *RASSF8* share two common phenotypes. Both have a rough eye phenotype as they are required for correct tissue morphogenesis in the developing retina, and also display a modest overgrowth (Langton et al., 2007, Langton et al., 2009). However, the eyes of flies lacking *RASSF9* appeared completely normal. To address whether there was a growth defect, I measured the wing size for *RASSF9* mutant and *RASSF9* control flies in density-controlled conditions. The measurements showed that the wings of *RASSF9*^{128} flies were significantly smaller (about 6 %) than those of control flies (P<0.001, n=19) (Figure 3.19). This suggests that RASSF9, unlike ASPP and RASSF8, is a positive rather than negative regulator of tissue size. Besides wing overgrowth, loss of *RASSF8* causes a wing rounding phenotype (Langton et al., 2009). This phenotype will be analysed in section 3.6.

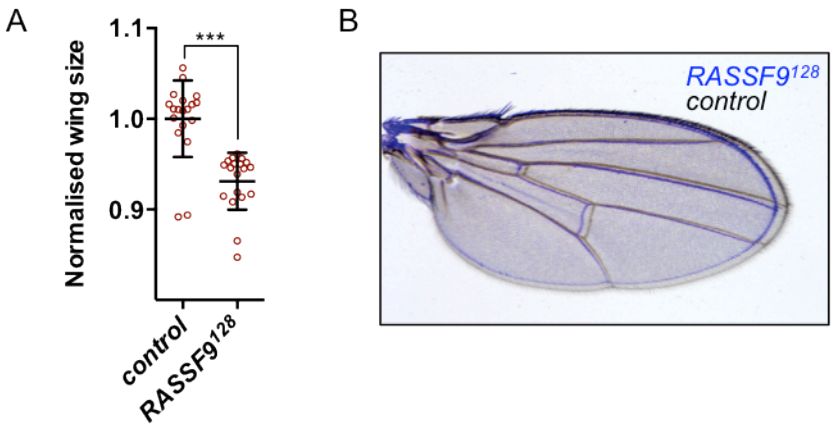

Figure 3.19 - *RASSF9* mutant flies have a mildly reduced wing size.

(A) The wing size (outline of the entire wing) was measured for *RASSF9*^{128} mutant and control flies (precise P-element excision) and normalised against the average wing size of the controls. 19 wings were measured for each genotype and error bars represent the mean ± standard deviation. *RASSF9*^{128} mutant wings are significantly smaller than control wings (Mann-Whitney test: ***P<0.001). (B) Adult wing of *RASSF9*^{128} mutant compared to control fly (precise excision).

3.5.2 Generation and characterisation of *RASSF10* loss-of-function alleles

To generate deletion mutants for *RASSF10/CG32150*, the CRISPR/Cas9 system was used (Port et al., 2014). This was done with the help of Maxine Holder from our lab, who designed and cloned the gRNAs and set up the initial crosses. The system takes advantage of the bacterial CRISPR (clustered regularly interspaced short palindromic repeats) associated nuclease (Cas), which causes site-specific double strand breaks in genomic sites, directed by a complementary CRISPR RNA-containing guide RNA (gRNA). The detailed strategy and description of the CRISPR/Cas9 system can be found in the Material and Methods section in 2.4.3. For the design of the guide RNAs, a gene that lies within the first intron of *RASSF10* had to be taken into account. It encodes for a micro RNA (mir-263b), which has been associated with loss of interommatidial bristles (Hilgers et al., 2010). So as not to interfere with the *mir-263b* expression, gRNA pair B was designed to target the Cas9 nuclease to cut just before exon 2 and within exon 4 and therefore theoretically excising 1546 bp, as seen in Figure 3.20A. As an alternative, gRNA pair C would induce cuts in the first intron and at the end of the first exon, removing 822 bp. Plasmid pairs (B and C) for the expression of the gRNAs were injected into embryos of a germ-line restricted *nos-Cas9* line.

The surviving potential founders were crossed to balancer stock and their progeny screened by PCR for the presence of deletions. For the screening it was important to consider, firstly, that not all of the progeny of one founder would be positive for deletions and, secondly, that deletions within the progeny could also differ. Therefore, I first identified positive founders by genotyping a pool of their female progeny by PCR for the presence of deletions (see Table 2.8 for primer sequences). This pre-screening revealed that gRNA pair B produced three positive founders (out of 35), while with gRNA pair C, one positive founder was obtained (out of 34). In the next step, several males of the progeny of the positive founders were crossed to a *RASSF10* deficiency line (*Df(3L)BSC575*), which would allow immediate phenotypical examination of the next generation and were subsequently genotyped. Using this approach, nine potential alleles for gRNA pair B and three for gRNA pair C were obtained. Subsequent sequencing to characterise the exact cleavage sites revealed that all of the deletions clustered around the predicted Cas9 cutting sites and showed, as expected, variability

within the progeny of one founder (Gratz et al., 2013, Port et al., 2014). I then picked one allele derived from gRNA pair B (*RASSF10*^{B221}) and one from gRNA pair C (*RASSF10*^{C321}) to further characterise. In order to have a *RASSF10* wild type control stock with the same genetic background, I followed the same cross scheme used for the *RASSF10* mutants, beginning with an uninjected male of the original *nos-Cas9* line.

RASSF10^{B221} has 1585 bp excised with an insertion of 3 bp (a 1546 bp deletion was predicted) leaving the 5' UTR and exon 1 unaffected and 635 bp of exon 4 remaining (Figure 3.20A, B). *RASSF10*^{C321} harbours a 839 bp deletion (822 bp were predicted), which excises the entire first exon (see Figure 3.20A, B). In order to test whether transcripts of the remaining exons were still detectable, I performed RT-PCRs. *RASSF10*^{B221} was positive for transcript expression of the 5' UTR and exon 1, and *RASSF10*^{C321} still expressed the remaining exons 2 to 4 (Figure 3.20C). Moreover the transcript levels were not detectably reduced compared to those of the *RASSF10* control.

The results from the RT-PCRs and the sequencing data imply the following regarding translations: *RASSF10*^{B221} mutants most likely express a truncated protein containing the first 118 amino acids encoded by exon 1, which are - depending on precision of the splicing of the remaining intron between exon 1 and exon 4 - followed by a premature stop codon or several missense substitutions and a stop codon. Within exon 4, just after the cleavage site, lies another ATG (out of frame with the first start codon), which could theoretically allow the expression of the C-terminus (aa 390-524). In the case of *RASSF10*^{C321}, a start codon right at the beginning of exon 2 could allow the expression of a N-terminally truncated protein containing 102 of the 107 amino acids of the RA domain and the complete rest of the sequence.

Both *RASSF10*^{B221} and *RASSF10*^{C321} could be kept as a healthy homozygous stock. Mutant flies, either as homozygotes or in *trans* to a deficiency, did not display any PCP defects, but presented sensory bristle defects: missing or additional macrochaetes on the thorax, duplicated bristles at the wing margin and split bristles on the thorax or abdomen. This phenotype will be explored in detail in Chapter 4.

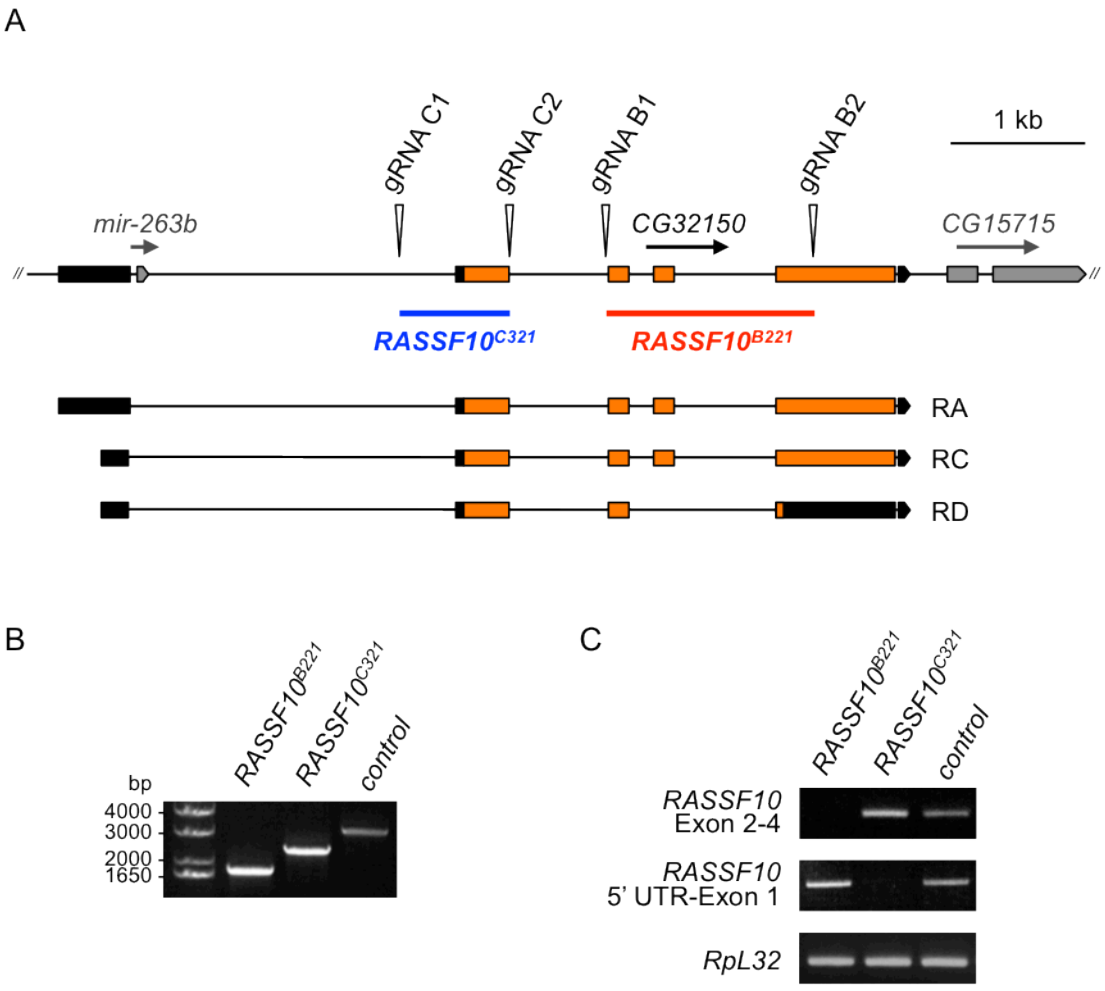

Figure 3.20 - Disruption of *RASSF10/CG32150* using the CRISPR/Cas9 system.

(A) Genomic map of the *RASSF10* (*CG32150*) locus, showing the predicted cut sites of the two gRNA pairs (B and C) used for CRISPR and the three predicted *RASSF10* transcripts (RA, RC and RD). *RASSF10* exons are highlighted in orange, untranslated regions in black. The neighbouring gene, *CG15715*, and the micro RNA *mir-263b* within the first intron of RASSF10 are highlighted in grey. Two different deletion mutants were generated with the CRISPR/Cas9 system. $RASSF10^{B221}$, derived from gRNA pair B (marked in red), has exon 2, exon 3 and part of exon 4 removed and $RASSF10^{C321}$ derived from gRNA pair C (marked in blue) and has the first exon excised. (B) PCR with primers flanking the *RASSF10* locus on DNA from *RASSF10* mutants or control flies confirming the deletions. (C) RT-PCR on mRNA from *RASSF10* mutants or control flies showing that truncated transcripts are still expressed for both deletions.

3.6 Redundancy between N-terminal RASSFs

I have previously shown that RASSF9 and RASSF10 share several binding partners of RASSF8 (3.2.1 and 3.3). Moreover flies mutant for *RASSF8*, *RASSF9* or *RASSF10* are homozygous viable and do not display severe phenotypes. This raised the question whether N-terminal RASSFs could be redundant. To address this hypothesis, I recombined the mutant alleles (*RASSF8* is located on 3R, *RASSF9* and *RASSF10* on 3L) to generate double mutants and a triple mutant. Double and triple mutants were then confirmed by genotyping PCR for the individual alleles. The $RASSF8^{6}$, $RASSF9^{128}$ double mutant flies were homozygous viable and could be kept as a homozygous stock, however, the adult flies seemed less active than their control counterparts. Recombination of $RASSF8^{6}$ and $RASSF10^{B221}$ resulted also in homozygous viable flies, which were very weak and could not be maintained as a homozygous stock. Triple mutants of $RASSF8^{6}$, $RASSF9^{128}$, $RASSF10^{B221}$ were, as with the $RASSF8^{6}$, $RASSF10^{B221}$ double mutants, homozygous viable but could not be kept as a homozygous stock. Double and triple mutants had, like the $RASSF8^{6}$ single mutant, an obvious eye roughness and round wings, which appeared even rounder than those of $RASSF8^{6}$.

Eunice Chan from our lab had previously examined the round wing phenotype of the $RASSF8^{6}$ mutants. She found that RASSF8, together with its binding partner Sec15 of the exocyst complex, are needed for the docking of Rab11 recycling endosomes to the membrane in pupal wings and eyes, as Rab11 containing endosomes were accumulated in both $RASSF8^{6}$ and *sec15* mutants (unpublished results). This led her to propose that RASSF8 is needed to facilitate polarised vesicle trafficking to the growing junctions thereby promoting cell-cell rearrangements leading to growth along the P-D axis. Since RASSF9 and RASSF10 were also able to bind Sec15 (see 3.3), I tested for redundancy between the N-terminal RASSFs in P-D wing elongation.

Firstly, I measured the wing roundness for the three N-terminal single mutants and their individual controls (Figure 3.21A). $RASSF8^{6}$ single mutants had 15% rounder wings than control. $RASSF9^{128}$ mutant wings were also slightly rounder, (2.5% when compared to the *RASSF9* control), whereas $RASSF10^{B221}$ mutants were modestly different from controls (1.3% rounder).

Next, I analysed the double and triple N-terminal RASSF mutants and compared them to the *RASSF8*^{6} single mutant (Figure 3.21B). Combinatorial loss of RASSF9 and RASSF10 led to a stepwise increase in wing roundness compared with *RASSF8*^{6} (2.5% for *RASSF8*^{6}, *RASSF9*^{128} double mutants; 5% for *RASSF8*^{6}, *RASSF10*^{B221} double mutants; 6.7% for, *RASSF8*^{6}, *RASSF9*^{128}, *RASSF10*^{B221} triple mutants). I then tested whether the double and triple mutants could be rescued by expression of *ubi-GFP-RASSF9/10* constructs. To have controls with the same genetic background as the *ubi-GFP-RASSF9/10* lines, I generated an *ubi-GFP* line with the plasmid used for the *ubi-GFP-RASSF9/10* lines (see 3.4.5), which was inserted using the PhiC31 integrase-mediated system into the same genomic locus (2L 28E7). I combined the three different lines accordingly with the *RASSF8*^{6} single, the *RASSF8*^{6}, *RASSF9*^{128} and the *RASSF8*^{6}, *RASSF10*^{B221} double mutants as well as the triple mutant and measured their wing roundness (Figure 3.21A, B).

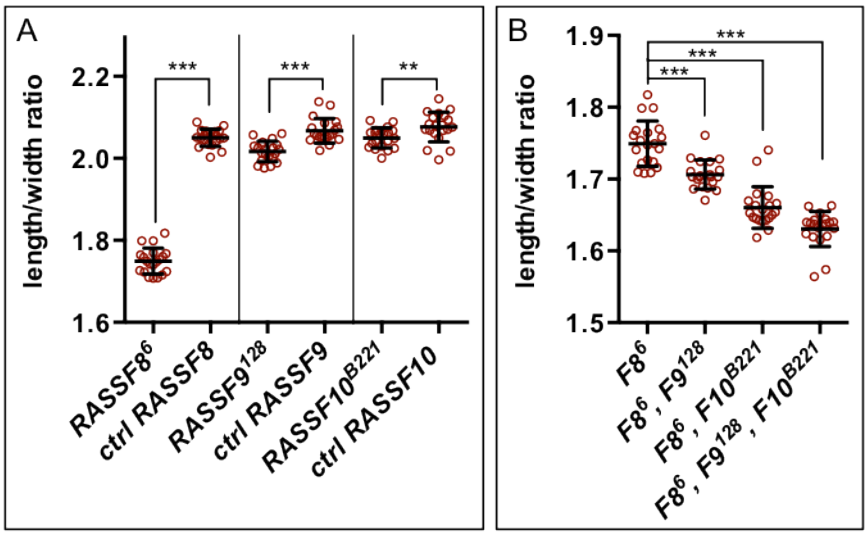

Figure 3.21 - Wing roundness of *RASSF8*^{6}, *RASSF9*^{128} and *RASSF10*^{B221} single, double and triple mutants.

The wing roundness was determined as described in Figure 3.17C. 20 wings were measured for each genotype and error bars represent the mean ± standard deviation. (A) Wings of N-terminal *RASSF* mutants are significantly rounder than wings of their controls (Mann-Whitney test: ***P<0.001, **P=0.0051). (B) The wing roundness of *RASSF8*^{6} mutants is significantly increased upon loss of *RASSF9*^{128} or/and *RASSF10*^{B221} (One-way ANOVA with Bonferroni's correction: ***P<0.001). n = 20 for all genotypes.

This analysis led to several puzzling observations. First, ectopic expression of RASSF9 under the *ubiquitin* promoter enhanced rather than rescued the wing roundness of the double and triple mutant combinations (Figure 3.22A). This is consistent with the previous finding that RASSF9 expression under control of *tubulin-Gal4* caused a slight round wing phenotype (Figure 3.17). Secondly, while it was clear that ectopic expression of RASSF10 under the *ubiquitin* promoter did not significantly rescue the double and triple mutant phenotypes, the enhancement of wing roundness in the triple mutant compared with the $RASSF8^{6}$, $RASSF10^{B221}$ double mutants (see Figure 3.21B) was no longer observed when combined with the *ubi-GFP* control construct (Figure 3.22B). Thus, it is likely that genetic background influences the wing roundness phenotypes elicited by N-terminal RASSF mutations. Although much care was taken in generating the correct control stocks for the wing roundness analysis of the mutant combinations in Figure 3.21, these results should be interpreted with caution in light of the rescue results. I therefore cannot conclude on the potential redundancy between N-terminal RASSF proteins based on these experiments.

The most robust cellular phenotype of the *RASSF8* mutants is the accumulation of Rab11 endosomes in the cytoplasm, while other endosomal markers such as Rab5 or Rab7 are unaffected (Eunice Chan, unpublished observations). In order to test the redundancy between N-terminal RASSF proteins using Rab11 localisation as a readout, I generated a triple mutant stock on a double *FRT82B, FRT2A* chromosome. Hence, within one imaginal disc, mitotic clones mutant for *RASSF8* or *RASSF9, RASSF10* or *RASSF8, RASSF9, RASSF10* (in overlapping areas) could be generated and compared to each other. Using this approach, I found that Rab11 strongly accumulated in $RASSF8^{6}$ mutant clones of wing imaginal discs (outlined in red), whereas loss of *RASSF9* and *RASSF10* (outlined in green) did not affect Rab11 distribution (Figure 3.23A-A’’’). Moreover, the Rab11 enrichment did not seem to be enhanced in the triple mutant clones (outlined in yellow) when compared to the *RASSF8* single mutant clones. I also tested whether E-cadherin, as a potential cargo of Rab11 endosomes (Figure 3.23B-B’’’), or their common binding partner Baz (Figure 3.23C-C’’’) were affected in triple mutant clones in wing imaginal discs. However, I saw no evidence of redundancy in L3 wing discs using these markers.

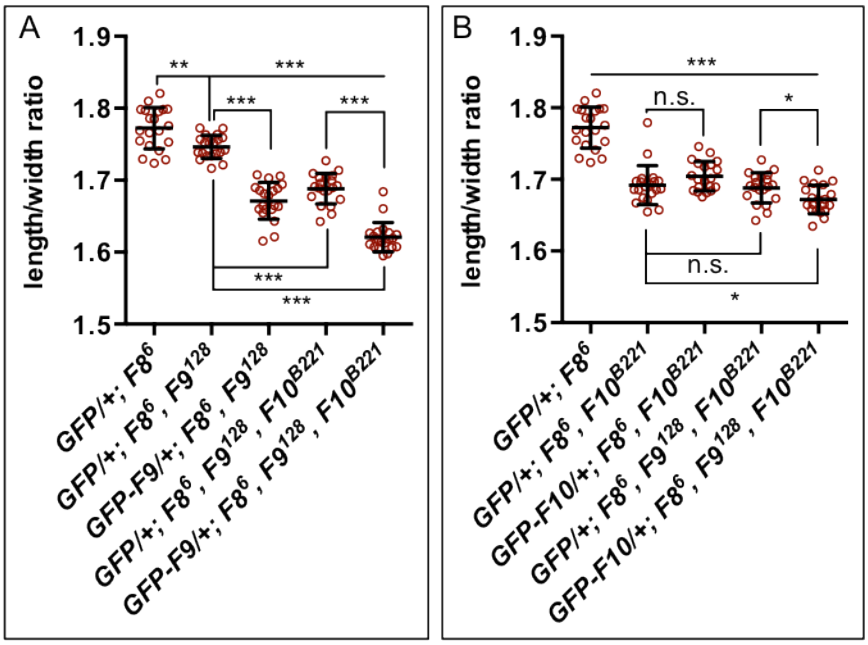

Figure 3.22 - Ectopic expression of RASSF9 or RASSF10 do not rescue the enhanced wing roundness of double and triple mutants.

The wing roundness was determined as described in Figure 3.17C. 20 wings were measured for each genotype and error bars represent the mean ± standard deviation. (A) Ubiquitous expression of GFP-RASSF9 does not rescue the phenotype of double and triple mutants and even makes the wings rounder (Mann-Whitney test: ***P<0.001, **P=0.0035). (B) Ubiquitous expression of GFP-RASSF9 does not rescue the phenotype of double and triple mutants (Mann-Whitney test: ***P<0.001, *P=0.0262).

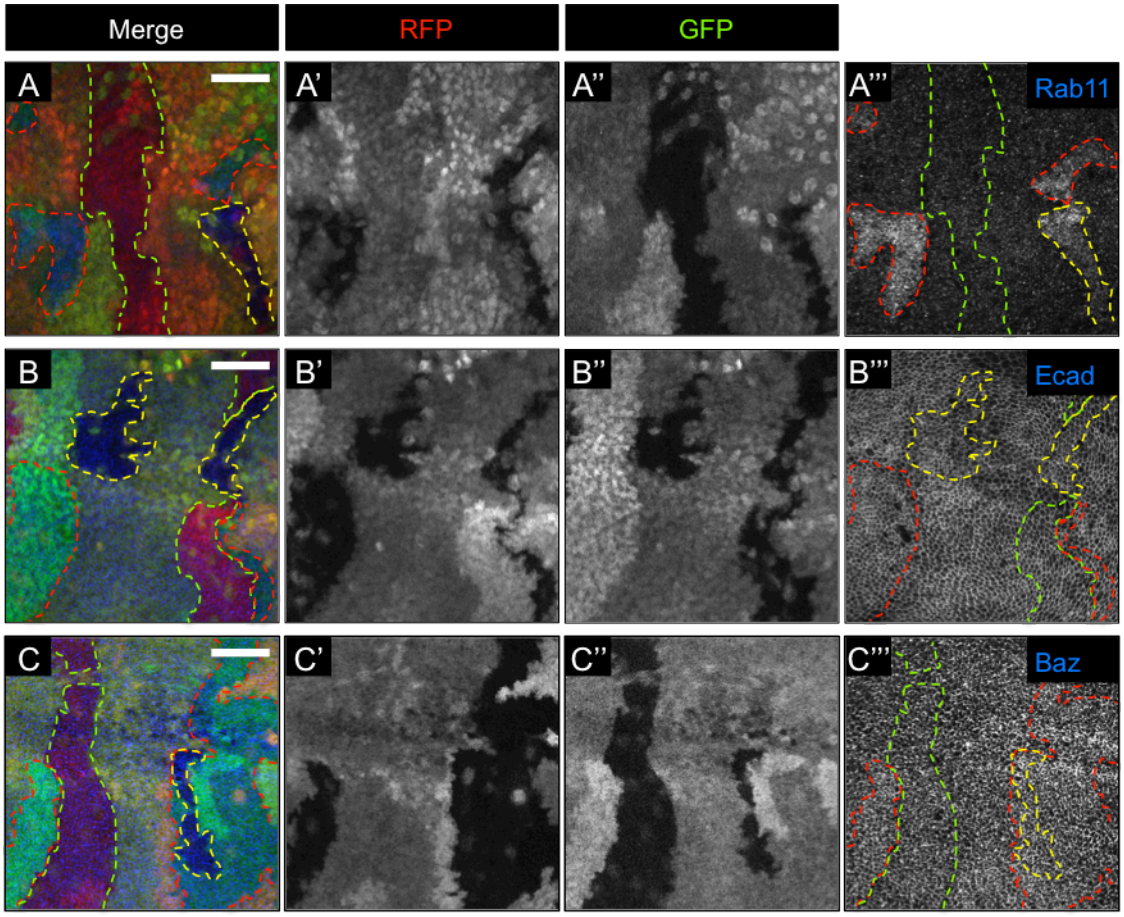

Figure 3.23 - Staining of Rab11, Ecad and Bazooka in *RASSF8*^{6} single, *RASSF9*^{128}, *RASSF10*^{B221} double and *RASSF8*^{6}, *RASSF9*^{128}, *RASSF10*^{B221} triple mutant clones.

Planar confocal sections of wing imaginal discs with *hsFLP* induced mitotic clones stained for Rab11 (A-A'''), Ecad (B-B''') or Baz (C-C'''). *RASSF8* wild type tissue is RFP positive and *RASSF8*^{6} mutant tissue is RFP negative (outlined in red). Wild type tissue for *RASSF9*, *RASSF10* is GFP positive and *RASSF9*^{128}, *RASSF10*^{B221} double mutants are GFP negative (outlined in green). Mitotic clones mutant for *RASSF8*^{6}, *RASSF9*^{128}, *RASSF10*^{B221} are outlined in yellow. Posterior is to the left and anterior to the right. Scale bar = 30 µm.

3.7 Concluding remarks

In this chapter, I have established an interaction network for *Drosophila* RASSF9 and RASSF10 performing co-IP experiments with S2 cells, based on the interactors of their potential human homologues. Even though RASSF9 and RASSF10 bear limited resemblance to their human counterparts, the interaction network is highly conserved.

They can form a trimeric complex with ASPP/PP1 and, moreover, associate independently of ASPP with all PP1 catalytic subunits. This gives RASSF9 and RASSF10 the potential to function both as regulatory subunits and as specificity subunits for PP1. However, whether they can function as such *in vivo* still needs to be established.

I have shown that RASSF9 and RASSF10 share other known RASSF8 binding partners - namely, Baz, Sec15 and SCAR - suggesting that N-terminal RASSFs might function in similar ways. Whether there is an overlap, and hence a redundancy, in their function or whether it is time and tissue-specific needs to be further investigated. I demonstrated that in the case of the round wing phenotype of *RASSF8* mutants, a redundancy between N-terminal RASSFs is unlikely to be biologically significant. First, despite the modest incremental increases in wing roundness in double and triple mutant combinations (Figure 3.21B), RASSF9 or RASSF10 ubiquitous expression did not rescue the triple mutant flies (Figure 3.22A, B). Furthermore, on a cellular basis, the Rab11 accumulation in *RASSF8* clones was not modified by RASSF9/10 loss (Figure 3.23A-A'''), at least in the L3 wing disc. These experiments could be repeated in pupal wings and eyes, where the RASSF8 defects are most obvious (Langton et al., 2009).

Thus, while it is doubtful that N-terminal RASSFs have redundant functions in the P-D axis elongation of the pupal wing, a redundancy in other tissues or developmental stages cannot be ruled out. The observation that $RASSF8^{6}$, $RASSF10^{B221}$ double mutants and $RASSF8^{6}$, $RASSF9^{128}$, $RASSF10^{B221}$ triple mutants were less healthy than the $RASSF8^{6}$ single mutant and that homozygous stocks could not be established, supports the possibility of redundant functions. However, this could also be due to a cumulative effect of losing the functions of several genes functioning in separate processes on fly viability. Therefore, the mechanistic basis for this viability would need to be established and studied in order to pursue the possible redundancy between N-terminal RASSF proteins.

RASSF9 and RASSF10 also have specific interactors, which are not associated with RASSF8. They can both bind to Dsh (Figure 3.8) and RASSF10 can also bind to Fz (Figure 3.11), suggesting a potential function in canonical Wg/Fz or PCP signalling. This connection is further supported by the ability of GFP-tagged transgenes to planar polarise in pupal wings (Figure 3.13). In the case of RASSF10, however, the evidence is

more suggestive, as its stability is dependent on both Dsh and Fz (Figure 3.14) and strong misexpression of RASSF10 can cause mild PCP defects, whereas no such effects were observed for RASSF9 (Figure 3.16). The *RASSF10* mutants, albeit not showing classical PCP defects, have a defect of their sensory bristles, which derive from a series of asymmetric cell divisions from a single SOP cell. The core PCP components and Baz, among others, are required to establish the polarity within the SOP cell prior to the first asymmetric division (Furman and Bukharina, 2011), thus suggesting that RASSF10 might be linked to these proteins in this context. This theory is supported by previous findings, which have shown *RASSF10* mRNAs to be highly enriched in the proneural clusters of the wing disc that give rise to the SOP cells (Reeves and Posakony, 2005) and SOP cells of the pupal notum (Buffin and Gho, 2010). Moreover, Baz, Dsh and Fz are all known to be phosphorylated on multiple residues and Baz can be dephosphorylated *in vitro* by PP1 (see 1.3.4 and 1.4.7). This led us to speculate these might be substrates of a RASSF10/PP1 complex in SOPs. *RASSF9* mutants exhibit no obvious phenotype, except for slight undergrowth (Figure 3.19), which makes it extremely difficult to address its developmental function. Thus, I decided to make the function of RASSF10 the focus of my research, as described in the next chapter, and addressed the function of RASSF9 only in this context.

Chapter 4 The function of RASSF9/10 in the formation of external sensory organs

The *Drosophila* external sensory organs (bristles), such as mechanoreceptors and chemoreceptors are part of the peripheral nervous system (PNS) and originate from a single cell - the sensory organ precursor (SOP). The selection of the SOP within the epithelial cell field is a complex process, which involves the action of different proneural proteins, their regulators and Notch-mediated lateral inhibition (see 1.7.1). Once the SOP cell is selected, it will divide asymmetrically into two cells of different fate and will, after subsequent asymmetric divisions, give rise to the four cells that form the sensory organ. In the case of mechanoreceptors, these are the neuron, the sheath, the socket and the shaft cell (see Figure 1.6). The key to the asymmetric division is the establishment of the asymmetric localisation of cell fate determinants. The three potential interactors of RASSF10 - Fz, Dsh and Baz- are all required to establish the asymmetry of the SOP cell. PCP facilitates the initial symmetry breaking within the SOP cell and also orients the division angle. Fz and Dsh promote the localisation of the Baz-aPKC-Par6 complex at the posterior cortex, whereas Stbm and Prickle promote the anterior localisation of the Dlg-Pins-Gα_i complex (see 1.7.2). The asymmetric and opposite localisation of the Baz-aPKC-Par6 complex and Dlg-Pins-Gα_i complex ultimately lead to the asymmetric localisation of the cell fate determinants, which, upon cell division, are unequally distributed into the daughter cells and ultimately induce them to adopt distinct identities - pIIa and pIIb (see 1.7). How Fz/Dsh link to the Baz-aPKC-Par6 complex to localise it to the posterior cortex of the SOP remains unknown, but RASSF10 is a potential candidate.

In this thesis chapter, I will address whether RASSF10 is linked to asymmetric cell divisions of SOPs. Therefore, I will first characterise the *RASSF10* loss-of-function phenotype and explore the subcellular localisation of endogenous RASSF10. Furthermore, I will present genetic interactions between *RASSF10* and different ACD machinery components. Finally, asymmetric divisions of SOPs in *RASSF10* mutants will be analysed by live imaging.

4.1 Loss of function of RASSF10 causes an external sensory organ defect

As described in section 3.5.2, the two different mutant *RASSF10* alleles, $RASSF10^{B221}$ and $RASSF10^{C321}$, display an external sensory bristle defect. The two most frequent defects were observed in the sensory bristles of the wing margin and in the thoracic macrochaetes. In the notal macrochaetes, two different defects were present: individual macrochaetes were either missing or occurred at random positions (Figure 4.1A). In a few cases, I observed duplications of individual thoracic microchaetes with a single socket (Figure 4.1B), which was most frequent in abdominal microchaetes (Figure 4.1C). Individual bristles of the wing margin were duplicated (Figure 4.1D, E).

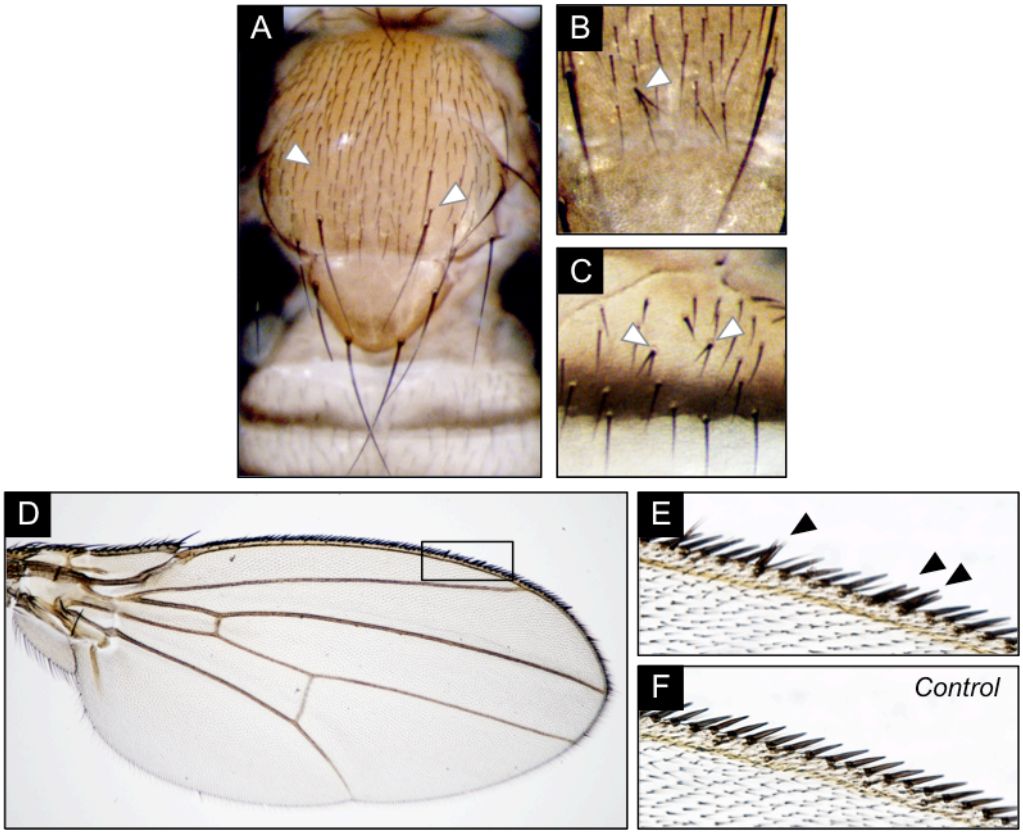

Figure 4.1 - *RASSF10* mutants have an external sensory organ defect.
(A-E) Images of an adult $RASSF10^{B221}$ mutant fly, bristle defects are indicated by white and black arrows. $RASSF10^{B221}$ mutants have missing and extra thoracic macrochaetes (A), split microchaetes on thorax (B) and abdomen (C). Wing of an adult $RASSF10^{B221}$ mutant fly (D, E) with duplicated stout bristles (E) and wild type control fly (F).

Overall the defect seemed stronger for the *RASSF10*^{B221} allele compared to *RASSF10*^{C321}, suggesting that *RASSF10*^{C321}, which encodes for a N-terminally truncated protein missing the first 134 aa, is a hypomorph. To address the question whether RASSF9 has redundant functions with RASSF10, I recombined the *RASSF9*^{128} allele with the *RASSF10*^{B221} allele using the same strategy as for the double and triple mutants (see 3.6). *RASSF9*^{128}, *RASSF10*^{B221} double mutants were homozygous viable and showed the same external sensory organ defects as *RASSF10*^{B221}.

4.1.1 *RASSF10* mutants have duplicated stout bristles

In order to characterise the different *RASSF10* mutants, I quantified the most frequent defects - the margin bristle defect and the thoracic missing/extra macrochaete defect.

The anterior wing margin harbours three types of bristles: firstly, the singly innervated stout (mechanosensory) bristles that are found on the dorsal side of the anterior wing margin, secondly, the singly innervated slender (mechanosensory) bristles located on the ventral side of the anterior wing margin and on the dorsal and ventral side towards the distal wing margin and lastly the multiply innervated recurved (chemosensory) bristles (see Figure 4.2B and (Hartenstein and Posakony, 1989)). The bristles of the posterior wing margin resemble the slender bristles, but are not innervated. I decided to quantify the defect for the stout bristles of the anterior wing margin (see Figure 4.2A, B), as these are thicker compared to the other bristles types and therefore defects are easier to score. I counted the number of duplicated bristles for both wings from 50 flies for each genotype. At the same time the flies were analysed for the missing and extra macrochaete defect (see 4.1.2).

Firstly, I analysed the defects for the different *RASSF10* alleles - *RASSF10*^{B221} and *RASSF10*^{C321} - and also for the *RASSF9*^{128}, *RASSF10*^{B221} double mutant. The quantification of the stout bristle defect in females revealed the following for the different alleles of *RASSF10* (Figure 4.2C). 60% of the wings of *RASSF10*^{B221} mutants had duplicated stout bristles. Wings harbouring the defect had 1 to 3 duplicated bristles, with an average of 0.87 duplicated bristles per wing. On the contrary, the defect was much milder in *RASSF10*^{C321} mutants, as just 10% of the wings of were affected (0.1 duplicated bristles per wing). *RASSF9*^{128}, *RASSF10*^{B221} double mutants caused a defect

comparable to the *RASSF10*^{B221} mutant (63%, 0.9 duplicated bristles per wing) (n.s.) (Table 7.3). *RASSF10* control flies did not show the defect (1%).

The defect of *RASSF10*^{B221} (56%, 0.74 duplicated bristles per wing) and *RASSF9*^{128}, *RASSF10*^{B221} double mutant (59%, 0.92 duplicated bristles per wing) was not enhanced over a deficiency (*Df(3L)BSC575*) (n.s.) (Table 7.3). This suggests that the *RASSF10*^{B221} allele is a null allele for *RASSF10* and that the N-terminal 118 aa, encoded by the first exon, are not sufficient for RASSF10 function. In contrast, the defect of *RASSF10*^{C321} was doubled over the deficiency (22%), supporting the notion that the N-terminally truncated protein might still retain some function and that the *RASSF10*^{C321} allele is likely to be a hypomorph (P=0.0381) (Table 7.3). Therefore the *RASSF10*^{B221} allele was exclusively used for all the following experiments. Moreover, only females were analysed, as the margin bristle defect was approximately half as strong in *RASSF10*^{B221} males compared to females (P<0.0001) (Table 7.3).

In order to confirm whether the bristle defect was indeed due to *RASSF10* loss of function, I tested whether expression of *ubi-GFP-RASSF10* could rescue the defect of *RASSF10*^{B221} and *RASSF9*^{128}, *RASSF10*^{B221}. Moreover, I wished to test whether expression of *ubi-GFP-RASSF9* could rescue loss of RASSF10, and therefore suggesting redundant functions for RASSF9 and RASSF10, even though loss of *RASSF9* on its own did not cause any stout bristle duplication (Figure 4.2E). Indeed, as seen in Figure 4.2D, expression of *ubi-GFP-RASSF10* almost completely abolished the stout bristle defect, for both *RASSF10*^{B221} (1%) and *RASSF9*^{128}, *RASSF10*^{B221} (3%). Expression of *ubi-GFP-RASSF9* could not rescue the defect of either mutant (n.s.) (Table 7.3) and on the contrary even seemed to slightly worsen the phenotype compared to the GFP control (P=0.0047) (Table 7.3). The defect of *RASSF10*^{B221} mutants significantly differed from *ubi-GFP; RASSF10*^{B221} flies (P=0.0031) (Figure 4.2 and Table 7.3), thus indicating that the *RASSF10*^{B221} stout bristle defect varies in different genetic backgrounds. Significances higher than this background noise P value should therefore be treated with caution, as such phenotypic differences might not be biologically relevant.

To further address whether there is a redundancy between the N-terminal RASSFs, I also quantified the defect for *RASSF8*^{6}, *RASSF10*^{B221} double mutants and *RASSF8*^{6}, *RASSF9*^{128}, *RASSF10*^{B221} triple mutants (Figure 4.2E).

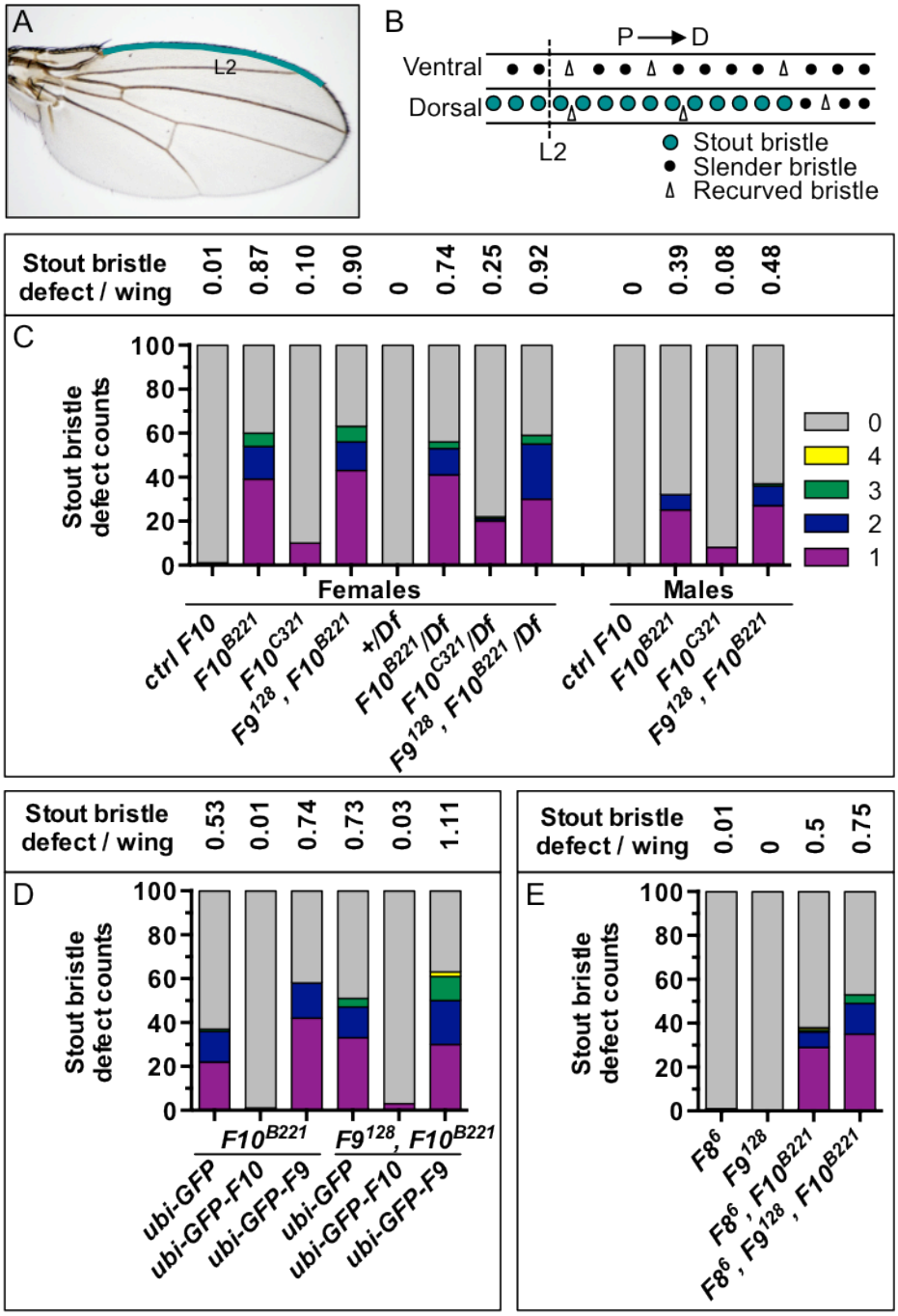

Figure 4.2 - Stout bristle duplication defect of *RASSF10* mutants.

(A) Wing of an adult fly outlining the stout bristle region on the anterior wing margin. (B) Schematic of the wing margin showing the different bristle types (adapted from (Hartenstein and Posakony, 1989)). The dorsal side of the anterior wing margin harbours singly innervated stout bristles and multiply innervated recurved bristles, whereas the ventral row consists of slender bristles and recurved bristles. (Continued on next page)

Figure 4.2 (Continued from previous page) - (C-E) Quantification of duplicated stout bristles for 100 wings (left and right wing of females, males in (C)) for each of the indicated genotype. For each wing, the number of duplicated bristles was counted. The average stout bristle defect per wing is written above the chart. (C) Stout bristle defect in different *RASSF10* mutants (*Df*: *Df(3L)BSC575,* deficiency line for *RASSF10*). (D) Expression of *ubi-GFP-RASSF10* but not *ubi-GFP-RASSF9* rescues the stout bristle defect of $RASSF10^{B221}$ and $RASSF9^{128}$, $RASSF10^{B221}$. (E) Stout bristle defect in $RASSF8^{6}$ single, $RASSF9^{128}$ single, $RASSF8^{6}$, $RASSF10^{B221}$ double and $RASSF8^{6}$, $RASSF9^{128}$, $RASSF10^{B221}$ triple mutants. Statistics can be found in Table 7.3 in the Appendix.

$RASSF8^{6}$, as with $RASSF9^{128}$, did not exhibit a defect on its own. The $RASSF8^{6}$, $RASSF10^{B221}$ double mutants (38%) and $RASSF8^{6}$, $RASSF9^{128}$, $RASSF10^{B221}$ triple mutants (53%) displayed duplicated stout bristles, however, the defect was slightly decreased and not increased compared to $RASSF10^{B221}$ alone (P= 0.0045 for $RASSF8^{6}$, $RASSF10^{B221}$ and n.s. for $RASSF8^{6}$, $RASSF9^{128}$, $RASSF10^{B221}$) (Table 7.3). Taken together, it seems very unlikely that N-terminal RASSFs share overlapping functions in the formation of the mechanoreceptors.

4.1.2 *RASSF10* mutants have a missing macrochaete defect

The thorax of an adult fly harbours exactly 22 macrochaetes (excluding the 4 humeral bristles of the prethorax), which are located at fixed positions (illustrated in Figure 4.3A). I counted for each thorax the number of missing macrochaetes and as well as the presence of extra macrochaetes.

The quantifications of the missing macrochaete defect (Figure 4.3C-E) overall mirror and thus support the results of the stout bristle defect. The missing macrochaete defect was stronger for $RASSF10^{B221}$ flies (40%) and than for $RASSF10^{C321}$ (12%) (Figure 4.3C). However, unlike the stout bristle defect, the defect was more pronounced in $RASSF9^{128}$, $RASSF10^{B221}$ double mutants (with 68%) and enhanced when crossed to the deficiency line for both, $RASSF10^{B221}$ and $RASSF10^{C321}$. Affected flies had in general one or two (less often three) mechanoreceptors missing. Unlike the stout bristle defect the difference between males and females was not significant (Table 7.3).

Furthermore, the rescue experiment with the different *ubi-GFP* lines (Figure 4.3D and Table 7.3), showed a clear rescue with the expression of *ubi-GFP-RASSF10* for both $RASSF10^{B221}$ single and $RASSF9^{128}$, $RASSF10^{B221}$ double mutants, whereas expression of *ubi-GFP-RASSF9* did not. The missing macrochaete defect supported the result of the stout bristle defect that N-terminal RASSFs are unlikely to be redundant in this context, as loss of *RASSF8*, or *RASSF8* and *RASSF9*, did not worsen the missing macrochaete phenotype of $RASSF10^{B221}$ (Figure 4.3E and Table 7.3).

The different macrochaetes on the notum are responsive to the expression of different prepatterning genes, such as Wingless, Pannier, Iroquois, which activate the expression of proneural genes in their expression zone (reviewed in (Simpson, 2007)). Interestingly, the positions of the missing macrochaete in $RASSF10^{B221}$ and $RASSF9^{128}$, $RASSF10^{B221}$ mutants (Figure 4.3B, the Wg expression zone is highlighted in green), did not display a specific pattern, as macrochaete on all positions were affected.

Unlike the two defects described above, the extra macrochaete phenotype (see Figure 4.4B and Table 7.3) did not appear to be linked to RASSF10 function. The two *RASSF10* alleles as well as the control flies, but not the $RASSF9^{128}$, $RASSF10^{B221}$ double mutants, all had extra macrochaetes (Figure 4.4A). However, when crossed to the deficiency line the $RASSF9^{128}$, $RASSF10^{B221}$ mutants showed extra macrochaetes to a similar degree as the single *RASSF10* mutants and also to the flies heterozygous for the deficiency. This suggests that a mutation eliciting the extra macrochaete defect is present in the background of the deficiency line. In addition, expression of *ubi-GFP-RASSF10* did not rescue the defect of $RASSF10^{B221}$ mutants (Figure 4.4C). Similar to the $RASSF9^{128}$, $RASSF10^{B221}$ double mutants, the other recombinants with $RASSF10^{B221}$, the $RASSF8^{6}$, $RASSF10^{B221}$ double mutants and the $RASSF8^{6}$, $RASSF9^{128}$, $RASSF10^{B221}$ triple mutants did not display a strong defect (Figure 4.3D), suggesting that the background defect was lost when the alleles were recombined. Taken together, the extra macrochaete phenotype is most certainly unrelated to loss of RASSF10 function and could have derived from the genetic background of the *RASSF10* deficiency line, when the stocks for the *RASSF10* alleles were originally made (see 3.5.2). Moreover, the differences in the genetic background could be the reason why the missing bristle defect was stronger in $RASSF9^{128}$, $RASSF10^{B221}$ double mutants compared to $RASSF10^{B221}$ single mutants, rather than a potential redundancy between RASSF9 and RASSF10.

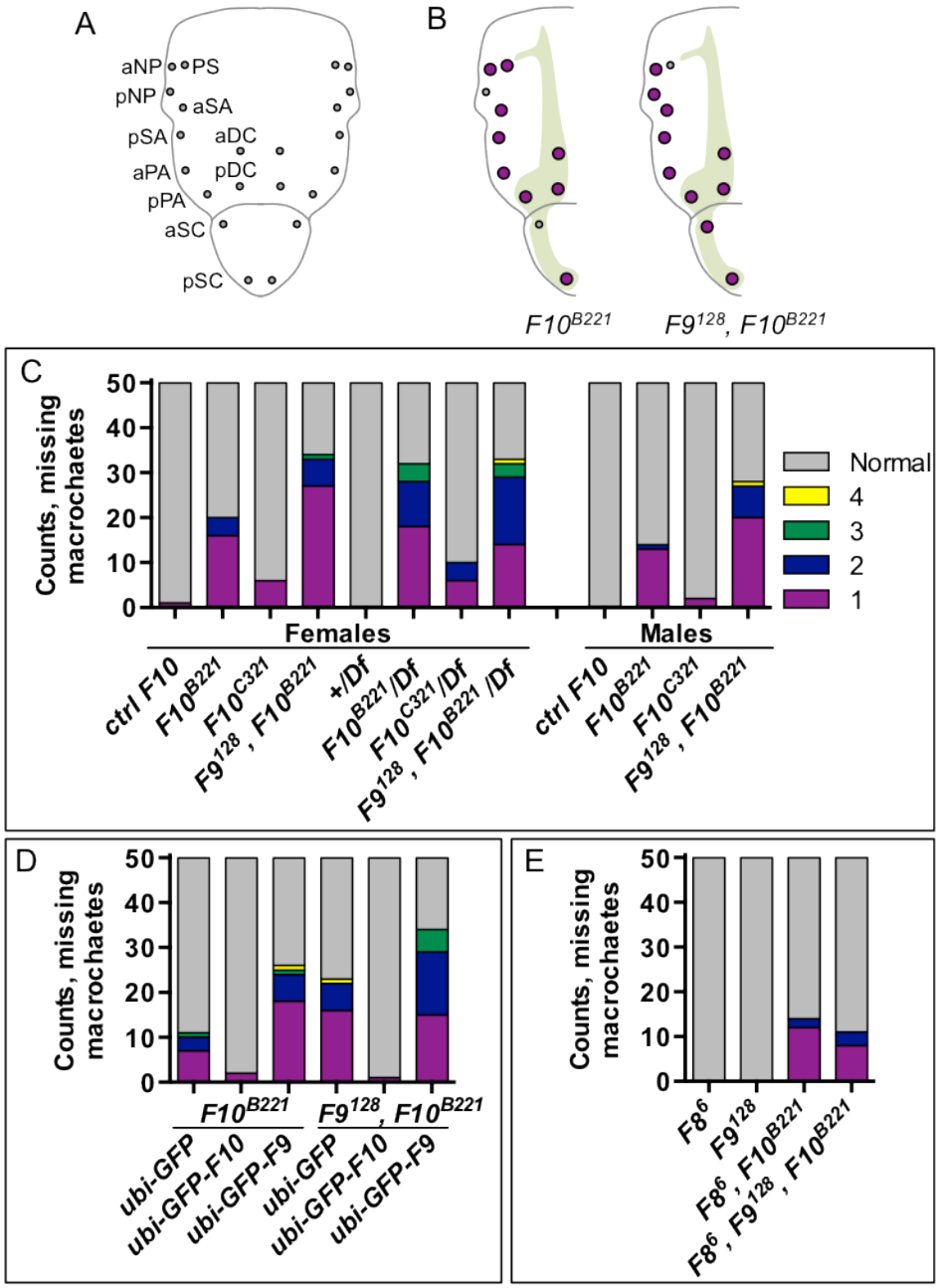

Figure 4.3 - *RASSF10* mutants have a missing macrochaete defect.

(A) Schematic outline of the notum of an adult fly. Grey circles indicate the position of macrochaetes and their shortened names are shown for the left side (identical for the right). a: anterior, p: posterior, NP: notopleural, PS: presutural, SA: supraalar, DC: dorsocentral, PA: postalar, SC: scutellar bristle. (B) Schematic of the affected macrochaetes (highlighted in purple), in *RASSF10*^{B221} and *RASSF9*^{128}, *RASSF10*^{B221} double mutants (Wingless expression pattern is highlighted in pale green, adapted from (Simpson, 2007)). (C-E) Quantification of missing thoracic macrochaetes of 50 female flies (and males in (C)) for each of the indicated genotype. (Continued on next page)

Figure 4.3 (Continued from previous page) **-** For each fly the number of missing macrochaetes without socket was counted. (C) Missing macrochaete defect in *RASSF10* mutants (*Df*: *Df(3L)BSC575*). (D) Expression of *ubi-GFP-RASSF10* but not *ubi-GFP-RASSF9* rescues the defect of $RASSF10^{B221}$ and $RASSF9^{128}$, $RASSF10^{B221}$. (E) Missing macrochaete defect in $RASSF8^{6}$ single, $RASSF9^{128}$ single, $RASSF8^{6}$, $RASSF10^{B221}$ double and $RASSF8^{6}$, $RASSF9^{128}$, $RASSF10^{B221}$ triple mutants. Statistics can be found in Table 7.3 in the Appendix.

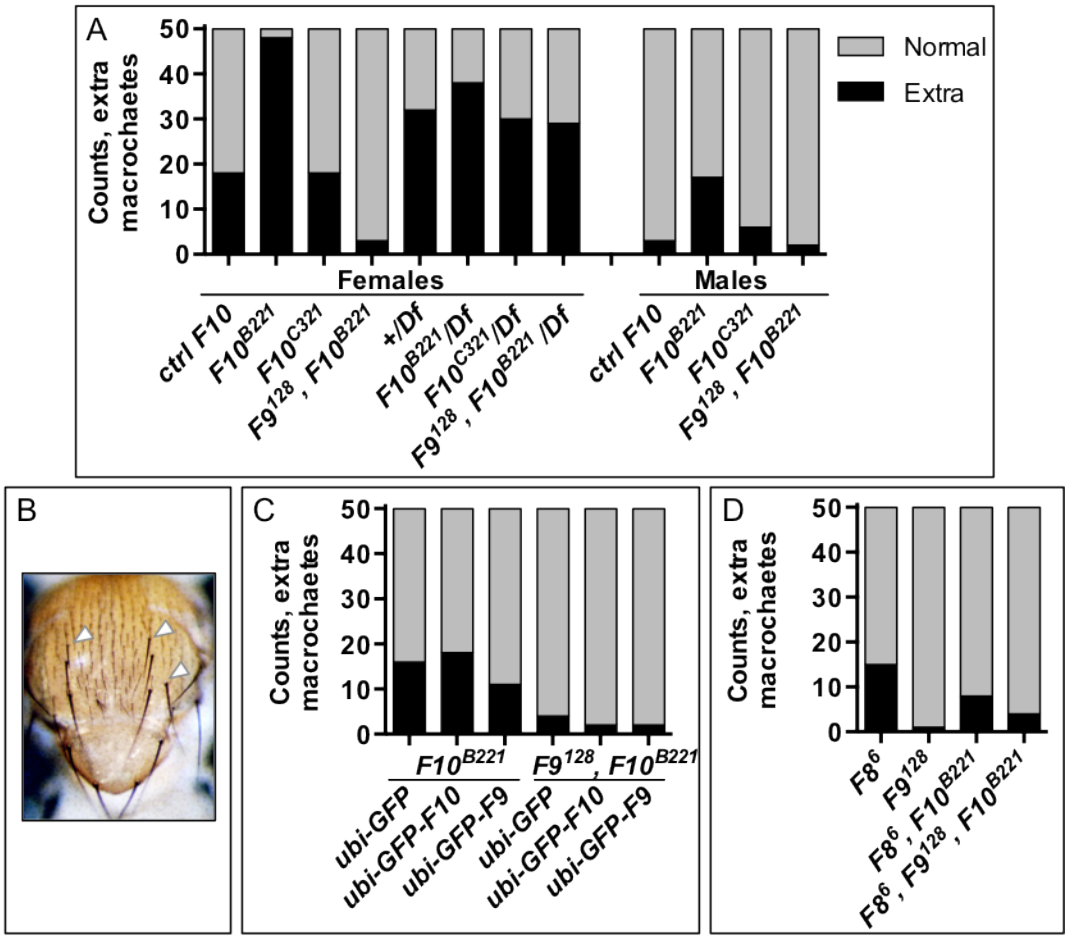

Figure 4.4 - *RASSF10* mutants and control flies have an extra macrochaete defect.
(A, C, D) Quantification of extra thoracic macrochaetes of 50 female flies (and males in (A)) for each of the indicated genotype (Extra: presence of extra bristle, Normal: no defect). (A) Extra macrochaete defect in *RASSF10* mutants (*Df*: *Df(3L)BSC575*). (B) Image of the notum of an adult $RASSF10^{B221}$ fly. Extra macrochaetes are indicated with a white arrow. (C) Expression of *ubi-GFP-RASSF10* or *ubi-GFP-RASSF9* does not affect the extra bristle defect of $RASSF10^{B221}$ and $RASSF9^{128}$, $RASSF10^{B221}$. (D) Extra macrochaete defects in $RASSF8^{6}$ single, $RASSF8^{6}$, $RASSF10^{B221}$ double and $RASSF8^{6}$, $RASSF9^{128}$, $RASSF10^{B221}$ triple mutants. Statistics can be found in Table 7.3 in the Appendix.

In conclusion, the quantification of both stout bristle defect and missing macrochaete defect revealed that, firstly, the *RASSF10*^{B221} mutant is most likely a null allele or at least a strong hypomorph, whereas *RASSF10*^{C321} is a hypomorphic allele. Secondly, both defects are caused by loss of function of *RASSF10*, as they could be rescued upon GFP-RASSF10 expression. Moreover, the other N-terminal RASSFs, RASSF8 and RASSF9 did not exhibit either of the two defects and the analysis of *RASSF8*^{6}, *RASSF10*^{B221} double mutants and the *RASSF8*^{6}, *RASSF9*^{128}, *RASSF10*^{B221} triple mutants showed no worsening of the *RASSF10* phenotype, and thus argue against a potential redundancy in this setting. Interestingly, the severity of the *RASSF10*^{B221} phenotype seemed to be supressed upon loss of RASSF8, which could be obviously due to genetic background changes, as seen for the wing roundness in 3.6. The *RASSF9*^{128}, *RASSF10*^{B221} double mutants were slightly more affected than the *RASSF10*^{B221} single mutant, however, expression of *GFP-RASSF9* did not rescue the defects of either of them. This suggests that RASSF10 is the major N-terminal RASSF in the SOP lineage, rather than redundancy being a major issue in these cells. Lastly, the stout bristle defect gave the more reliable results and represents therefore a good system to perform genetic interactions, as the background extra macrochaete defect might interfere with the analysis of the missing macrochaete defect.

4.1.3 The phenotype of *RASSF10* mutants suggests defects in ACD

The phenotype of the *RASSF10* mutants, though relatively weakly penetrant, resembles phenotypes seen for components involved in the asymmetric cell divisions of SOPs and hence, cell fate determination of the daughter cells. Defects in asymmetric cell divisions lead to daughter cells adopting the wrong cell fate and therefore defects in the adult external sensory bristle, such as multiple or missing neurons/sheath cells and/or bristles/sockets, depending on which or how many of the asymmetric divisions were affected. Knockdown of the known ACD proteins, Pins or $Ga_{o/i}$ (Kopein and Katanaev, 2009), or Baz (Figure 4.12A, A'), cause the appearance of duplicated stout bristles, as seen for *RASSF10* loss of function. Similarly, mis-expression of Numb results in duplication of margin bristles, twinning and loss of macrochaetes (Frise et al., 1996, Yaich et al., 1998).

Interestingly, the bristle defect of *RASSF10* is distinct from the bristle defect caused by loss or overexpression of planar cell polarity proteins. Mutants for Fz, Dsh, Stbm and Pk show a randomised orientation of the external sensory organs (reviewed in (Shulman et al., 1998)), but no defects of cell fate determination. This is because planar cell polarity is required to establish the initial polarity within the SOP cell and also orients cell division within the tissue axis, but is not required for the asymmetric localisation of cell fate determinants (reviewed in (Segalen and Bellaiche, 2009)). As loss of *RASSF10* function does not cause random orientation of bristles, it seemed unlikely that RASSF10 is involved in establishing the initial polarity together with Fz/Dsh, but rather suggests that RASSF10 acts downstream of these.

4.1.4 Loss of *RASSF10* function does not affect canonical Wg/Fz signalling

Canonical Wg/Fz signalling is required for the prepatterning of the wing margin and for the selection and specification of the SOPs. The Wg target gene Senseless is required for the specification of the SOP cells and regulates the expression of proneural proteins (Acar et al., 2006, Jafar-Nejad et al., 2003, Jafar-Nejad et al., 2006, Nolo et al., 2000). Hence, loss of Wg (Couso et al., 1994) or Senseless (Jafar-Nejad et al., 2006) function in larval stages results in wings without any margin bristles, as no sensory organs are formed. Subsequently gain of function of canonical Wg/Fz signalling causes the formation of ectopic, but normally composed, bristles on the wing (Jafar-Nejad et al., 2006, Axelrod et al., 1996). As RASSF10 interacts with Dsh/Fz, key players in the Wg signal transduction, it was possible that RASSF10 functions in the canonical Wg/Fz signalling pathway. However, this seemed unlikely for the following reasons: firstly, the duplicated stout bristle defect of *RASSF10* mutants is clearly distinct from canonical Wg/Fz signalling-related phenotypes, secondly, the missing macrochaete defect also affected bristles outside of the Wg expression zone (Figure 4.3) and lastly, strong ectopic expression of RASSF10 did not cause the appearance of ectopic bristles, but caused a mild PCP defect (3.4.7). Taken together, this supported the idea that RASSF10 is involved in the process of ACD of SOPs cells and might be connected to Fz/Dsh in the context of PCP, rather than in canonical Wg/Fz signalling and/or selection of SOP cells.

To validate the phenotypic observations I examined the expression of Wg and its target genes Distal-less (Dll) and Senseless (Sens) in wing imaginal discs of *RASSF10*^{B221} mutants. I could not detect obvious differences in the expression pattern of Wg, Dll or Sens in *RASSF10*^{B221} mutants (Figure 4.5A'-C') compared to wild type wing discs (Figure 4.5A-C). The stainings for Sens together with the stainings for Hindsight (Hnt) (Figure 4.5D, D'), a marker for specified, mature SOP cells whose expression is activated by Sens (Koelzer and Klein, 2003), revealed that SOPs are still specified in *RASSF10* mutants. Taken together, these results showed, that loss of *RASSF10* function had no obvious effect on the expression of Wg and its target genes Dll and Sens or on the specification and selection of SOPs.

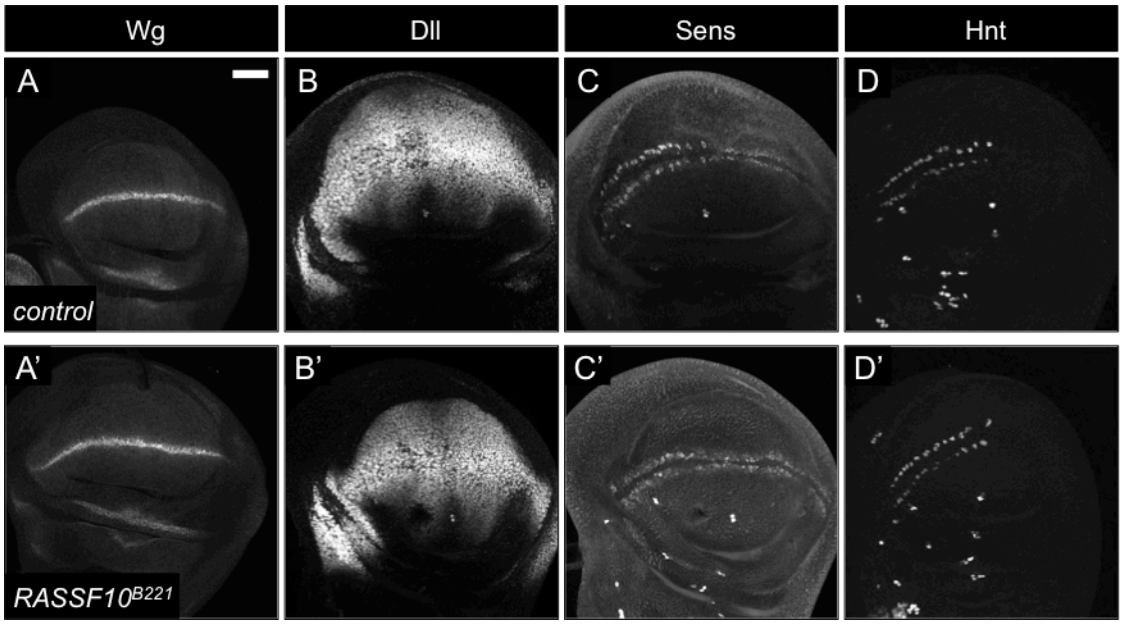

Figure 4.5 - Loss of *RASSF10* does not affect canonical Wg/Fz signalling or the specification of SOP cells.

Planar confocal sections of wild type *RASSF10* control (A-D) or *RASSF10*^{B221} (A'-D') wing imaginal discs either stained for Wingless (Wg, A-A'), Distal-less (Dll, B-B'), Senseless (Sens, C-C') or Hindsight (D-D', images are identical to those in Figure 4.6A'', B''). Loss of *RASSF10* does not affect Wg expression (A-A'), or the expression of Wg target genes Dll (B-B') and Sens (C-C'). SOPs are specified normally in *RASSF10* mutants as seen by the staining of the SOP marker Hnt (D-D') and Sens (C-C'). Anterior is to the left and posterior to the right. Scale bar = 50 µm.

4.2 RASSF10 localisation

4.2.1 Endogenous RASSF10 localises exclusively in SOP cells in imaginal discs

In order to study the endogenous localisation of RASSF10, I generated an antibody that targets a C-terminal region of RASSF10 (aa 375-486) (see Material and Methods 2.8).

In control *RASSF10* wing discs RASSF10 was exclusively detected in SOP cells (identified by the presence of the SOP marker Hnt) (Figure 4.6A-A''). In contrast, no signal was detected in $RASSF10^{B221}$ mutant discs (Figure 4.6B-B'') or in *hsFLP*-induced mitotic clones of $RASSF10^{B221}$ (Figure 4.6C-C'), thus confirming that the signal was specific for RASSF10. This supported the previous findings that *RASSF10* mRNA was highly expressed in SOP cells of wing imaginal discs and therefore suggested *RASSF10* was an SOP-specific gene (Reeves and Posakony, 2005). The SOPs present in the late L3 wing imaginal disc give rise to the macrochaete of the notum and also to some of the bristles of the wing margin (as illustrated in Figure 4.6F). The clear double row of SOPs in the L3 wing pouch are the precursors of the chemosensory bristles of the anterior wing margin (Huang et al., 1991). Most interestingly, in co-stainings with E-cadherin to outline the cell cortex, RASSF10 was found not only localised to the membrane, but also highly asymmetrically enriched at one side at the cell cortex (Figure 4.6D-E''). The SOP cells of the wing imaginal discs are selected and specified at different time points, with the SOPs, which give rise to the macrochaete of the notum appearing first and the SOPs of the wing margin appearing at late L3 (Huang et al., 1991). Indeed, looking at different stages of wing imaginal discs the occurrence of RASSF10 expression correlated with the presence of the SOP-marker Hnt (Figure 4.7A-C'), thus suggesting that RASSF10 expression is activated upon specification of the SOPs.

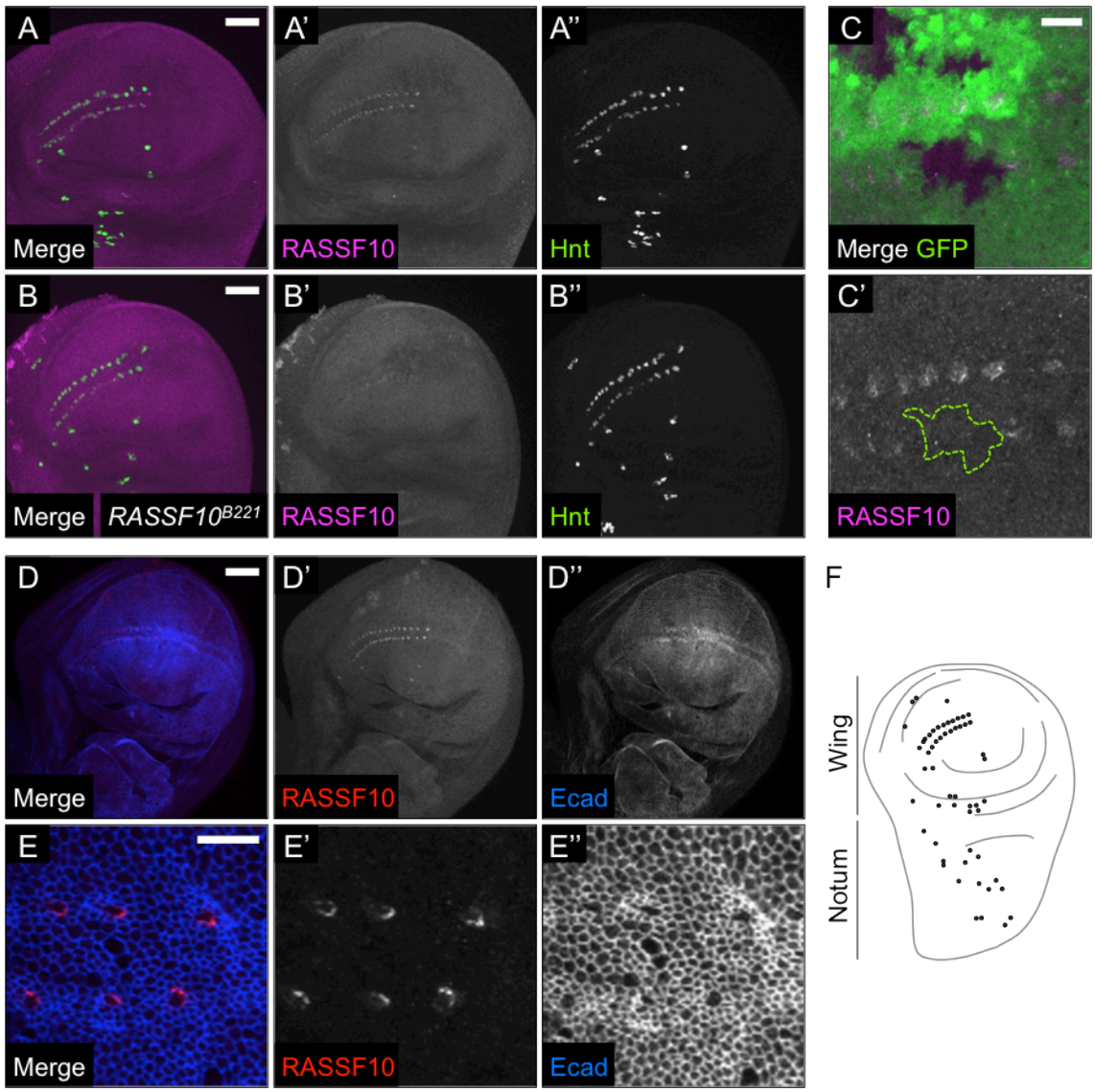

Figure 4.6 - Endogenous RASSF10 localises exclusively in SOP cells in late third instar wing imaginal discs.

(A-E'') Planar confocal sections of L3 wing imaginal discs. (A-B'') Wing discs stained for RASSF10 and the SOP marker Hnt. RASSF10 is expressed exclusively in SOP cells (A-A'') and cannot be detected in wing discs of *RASSF10*^{B221} mutants (B-B''). (C-C') *hsFLP* induced mitotic clones of *RASSF10*^{B221} stained for RASSF10. Wild type tissue for *RASSF10* is GFP positive and *RASSF10*^{B221} mutant tissue is GFP negative (outlined in green). Wing disc stained for RASSF10 and E-cadherin (D-D'') and a close up of the same disc showing the margin SOP region (E-E''). Scale bar = 50 µm (A-B'', D-D'') or 10 µm (C-C', E-E'). Anterior is to the left and posterior to the right. (F) Outline of a late L3 wing imaginal discs showing the position of the SOP cells (adapted from (Simpson, 2007).

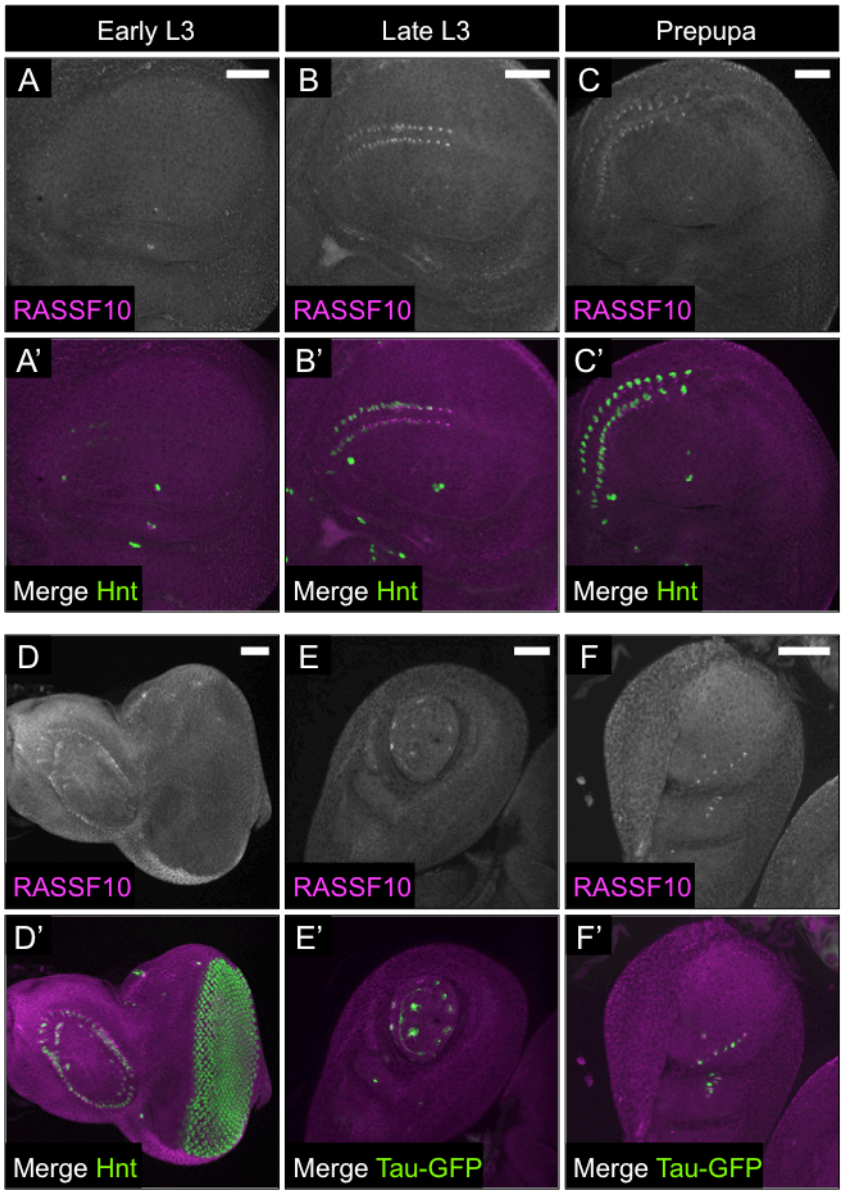

Figure 4.7 - RASSF10 expression in wing imaginal discs of different larval stages and in various imaginal discs.

Planar confocal sections of imaginal discs stained for RASSF10. SOP cells were marked either by staining for Hnt (A-D') or by the *neuralized-Gal4* driven expression of Tau-GFP (E-F'). RASSF10 protein expression correlates with the expression pattern of Hnt in early L3, late L3 and prepupal wing discs (A-C'). Anterior is to the left and posterior to the right (A-C'). RASSF10 is also expressed in SOP cells of the eye-antennal disc (D, D'), leg disc (E-E') and haltere disc (F, F'). Scale bar = 50 µm.

This is in accordance with previous findings that RASSF10 transcription in wing imaginal disks is dependent on the presence of the proneural Achaete-Scute complex (Reeves and Posakony, 2005). RASSF10 was also expressed in SOPs of the eye-antennal disc, the leg disc and the haltere disc (Figure 4.7F-F'). Thus, the endogenous RASSF10 protein is specifically expressed in SOP cells in different imaginal discs, appears upon SOP cell specification, and is localised asymmetrically at the SOP cell cortex.

4.2.2 RASSF10 co-localises with polarity determinants in SOPs

Intrigued by the finding that RASSF10 localised asymmetrically in wing imaginal disc SOPs, I went on to test whether it would co-localise with its binding partners Baz, Fz and Dsh and also with PCP components Stbm and Fmi. Interestingly, Baz-GFP, Fz-GFP, Dsh, Stbm and Fmi were all asymmetrically distributed in the wing margin SOPs, while E-cadherin or Arm showed no difference between SOP and the surrounding epithelial cells (Figure 4.8 and Figure 4.9). Baz-GFP (endogenously tagged) was found asymmetrically enriched on the same side as RASSF10, where its localisation overlapped with RASSF10 (Figure 4.8A-B'''). The same was true for the localisation of Fz-GFP (*arm-fz-GFP* line, Figure 4.8C-D''') and Dsh (Figure 4.9A-B'''). On the contrary, Stbm did not localise with RASSF10, but was found highly asymmetrically enriched in the neighbouring cell adjacent to RASSF10 (Figure 4.9C-D'''). Lastly, RASSF10 localised with Fmi at the cell cortex, though their localisation did not completely overlap (Figure 4.9E-F''').

Thus, RASSF10 co-localises with Baz, Dsh and Fz and all are asymmetrically enriched in the wing margin SOPs of the wing disc. As mentioned above, the SOP cells of the wing margin will not enter mitosis until after puparium formation (Hartenstein and Posakony, 1989), thus suggesting that the initial polarity within the SOP cell might already be established hours before the actual divisions start. Moreover it supports the finding that Fz and Dsh initiate the asymmetric localisation of the Baz-Par6-aPKC complex prior to mitosis in SOPs of the pupal notum, independently of Aurora A kinase activity (Besson et al., 2015). Together, the study of the Schweisguth lab (Besson et al., 2015) and our findings that RASSF10 can bind to Baz as well as Fz/Dsh, with which

they co-localise in wing disc SOP cells prior to entry into mitosis, led us to hypothesise that RASSF10 might be the link that facilitates the association of Fz/Dsh with Baz.

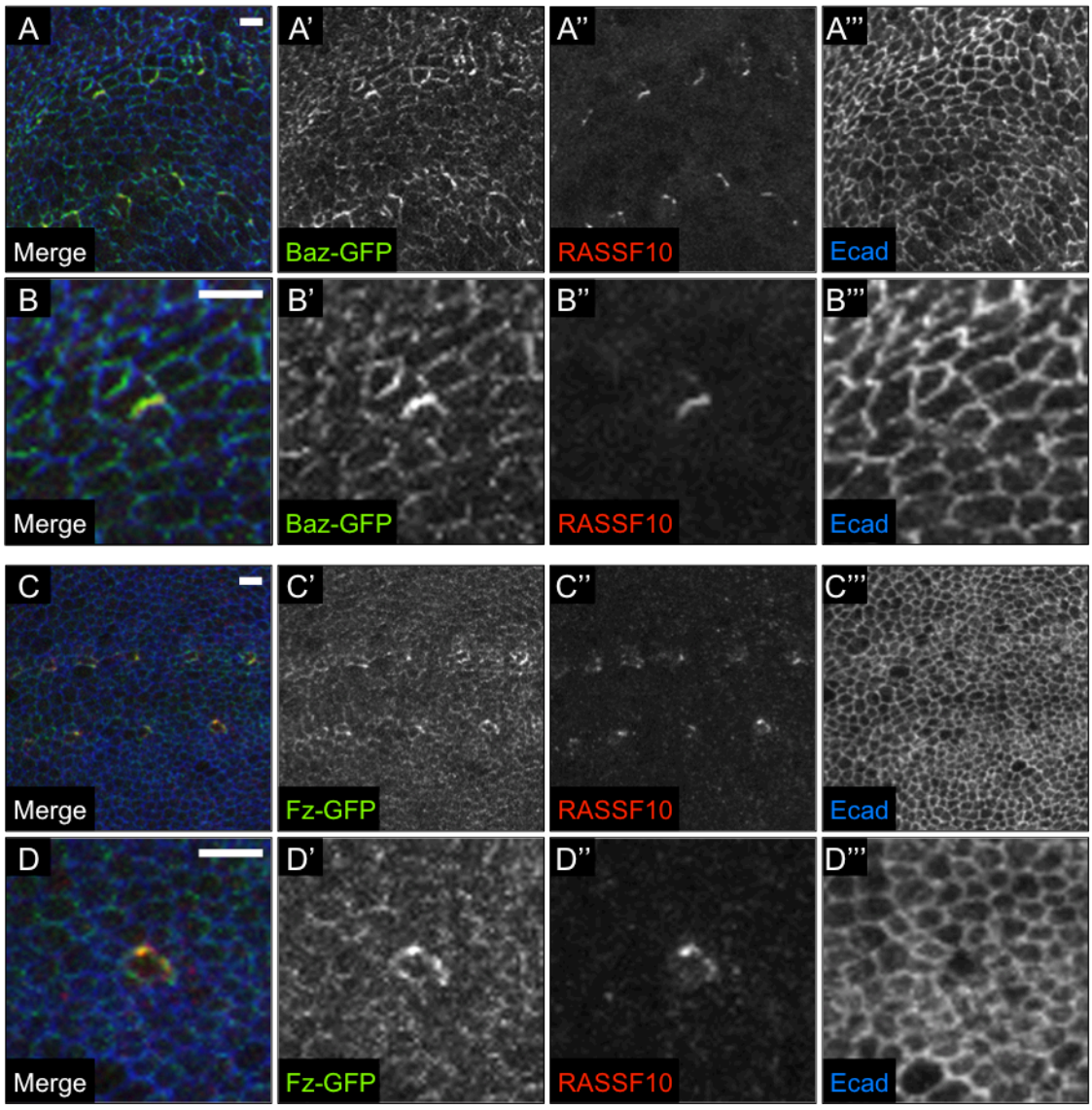

Figure 4.8 - RASSF10 co-localises with Baz and Fz in wing imaginal disc SOPs.
Planar confocal sections of wing discs from late third instar larvae or white prepupae stained for RASSF10 and E-cadherin. RASSF10 co-localises with Baz-GFP (A-B''') and Fz-GFP (C-D''') in wing disc SOP cells. Close up of a single margin SOP cell (B-B''', D-D'''). Anterior is to the left and posterior to the right. Scale bar = 5 µm.

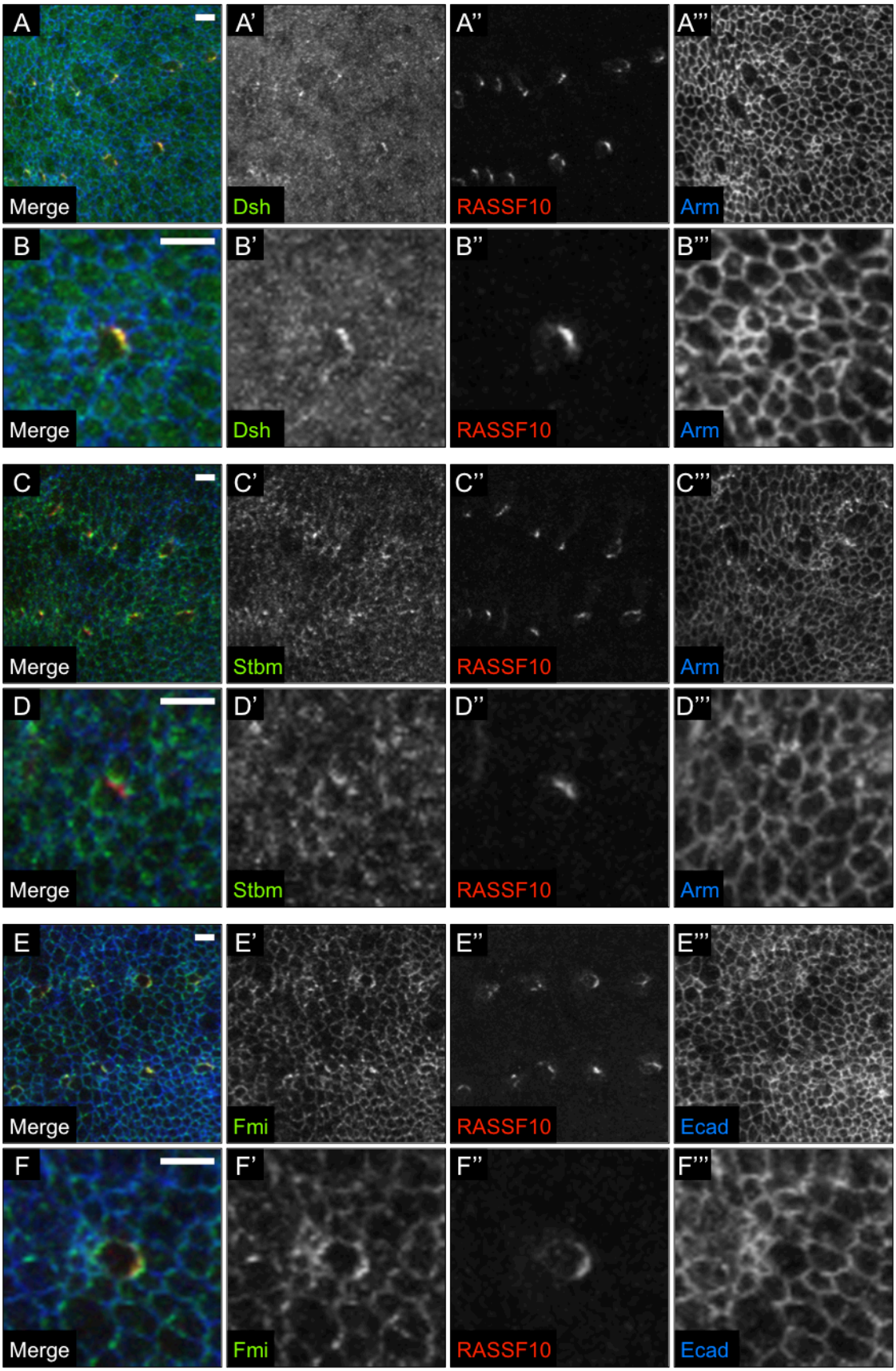

Figure 4.9 - Description see following page.

Figure 4.9 - RASSF10 co-localises with Dsh and Fmi, but not with Stbm in wing imaginal disc SOPs.

Planar confocal sections of wing discs from late third instar larvae or white prepupae stained for RASSF10 and either, Dsh and Arm (A-B’’’) or Stbm and Arm (C-D’’’) or Fmi and E-cadherin (E-F’’’). Close up of a single margin SOP cell (B-B’’’, D-D’’’, F-F’’’). RASSF10 co-localises with Dsh (A-B’’’) and partly with Fmi (E-F’’’), but not with Stbm (C-D’’’) in wing disc SOP cells. Anterior is to the left and posterior to the right. Scale bar = 5 µm.

4.3 Genetic interactions with ACD polarity components

In order to substantiate the hypothesis that RASSF10 might function together with Fz/Dsh and Baz in the context of ACD of SOP cells, I looked at genetic interactions between the *RASSF10*^{B221} mutant and different ACD polarity components using the duplicated stout bristle defect as a readout. In addition, I tested *RASSF9*^{128} for the same genetic interactions.

4.3.1 Dsh

Firstly, I tested whether RASSF9 and RASSF10 genetically interacted with Dsh. I combined *dsh*^{1} with either *RASSF10*^{B221} or *RASSF9*^{128}. The *dsh*^{1} allele has an amino acid substitution (K417M) in its DEP domain and is a PCP-specific allele that is not thought to affect Wg signalling (Axelrod et al., 1998). *dsh*^{1} mutant flies can be kept as a homozygous stock and show random orientation of sensory bristles as well as trichomes on the body and wing. The stout bristle defect was found rather rarely (3% of wings, 0.03 duplicated stout bristles per wing) in *dsh*^{1} single and *dsh*^{1}*;; RASSF9*^{128} double mutants and no defect was seen for *dsh*^{1} mutants heterozygous for *RASSF9*^{128} (Figure 4.10A). In contrast, the stout bristle defect of *dsh*^{1}*;; RASSF10*^{B221} double mutants (83% of wings, 2.21 defects per wing) was strongly increased compared to *RASSF10*^{B221} alone (60%) ($P<0.0001$) (Figure 4.10A and Table 7.3). Besides wings with 1 to 3 duplicated stout bristles (as seen for loss of function of *RASSF10*) some wings contained up to 6 duplicated bristles. Moreover, 98% of the *dsh*^{1}*;; RASSF10*^{B221} animals analysed had a strong missing macrochaete defect (over 4 thoracic macrochaetes), compared to 40% of

RASSF10 (P<0.0001) or 16% of *dsh* single mutants (P<0.0001) (Figure 4.10B and Table 7.3).

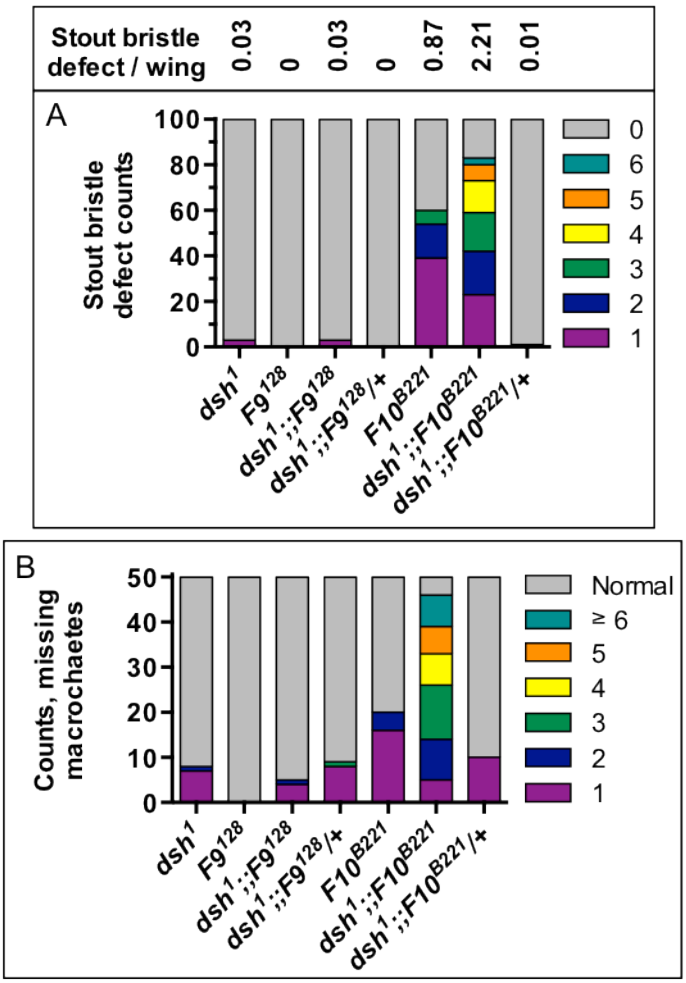

Figure 4.10 - Flies double mutant for *dsh*^{1} and *RASSF10* have a strong bristle defect.
(A) Duplicated stout bristles of the anterior wing margin (n=100) were quantified as described in Figure 4.2. The average stout bristle defect for 100 wings is indicated above the chart. (B) Flies (n=50) were also analysed for missing thoracic macrochaetes as described in Figure 4.3. The *RASSF10*^{B221} stout bristle defect (A) and missing macrochaete defect (B) are strongly enhanced in combination with *dsh*^{1}, whereas *dsh*^{1}*;; RASSF9*^{128} double mutants show no difference compared to *dsh*^{1} alone. Statistics can be found in Table 7.3 in the Appendix.

Strikingly, besides the stout bristle and the macrochaete defect, *dsh*^{1}*;; RASSF10*^{B221} double mutants displayed other notable defects, while *dsh*^{1}*;; RASSF9*^{128} double mutants behaved like single *dsh*^{1} mutants. *dsh*^{1}*;; RASSF10*^{B221} double mutants, were very unhealthy and died within 2 or 3 days. The animals were almost immobile, unable to fly and displayed a held-up wing phenotype, indicating a potential flight muscle defect. Interestingly, muscle progenitors were shown to divide asymmetrically, with Numb being unequally distributed onto the daughter cells (Gunage et al., 2014, Carmena et al., 1998). Thus we could speculate that RASSF10 and Dsh might also be involved in ACD of muscle progenitors.

4.3.2 Frizzled

Next, I investigated whether *RASSF10* genetically interacts with *frizzled*. I tested the effect of *fz* mis-expression under control of *nubbin-Gal4* upon loss of function of *RASSF10* (*RASSF9* and *RASSF9, RASSF10*). Mis-expression of Fz causes swirly trichomes and randomised orientation of the margin bristles and resembles the PCP loss-of-function phenotype, but does not induce ectopic Wingless signalling (Zhang and Carthew, 1998). Ectopic expression of Fz did not cause duplicated stout bristles (0.02 duplicated bristles per wing) in *RASSF10* control, *RASSF9*^{128} homo- or heterozygous flies (Figure 4.11). However, the number of affected wings strongly increased for *RASSF10*^{B221} (86%, 2.06 duplicated bristles per wing) upon expression of *fz* compared to *RASSF10*^{B221} combined with *nubbin-Gal4* alone (39%, 0.51 duplicated bristles per wing) ($P<0.0001$) (Figure 4.11 and Table 7.3). The defect increased even more for the *RASSF9*^{128}, *RASSF10*^{B221} double mutant (97%, 2.80 duplicated bristles per wing) ($P<0.0001$). However, *RASSF9*^{128}, *RASSF10*^{B221} double mutants in the *nubbin-Gal4* background were already more affected (59%, 0.76 duplicated bristles per wing) than *RASSF10*^{B221}.

To check whether the stout bristle defect of *RASSF10*^{B221} could increase upon induction of ectopic Wg signalling I mis-expressed *arm* with *nubbin-Gal4* in the different genetic backgrounds. Though gain of function of Arm caused the appearance of ectopic bristles on the wing, the quantification revealed that it did not induce duplicated stout bristles (Figure 4.11 and Table 7.3). Moreover, the stout bristle defect did not increase for *RASSF10*^{B221} or *RASSF9*^{128}, *RASSF10*^{B221}. This further supports the

previous observation that RASSF10 does not interfere with canonical Wg/Fz signalling (4.1.4). Interestingly, ectopic expression of Fz already caused a slight stout bristle defect in the *RASSF10*^{B221} heterozygous (10%) and the *RASSF9*^{128}, *RASSF10*^{B221} (12%) heterozygous background, which was not seen for ectopic expression of Arm in these backgrounds (Figure 4.11).

In conclusion, *RASSF10* genetically interacts with *dsh* and *fz*, as loss of *dsh* function or mis-expression of *fz* worsens the stout bristle defect of *RASSF10*^{B221}. On the contrary no genetic interactions were detected for *RASSF9*.

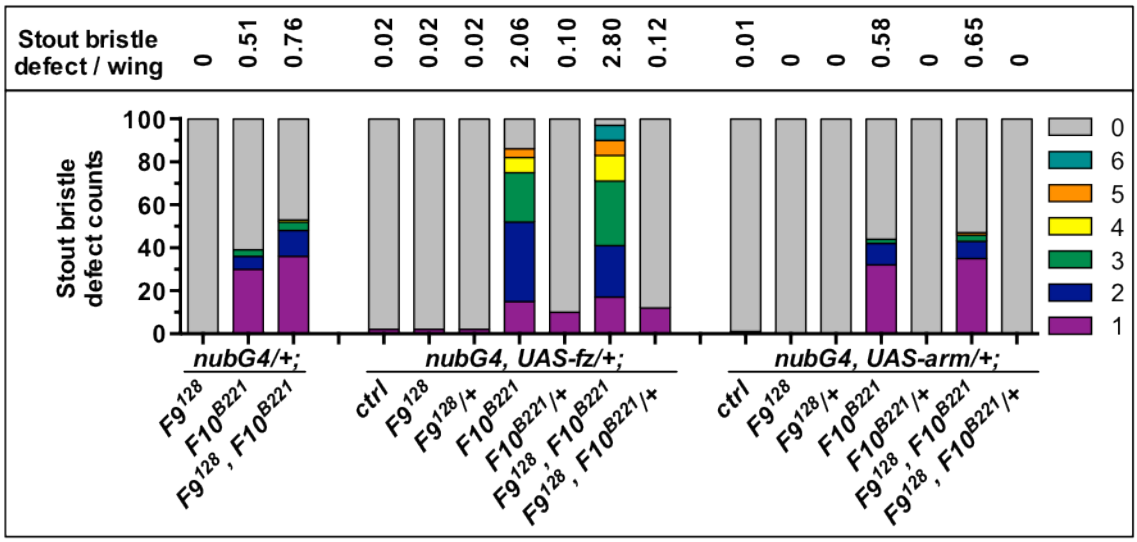

Figure 4.11 - Ectopic expression of Frizzled but not Arm increases the stout bristle defect of *RASSF10* mutants.

Duplicated stout bristles of the anterior wing margin (n=100) were quantified as described in Figure 4.2. The average stout bristle defect for 100 wings is indicated above the chart. Fz and Arm were expressed under control of *nubbin-Gal4*. Mis-expression of Fz, but not Arm, under control of *nubbin-Gal4* strongly increases the stout bristle defect of *RASSF10* mutants. Statistics can be found in Table 7.3 in the Appendix.

4.3.3 Bazooka and Pins

Having examined genetic interactions with *dsh* and *fz*, I tested the effect of knocking down Baz on the stout bristle defect in the different *RASSF9/10* mutant backgrounds. *baz* dsRNAs were expressed under control of the *nubbin-Gal4* driver. Knockdown of Baz alone caused a relatively strong stout bristle defect, with 83% of the wings affected (1.87 duplicated bristles per wing) (Figure 4.12A, A', E). Strikingly, in combination with $RASSF10^{B221}$ or $RASSF9^{128}$, $RASSF10^{B221}$ the expression of the RNAi against Baz caused a very strong margin bristle defect (P<0.0001) (Figure 4.12C-D' and Table 7.3). Many bristles were completely missing and almost all of the remaining ones were duplicated. Most interestingly, the stout bristle defect of the Baz knockdown increased upon loss of *RASSF9* with an average of 4.4 duplicated stout bristles per wing and 99% of the wings being affected (P<0.0001) (Figure 4.12B, B', E and Table 7.3).

All the genetic interactions described so far were with posterior ACD components. Pins (partner of Inscuteable), localises together with Disc-large (Dlg) and $G\alpha_i$ at the anterior cortex and is important to restrict Baz localisation to the posterior side (Bellaiche et al., 2001b, Schaefer et al., 2001). Pins expression was silenced by RNAi expression under control of *nubbin-Gal4* causing a mild stout bristle defect (17%, 0.18 duplicated stout bristles per wing). Strikingly, in combination with $RASSF10^{B221}$, the stout bristle defect was present in all of the wings with an average of 6.5 duplicated bristles per wing (P<0.0001) (6.95 for $RASSF9^{128}$, $RASSF10^{B221}$, P<0.0001) (Figure 4.12E and Table 7.3). Moreover, knockdown of Pins in $RASSF9^{128}$ mutants also led to an increased defect (55% of the wings, 0.76 duplicated bristles per wing, P<0.0001).

Thus, knockdown of Baz or Pins function, which are both required for the asymmetric localisation of the cell fate determinants, caused duplicated stout bristles on the anterior wing margin and the defect was strongly increased upon loss of *RASSF10*. The genetic interaction of *RASSF10* with *fz* and *dsh*, as well as *baz* and *pins* strongly supported the involvement of RASSF10 in ACD of SOPs. Moreover, *RASSF9* also genetically interacted with *baz* and *pins*, suggesting it may have some role in ACD, despite not causing an obvious defect on its own.

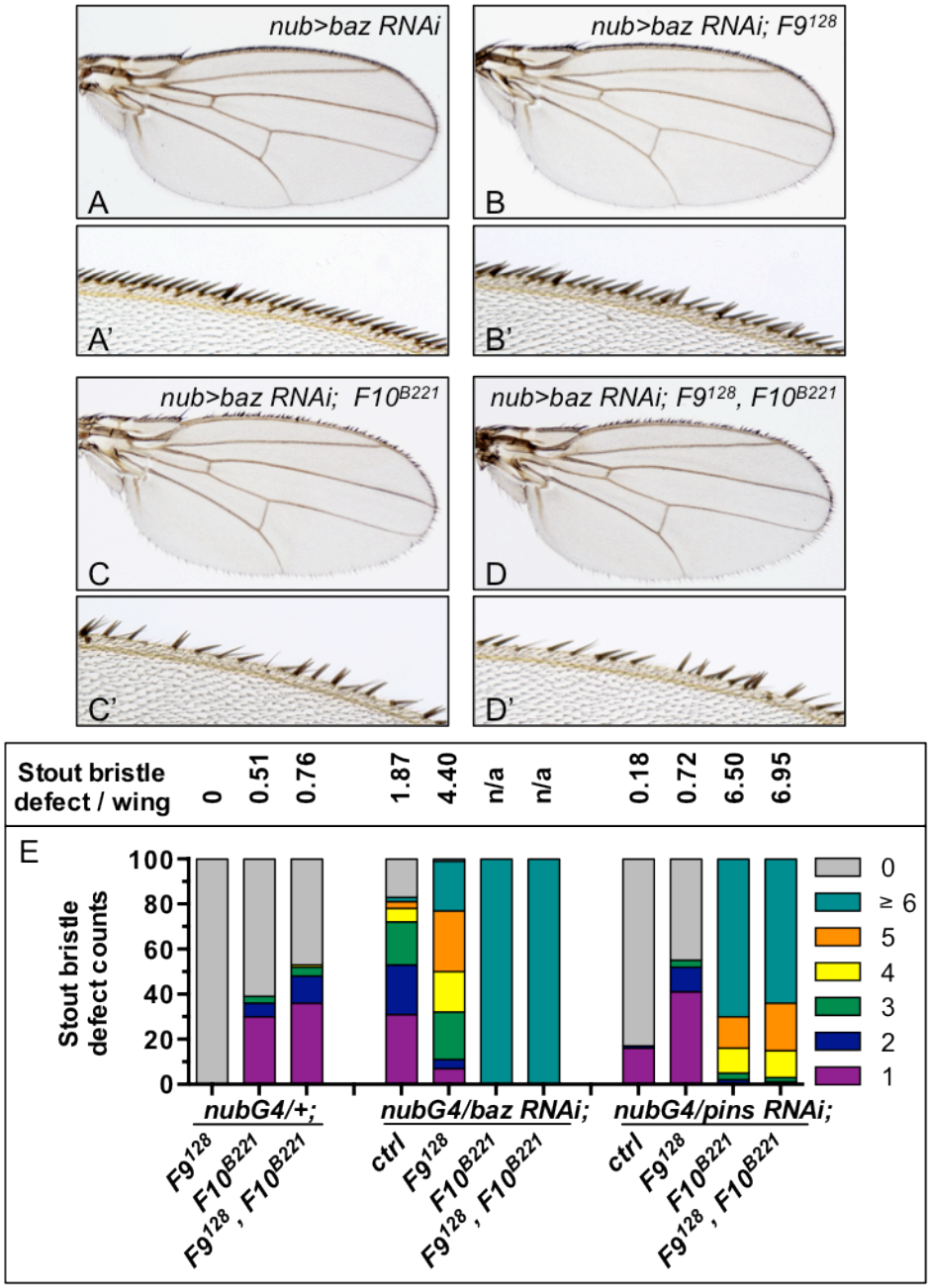

Figure 4.12 - Knockdown of *baz* or *pins* strongly increases the stout bristle defect of *RASSF10* mutants.

Images of adult wings (A-D) and close up of anterior margin of the same wings (A'-D'), expressing *baz* RNAi with *nubbin-Gal4* in wild type, $RASSF9^{128}$ single, $RASSF10^{B22}$ single or $RASSF9^{128}$, $RASSF10^{B221}$ double mutants. (E) Duplicated stout bristles of the anterior wing margin (n=100) were quantified as described in Figure 4.2. The average stout bristle defect for 100 wings is indicated above the chart. *baz* RNAi and *pins* RNAi were expressed in the different genetic backgrounds with *nubbin-Gal4* (*nubbin-Gal4 /+* controls are identical to the ones in Figure 4.11). (Continued on next page)

Figure 4.12 (Continued from previous page) **-** (E) Knockdown of Baz or Pins cause duplicated stout bristles on their own and strongly increase the defect in *RASSF10*^{B221} single or *RASSF9*^{128}, *RASSF10*^{B221} double mutants. Loss of *RASSF9* increases the defects caused by silencing of Baz or Pins function. Statistics can be found in Table 7.3 in the Appendix.

4.4 Is the function of RASSF10 in SOP cell division linked to the ASPP-PP1 phosphatase complex?

The data presented so far suggests that RASSF10 is most likely involved in establishing the asymmetric distribution of cell fate determinants in SOP cells together with Fz, Dsh and Baz. Considering the previous findings that RASSF10 can bind to ASPP and all PP1 catalytic subunits and thus might be part of a PP1 complex (see 3.2), I was interested in testing, whether RASSF10 could function in ACDs as part of a phosphatase complex. Although RASSF10 could bind to PP1 catalytic subunits independently of ASPP, it is possible that ASPP is required *in vivo*. I had found that strong simultaneous over-expression of RASSF10 and ASPP with *tubulin-Gal4* was lethal, whereas co-expression of a PP1-binding mutant of ASPP (ASPP^{VFAA}) was not. The synthetic lethality could obviously be due to gain-of-function artefacts, however it might also indicate, that RASSF10 and ASPP might function together *in vivo*.

Firstly, I checked whether loss or RNAi-mediated depletion of ASPP caused a stout bristle defect similar to *RASSF10*^{B221}. Neither the *ASPP*^{D} mutant (a null allele of ASPP), nor the expression of RNAi using *nubbin-Gal4* displayed any stout bristle defects (Figure 4.13A and Table 7.3). However, knockdown of *ASPP* caused a slight increase of the stout bristle defect of *RASSF10*^{B221} with 58% of the wings being affected (0.86 duplicated bristles per wing) compared to *RASSF10*^{B221} on its own (39%, 0.51 duplicated bristles per wing) (P=0.0375). This effect was also seen for the *RASSF9*^{128}, *RASSF10*^{B221} double mutants (75%, 1.12 duplicated bristles per wing) compared to their *nubbin-Gal4* control (59%, 0.76 duplicated bristles per wing) (P=0.0209), whereas *RASSF9*^{128} mutants displayed no defect with or without knockdown of *ASPP*. Similar to the genetic background effects described for *RASSF10*^{B221} and *ubi-GFP*; *RASSF10*^{B221} in 4.1.1, the stout bristle defect differed significantly between *RASSF10*^{B221} and *nubbin-*

Gal4/+; RASSF10^{B221} flies (P=0.0153) (Table 7.3). The P values obtained for the enhancement of the *RASSF10*^{B221} phenotype upon *ASPP* knockdown are higher than this background noise P value and thus the stout bristle defect differences might not be biologically relevant.

In addition to the genetic interactions, I looked at the localisation of ASPP in SOP cells of the wing imaginal discs. ASPP localised as in the neighbouring epithelial cell at the adherens junctions with E-Cadherin in SOPs and showed neither asymmetric enrichment nor overlapping localisation with RASSF10 (Figure 4.13B). However, this result does not rule out a transient co-localisation between ASPP and RASSF10, for instance during SOP division, which would not be visible in stainings.

In order to investigate whether ASPP and PP1 are, similarly to RASSF10, involved in asymmetric cell divisions, I checked whether partial loss of ASPP or different PP1 catalytic subunits would cause stout bristle duplications in combination with *nubbin-Gal4* driven Fz mis-expression or Baz knockdown. The following alleles for three different catalytic subunits of PP1 were tested: *flw*^{1}, a hypomorphic allele for *PP1β9C*, *PP1α87B*$^{Bg-3}$, a null allele for *PP1α87B* (homozygous lethal) and *PP1α96A*^{2}, a null allele for *PP1α96A*.

Firstly, neither knockdown of ASPP nor partial loss of the PP1 alleles caused a stout bristle defect in combination with Fz mis-expression (Figure 4.14). However, the severity of the stout bristle defect caused by Baz knockdown (80%, 1.45 duplicated bristles per wing) was significantly increased upon reduction of PP1β9C (89%, 2.18 duplicated bristles per wing) (P=0.0012), PP1α87B (94%, 2.8 duplicated bristles per wing, P<0.0001) or ASPP (95%, 3.04 duplicated bristles per wing) (P<0.0001) dosage (Figure 4.14 and Table 7.3). On the contrary, the Baz knockdown phenotype was not affected in the *PP1α96A*^{2} heterozygous background (77%, 1.59 duplicated bristles per wing) (n.s.).

These preliminary results allow us to make the following considerations. If the *RASSF10* mutant phenotype was solely caused by loss of its function as part of a phosphatase complex in ACD, one might expect similar phenotypes for loss of ASPP or PP1 catalytic subunits. However, knockdown or loss of ASPP does not cause ACD bristle defects (Figure 4.13).

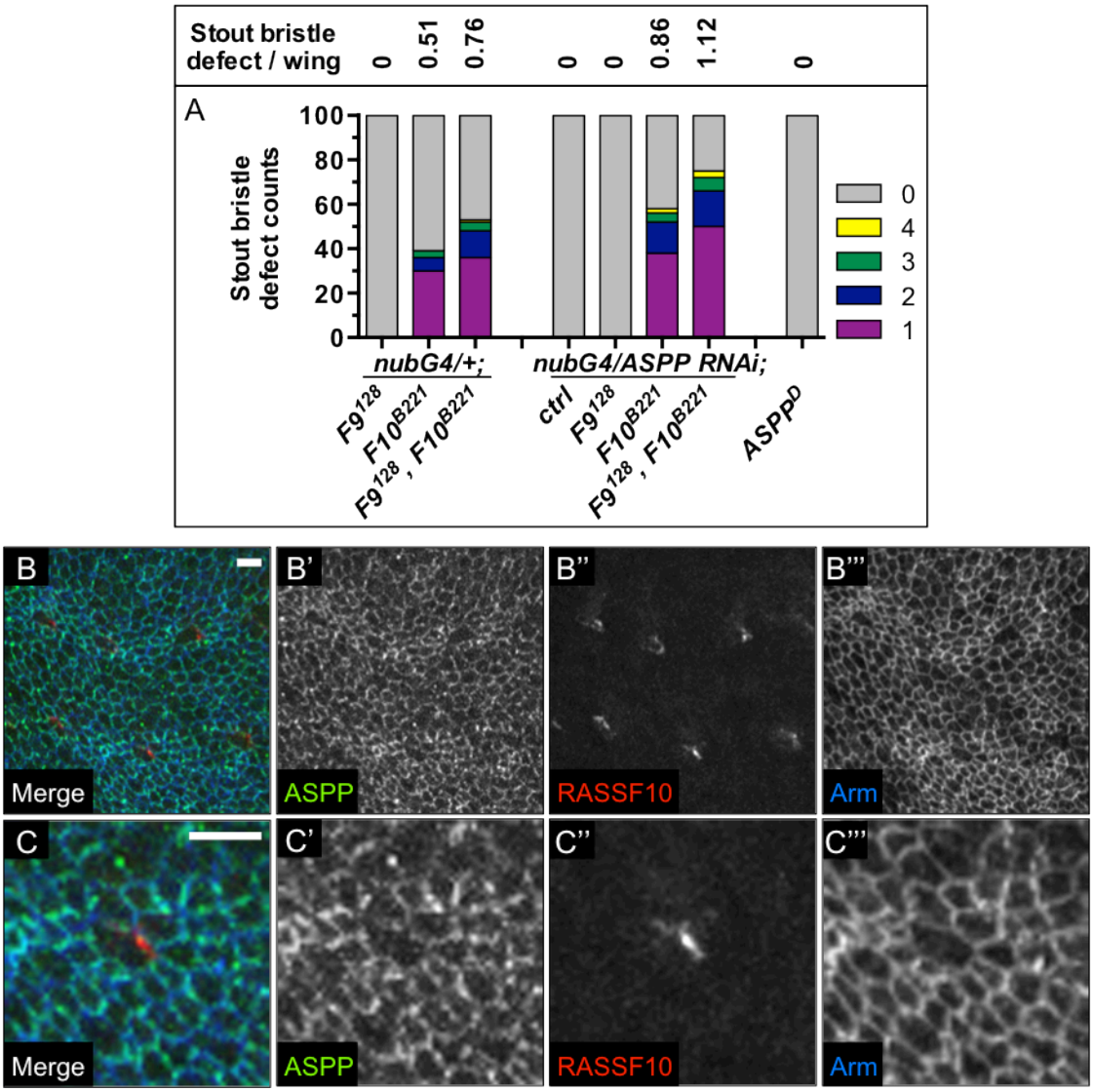

Figure 4.13 - Genetic interaction between RASSF9/10 and ASPP and localisation ASPP in wing imaginal disc SOPs.

(A) Duplicated stout bristles of the anterior wing margin (n=100) were quantified as described in Figure 4.2. The average stout bristle defect for 100 wings is indicated above the chart. RNAi against ASPP was expressed with *nubbin-Gal4* (*nubbin-Gal4 /+* controls are identical to the ones in Figure 4.11). Knockdown of ASPP mildly increases the stout bristle defect of $RASSF10^{B221}$ single or $RASSF9^{128}$, $RASSF10^{B221}$ double mutants. (B-C''') Planar confocal sections of wing discs in late third instar larvae stained for RASSF10, ASPP and E-Cadherin. Close up of a single margin SOP cell (C-C'''). ASPP does not co-localise with RASSF10 in L3 wing disc SOP cells. Anterior is to the left and posterior to the right. Scale bar = 5 µm. Statistics can be found in Table 7.3 in the Appendix.

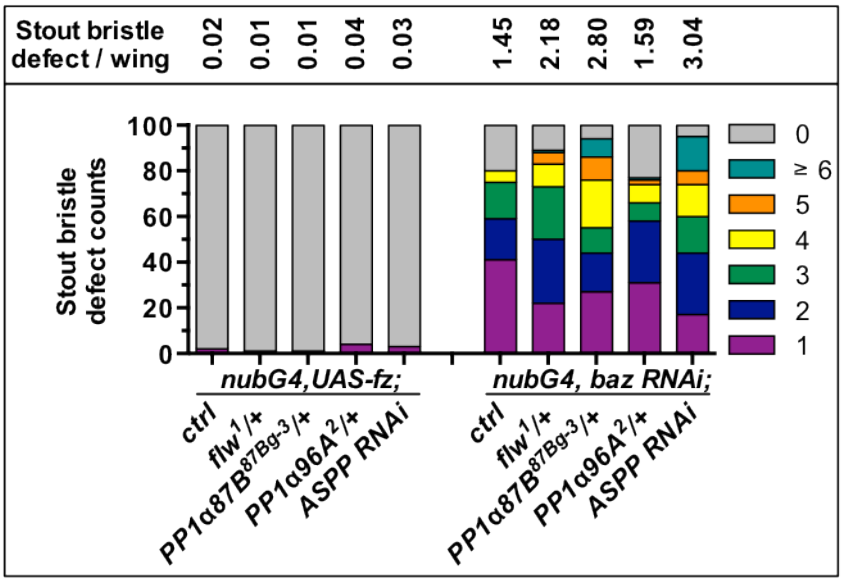

Figure 4.14 - Genetic interactions between different PP1 catalytic subunits or *ASPP* with *fz* and *baz*.

Duplicated stout bristles of the anterior wing margin (n=100) were quantified as described in Figure 4.2. The average stout bristle defect for 100 wings is indicated above the chart. *UAS-Fz* or *UAS-Baz RNAi* lines were recombined with *nubbin-Gal4* and tester stocks were subsequently crossed to wild type flies (control), different PP1 mutant alleles (flw^{1}, $PP1\alpha87B^{Bg-3}$, $PP1\alpha96A^{2}$) or *ASPP* RNAi. Partial loss of PP1 alleles or *ASPP* does not cause duplicated stout bristles upon Fz mis-expression, whereas loss of one copy of flw^{1} or $PP1\alpha87B^{Bg-3}$ as well as ASPP knockdown increase the stout bristle defect induced by *baz* knockdown. Statistics can be found in Table 7.3 in the Appendix.

Furthermore, I did not observe RASSF10-like defects in homozygous flw^{1} or $PP1\alpha96A^{2}$ homozygous or $PP1\alpha87B^{Bg-3}$ heterozygous flies. However, this could be due to redundancy between the different PP1 catalytic subunits and double or triple mutants would have to be combined and analysed to see whether ACD defects are visible. These experiments might prove difficult due to the multitude of PP1 substrates.

The effect of the ASPP knockdown on both the *RASSF10* loss-of-function phenotype and the Baz knockdown suggests that ASPP might be required for ACD, possibly independently of RASSF10. Similarly to the ASPP RNAi, the reduction of PP1β9C and PP1α87B gene dosage increased the stout bristle phenotype caused by knockdown of

Baz. These preliminary findings open up the possibility that RASSF10 might function as part of a phosphatase complex in ACD, though further work is required to test this directly. In pupal retinas, Baz is mis-localised in *ASPP* mutant clones and ASPP/PP1 can dephosphorylate Baz *in vitro* (Yanxiang Zhou, unpublished result). Hence, it is possible that ASPP/PP1 could regulate Baz independently of RASSF10. Another point worth considering is that PP1α87B is required for mitosis (Axton et al., 1990, Rodrigues et al., 2015) and subsequently the worsening of the phenotype could be due to an independent effect on SOP cell division. Future experiments will be necessary to substantiate the RASSF10/PP1 hypothesis and this will be addressed in the discussion (see 6.2 and 6.3.2).

4.5 Asymmetric cell division of SOPs in the pupal notum

The asymmetric localisation of RASSF10 in SOP cells in the wing imaginal discs of late L3 larvae, the association with Fz, Dsh and Baz and the genetic interactions with the different ACD components all support the hypothesis that RASSF10 might be required to establish asymmetry within the SOP. However, as mentioned above, the SOP cells that give rise to the chemosensory bristles of the wing margin do not enter mitosis until after puparium formation (Hartenstein and Posakony, 1989, Huang et al., 1991). At this point, the morphogenetic movements of wing eversion are ongoing, making this system inappropriate to perform high-resolution live imaging. In order to image asymmetric cell division, I decided to use the pupal notum, a well-established system to study ACD of SOPs (Schweisguth, 2015). At approximately 15-16 hours APF, the SOPs, which will give rise to the thoracic microchaetes start to divide along the anterior-posterior axis. Expression of fluorescently tagged proteins can be used to follow this process dynamically.

4.5.1 Localisation of RASSF10 and RASSF9 in SOPs of the pupal notum

In order to examine the localisation of RASSF10 in SOP cells of the pupal notum, I first tried to detect endogenous RASSF10 with the RASSF10 antibody in pupal nota at 15-16 hours APF. Unfortunately, the initial stainings for RASSF10 did not detect any

signal, while the co-staining for E-cadherin worked and thus would have required optimisation of the staining protocol. However, it is highly likely that endogenous RASSF10 is expressed in SOPs of the pupal notum, as *RASSF10* mRNA had been previously shown to be highly enriched in pupal notum SOPs (Buffin and Gho, 2010) and *RASSF10*^{B221} mutants exhibited split microchaete defects.

Hence, instead of looking at the endogenous RASSF10 protein, I decided to use the GFP-tagged UAS lines for live imaging before and during asymmetric divisions. GFP-RASSF10 (or GFP-RASSF9) was specifically expressed in SOPs with the *neuralized-Gal4* driver (Bellaiche et al., 2001a).

The live imaging revealed that GFP-RASSF10 localised apically to the membrane and was asymmetrically enriched at the posterior cortex prior to mitosis (Figure 4.15A, A'), similar to Fz, Dsh and Baz (Bellaiche et al., 2001a, Segalen et al., 2010, Roegiers et al., 2001a), and consequently opposite to Stbm, Pk, the Dlg-Pins-Gα_i complex and cell fate determinants. Interestingly, just before onset of mitosis GFP-RASSF10 lost its asymmetric localisation and localised uniformly around the membrane (apically and basolaterally) and was partitioned into both daughter cells (pIIa and pIIb). This observation was puzzling, as ACD polarity determinants generally keep their asymmetric localisation (either anterior or posterior) during mitosis (Bellaiche et al., 2001b, Bellaiche et al., 2004, Segalen and Bellaiche, 2009). It is possible that overexpression of GFP-RASSF10 causes it to lose its asymmetric distribution prior to mitosis as overexpression might saturate the proteins, required for RASSF10 asymmetric localisation (presumably Dsh/Fz).

In contrast, GFP-RASSF9 showed no asymmetric localisation prior to mitosis and was also found in the cytoplasm (Figure 4.15B, B'). Upon the onset of mitosis, GFP-RASSF9 lost its membrane localisation completely and was evenly segregated into both pII cells.

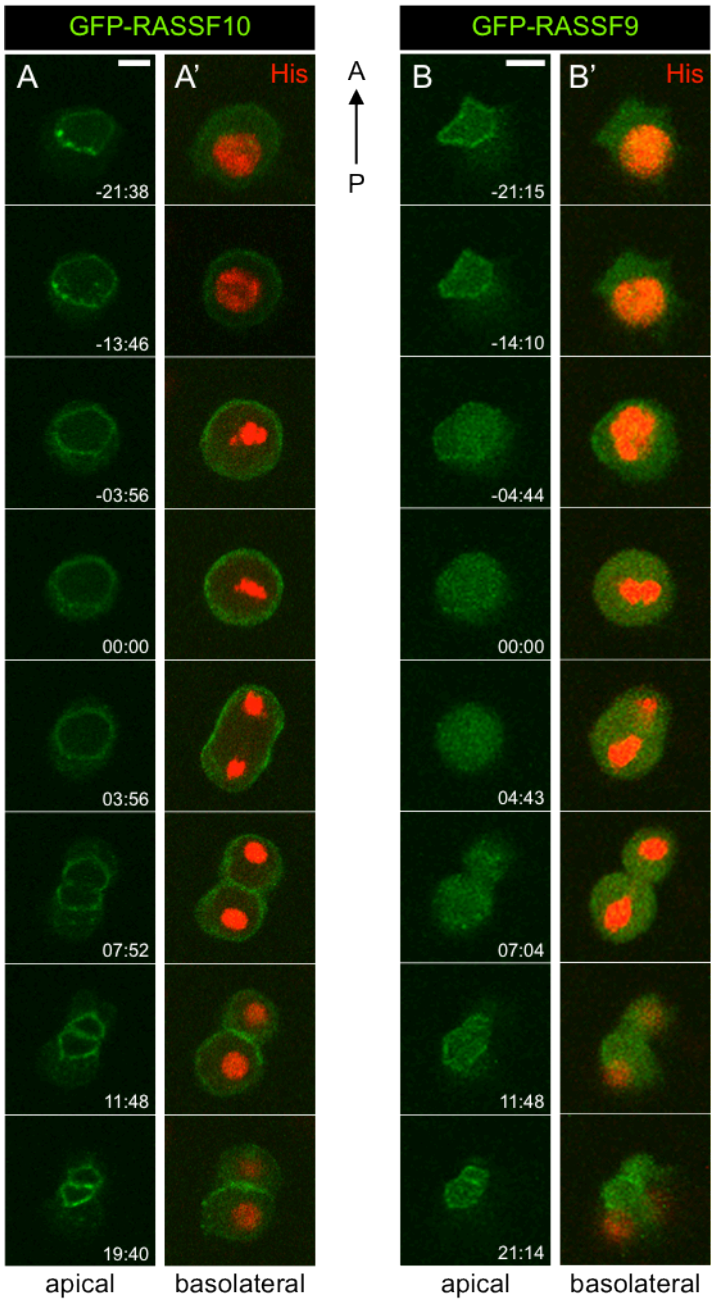

Figure 4.15 - Localisation of GFP-RASSF10 and GFP-RASSF9 in SOP cells of the pupal notum.

(A-B') Frames from a time-lapse movie of planar confocal sections showing a dividing SOP cell. Histone2B-RFP and GFP-RASSF9/10 were expressed under the control of *neuralized-Gal4*. Pupal nota were live imaged at 15-17 hours APF. Images are oriented with the anterior to the top and the posterior to the bottom. Apical stack (A, B) and basolateral stack (A', B') are shown for each time point. Time is given in minutes relative to the onset of mitosis (00:00). Scale bar = 5 µm. (Continued on next page)

Figure 4.15 (Continued from previous page) **-** (A, A') GFP-RASSF10 localises apically and is asymmetrically enriched at the posterior side of the SOP cell prior to mitosis and loses its asymmetric localisation just before onset of mitosis. RASSF10 is equally distributed onto the pIIa and pIIb cell. (B, B') GFP-RASSF9 is found apically localised to the membrane, as well as in the cytoplasm prior to mitosis, and loses its membrane localisation completely at mitosis onset, then partitions equally into pIIa and pIIb.

4.5.2 The role of RASSF10 in asymmetric cell division of sensory organ precursors

Finally, I went on to test whether *RASSF10*^{B221} mutants would show defects in pI asymmetric cell divisions - as suggested by their phenotype, by the localisation of RASSF10 and by the genetic interactions. Pon-GFP (GFP-tagged Partner of Numb) was expressed under control of *neuralized-Gal4* in SOP cells in either wild type, *RASSF10*^{B221} mutant or *RASSF10*^{B221} heterozygotes, and its segregation was followed during the first division of the pI cell in the pupal notum at 15-17 hours APF. In the wild type, Pon-GFP localises at the anterior cortex of pI cells just before entry into mitosis (see Figure 4.16A and (Roegiers et al., 2001b)). The pI cell divides along the anterior-posterior axis and Pon-GFP is segregated unequally into the pIIb cell. *RASSF10*^{B221} heterozygotes behaved like the wild type pupae (Figure 4.16C). Strikingly, the *RASSF10*^{B221} mutants showed a clear Pon-GFP mis-segregation phenotype in many of the divisions. Prior to mitosis the Pon-GFP crescent was often not orientated along the posterior-anterior axis Figure 4.16B) and moreover the division angle was not aligned to the Pon-GFP crescent, leading to mis-segregation of Pon-GFP into both daughter cells (Figure 4.16B, B'). The Pon-GFP crescent appeared broader and occasionally spread over almost the entire pI cell, also resulting in a Pon-GFP mis-segregation (Figure 4.16B''). Moreover, the division of the pI cell was in some cases not aligned to the anterior-posterior axis. Figure 4.17A-C illustrates the phenotypes observed in *RASSF10*^{B221} mutants compared to the wild type situation.

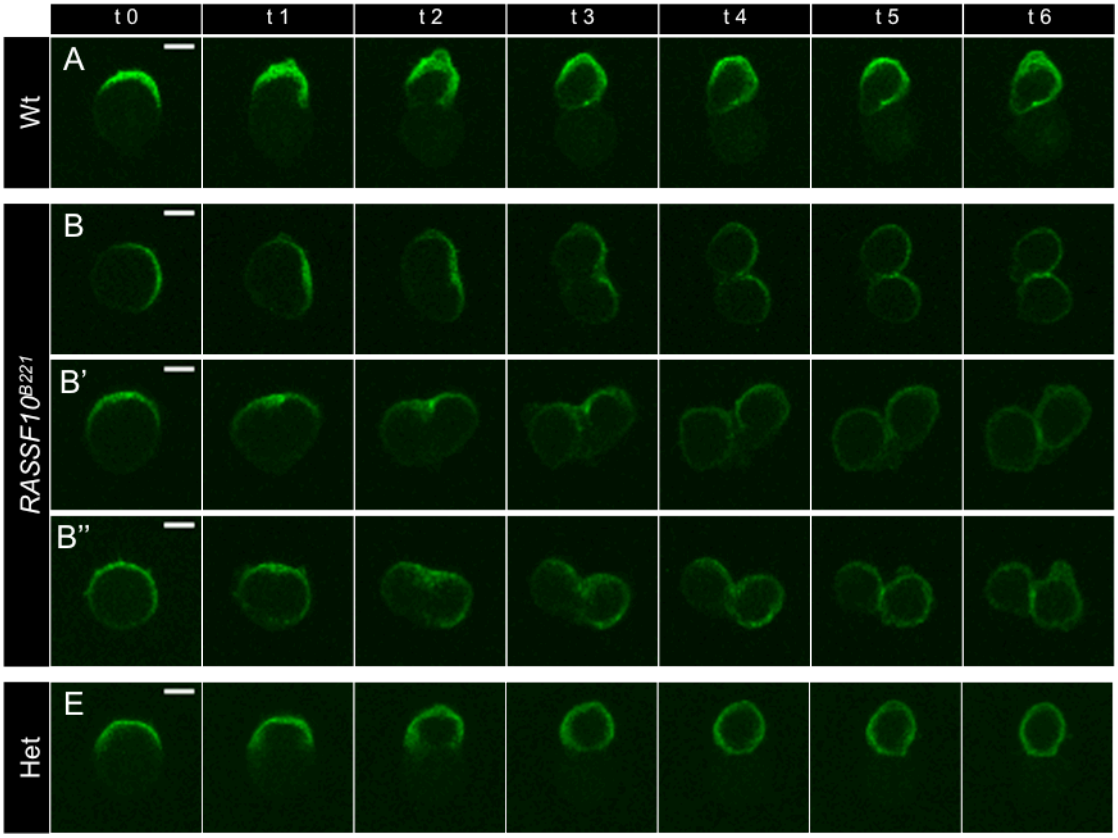

Figure 4.16 - Asymmetric divisions of pupal notum pI cells in *RASSF10* mutants and controls.

Frames from a time-lapse movie of planar confocal sections showing the localisation of Pon-GFP during the asymmetric division of a single SOP cell in the pupal notum at 15-17 hours APF. Pon-GFP was expressed under the control of *neuralized-Gal4* and the interval between each time point is 51.6 seconds. The images are oriented with anterior to the top and posterior to the bottom. Scale bar = 0.5 µm. (A) In wild type pupae, Pon-GFP localises asymmetrically to the anterior of the pI cell and is distributed into the pIIb cell. (B-B'') Examples of SOP divisions in $RASSF10^{B221}$ mutants all resulting in a mis-segregation of Pon-GFP into both daughter cells. (B) The Pon-GFP crescent is not oriented towards the anterior and the division angle is not aligned to the Pon-crescent. (B') The Pon-GFP crescent shows a normal orientation, but the division angle is randomised. (B'') No clear Pon-GFP crescent is formed. (C) Divisions in $RASSF10^{B221}$ heterozygous pupae mostly behave like the wild type.

I then analysed the asymmetric divisions of the different genotypes quantifying the following defects: the polarity of the Pon-GFP crescent, the mis-segregation of Pon into the two pII daughter cells and the division angle relative to the anterior-posterior body axis (as illustrated in Figure 4.18A). 60 divisions for each genotype were quantified for the three defects and the detailed description of how the defects were analysed can be found in the materials and methods (2.6.3).

The polarity of the Pon-GFP crescent was determined by calculating the polarisation coefficient using a Fourier transformation (in case of no polarisation, the polarisation coefficient will approach 0). In *RASSF10*^{B221} mutants the Pon-GFP crescent was significantly less polarised (mean±SD: 0.2356±0.07729) compared to wild type (0.4188±0.04821) ($P<0.001$) and interestingly, heterozygotes already displayed a slight defect compared to wild type ($P<0.001$) (Figure 4.17D).

In order to see whether Pon-GFP was mis-segregated onto the two daughter pII cells, the ratio of the Pon-GFP signal intensity from the two pII cells was quantified (in case of an equal distribution, the ratio will equal one). The intensity ratios in *RASSF10*^{B221} mutants (mean±SD: 0.7228±0.1523) were significantly increased compared to wild type (0.4898±0.05602). Pon-GFP was mis-segregated into the pIIa and pIIb cells in approximately 73% of SOP divisions in *RASSF10*^{B221} mutants and in 12% of the heterozygotes (mis-segregation being defined as intensity ratios higher than the maximal ratio of the wild type).

Lastly, the analysis revealed that the angle of division relative to the anterior-posterior body axis was more randomised in *RASSF10*^{B221} mutants compared to wild type and heterozygotes (Figure 4.18B). Division angles were determined as illustrated in Figure 4.18A. The randomisation can be seen by means of the standard deviation (SD) of the division angles, which was almost twice as high for *RASSF10*^{B221} mutants (SD=68.33) as for wild type (SD=35.44) or for heterozygotes (SD=36.29).

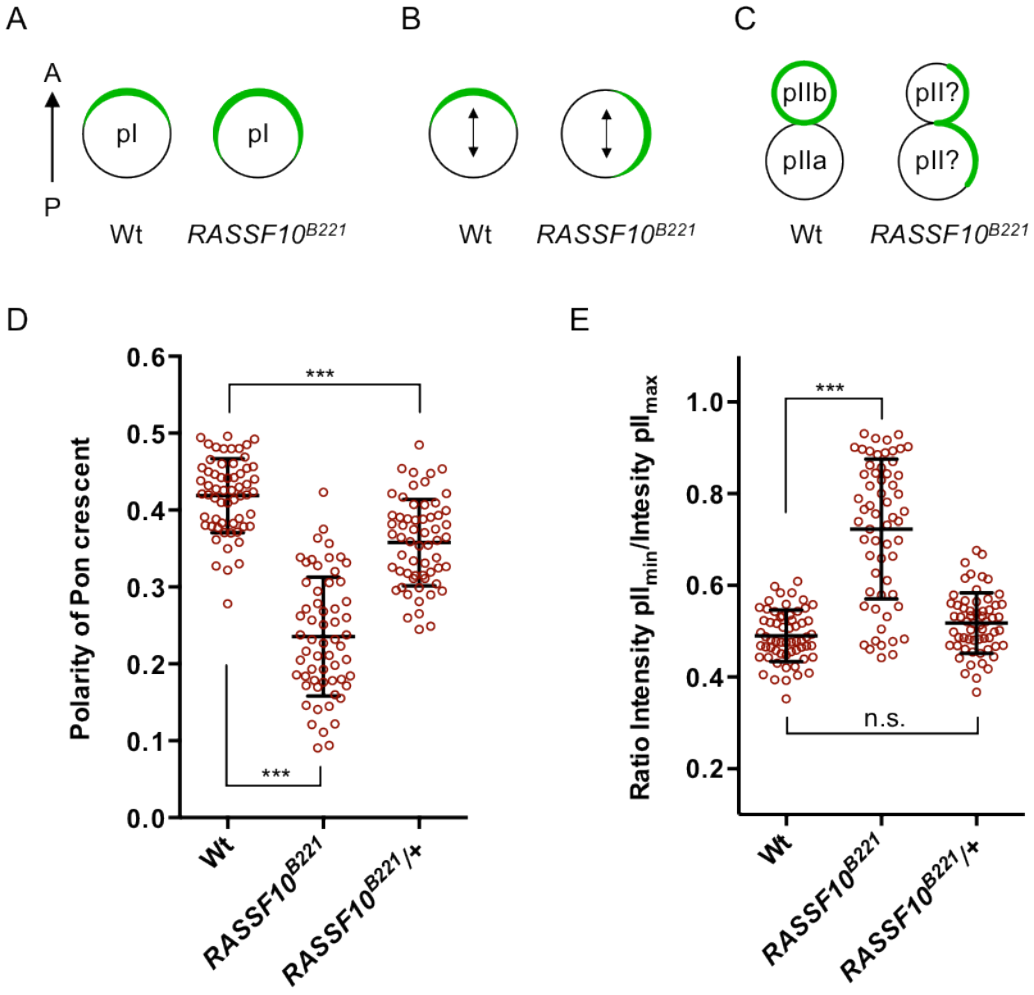

Figure 4.17 - Polarity of Pon crescent in pI cells and Pon distribution onto pII cells in *RASSF10* mutants.

(A, B, C) Schematic of the observed phenotypes in *RASSF10* mutants compared to the wild type situation. (A) Most pI cells of *RASSF10* mutants have a widened Pon-GFP crescent. In many cases the direction of division is not aligned to the Pon-GFP crescent in pI cells (B), resulting in partitioning of Pon-GFP into both daughter pII cells instead of solely pIIb (C). (D) Quantification of the polarity coefficient of the Pon crescent of pI cells (no polarity = 0). (E) Quantification of Pon-GFP mis-segregation. The distribution of Pon-GFP into the two daughter cells was measured by dividing the mean grey value intensities of the daughter cells. In case of mis-segregation ratios will be approaching 1. n=60 for each genotype from 3 pupae and error bars represent the mean ± standard deviation. (One-way ANOVA with Bonferroni's correction: ***P<0.001)

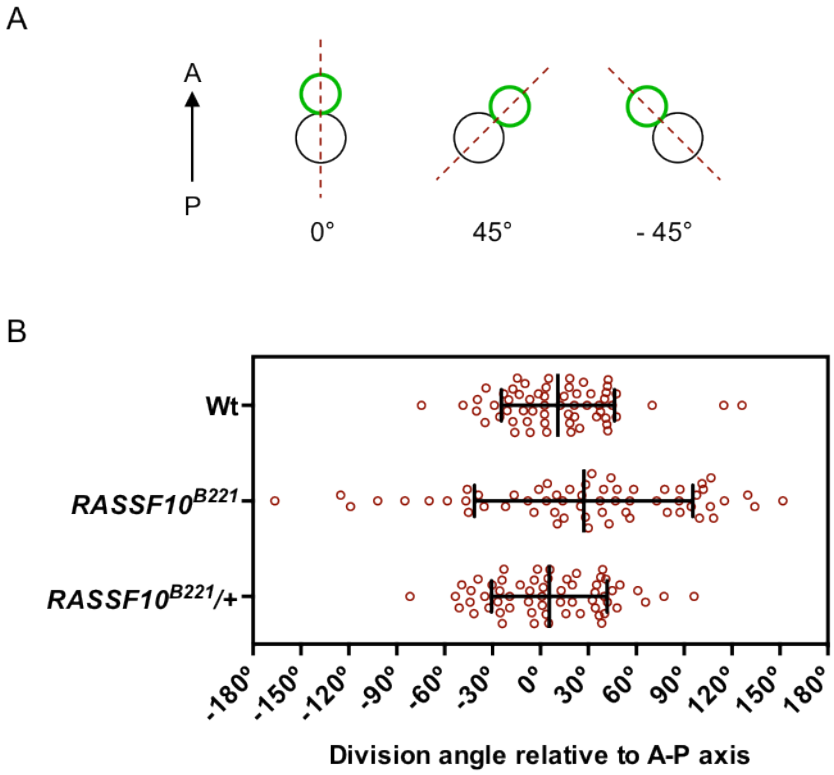

Figure 4.18 - The angle of SOP divisions relative to the anterior-posterior axis is randomised in *RASSF10*^{B221} mutants.

(A) Illustration of how the division angle relative to the anterior-posterior axis was determined. A line through the centre of both pII daughter cells was drawn and the angle relative to the A-P axis was measured. (B) The angle of asymmetric SOP divisions relative to the anterior-posterior axis is randomised in *RASSF10*^{B221} mutants compared to in wild type control or in *RASSF10*^{B221} heterozygous. n=60 for each genotype from 3 pupae and error bars represent the mean ± standard deviation.

Loss of function of Fz (Bellaiche et al., 2001a, Bellaiche et al., 2004) or Dsh (Bellaiche et al., 2004, Gomes et al., 2009) both cause only a mild Pon-GFP mis-segregation phenotype, as the antagonism between Baz and Pins in not affected in these mutants and maintains the asymmetric localisation of cell fate determinants consistent with the spindle orientation. However, the division angle relative to the anterior-posterior axis is randomised, as Fz/Dsh are required to orient the spindle in the plane of the epithelium by direct interaction with Mud (Segalen et al., 2010). In contrast, in *baz* and *pins*

mutants, either a weak Pon/Numb-crescent is present or no crescent forms at all and Pon/Numb are uniformly spread in pI cells, as Baz and Pins are required for cell fate determinant asymmetric localisation (Roegiers et al., 2001a, Bellaiche et al., 2001b). However, in both mutants the division angle remains orientated along the anterior-posterior axis (Bellaiche et al., 2001b). Thus, the *RASSF10*^{B221} mutant ACD phenotype has elements of both Fz/Dsh and Baz/Pins disruption. Firstly, loss of RASSF10 function causes a broadening of the Pon crescent and a strong Pon-GFP mis-segregation defect (73%) similarly to Baz and secondly the randomised division angles relative to the anterior-posterior body axis resembles Fz/Dsh loss of function. As no spindle marker was expressed in this experiment, I did not analyse spindle orientation relative to the Pon crescent, which should be addressed in the future.

4.5.3 Is RASSF10 required for the asymmetric localisation of Bazooka in SOPs?

So far, I have demonstrated that RASSF10 is required for correct SOP ACDs. But what is the molecular mechanism underlying RASSF10's function in ACD? One possible role for RASSF10 could be to facilitate the association of the Baz-Par6-aPKC complex with Fz/Dsh, by bridging the interaction between Baz and Fz/Dsh. This idea is supported by the findings that RASSF10 can bind to Baz and Fz/Dsh in co-IP experiments (Figure 3.6, Figure 3.8 and Figure 3.11), and co-localises with them in wing disc SOPs (Figure 4.8 and Figure 4.9). It has been recently shown that the asymmetric localisation of the Baz-Par6-aPKC is dependent on Fz/Dsh prior to mitosis (Besson et al., 2015). However, upon entry into mitosis, Fz/Dsh are dispensable for the asymmetric localisation of the Baz-Par6-aPKC complex, as *dsh* of *fz* mutants, Pins facilitates the asymmetric localisation of Baz opposite from the Dlg-Pins-Gα_i complex, albeit with a random orientation with regards to the anterior-posterior axis (Bellaiche et al., 2001b, Bellaiche et al., 2004).

In order to test whether RASSF10 is required for the initial asymmetric localisation and hence polarisation of Baz in SOP cells of the pupal notum prior to mitosis, I looked at the localisation of Baz in *RASSF10*^{B221} mutants. In wild type nota, Baz is found asymmetrically enriched in SOP cells at 15 hours APF (Figure 4.19A-A''). In contrast, in *RASSF10*^{B221} mutants, Baz was not enriched in SOP cells compared to the

surrounding epithelial cells and appeared less polarised (Figure 4.19B-B''). This suggests that RASSF10 might indeed be required for initial asymmetric localisation of Baz. This very preliminary experiment should be followed up by quantifications of the polarisation of Baz, similarly to the Besson et al. study, using the Baz-GFP line for live imaging. Moreover, live imaging will reveal whether RASSF10 is needed for the asymmetric localisation of Baz during mitosis or if Baz still asymmetrically localises (due to Pins) during mitosis, similar to Fz/Dsh loss.

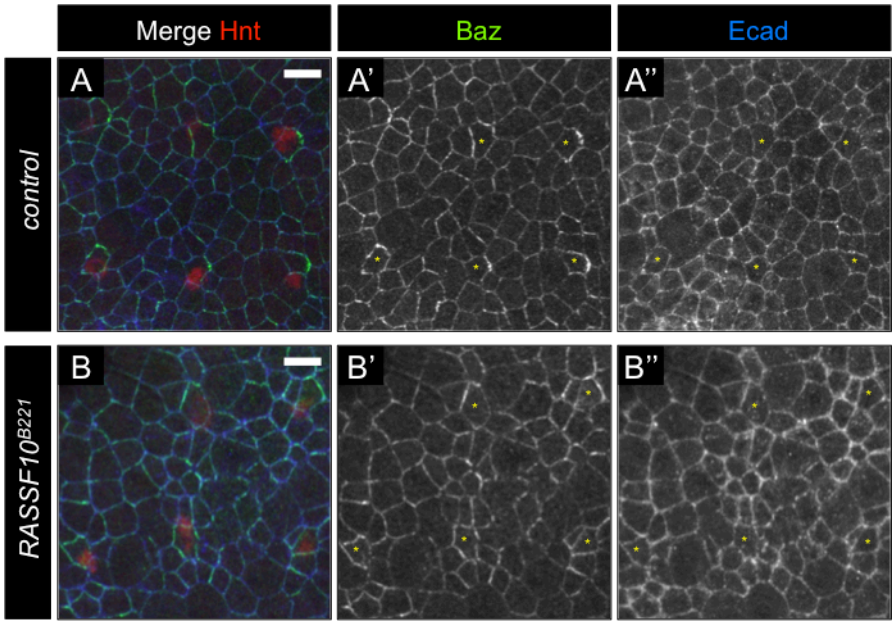

Figure 4.19 - Loss of *RASSF10* affects the asymmetric localisation of Bazooka.
Planar confocal sections of pupal nota at 15 h APF stained for Baz, Hnt and Ecad. pI cells were identified by the presence of the SOP marker Hnt (and are labelled with asterisk). Baz is asymmetrically enriched in pI cells of *RASSF10* control nota (A-A''). The asymmetric localisation of Baz in pI cells is less pronounced in the $RASSF10^{B221}$ mutant (B-B'). Scale bar = 10 μm.

4.6 Concluding remarks

In this chapter I have added substance to the hypothesis that RASSF10 is required for correct ACD of SOPs of the peripheral nervous system in *Drosophila*. Firstly, $RASSF10^{B221}$ mutants exhibit a bristle phenotype, which is linked to defects in ACD of

SOPs. The requirement for RASSF10 function in ACD was supported by the genetic interactions with ACD polarity determinants such as *fz*, *dsh*, *baz* and *pins*. Furthermore, I demonstrated that RASSF10 is specifically expressed in SOPs of the wing imaginal disc and is found asymmetrically enriched at the cell cortex together with its binding partners Fz, Dsh and Baz. Moreover, RASSF10 localises in SOP cells of the pupal notum at the posterior cortex prior to mitosis, as is the case for Fz, Dsh and the Baz-Par6-aPKC complex. In order to confirm the mitotic behaviour of GFP-RASSF10 live imaging could be repeated in the $RASSF10^{B221}$ mutant background, or a GFP-RASSF10 (also for GFP-RASSF9) knockin at the endogenous locus could be generated with CRISPR/Cas9. In addition, the staining protocol for endogenous RASSF10 will need to be optimised.

Ultimately, ACD of SOPs of the pupal notum display several defects in $RASSF10^{B221}$ mutants. Firstly, the asymmetric localisation of the cell fate determinant Pon is less pronounced in pI cells and Pon is mis-segregated onto both daughter cells, instead of solely pIIb. In addition, the division angle of the SOP cells relative to the anterior-posterior body axis is markedly randomised. Taken together, these findings suggest that RASSF10 might function together with Dsh, Fz and Baz at the posterior cortex to establish the asymmetric distribution of cell fate determinants.

However the exact mechanism of how RASSF10 functions at the posterior cortex remains unanswered. One possible hypothesis is that RASSF10 functions as the linker between Fz/Dsh and Baz. Fz/Dsh (together with the other PCP components) establish the initial polarity in SOPs and could localise the Baz-Par6-aPKC complex by recruiting RASSF10 at the posterior cortex prior to mitosis. This model is supported by the preliminary finding that the asymmetric localisation of Baz prior to mitosis was impaired in $RASSF10^{B221}$ mutants (Figure 4.19). However, RASSF10 must also have additional functions, as loss of function of RASSF10 causes stronger and additional ACD phenotypes than mutants of PCP components, which cannot be explained by a simple linker role (Bellaiche et al., 2001a, Bellaiche et al., 2004, Gomes et al., 2009). I will address the potential roles of RASSF10 in more detail in the discussion (see 6.3) and will also propose future experiments to elucidate the function of RASSF10 in ACD.

Chapter 5 The function of the ubiquitin system around Spc25 at the kinetochore

In this chapter of my thesis I will present the project I worked on in Helle Ulrich's lab. My main focus lay on studying the function of the ubiquitin binding of Spc25 in the context of the kinetochore, and consequently revealing the interactors and underlying regulation, as well as to further characterise the ubiquitin-binding domain of Spc25. In this way, I hoped to build on Shengkai Zhao's work ((Zhao, 2010), see 1.10.4) and to ascertain whether substance can be added to the theory it implies - namely that the ubiquitin binding of Spc25 might be prerequisite in the stable maintenance of the kinetochore complex.

5.1 Genetic interactions of *spc25 (L109A)* with temperature-sensitive mutants of kinetochore components

The ubiquitin-binding defective *spc25 (L109A)* mutant has no obvious phenotype. Therefore, it is difficult to predict the function of the ubiquitin binding of Spc25. One hint regarding the function was the synthetic interaction of *spc25 (L109A)* with temperature-sensitive alleles of *DSN1*. The *spc25 (L109A)* mutation led to an increased temperature sensitivity of *dsn1-7* and *dsn1-8* (Zhao, 2010) (see 1.10.4). This could mean that the function of ubiquitin binding lies in maintaining the stability of the kinetochore. However, is the genetic interaction specific for *DSN1*? This would indicate that the Dsn1 protein might be the direct ubiquitylated interactor of Spc25. Or, does the Spc25 (L109A) mutation further destabilise already unstable kinetochore proteins in general? In order to investigate these two options I decided to systematically analyse the genetic interactions of the *spc25 (L109A)* mutant with temperature-sensitive mutants of other kinetochore proteins. I tested the effect of the *spc25 (L109A)* mutation on different temperature-sensitive alleles of inner, outer and central kinetochore components (*ask1-22*, *dad1-13*, *dam1-31*, *duo1-61*, *mtw1-11*, *ndc10-1*, *ndc80-1*, *nnf1-77*, *nsl1-5*, *nsl1-6*, *nuf2-61*, *spc24-1*, *spc105-4* and *spc105-15* (Nekrasov et al., 2003)). In Figure 5.1A the

tested mutants are grouped according to the kinetochore complex they belong to and Figure 5.1B illustrates the position of the tested mutants within the kinetochore.

Double mutants were created by mating of *spc25 (L109A)* with different temperature-sensitive mutants, followed by tetrad dissection. For the temperature sensitivity test cultures were spotted on YPD plates in serial dilutions and then grown at different temperatures.

Firstly, I was able to confirm the previous result that the *spc25 (L109A) dsn1-7* and *spc25 (L109A) dsn1-8* double mutants were more sensitive to higher temperatures than the temperature-sensitive mutants alone and that the L109A mutation of *spc25* on its own had no effect (Figure 5.2). By contrast, the *spc25 (L109A)* mutation had no influence on the temperature sensitivity of *ndc10-1*, *mtw1-11*, *nnf1-77*, *nsl1-5*, *nsl1-6*, *dam1-31*, *duo1-61*, *dad1-13*, *ask1-22*. However, I did find additional genetic interactions for *spc25 (L109A)* as it worsened the phenotypes of *spc105-4*, *spc105-15*, *nuf2-61* and *ndc80-1* (Figure 5.2). The strongest impact was observed for the temperature-sensitive alleles of *SPC105*. For both *spc105-4* and *spc105-15* the permissive temperature was reduced from 35 °C to 31 °C, which was an even stronger effect than was seen with Dsn1.

When I was trying to cross *spc24-1*, a temperature-sensitive allele of *SPC24,* with the *spc25* mutant, I discovered a synthetic lethality between those two mutants. I performed several tetrad dissections, but a double mutant was never obtained. The *spc24-1* mutant has overall 8 amino acid substitutions, which are scattered from the C- to the N-terminus of Spc24 (Wigge and Kilmartin, 2001). In order to determine whether the synthetic lethality is specific for this mutant or whether other temperature-sensitive alleles carrying different mutations of *SPC24* are also lethal in combination with *spc25 (L109A)*, I tested *spc24-12* and *spc24-13* (Le Masson et al., 2002). For both of them, initial crossings with *spc25 (L109A)* resulted only in single mutants. The *spc24-12* allele expresses a truncated version of Spc24 (amino acids 1-183) that lacks the N-terminus and *spc24-13* has just a single substitution (L38P) (Le Masson et al., 2002).

From these preliminary results I could conclude that the synthetic lethality is clearly not specific for the *spc24-1* allele.

A

Kinetochore component	*ts* mutant
Ndc10/Cbf3 complex	*ndc10-1*
Mtw1 complex	*dsn1-7/8* *mtw1-11* *nnf1-77* *nsl1-5/6*
Spc105 complex	*spc105-4/15*
Ndc80 complex	*ndc80-1* *nuf2-61* *spc24-1*
Dam1 complex	*ask1-22* *dad1-13* *dam1-31* *duo1-61*

B

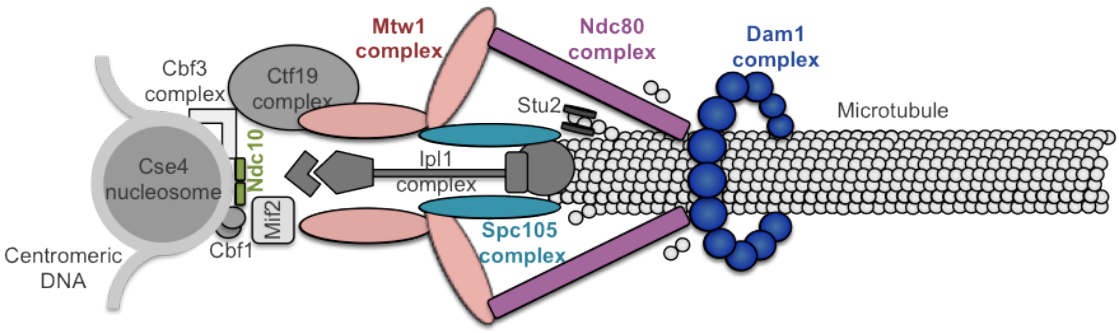

Figure 5.1 - Temperature-sensitive mutants of kinetochore components tested for genetic interaction with *spc25 (L109A)*.

(A) Grouping of the temperature-sensitive (*ts*) mutants screened for genetic interaction with *spc25 (L109A)* according to their kinetochore complex. Spc25 is a member of the Ndc80 complex. (B) Position of the relevant complexes (highlighted in colour) within the kinetochore (figure adapted from (Westermann et al., 2007)).

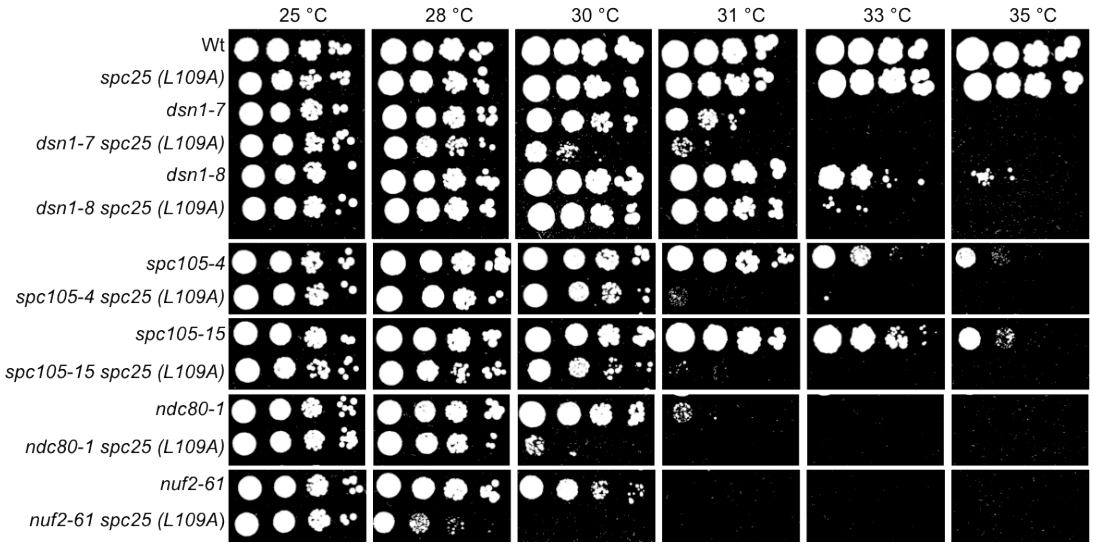

Figure 5.2 - *spc25 (L109A)* increases the temperature sensitivity of other kinetochore mutants.

Double mutants were created by mating and tetrad dissection. 3.3 µL of each yeast culture (OD_{600} = 0.2) and three serial 10-fold dilutions were spotted on YPD plates and grown for three days at 25, 28, 30, 31, 33 and 35 °C.

In summary, I was able to show that the genetic interactions of *spc25 (L109A)* with temperature-sensitive alleles of *DSN1* are not specific for Dsn1 of the Mtw1 complex as the L109A mutant also affects the temperature sensitivity of other kinetochore protein mutants. Interestingly, all of the mutants were in close proximity to Spc25, namely Spc105 and the remaining members of the Ndc80 complex in which Spc25 resides. Additionally, there was no effect on temperature-sensitive alleles of *NDC10*, the remaining Mtw1 complex (Nsl1, Mtw1, Nnf1) and members of the Dam1 complex (Dam1, Duo1, Ask1, Dad1).

5.2 Are the genetic interactions of *spc25 (L109A)* due to the ubiquitin-binding deficiency?

These results raised the question of whether the observed synthetic effects were caused by the defect of the ubiquitin-binding domain of Spc25 or whether the L109A mutation affects the temperature-sensitive mutants in an ubiquitin-independent manner?

To answer this question I tested whether the fusion of different ubiquitin-binding domains to the C-terminus of Spc25 (L109A) or to Spc24 would rescue the phenotype of the *spc105-15 spc25 (L109A)* double mutant or the synthetic lethality of *spc24-1* and *spc25 (L109A)*. I chose the *spc105-15 spc25 (L109A)* double mutant as it held the strongest increase for the temperature sensitivity, so that a rescue would be more obvious. In addition, the synthetic lethality with *spc24-1* was chosen, as the rescue would mean the survival of double mutants. If a different ubiquitin-binding domain and therefore the restoration of the ubiquitin-binding ability of Spc25 (L109A) rescued the double mutants, one could assume that the phenotype was linked to the defect in ubiquitin binding. I decided to use the following two UBDs for the fusion: the UIM-1 (ubiquitin-interacting motif) domain of yeast Vps27 and the MIU (motif interacting with ubiquitin) domain of human Rabex-5. The UIM-1 (256-278) domain binds ubiquitin with a low to intermediate affinity (K_D = 277 μM) (Swanson et al., 2003), while the MIU (48-74) domain has a comparatively higher affinity for ubiquitin (K_D = 28.7 μM) (Penengo et al., 2006). Both of them interact with ubiquitin via a single α-helix. In order to fuse them to the C-terminus of Spc24 and Spc25 (see Figure 5.3A), I modified a 3xFLAG-HIS3MX6 tagging cassette (Funakoshi and Hochstrasser, 2009) to the following construct: a 6 amino acid linker, the UBD (UIM or MIU), then another linker (six glycine residues) and lastly the 3xFLAG-tag for the detection (Figure 5.3B). The yeast strains were transformed with the cassettes and positive transformants were selected on plates lacking histidine.

Figure 5.4A-B shows that all the fusion proteins for Spc24 and Spc25 were expressed in the different strains. However, looking at the fusions to spc24-1 (Figure 5.4A), it was noticeable that the protein behaved differently for all the constructs compared to the wild type Spc24, as the signal was weaker and ran higher on an SDS PAGE gel. This already indicated that the mutant protein is likely quite unstable.

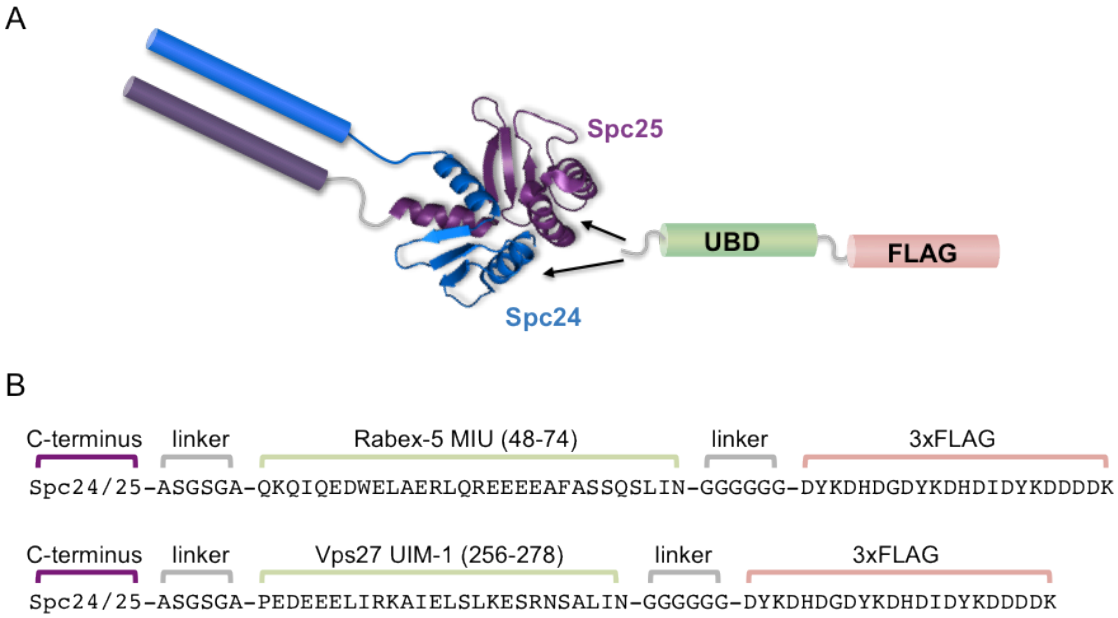

Figure 5.3 - Fusion of ubiquitin-binding domains to the C-terminus of Spc24 or Spc25.
(A) Model of the fusion of a UBD to the C-terminus of either Spc24 or Spc25 (structure of the Spc24/25 globular domains: PDB access code 2FV4). (B) Protein sequences of the two tagging cassettes for the fusions of the UBD.

After confirming that all fusions were expressed I started the rescue experiments. Fusion of neither the UIM nor the MIU domain to Spc25 (L109A) rescued the synthetic lethality with *spc24-1* as none of the crossings resulted in the formation of viable double mutants. I then examined the temperature sensitivity of single mutants harbouring the fusions. The wild type strains expressing the FLAG-tagged Spc25, the UIM or MIU domain fusions to Spc25 behaved as the original strain (Wt) as seen in Figure 5.5. Also the different fusions (FLAG, UIM or MIU) to *spc25 (L109A)* did not result in any difference in the temperature sensitivity compared to the original *spc25 (L109A)* strain. Therefore, I could be relatively sure that the fusion did not affect Spc25. Also, expression of FLAG-tagged Spc25 did not influence the temperature sensitivity of the *spc24-1* mutant. However, the fusion between Spc25 and the UIM or the MIU domain reduced the permissive temperature of the mutant. Similarly, there was no sign of the fusions rescuing the increased temperature sensitivity of *spc105-15 spc25 (L109A)* double mutant and for the UIM domain the phenotype was even further debilitated

(Figure 5.5). Even for the *spc105-15* mutant alone, fusion of the UIM and MIU domain to Spc25 made the strain even more sensitive, while the FLAG-tag had no effect.

Next, I tested whether there is a rescue-effect by fusing the UBDs to the C-terminus of Spc24. At first, there was a surprising result, because I suddenly got double mutants when I crossed the *spc25 (L109A)* mutant with the *spc24-1* fusions (FLAG, UIM and MIU), even for the FLAG-tagged *spc24-1* control. From there the next step was to test whether the fusion of the UIM or MIU domain had an effect on the temperature sensitivity of the double mutants compared to the FLAG-tag alone.

Checking the behaviour at higher temperatures for the *spc24-1* mutant as well as all the different fusion constructs (Figure 5.6A) showed that all three increased the permissive temperature from 30 °C to 32 °C. The double mutants with the different fusion proteins reflected exactly the same pattern as that of the *spc24-1* mutant fusions alone, just with a slightly increased sensitivity, as seen in Figure 5.6A. I concluded from these findings and the protein expression results (Figure 5.4A) that the protein of *spc24-1* seemed to be quite unstable, such that even the fusion of a FLAG-tag alone somehow had the ability to stabilise it. The rescue of the synthetic lethality of *spc25 (L109A)* and *spc24-1* had therefore nothing to do with the potentially restored ubiquitin binding of Spc25 (L109A), but more so with the stabilisation of the *spc24-1* protein itself.

The last rescue I tested was the fusion of the UBDs to Spc24 and its impact on the *spc105-15 spc25 (L109A)* double mutant. For the *spc105-15* control, all of the constructs acted as the original strain, although the UIM-fusion seemed to slightly worsen the phenotype in the temperature sensitivity screen (Figure 5.6A). This UIM fusion showed no rescue effect for the double mutant and actually caused the opposite - an increase of the temperature sensitivity. However, I found that the fusion of the MIU domain to Spc24 led to a very marginal rescue of *spc105-15 spc25 (L109A)* compared to the FLAG-tag control and the untagged double mutant at 31 °C, which was noticeable in more dense colonies for the MIU fusion.

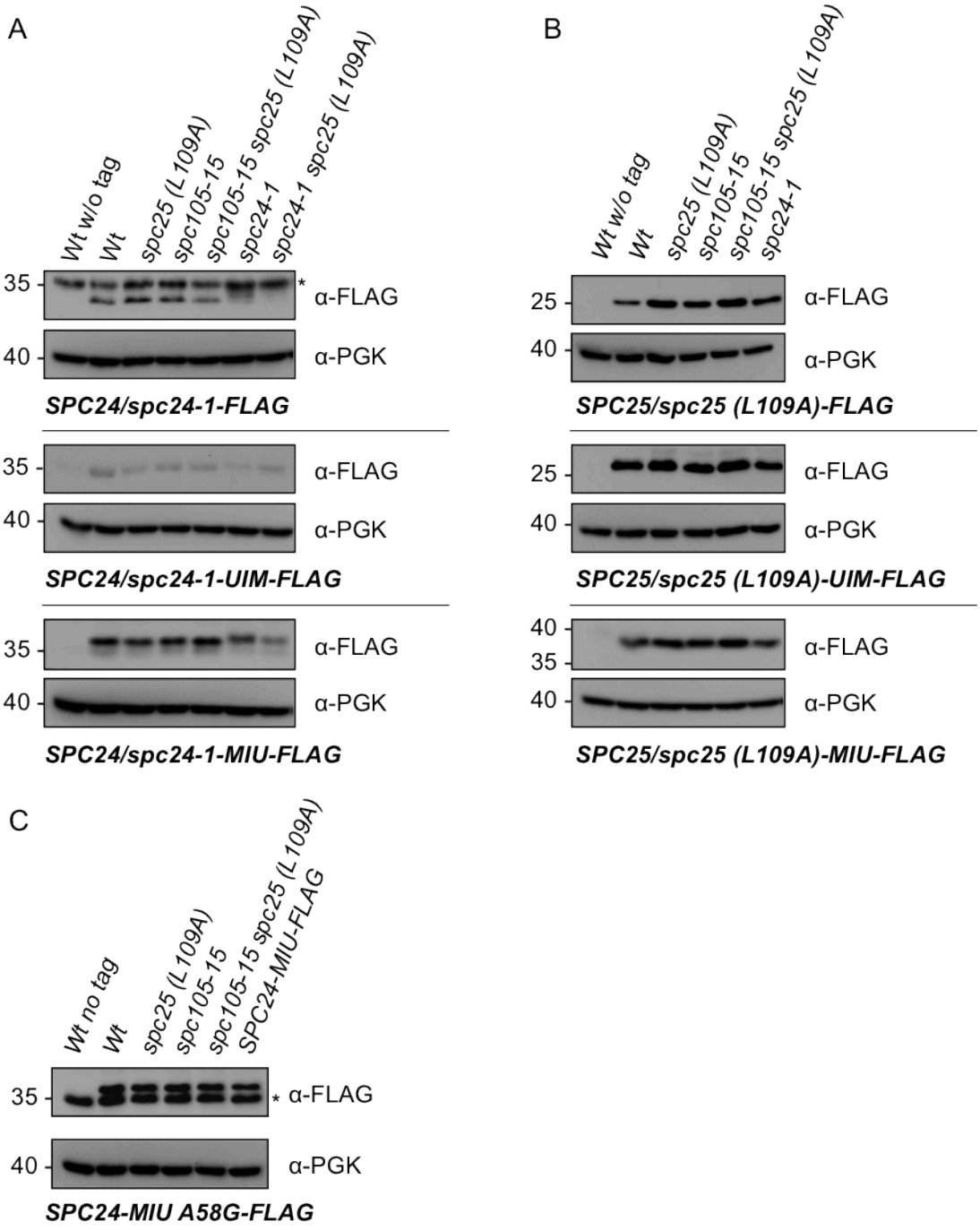

Figure 5.4 - Expression of the different Spc24- and Spc25-UBD-fusion proteins in the different strain backgrounds.

In order to fuse the FLAG-tag or the UBD constructs to the C-terminus of Spc24/Spc25 the different strains were transformed with the tagging cassettes. Tagging cassettes consisted of a FLAG-tag alone or an UBD-FLAG-tag. To test the expression of the created UBD-fusions proteins in the different strain backgrounds total protein extracts were analysed in western blots using anti-FLAG antibody. PGK was used as a loading control. (Continued on next page)

Figure 5.4 (Continued from previous page) **-** Cross-reacting, unspecific bands are labelled with an asterisk. (A) Expression of Spc24/spc24-1 fusion proteins. (B) Expression of Spc25/spc25 (L109A) fusion proteins. (C) Expression of Spc24-MIU A58G-FLAG.

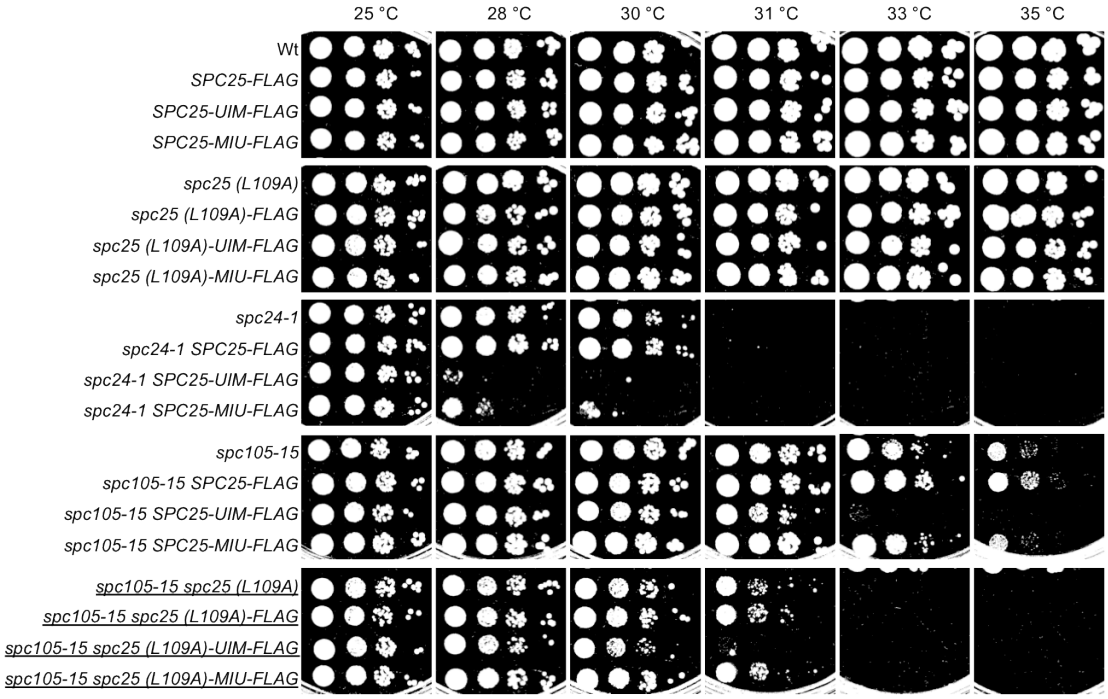

Figure 5.5 - The fusion of the UIM or MIU ubiquitin-binding domain to Spc25 (L109A) does not rescue the phenotype of the double mutants.

Strains expressing the Spc25-UBD fusions were created by PCR-based epitope tagging. For the temperature sensitivity test cultures were prepared and spotted as described in Figure 5.2.

In order to prove that this little rescue is due to a restored ubiquitin binding and not to other interactions, I mutated the alanine 58 residue of the MIU domain to glycine, as this mutation was shown to cause loss of the interaction with ubiquitin (Penengo et al., 2006). The strains with the fusion of the MIU (A58G) domain to Spc24 were created as previously described and Figure 5.4C confirms that all strains expressed the fusion and that protein levels were the same as for the wild type MIU (last lane). The temperature sensitivity screen in Figure 5.6B shows that the ubiquitin-binding deficient mutant of the MIU domain behaved exactly as the functional MIU domain. The tiny rescue by the fusion of the MIU domain to Spc24 of *spc105-15 spc25 (L109A)* could not therefore be associated with a re-establishment of ubiquitin binding.

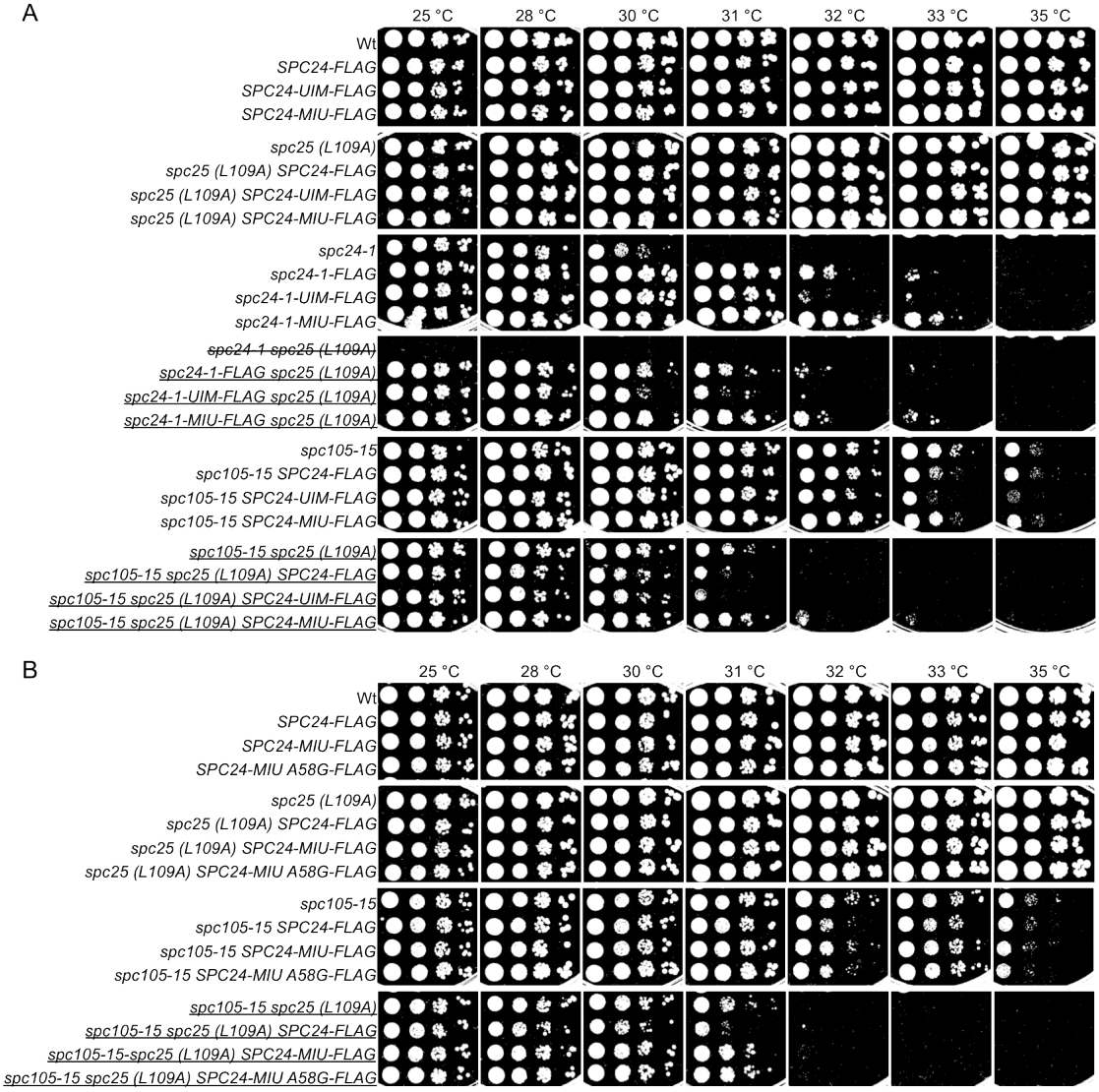

Figure 5.6 - The fusion of the UIM or MIU domain to Spc24 does not rescue the phenotype of the double mutants.

Strains expressing the Spc24-UBD fusions were created by PCR-based epitope tagging. For the temperature sensitivity test cultures were prepared and spotted as described in Figure 5.2.

In conclusion, the *spc25 (L109A)* mutation did not only affect temperature-sensitive alleles of *DSN1*, but also those of *SPC105*, *NUF2*, *NDC80* and *SPC24*. Unfortunately, I could not link the observed genetic interactions of *spc25 (L109A)* to the deficiency in ubiquitin binding, as none of the rescue attempts with the UBD fusions to Spc24/25 were successful. However, this negative result is inconclusive and does not rule out the connection to the ubiquitin system.

5.3 Ubiquitylation of kinetochore proteins

5.3.1 Dsn1, Nsl1 and Spc105 are ubiquitylated

The genetic interaction studies have shown that the L109A mutation of Spc25 affected several kinetochore mutants located close to Spc25 in the kinetochore. However, I could not prove a connection to the ubiquitin-binding deficiency. Another approach to reveal the function of the ubiquitin binding of Spc25 was trying to find the ubiquitylated protein(s) that interact(s) with the UBD of Spc25. Using a TAP-tagged strain collection, it has previously been shown in the laboratory that several kinetochore proteins were ubiquitylated *in vivo* (Zhao, 2010). Most interestingly, Dsn1 of the Mtw1 complex was found to be monoubiquitylated and also Mtw1 and Nnf1 were ubiquitylated. Based partly on my previous findings with the temperature-sensitive mutants, I decided to focus on kinetochore proteins in close proximity to Spc25 (Joglekar et al., 2009). Therefore, I checked ubiquitylation for the members of the Mtw1 complex (Dsn1, Nsl1, Nnf1 and Mtw1) and Spc105.

To analyse the *in vivo* ubiquitylation of kinetochore proteins I used TAP-tagged alleles of members of the Mtw1 complex. For the purpose of confirming the previous results I also tagged Dsn1 with a 6xHA- or with a 9xmyc-tag and I did the same for Spc105, as there was no TAP-tagged allele available. Strains harbouring tagged alleles were then transformed with an episomal expression vector for copper-inducible expression of His-tagged ubiquitin, and pull-downs of total ubiquitin conjugates were performed under denaturing conditions (Ulrich and Davies, 2009). Pull-down and input samples were analysed by western blot using tag-specific antibodies.

Firstly, I reproduced the finding that TAP-tagged Dsn1 is ubiquitylated, as is indicated by a shift of the input band (I, +/− His-Ubi) to a higher molecular weight for the pull-down sample (P, + His-Ubi) in Figure 5.7A. The ubiquitylation was also present for HA- and myc-tagged Dsn1 (Figure 5.7B). Above the band representing the monoubiquitin signal were faint bands of a higher molecular weight visible for the TAP- and HA-tagged versions. I concluded from this that Dsn1 is mainly monoubiquitylated, but also polyubiquitylated. In all Dsn1 pull-down samples (P, + His-Ubi) as well as the negative control without expression of His-tagged ubiquitin (P, − His-Ubi), a band was detectable on the same height as unmodified Dsn1, indicating

that Dsn1 itself bound to the Ni-NTA beads. I discovered that TAP-tagged Nsl1 was also ubiquitylated (P, + His-Ubi), with a strong signal for monoubiquitin as well as the presence of an additional band at a higher molecular weight, which I interpreted as diubiquitylation (Figure 5.7A). However, I could not detect any ubiquitylation signals for TAP-tagged Mtw1 (P, + His-Ubi) and Nnf1 (P, + His-Ubi) (Figure 5.7A). The pull-downs with HA- and myc-tagged Spc105 (Figure 5.7C) revealed the ubiquitylation of Spc105. As Spc105 has a high molecular weight it was not possible to distinguish between mono- and polyubiquitylation.

In conclusion Dsn1 and Nsl1 of the Mtw1 complex and Spc105 of the Spc105 complex were shown to be positive for ubiquitylation.

To be sure that the ubiquitylation signals of Dsn1, Spc105 and Nsl1 were not due to degradation caused by the tag, I checked the stability of the tagged proteins in a cycloheximide assay. Cycloheximide inhibits the *de novo* protein synthesis and was therefore used to study the amount of tagged proteins over a period of time. For this purpose, cells expressing the tagged alleles were treated with 100 mg/mL cycloheximide. Samples were taken at several different time points and analysed by western blot.

The results showed there was no difference detectable for HA-, myc- and TAP-tagged Dsn1, as seen in Figure 5.8. The tagged proteins remained stable for 3 hours and only after 21 hours was a reduction of the protein amount detectable. HA- and myc-tagged Spc105 behaved in the same pattern. Only TAP-tagged Nsl1 seemed to be less stable as in this instance the signal decreased gradually within 3 hours.

It was apparent that the identity of the tag did not influence the stability of Dsn1 and Spc105. Therefore, I was fairly sure that their ubiquitylation was not caused by the presence of the tags. It was, however, possible that the ubiquitylation of Dsn1 and Spc105 was a signal for degradation via the 26S proteasome. Therefore, I tested the effect of inhibition of the proteasome using the inhibitor MG132 on the ubiquitylation of Dsn1 and Spc105. Under those conditions polyubiquitin conjugates, which are normally degraded by the proteasome, will accumulate.

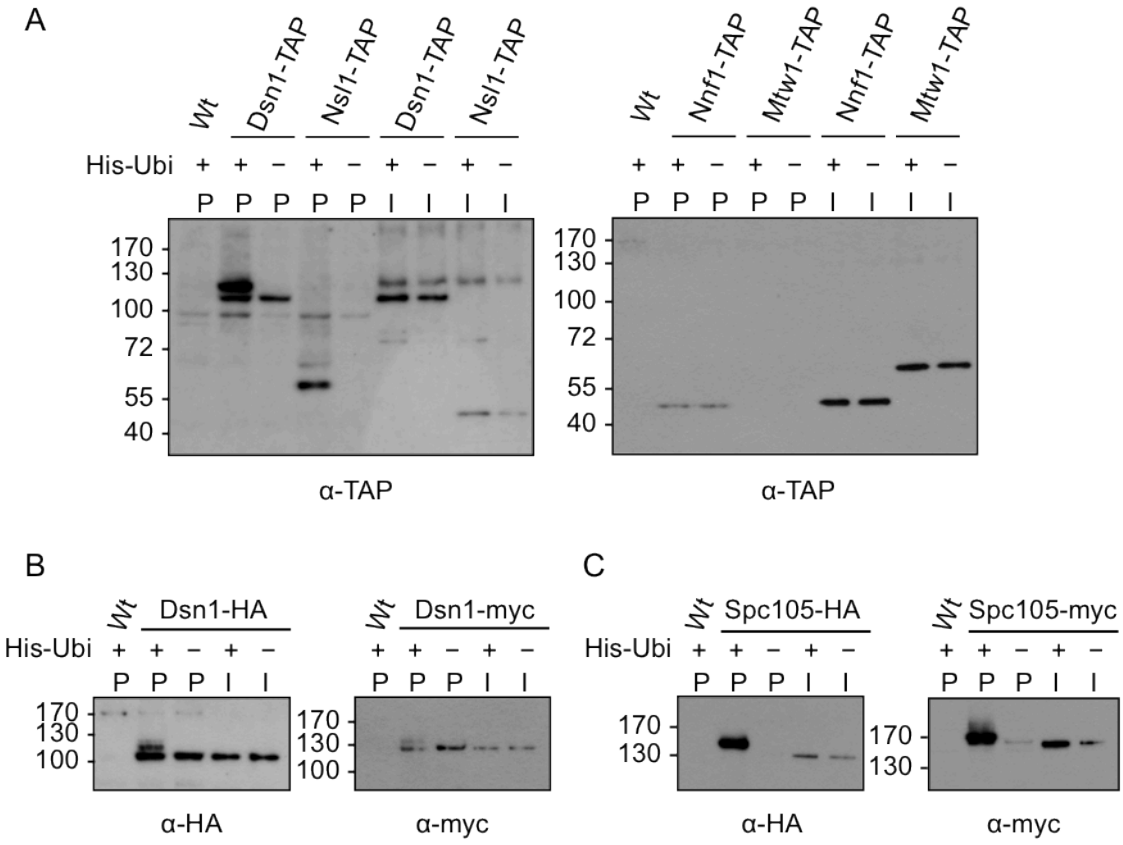

Figure 5.7 - *In vivo* ubiquitylation of different kinetochore proteins.

Yeast cells harbouring HA-, myc- or TAP-tagged alleles of the relevant genes were transformed with a vector expressing His-tagged ubiquitin (+His-Ubi) or an empty vector (−His-Ubi). His-Ubi expression was induced by addition of copper and Ni-NTA pull-downs under denaturing condition were performed with lysates prepared under denaturing conditions. Pull-down (P) and input samples (I) were analysed by western blot using the appropriate antibodies according to the respective tags. (A) Ubiquitylation of components of the Mtw1 complex (TAP-tagged strains). (B) Ubiquitylation of HA- and myc-tagged Dsn1. (C) Ubiquitylation of HA- and myc-tagged Spc105.

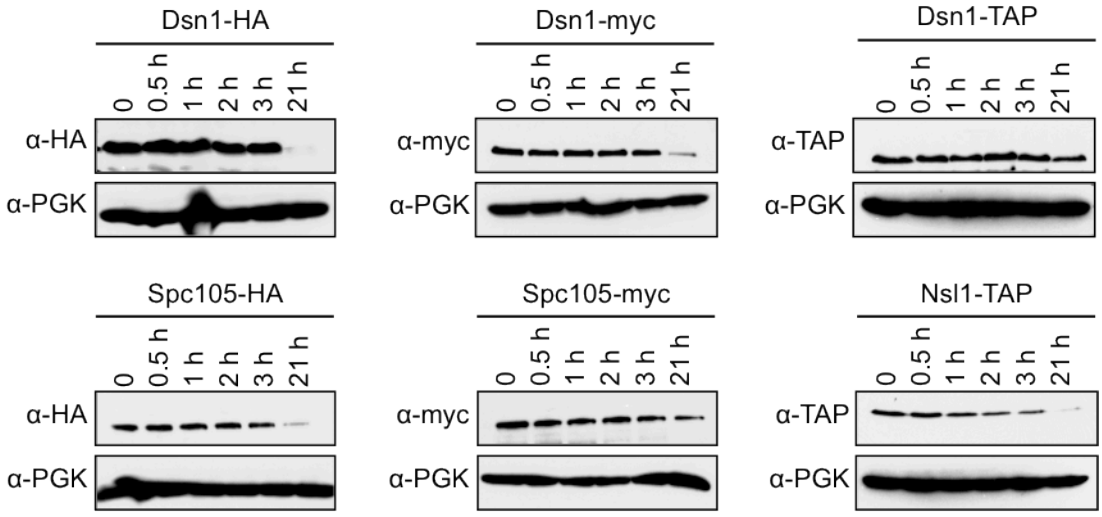

Figure 5.8 - Cycloheximide chase assays to test the stability of tagged Dsn1, Spc105 and Nsl1.

The tagged strains were treated with 100 µg/mL cycloheximide, samples were taken at the indicated time points and the protein extracts were analysed by western blot. PGK was used as a loading control.

If ubiquitylation of Dsn1/Spc105 was due to degradation, an increased ubiquitin signal would occur. To enable the uptake of the inhibitor in the yeast cells I deleted *PDR5*, thereby increasing the permeability for the drug. Strains harbouring the tagged allele of Dsn1 or Spc105 and the deletion of *PDR5* were then transformed with the episomal vector for copper-inducible His-Ubi expression. Cultures were then treated with 50 µM MG132 for two hours before performing the Ni-NTA pull-downs under denaturing conditions. Figure 5.9 shows the result from the pull-down experiments with the proteasomal inhibitor MG132. The monoubiquitylation band of Dsn1-HA for cells treated with MG132 (+ MG132, + His-Ubi, *Δpdr5*) was comparable to those without (− MG132, + His-Ubi, *Δpdr5*), while the intensity of the higher bands, representing polyubiquitylated Dsn1, was increased. The ubiquitin signal of Spc105-HA showed no difference (−/+ MG132, + His-Ubi, *Δpdr5*). As a control for successful inhibition of the proteasome pull-down, input samples (whole protein extracts) were blotted with an anti-Ubiquitin antibody and - as shown in Figure 5.9 - total ubiquitin conjugates increased when cells were treated with MG132 (−/+ MG132). For both Dsn1 and Spc105 pull-

down experiments, a band was present at around 170 kDa (labelled with an asterisk), and its intensity strongly increased in the MG132 treated samples. This band ran close to the band representing ubiquitylated Spc105. However, it was also present in controls without His-Ubi expression (+ MG132, − His-Ubi, *Δpdr5*), confirming that it was indeed an unspecific cross-reacting band and not ubiquitylated Spc105.

These results indicated that monoubiquitylation of Dsn1 and ubiquitylation of Spc105 was independent of proteasome activity, whereas the polyubiquitin signal on Dsn1 was likely to be targeted by the proteasome.

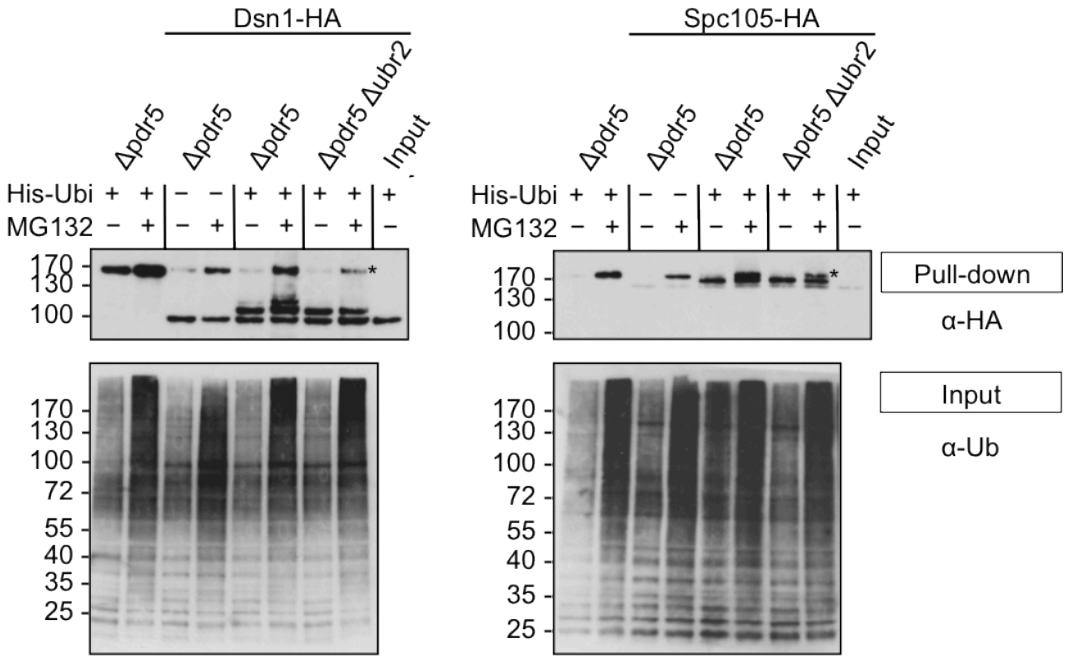

Figure 5.9 - Test of *in vivo* ubiquitylation of tagged Dsn1 and Spc105 upon inhibition of the proteasome.

PDR5 was deleted in HA-tagged Dsn1 and Spc105 strains in order to increase the cellular uptake of the proteasomal inhibitor MG132. Ni-NTA pull-downs were performed as described in Figure 5.7 with the difference that cells were treated with or without 50 µM MG132 (+ / − MG132) at an OD_{600} of 1 for 2 hours. Pull-down (P) and input samples (I) were analysed by western blot with the indicated antibodies. Upper panel: Ubiquitylation of HA-tagged Dsn1 and Spc105. Lower panel: Total ubiquitin-conjugates of input samples. Cross-reacting, unspecific bands are labelled with an asterisk.

In summary, these findings revealed that Dsn1, Nsl1 and Spc105 were ubiquitylated and could therefore all be potential interactors of the ubiquitin-binding domain of Spc25. Moreover, the experiments showed that monoubiquitylation of Dsn1 and Spc105 was independent of proteasome activity. Although Spc105 and Nsl1 were also possible candidates, I decided to begin by focussing on Dsn1 for my further studies.

5.3.2 What is the ubiquitylated site within Dsn1?

The next challenge was to prove that ubiquitylated Dsn1 actually binds to the UBD of Spc25. I therefore wanted to find an ubiquitylation deficient mutant of Dsn1. If this were true and Dsn1 was the ubiquitylated interactor, this mutant should be epistatic to the *spc25 (L109A)* mutant. However, Dsn1 contains a total of 46 lysine residues. Instead of mutating every single lysine in Dsn1, I ordered Dsn1 mutants synthesised from Addgene, in which the lysine residues were mutated in groups, as depicted in Figure 5.10A. The Dsn1 constructs had a C-terminal HA-tag and were cloned in an integrative expression vector for integration in the yeast genome. Vectors contained the promoter region of Dsn1 to allow expression similar to a wild type level. As a control, wild type Dsn1 was also cloned in the integrative plasmid. Strains expressing HA-tagged mutants and wild type Dsn1 (besides the normal untagged Dsn1) were created by integration of the vector into the *LEU2* locus of the yeast genome. To study the *in vivo* ubiquitylation of Dsn1, strains were transformed, as before, with an episomal expression vector for the copper-inducible expression of His-tagged ubiquitin, and pull-downs under denaturing conditions (Ulrich and Davies, 2009) were performed.

Unfortunately, the result of the *in vivo* ubiquitylation of the Dsn1 lysine mutants was inconclusive, as all four mutants (a-d) were still ubiquitylated (as seen in Figure 5.10B). Mutant b and c seemed to be ubiquitylated even more strongly than the wild type. The input samples, however, showed that the expression of those two mutants was much stronger compared to the other samples. It is possible that there is no specific acceptor lysine residue in Dsn1 or that there is redundancy between the ubiquitylation sites. This would make it extremely difficult to create an ubiquitylation-deficient mutant of Dsn1.

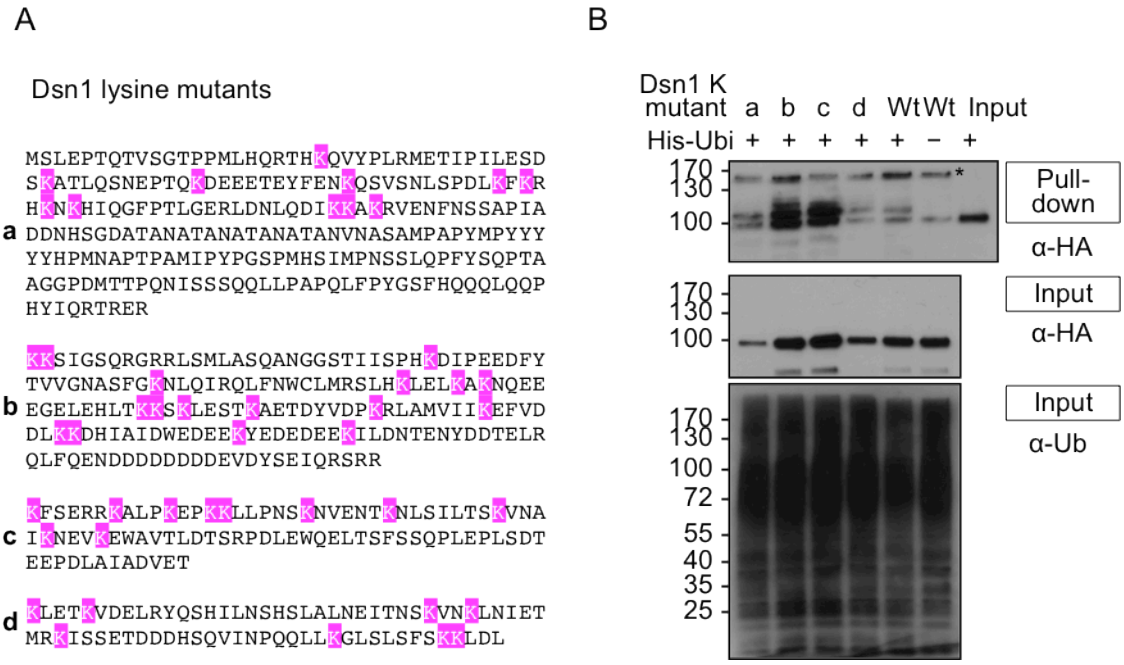

Figure 5.10 - All four Dsn1 lysine group mutants are all positive for *in vivo* ubiquitylation. (A) Lysine residues (highlighted in pink) of Dsn1 were mutated in groups, as Dsn1 has 46 lysine residues. Each of the Dsn1 lysine mutants (a-d) contained several mutations. (B) For expression of the four different lysine mutants and wild type Dsn1 (all HA-tagged) vectors were integrated into the *LEU2* locus in the yeast genome and Ni-NTA pull-downs were done as described in Figure 5.7. Pull-down (P) and input samples (I) were analysed by western blot with the indicated antibodies. Upper panel: Ubiquitylation of Dsn1 lysine mutants and wild type. Middle panel: Expression of Dsn1 lysine mutants (a-d) and wild type of input samples. Lower panel: Total ubiquitin-conjugates of input samples. Cross-reacting, unspecific bands are labelled with an asterisk.

5.3.3 Dsn1 ubiquitylation factors

As my strategy of creating an ubiquitylation-deficient lysine mutant of Dsn1 turned out to be extremely difficult, I decided to change my approach. Instead of creating an ubiquitylation deficient Dsn1 mutant, I hoped to be able to abolish ubiquitylation of Dsn1 by inactivating the responsible ubiquitin ligase E3 and/or ubiquitin-conjugating enzyme E2. A recent report from the Biggins group indicates that Ubr2 is the ubiquitin ligase responsible for ubiquitylation of Dsn1 (Akiyoshi et al., 2013b). Ubr2 has thus far been shown to work together with the ubiquitin-conjugating enzyme Rad6 on the ubiquitin-mediated degradation of the transcription factor Rpn4 (Ju et al., 2004, Wang et al., 2004) and the ribonucleotide reductase inhibitor Sml1 (Andreson et al., 2010).

In order to confirm the observation of the Biggins group, I tested the effect of an *UBR2* deletion on the *in vivo* ubiquitylation of Dsn1. Standard pull-down experiments for HA- and TAP-tagged Dsn1 (Figure 5.11) revealed that Ubr2 had no effect on the monoubiquitylation (P, + His-Ubi, *Δubr2*) compared to tagged Dsn1 in the wild type background (P, + His-Ubi). However, it seemed that the polyubiquitin signal was abolished in the *Δubr2* background. This became even more obvious under conditions of proteasome inhibition (Figure 5.9). In the *Δubr2* background and upon inhibition of the proteasome there was no polyubiquitin signal at all (+ MG132, + His-Ubi, *Δubr2 Δpdr5*). Meanwhile, I observed a strong increase in polyubiquitylation for inhibition of the proteasome alone (+ MG132, + His-Ubi, *Δpdr5*). This experiment confirmed that the monoubiquitin signal was unaffected by *Δubr2* and inhibition of the proteasome.

As there was a chance that Ubr2 might be involved in ubiquitylating Spc105 and Nsl1, I also tested the deletion of *UBR2* for these two. However Ubr2 did not seem to be the responsible ubiquitin ligase in their case (Figure 5.11). The bands representing ubiquitylation of TAP-tagged Nsl1 were still present (P, + His-Ubi, *Δubr2*) and, for HA-tagged Spc105, there was even an increase of the signal (P, + His-Ubi, *Δubr2*). This was supported by the notion that the *UBR2* knockout had no effect on the ubiquitylation of Spc105-HA upon inhibition of the proteasome (Figure 5.9).

In summary, these results elucidated that Ubr2 was responsible for polyubiquitylation of Dsn1, but was not the ubiquitin ligase involved in the monoubiquitylation.

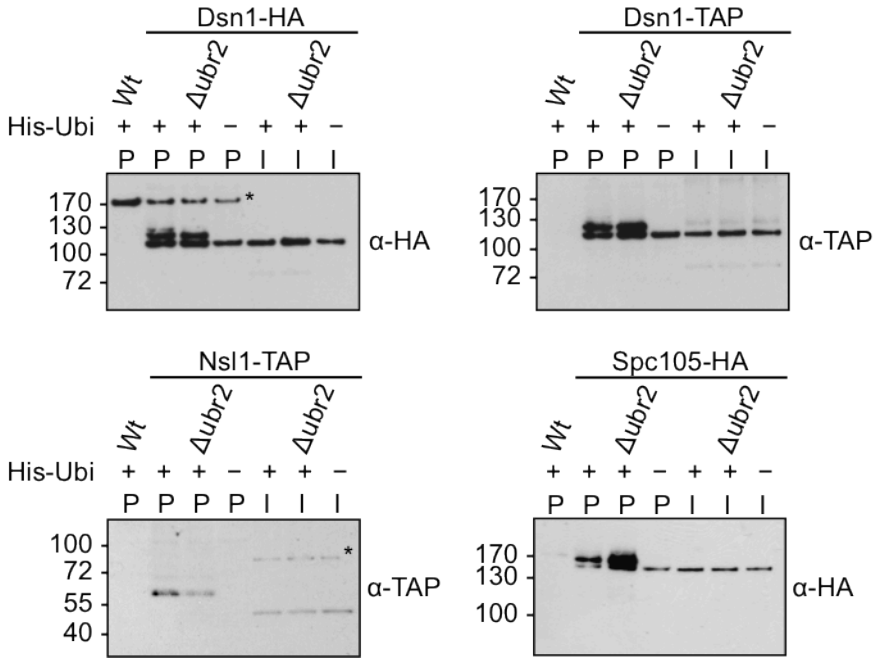

Figure 5.11 - *In vivo* ubiquitylation of tagged Dsn1, Nsl1 and Spc105 in the *Δubr2* background.

UBR2 was deleted in tagged Dsn1, Nsl1 and Spc105 strains. Ni-NTA pull-downs were performed as described in Figure 5.7. Pull-down (P) and input samples (I) were analysed by western blot using the appropriate antibodies according to the tags. Cross-reacting, unspecific bands are labelled with an asterisk.

As there was also the possibility that polyubiquitylated Dsn1 interacts with the ubiquitin-binding domain of Spc25, I was interested in the effect of an *UBR2* deletion on the synthetic temperature sensitivities involving the *spc25 (L109A)* mutation (see 5.1). If Ubr2 was the responsible ubiquitin ligase and if Dsn1 was the ubiquitylated interactor of Spc25, *Δubr2* and *spc25 (L109A)* should be epistatic with respect to their effect on other kinetochore mutants (epistatic effect being defined as *spc25 (L109A)* or *Δubr2* single mutants showing similar synthetic interactions with the temperature-sensitive mutants and the effect of *Δubr2 spc25 (L109A)* double mutants mirroring the effect of the single mutants). I therefore created double and triple mutants by transformations and crossings (*Δubr2*, temperature-sensitive mutant and *spc25 (L109A)*).

I then tested the effect of the *UBR2* deletion using a temperature sensitivity assay. However, an epistatic effect could not be observed for any of the temperature-sensitive

mutants, as seen in Figure 5.12. *dsn1-7 Δubr2* and *dsn1-7 Δubr2 spc25* showed higher temperature sensitivities, with the triple mutant being more sensitive, whereas in combination with the *dsn1-8* mutant, deletion of *UBR2* actually suppressed the synthetic phenotype to a certain degree and the phenotype of the triple mutants differed from both double mutants. The phenotypes of both alleles of the *spc105* temperature-sensitive mutants were also attenuated by the *ubr2* deletion (mild suppression) and triple mutant phenotypes differed from both double mutants. Although the mutants of the Ndc80 complex (*ndc80-1* and *nuf2-61*) exhibited increased temperature sensitivities in combination with *Δubr2*, similar to the effect of *spc25 (L109A),* the triple mutants displayed an even stronger phenotype. As earlier mentioned, the *spc25 (L109A) spc24-1* double mutant was not viable, and neither were the *spc25 (L109A) spc24-1 Δubr2* triple mutants. The *spc24-1 Δubr2* mutant was viable and displayed a higher temperature sensitivity than the *spc24-1* mutant alone.

Taken together, these results suggested that there must be at least two independent pathways of the ubiquitin system present at the kinetochore, one of them involving Ubr2 and the other involving the ubiquitin binding by Spc25. Ubr2 was responsible for polyubiquitylation of Dsn1, which seemed to be independent of the ubiquitin-binding deficiency of Spc25. Therefore, I strongly suspected that monoubiquitylated Dsn1 might be interacting with the ubiquitin-binding domain of Spc25.

As mentioned previously, both the ubiquitin ligase E3 and the ubiquitin-conjugating enzyme E2 would allow me to abolish monoubiquitylation of Dsn1 and therefore link it to the UBD of Spc25. This attempt to find the responsible E3 did not succeed, so I tried to find the E2 involved in the monoubiquitylation of Dsn1. In order to reveal the responsible E2, I looked at the *in vivo* ubiquitylation of HA-tagged Dsn1 in E2 deletion or temperature-sensitive strains. E2 candidates were Ubc1, Rad6 (Ubc2), Cdc34 (Ubc3), Ubc4, Ubc5, Ubc6, Ubc7, Ubc8, Ubc10, Ubc11 and Ubc13. I tagged Dsn1 with an HA-tag in the different strain backgrounds. As before, episomal expression of His-tagged ubiquitin was induced by the addition of copper and pull-downs took place under denaturing conditions. For Cdc34, a temperature-sensitive mutant was used as the deletion mutant is inviable (Goebl et al., 1988), and cultures were grown at the permissive temperature until an OD of 1 was reached and then shifted for 3 hours to the non-permissive temperature.

With the exception of Rad6 none of the E2s influenced the *in vivo* ubiquitylation of Dsn1 (Figure 5.13A,B), as in all the pull-down samples (P, + His-Ubi, Dsn1-HA, ΔE2) at least two, compared to the input band, higher bands were detectable. In the *Δrad6* mutant, however, polyubiquitylation (but not monoubiquitylation) of Dsn1 was abolished, which is consistent with the cooperation between Rad6 and Ubr2 described earlier. After having looked at the genetic aspects of the project, I focused on the structural analysis of the ubiquitin binding of Spc25 in the following sections.

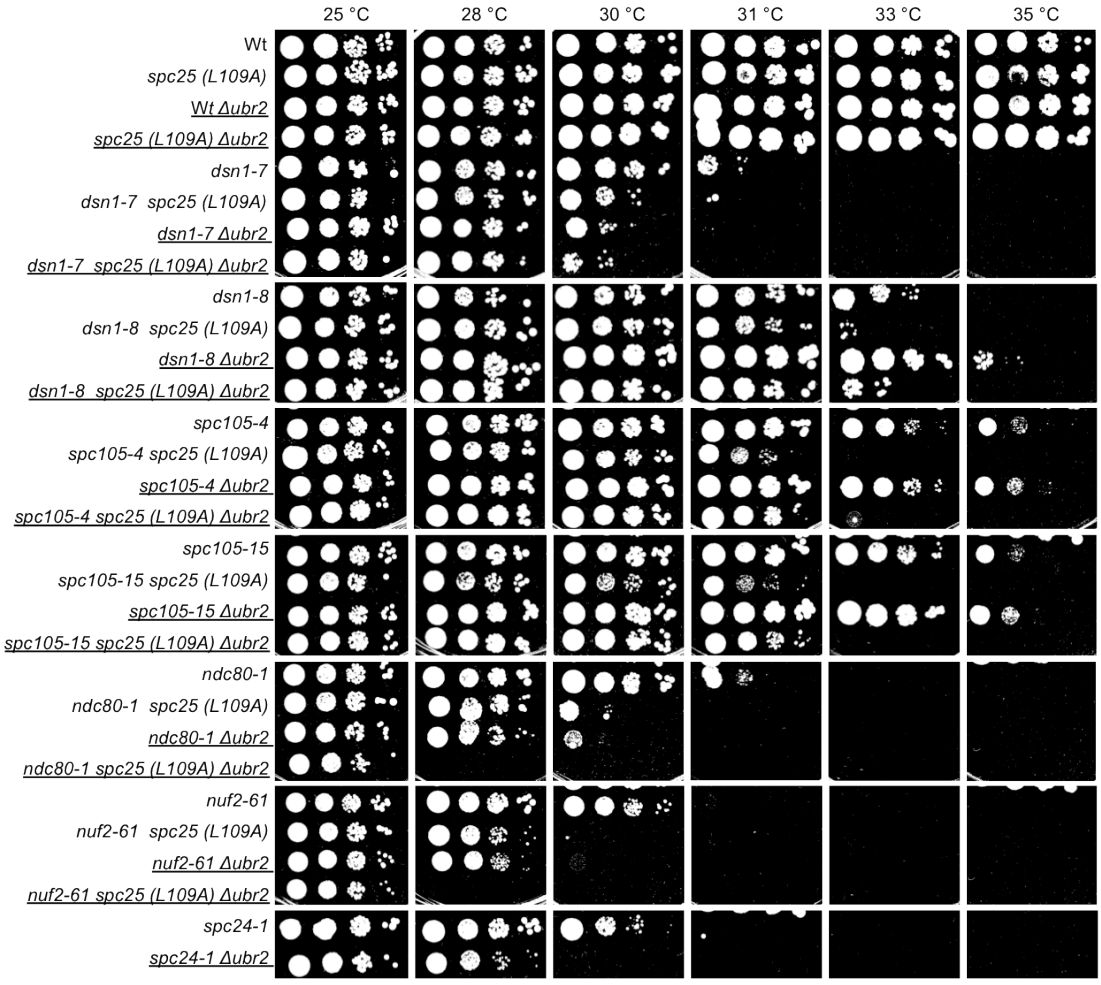

Figure 5.12 - Genetic interactions of *spc25 (L109A)* and *Δubr2* with temperature-sensitive mutants.

UBR2 was deleted in the relevant single and double mutants and temperature sensitivity was tested. Therefore, 3.3 µL of each yeast culture (OD_{600} = 0.2) and three serial 10-fold dilutions were spotted on YPD plates and grown for three days at 25, 28, 30, 31, 33 and 35 °C.

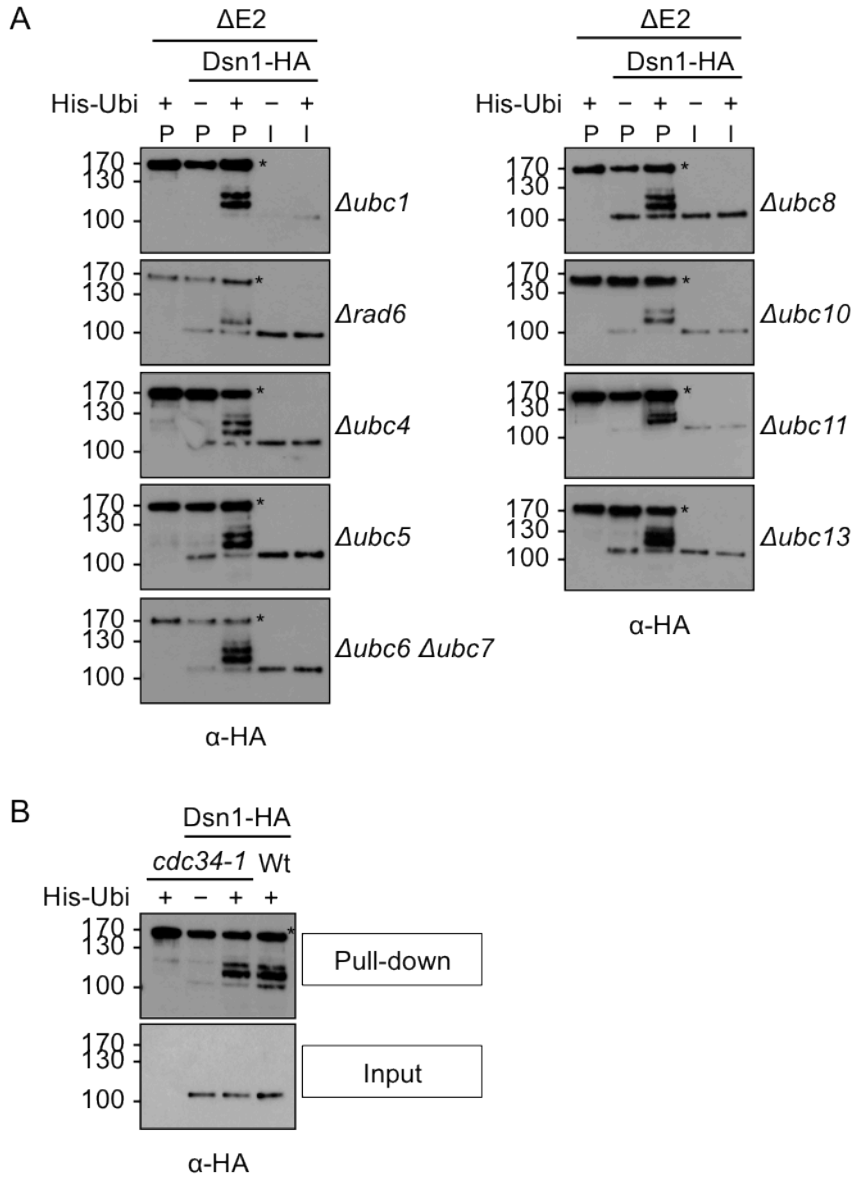

Figure 5.13 - Effect of the deletion of different E2s on the *in vivo* ubiquitylation of tagged Dsn1.

Dsn1 was HA-tagged in the different E2 mutants and the ubiquitylation was monitored in pull-downs under denaturing conditions (as described in Figure 5.7). For the *cdc34-1* temperature-sensitive mutant the cultures for the pull-downs were grown at 25 °C until an OD_{600} of 1 was reached, and then they were shifted to the non-permissive temperature of 37 °C for 3 hours. Pull-down (P) and input samples (I) were analysed by western blot using anti-HA antibody. (A) Pull-downs for the different E2 deletion mutants. (B) Pull-down (upper panel) and input (lower panels) samples for the *cdc34* temperature-sensitive mutant. Cross-reacting, unspecific bands are labelled with an asterisk.

5.4 Characterisation of the ubiquitin binding of Spc25

5.4.1 Crystallisation trials of Spc25-Spc24 with ubiquitin

The ubiquitin-binding domain of Spc25 is unknown and there is no sequence similarity to any of the so far identified UBDs. It has been shown that the linker region as well as the globular domain are needed and that the conserved L109 residue is critical for the ubiquitin binding (Zhao, 2010). Furthermore, *in vitro* experiments revealed that the Spc25 UBD binds ubiquitin via the hydrophobic I44 patch of the β-sheet. However, the exact sites of ubiquitin binding on Spc25 remained unknown. Though Spc24 was negative for interaction with ubiquitin in the yeast two-hybrid system, it is quite possible that Spc24 is also involved in the binding. When I started working on the project I was very keen to identify the residues on Spc25 (and also Spc24) involved in the interaction with ubiquitin. In order to do so, I decided to crystallise the Spc25-Spc24 complex with ubiquitin to reveal their structure in collaboration with Martin Singleton.

Considering that the structure of the C-terminal globular domains of the Spc25-Spc24 complex has already been solved (Wei et al., 2006), I thought it would also be best to use a truncated version rather then the full-length complex. Additionally, I had to include the linker region of Spc25 (107-132), as it is also required for successful binding to ubiquitin (see 1.10.4). Hence, the truncated complex for the crystallisation trials with ubiquitin consisted of the globular domain of Spc24 (154-213) and the linker together with the globular domain of Spc25 (107-221) (Figure 5.14A) to which I will subsequently refer to as Spc24(G) and Spc25(L+G).

For the crystallisation trials, large amounts of highly pure proteins were required. Therefore, I first had to establish and optimise the purification of the Spc25(L+G)-Spc24(G) complex. Spc24(G) and Spc25(L+G) were co-expressed in BL21 Codon^{2+} cells to maintain the solubility of the proteins. The Spc24(G) construct had a N-terminal cleavable 6xhistidine-tag, which allowed Ni-NTA affinity purification. The His-tag of Spc24 was afterwards cleaved with TEV protease, followed by two Ni-NTA purification steps to remove the protease and the His_6-peptide. The sample was then further purified, taking advantage of the fact that the complex just weakly bound to a strong anion exchange column. In the presence of 100 mM salt, Spc25(L+G)-Spc24(G) did not bind to the anion exchanger, but most of the other contaminating proteins did. In

the next step, Spc25(L+G)-Spc24(G) was under low-salt conditions loaded onto an anion exchange column, which allowed binding. Elution was achieved by a salt gradient. The purified complex was then run over a S75 16/60 gel filtration column. As seen in Figure 5.14B, Spc25(L+G) and Spc24(G) eluted as a heterodimeric complex with a molecular weight of about 20 kDa. Ubiquitin (from Sigma-Aldrich) was also loaded on the S75 16/60 gel filtration column and eluted, as expected, at around 8.5 kDa (Figure 5.14C). The purified Spc25(L+G)-Spc24(G) complex and ubiquitin were then finally sent to Martin Singleton's lab for crystallisation.

Unfortunately, none of the crystallisation attempts, performed by Silva Zakian from Martin Singleton's lab, led to the formation of ubiquitin-Spc24-Spc25 crystals and solely ubiquitin crystals were detectable. My concern now was that the interaction with ubiquitin was not strong enough for the formation of crystals. This was consistent with the fact that ubiquitin and the Spc25(L+G)-^{His}Spc24(G) complex (without cleavage of the His-tag) did not coelute when loaded onto a sizing column (ratio of 2:1), which would have been visible in a shift to a higher molecular weight in the elution profile. Instead, there were two separate peaks present, one for Spc25-Spc24, which was at the same position as the control of the complex alone and another for ubiquitin (Figure 5.15A). The Coomassie stained gels showed that fractions of the first peak contained only the complex and no ubiquitin, while ubiquitin was detectable in the fractions of the second peak (Figure 5.15B).

In summary, my approach to reveal the exact binding sites between the Spc25-Spc24 complex and ubiquitin by crystallisation did not succeed, as no crystals were obtained. Also, the interaction of the Spc25(L+G)-Spc24(G) with monoubiquitin was too weak to be maintained in a sizing column.

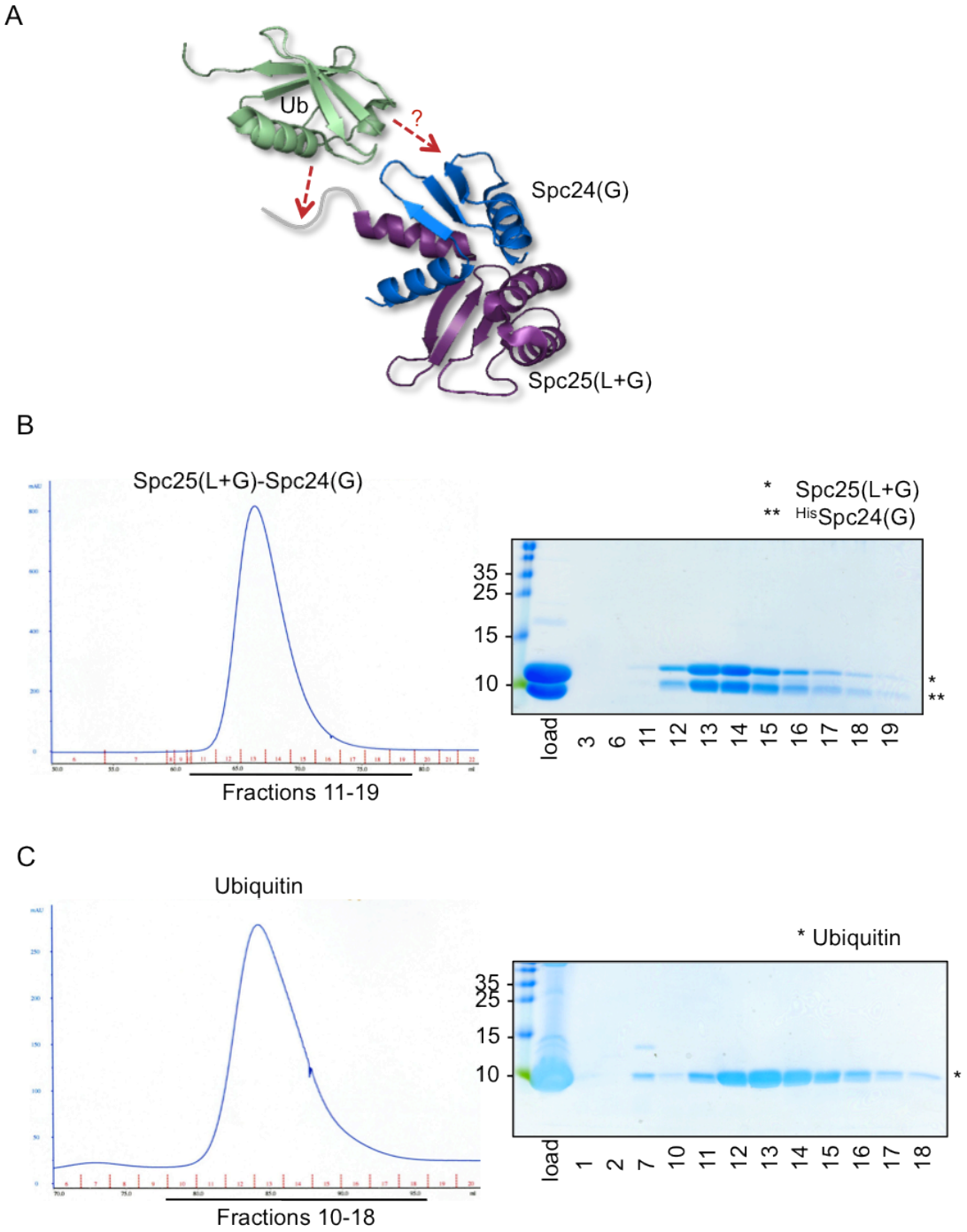

Figure 5.14 - Purified Spc25(L+G)-Spc24(G)-complex and ubiquitin for the crystallisation. (A) Model of the truncated Spc25-Spc24 complex used for the crystallisation with ubiquitin. Ubiquitin (Ub, PDB access code: 1D3Z) interacts with the linker region of Spc25 (in grey). The binding sites of the globular domain of Spc25 and potentially Spc24 are unknown (PDB access code: 2FV4). (B) For the final purification step of the Spc25(L+G)-Spc24(G) complex a S75 16/60 gel filtration column was used. (Continued on next page)

Figure 5.14 (Continued from previous page) **-** The peak fractions of the elution profile can be seen in the Coomassie stained gel and those containing Spc24 and Spc25 in a 1:1 ratio were sent off for the crystallisation. (C) Ubiquitin was also loaded onto the S75 16/60 gel filtration column and the ubiquitin containing fractions were used for the crystallisation trials.

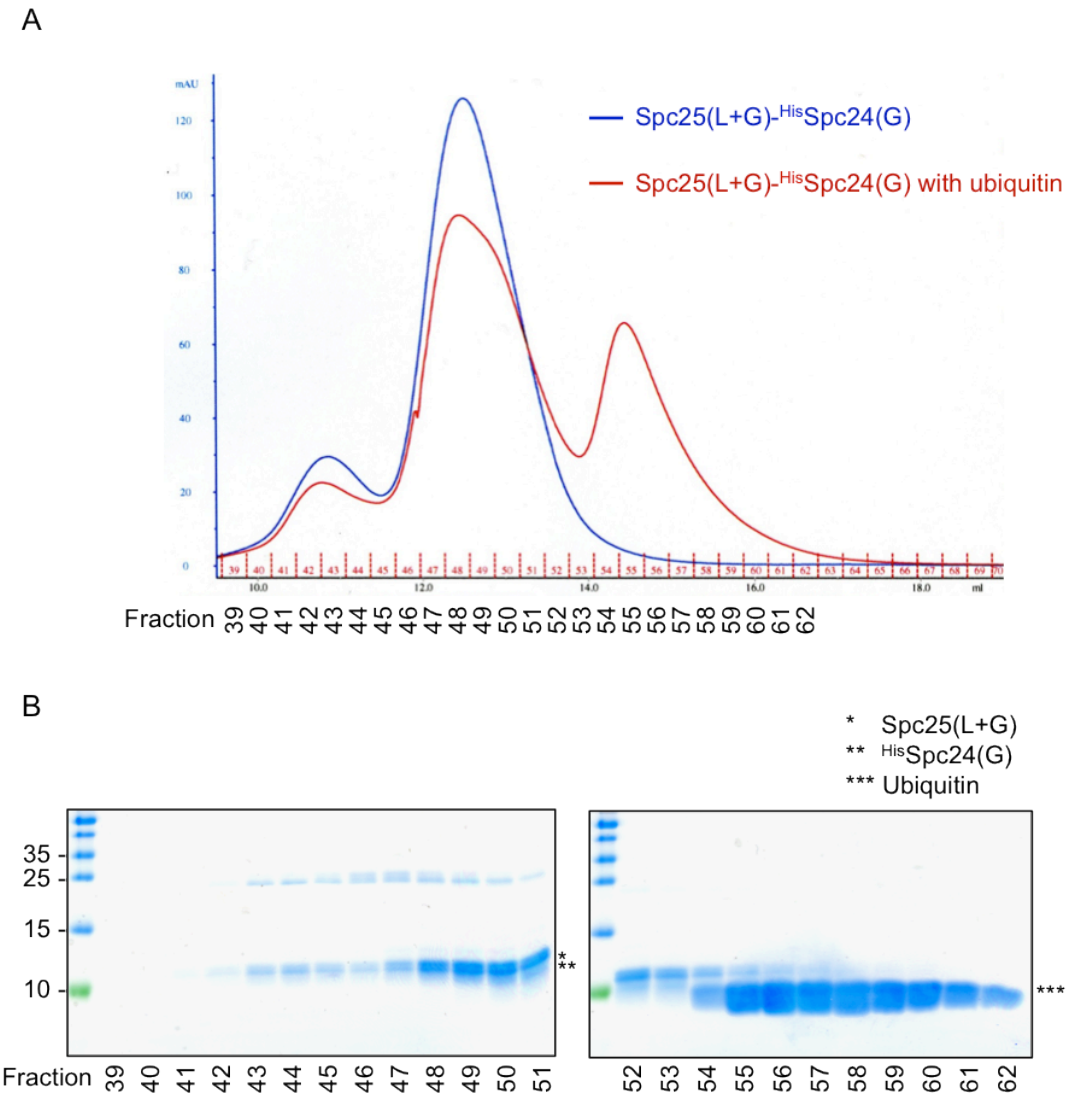

Figure 5.15 - Ubiquitin does not coelute with the Spc25(L+G)-Spc24(G) complex in a sizing column.

The purified Spc25(L+G)-^{His}Spc24(G) complex was mixed in a 1:2 ratio with ubiquitin and loaded onto a S75 16/60 gel filtration column. (A) Elution profile of Spc25(L+G)-^{His}Spc24(G) and ubiquitin (red) or Spc25(L+G)-^{His}Spc24(G) alone as a control (blue). (B) Coomassie stained gel shows the corresponding fractions of the gel filtration.

5.4.2 The ubiquitin binding of the Spc25 (L109A) mutant is reduced but not abolished

The unsuccessful crystallisation trial and the negative interaction in the sizing column already indicated that the binding between Spc25/Spc24 and ubiquitin was fairly weak. I therefore wanted to further characterise the interaction of Spc25 with ubiquitin. It has already been described that the dissociation constant for the ^{His}Spc25(L+G)-^{His}Spc24(G) complex and ubiquitin was 14.2 μM (Zhao, 2010). The L109A mutant of Spc25 was unable to bind ubiquitin in the yeast two-hybrid system. However, cells harbouring that mutation displayed no obvious phenotype. I wanted to test how this mutation affected the affinity to ubiquitin using the BIACORE system (based on surface plasmon resonance) and compare it to the wild type affinity.

To this end, I purified the ^{His}Spc25(L+G)-^{His}Spc24(G) complex and the L109A mutant complex (Figure 5.16A). First, I wanted to confirm the described dissociation constant of 14.2 μM for the wild type complex. For the BIACORE analysis, 9000 RU of anti-GST antibody was immobilized on a CM5 sensor chip in order to capture equimolar amounts of GST (662 RU) in one cell and GST-tagged ubiquitin (^{GST}Ub, 895 RU) on the other cell. Increasing concentrations (double measurements) of purified ^{His}Spc25(L+G)-^{His}Spc24(G) (1-40 μM) or the mutant ^{His}Spc25 (L109A)(L+G)-^{His}Spc24(G) complex (10-400 μM) were passed through both cells of the sensor chip and the SPR signal (RU) was measured over 300 seconds. The background signals of the GST cell were then subtracted from the ^{GST}Ub SPR signal. For the calculation of the dissociation constant K_D, the SPR signals were derived from the equilibrium state of every concentration and plotted against the respective concentrations.

The binding between ubiquitin and the truncated wild type complex revealed a dissociation constant of approximately 1 mM (Figure 5.16B), while the L109A mutant reduced the binding to a K_D of approximately 6 mM (Figure 5.16C). However, these numbers were not considered reliable, as the R_{max} values representing the theoretical binding capacity were far too high ($1\text{-}2x10^3$). I repeated the measurements, but the obtained values remained similar.

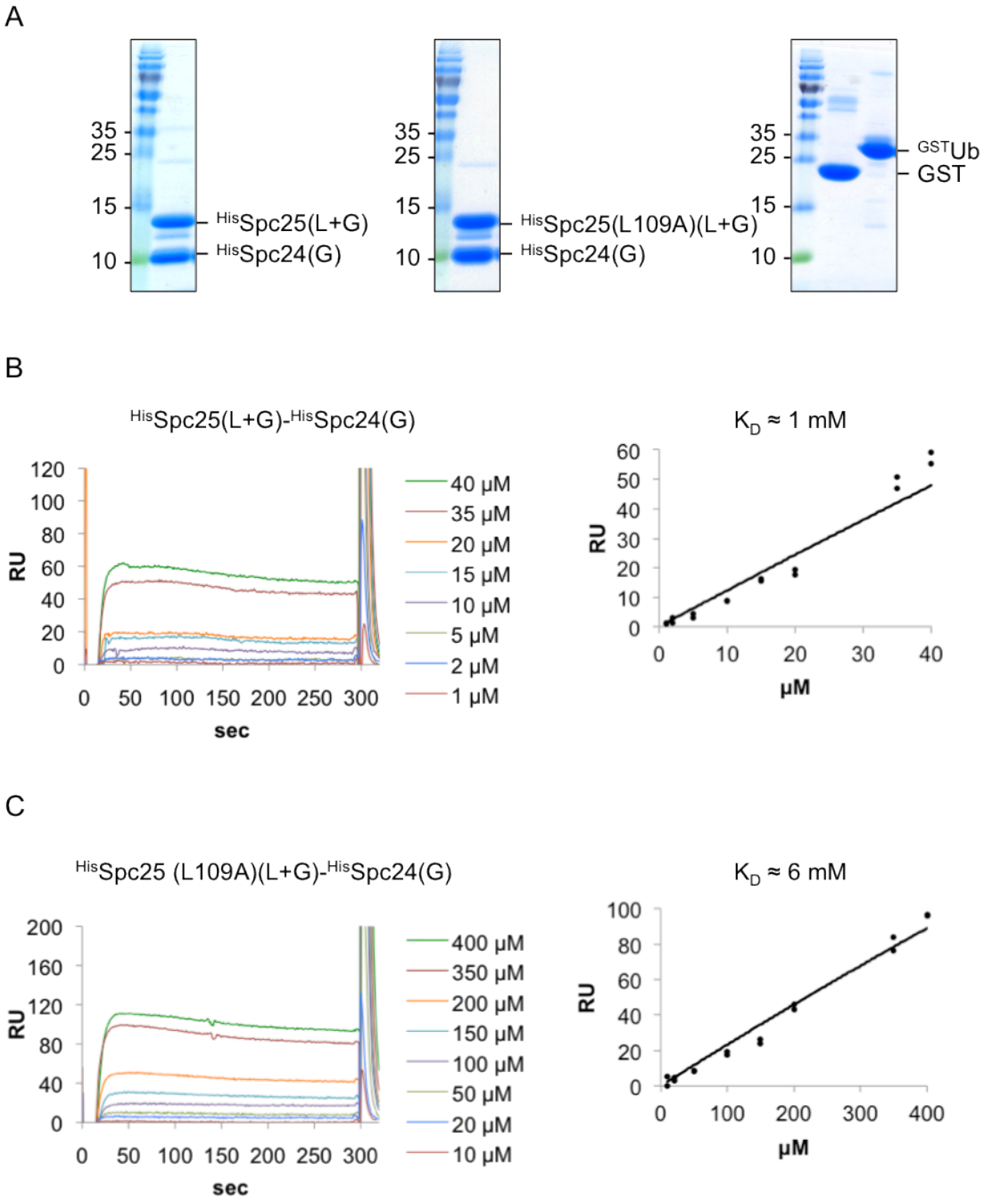

Figure 5.16 - The L109A mutation of Spc25 reduces but does not abolish the binding to ubiquitin.

BIACORE surface plasmon resonance technology was used to measure the dissociation constants of wild type ^{His}Spc25(L+G)-^{His}Spc24(G) complex versus the L109A mutant complex. (A) Coomassie stained gels showing purified ^{His}Spc25(L+G)-^{His}Spc24(G) complex, purified ^{His}Spc25(L109A)(L+G)-^{His}Spc24(G) complex and provided GST and ^{GST}Ub for the BIACORE analysis. (B) Interaction with ubiquitin for ^{His}Spc25(L+G)-^{His}Spc24(G). (C) Interaction with ubiquitin for ^{His}Spc25(L109A)(L+G)-^{His}Spc24(G). (Continued on next page)

Figure 5.16 (Continued from previous page) - (B+C) 9000 RU of anti-GST antibody were coupled to an activated CM5 sensor chip. Equimolar amounts of GST (662 RU) and ^{GST}Ub (895 RU) were captured with the immobilized anti-GST. Increasing concentrations of wild type (1-40 mM) and mutant (10-400 mM) Spc25-Spc24 complex where injected and the change of the response in RU was measured twice for every concentration over a period of 300 seconds (B+C left panel: sensorgrammes are shown for only one measurement per concentration). The dissociation constant K_D was obtained by plotting the RU signal (equilibrium state) against the ligand concentration (B+C right panel).

In conclusion, I was unable to reproduce the dissociation constant of 14.2 μM for the wild type complex (Zhao, 2010), instead the binding was approximately a hundred-fold weaker. However, I was able to show that the affinity of the L109A mutant Spc25-Spc24 complex for ubiquitin was estimated to be at least 6-fold reduced compared to the wild type, indicating that this residue is indeed important for the binding, but also that ubiquitin binding is not completely abolished in this mutant.

5.4.3 No evidence for ubiquitin binding by human Spc25

One striking question was whether the ubiquitin system at the kinetochore is conserved in other organisms. Human Spc25 (hSpc25) and yeast Spc25 have very little sequence homology. However, it was shown that the globular domains of the human Spc25-Spc24 complex and *S. cerevisiae* are structurally very similar (Ciferri et al., 2008). As the structures were related there was a chance that human Spc25 would also be able to interact with ubiquitin. I therefore tested the ubiquitin-binding ability of human Spc25 in a yeast two-hybrid experiment. Yeast Spc25 was shown to bind to polyubiquitin (chain of four ubiquitin separated by a short linker) in the yeast two-hybrid system (Zhao, 2010). As yeast Spc25 requires Spc24 *in vitro* and for ectopic expression, I decided to co-express human Spc24 for the two-hybrid experiment. Consequently yeast cells were transformed with the respective plasmids and hSpc25 was expressed as a fusion to the Gal4 activation domain or as a fusion to the Gal4 binding domain and ubiquitin constructs were fused to the opposite Gal4 domain.

Unfortunately, none of the ubiquitin constructs used (monoubiquitin, a linear chain of four ubiquitin, a chain of four ubiquitin connected by a short linker) were positive for interaction with human Spc25 (with or without expressing human Spc24), while the yeast Spc25 positive control bound to ubiquitin (Figure 5.17A,B). From this first result, however, it cannot be ruled out that human Spc25 does interact with ubiquitin.

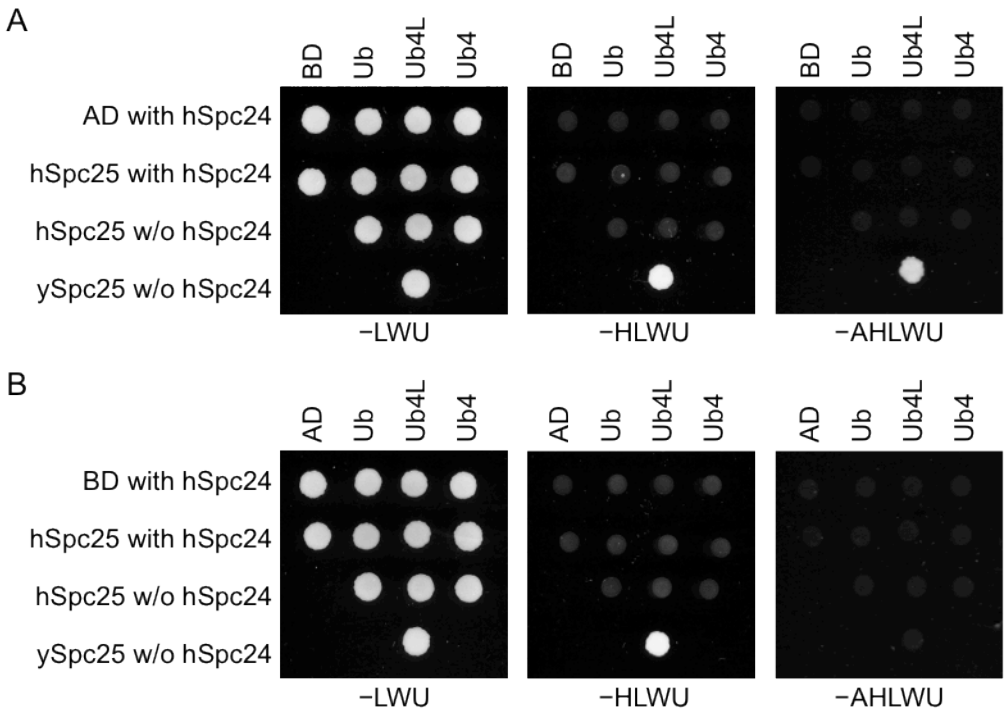

Figure 5.17 - Human Spc25 does not interact with ubiquitin in the yeast two-hybrid system.

Yeast two-hybrid analysis was performed to investigate the protein-protein interaction between ubiquitin and human Spc25 under co-expression of human Spc24. Five colonies of each transformation were picked, resuspended in 500 µL water and 3.3 µL cells were spotted on selective plates and grown for three days at 30 °C. Growth on –LWU plates represented the control for the individual transformations, growth on –HLWU showed week interactions and growth on –AHLWU stronger interactions (−LWU: lacking leucine, tryptophan, uracil; −HLWU: lacking histidine, leucine, tryptophan, uracil; –AHLWU: lacking adenine, histidine, leucine, tryptophan, uracil). Yeast Spc25 and Ub4L were used as a positive control as they were previously shown to interact (Zhao, 2010). Ub: monoubiquitin, Ub4L: linear chain of four ubiquitin separated by a short linker (VQIQ), Ub4: linear chain of four ubiquitin.

Chapter 6 Discussion

This thesis investigates the function of RASSF9 and RASSF10 in *Drosophila*, by examining their interaction network, subcellular localisation, gain- and loss-of-function phenotypes and genetic interactions with binding partners. In the following subchapters I will discuss the main findings, focusing on the function of RASSF10, and what will be necessary to further substantiate them.

In the last part of this chapter, I will discuss the separate project I worked on in Helle Ulrich's lab, where I tried to elucidate the function of the ubiquitin binding of the kinetochore component Spc25.

6.1 Summary of results

Little is known about the function of the two N-terminal RASSFs, RASSF9 and RASSF10 in humans and even less in *Drosophila* (see 1.2.2 and 1.2.3). The starting point for my investigations was the interaction network of human N-terminal RASSFs placing RASSF9/10 closely interconnected to the ASPP/PP1 phosphatase complexes, PCP proteins and the polarity determinant Par3/Baz (Hauri et al., 2013). In summary (see Figure 6.1) I showed using co-IP experiments that the human interaction network of RASSF9 and RASSF10 (see Figure 1.3 and (Hauri et al., 2013)) is largely conserved in *Drosophila*, with the difference that RASSF9/10 seem to be specifically linked to the Fz/Dsh PCP group rather than to the Stbm/Pk group (see 3.4). I also showed that RASSF9/10 bind to other known RASSF8 interactors (see 3.3). While the initial characterisation of RASSF9 could not reveal its biological role (see 6.4), I found *in vivo* evidence that RASSF10 is indeed connected to Fz/Dsh and Baz. This work suggests that RASSF10 specifically functions, together with Fz/Dsh and Baz in asymmetric divisions of SOPs, most likely in establishing the initial asymmetry (see Chapter 4). However, many questions remain open and I will address these in the following sections.

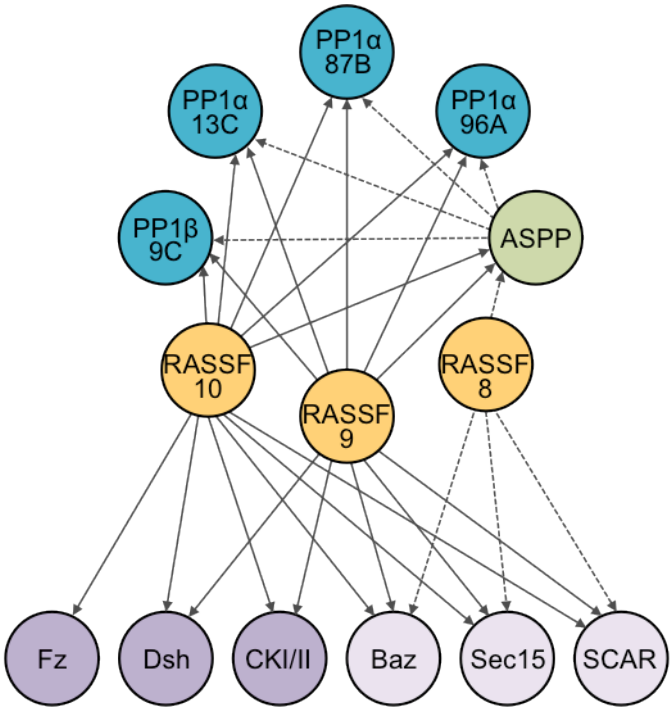

Figure 6.1 - The interaction network of N-terminal RASSFs in *Drosophila*.
The interaction network is based on co-IP experiments in S2 cells (dashed lines indicate previously described interactions). *Drosophila* RASSFs (orange) are found in an interaction network with ASPP (green) and PP1 catalytic subunits (blue). RASSF9 and RASSF10 bind to all catalytic subunits, similar to the known PP1 regulatory subunit ASPP, while RASSF8 requires ASPP for PP1 interaction. RASSF8, RASSF9 and RASSF10 have several interactors (light purple) in common. RASSF9 and RASSF10 have also specific binding partners (darker purple).

6.2 N-terminal RASSFs and their connection to PP1

Drosophila RASSF9 and RASSF10 can both form complexes with ASPP/PP1 (Figure 3.4) and moreover can bind PP1 catalytic subunits independently of ASPP (Figure 3.5), giving them, like human N-terminal RASSFs (Hauri et al., 2013) and *Drosophila* RASSF8 (Zhou, 2014), the potential to act as substrate specifying subunits of PP1 complexes. While *Drosophila* RASSF8 requires ASPP, which binds to PP1 through its RVxF motif, for association with PP1 (Figure 3.4) (Zhou, 2014), it is not clear whether RASSF9/10 bind directly to PP1, through another regulatory subunit or through ASPP

(see 4.4 for discussion). This could be initially tested with *in vitro* pull-downs using bacterially expressed proteins. If the binding is direct, it will be crucial to identify the PP1-binding motif in order to generate PP1-binding deficient mutants. These mutants will ultimately allow us to test whether RASSF9/10 function *in vivo* as substrate specifying subunits (in the case of RASSF10 in ACD of SOPs), as they should phenocopy the null mutants. Obvious PP1-binding motifs (see 3.2.3) are not present in *Drosophila* RASSF9 and RASSF10. In depth sequence analysis of RASSF9/10 and their homologues in other species could reveal homology regions required for PP1 interaction. Despite the fact that the *in vivo* relevance of RASSF9 or RASSF10 phosphatase complexes remains to be elucidated, I will discuss how potential RASSF10/PP1 complexes might function in ACD of SOPs in 6.3.2. If *in vivo* evidence confirms that RASSF10 indeed functions with PP1, different biochemical approaches can be taken to further characterise the potential substrates, such as mass spectrometry on extracts from *RASSF10* mutant versus wild type tissue and *in vitro* phosphatase assays in S2 cells.

Interestingly, although classical and N-terminal RASSFs are two distinct groups, which have little in common besides the RA domain (Sherwood et al., 2010), they all appear to be part of phosphatase complexes. The only *Drosophila* homologue of classical RASSFs regulates the phosphorylation and thus activity of Hippo as part of a PP2A phosphatase complexes (Ribeiro et al., 2010) and one of its human homologues, RASSF3, can interact with PP2A complexes (Hauri et al., 2013).

6.3 The function of RASSF10 in ACD of SOPs

6.3.1 Summary

The external sensory organs, which are part of the peripheral nervous system, derive from a series of asymmetric cell divisions (ACD) starting from a single SOP (see 1.7.1). In the first asymmetric division, the unequal distribution of cell fate determinants into the pIIa and pIIb daughter cells, which defines their fate, depends on the interplay between PCP proteins and polarity determinants (see 1.7.2). PCP proteins define the polarity along the tissue axis (anterior-posterior in case of the pupal notum), and promote the planar polarisation of the Baz-aPKC-Par6 complex to the posterior

(mediated by Fz/Dsh) and the Dlg-Pins-Ga_i complex to the anterior cell cortex (mediated by Stbm/Pk) upon mitotic entry in the case of the pupal notum (see Figure 1.7). The opposing asymmetric localisation of the two polarity determinant complexes then positions cell fate determinants to the anterior cortex.

A recent study provided evidence that the Baz-aPKC-Par6 complex already becomes polarised in a PCP-dependent manner during interphase and moreover that the formation of the Par complex at this stage is independent of Aurora A (Besson et al., 2015). In this study, Besson et al, raise an important issue: PCP does not affect the localisation of Baz (or aPKC or Par6) in neighbouring epithelial cells and therefore specific factors must exist that allow the Baz-aPKC-Par6 complex to interpret the PCP signal in SOPs. Indeed, the mRNA expression profiles of SOPs and the adjacent epithelial cells differ vastly (Reeves and Posakony, 2005, Buffin and Gho, 2010) and both of these studies found *RASSF10* mRNA to be highly expressed in SOPs. Moreover, *RASSF10* mRNA expression was dependent on the expression of proneural genes (Reeves and Posakony, 2005). Consistent with this, I found endogenous RASSF10 protein exclusively localised in wing imaginal disc SOPs (see 4.2.1).

In this thesis I present data showing the requirement of RASSF10 for ACD of SOPs. Firstly, *RASSF10* mutant flies exhibit bristle defects that resemble the defects of reduced Baz or Pins function (Figure 4.1) (Kopein and Katanaev, 2009). Secondly, *RASSF10* strongly genetically interacted with PCP components and polarity determinants (see 4.3). Ultimately, loss of *RASSF10* causes several defects in the actual ACD of SOPs (see 4.5.2): it affects the polarisation of the Pon crescent, causes Pon mis-segregation into pIIa and pIIb daughter cells (Figure 4.17), similar to loss of *baz* or *pins* (Roegiers et al., 2001a, Bellaiche et al., 2001b) and the anterior-posterior division angle is not properly aligned along the tissue axis (Figure 4.18), similar to loss of *fz* or *dsh* (Bellaiche et al., 2001a, Bellaiche et al., 2004, Gomes et al., 2009). Together with the findings that (a) RASSF10 can bind to Fz/Dsh (Figure 3.8 and Figure 3.11) as well as Baz (Figure 3.6), (b) that it co-localises with them to one side of the cell cortex in wing imaginal disc SOPs (Figure 4.8 and Figure 4.9) and localises to the posterior cell cortex in pupal nota SOPs (Figure 4.15) and (c) that polarisation of Baz seems impaired in interphase SOPs upon loss of *RASSF10* (Figure 4.19), my work strongly suggests that RASSF10 functions together with Fz/Dsh and Baz in SOP initial polarisation and ACD.

Furthermore, RASSF10 is most likely recruited to the membrane by Fz and Dsh, as ectopically expressed GFP-RASSF10 is planar polarised in epithelial cells (Figure 3.13) and membrane localisation is dependent on the presence of both Fz and Dsh (Figure 3.14). In order to better understand the hierarchy of the Fz/Dsh-RASSF10-Baz network, it will be necessary to examine RASSF10 localisation in *baz* mutants. However, the molecular function of RASSF10 remains unexplored. In the following subchapter I will present different possible scenarios for how RASSF10 might act on Dsh, Fz or Baz.

6.3.2 Possible mechanisms for the function of RASSF10 in ACD

One possible mechanism is that RASSF10, as an SOP-specific factor, could promote the interaction between Fz/Dsh and Baz-aPKC-Par6, either by bridging a Fz-Baz or a Dsh-Baz association. This could be initially tested in co-IP experiments and also in pupal nota stainings of *RASSF10* mutants, as Baz localisation should in this situation be randomised relative to the Fz/Dsh localisation. In addition, ectopically expressed RASSF10 might lead to the planar polarisation of Baz in normal epithelial cells. However, as discussed in 4.6, RASSF10 must have additional functions, as the adult bristle phenotype as well as the Pon-segregation analysis differs from PCP mutants.

One additional or alternative mechanism could be that RASSF10 is required to stabilise Fz and/or Dsh and/or Baz at the posterior cell cortex. The levels of Fz, Dsh and Baz are highly enriched in SOPs compared to the surrounding epithelial cells in wing imaginal discs (see 4.2.2) and in the pupal notum (e.g. (Bellaiche et al., 2004, Bellaiche et al., 2001b)). This hypothesis would be consistent with the observations that, upon co-expression RASSF10, Fz and Dsh (Figure 3.15) all components appear stabilised in S2 cell lysates. Furthermore, Baz levels seem less enriched at the posterior cell cortex in *RASSF10* mutants compared to wild type tissue (Figure 4.19) and it will be important to test whether the same is true for Dsh and Fz. Lower levels of Fz/Dsh, could also explain the randomisation of the division angle relative to the anterior-posterior axis in *RASSF10* mutant (Figure 4.18). Fz/Dsh position the spindle through direct binding between Dsh and Mud/NuMA (see 1.7.3) (Segalen et al., 2010). Reduced Fz/Dsh levels could therefore lead to less stable anchoring of the spindle at the apical posterior cell cortex. This can be tested through live imaging the spindle in *RASSF10* mutants.

It is possible that RASSF10 could function as a regulatory subunit of PP1 to stabilise the components of the posterior cortex. RASSF10 could recruit PP1 to the posterior cell cortex to dephosphorylate and thus stabilise either Fz or Dsh or Baz (see below). All three are plausible substrates for potential RASSF10/PP1 complexes.

Firstly, Fz can be inhibited by aPKC-dependent phosphorylation on two serine residues at the C-terminal cytoplasmic tail, leading to its destabilisation and removal from the membrane, at least in photoreceptors of the eye disc (Djiane et al., 2005). This study presented a model in which Baz binding to aPKC (in the planar polarised R3 and R4) would protect Fz from phosphorylation. In SOPs, Fz and the Baz-aPKC-Par6 complex co-localise and it is likely that residual aPKC activity could still lead to Fz phosphorylation. Dephosphorylation by RASSF10/PP1 complexes could therefore hypothetically stabilise Fz.

Secondly, RASSF10/PP1 complexes could regulate Dsh levels by dephosphorylation. In pupal wings, Dsh (most likely a hyperphosphorylated form) is targeted by the Cullin-3/Diablo/Kelch ubiquitin ligase complex (Strutt et al., 2013a). Interestingly, mammalian Dvl is targeted for ubiquitin-mediated degradation by the E3 ubiquitin ligase Itch (*Drosophila* Suppressor of deltex, Su(Dx)) and partial dephosphorylation by PP1 (in association with the kinase Hipk2) can prevent this degradation *in vitro* (Shimizu et al., 2014). In order to test whether RASSF10/PP1 complexes prevent ubiquitin-mediated degradation of either Fz or Dsh, mutants of different E3 ligases could be combined with the *RASSF10* mutant and the responsible E3 would be expected to rescue the *RASSF10* mutant bristle defect. As discussed in 6.2, it will be crucial to generate a PP1-binding deficient mutant of RASSF10 to prove that RASSF10 does indeed act as a substrate specifying subunit of PP1.

Lastly, in the case of Baz, RASSF10/PP1 complexes could promote Baz association with aPKC/Par6. In several types of epithelial cells Baz localises at the adherens junctions and is separate from aPKC/Par6, which localises more apically (Walther and Pichaud, 2010, Morais-de-Sa et al., 2010, Harris and Peifer, 2005). The apical exclusion of Baz is based on two events: phosphorylation of Baz on Ser980 by aPKC, as well as competition between Crb and Baz for aPKC/Par6 binding (Morais-de-Sa et al., 2010, Walther and Pichaud, 2010). Assuming that this might also be true for epithelial cells and SOPs of the pupal notum, this would require a special regulatory mechanism, which

allows the formation of Baz-aPKC-Par6 complexes in SOPs at interphase (before Aurora A is active). PP1 can dephosphorylate the Ser980 residue of Baz/Par3 *in vitro* (Yanxiang Zhou, unpublished result) (Traweger et al., 2008). In neuroblasts and oocytes Ser980 phosphorylation does not affect the association of Baz with aPKC/Par6, as Crb is not present (Morais-de-Sa et al., 2010, Hong et al., 2001). Therefore the requirement of dephosphorylation of Ser980 to keep Baz associated to aPKC/Par6 would only occur if Crb was present in SOPs. However, there are no reports on Crb function in SOPs and this can first be addressed by testing Crb expression in SOPs. In addition, it will be important to look at the localisation of aPKC and Par6 in *RASSF10* mutants to see whether they co-localise with Baz, or whether Baz is excluded from the aPKC crescent. Moreover, if this is the case, Ser980 phosphomimicking Baz mutants should phenocopy *RASSF10* mutants. Alternatively, RASSF10/PP1 could stabilise Baz at the anterior cell cortex by dephosphorylating the Rho-kinase phosphorylation sites at the C-terminus of Baz, which were shown to disrupt Baz cortical localisation (Krahn et al., 2010b).

A contrasting model is that RASSF10 could promote the stabilisation of Fz/Dsh and Baz independently of PP1 function. For example RASSF10 could promote polarised transport of Rab11 endosomes containing Fz, Dsh or Baz via its physical binding partner Sec15 (Figure 3.7) in SOPs, as seen for RASSF8 in L3/pupal wings. There are many other possible scenarios for how RASSF10 might function in ACD, and future research as proposed in this discussion will shed light into the mechanism(s) involved. It might also be informative to test RASSF10 in the subsequent divisions of the SOP lineage. While Baz is important for pIIa, pIIb and pIIIb divisions, PCP proteins do not appear to be involved (see 1.7.3) (Roegiers et al., 2001a, Roegiers et al., 2001b). pIIb and pIIIb asymmetric division are similar to neuroblast divisions as they involve Inscuteable (see 1.7.3). However, the mechanisms of pIIa divisions are unexplored and RASSF10 might function together with Baz in this process.

6.3.3 Regulation of RASSF10 in SOPs

RASSF10 transcription in SOPs is, as mentioned above, regulated by proneural genes (Reeves and Posakony, 2005). This study identified proneural protein binding sites 5 kbp upstream of the *RASSF10* locus, which are responsive to Achaete-Scute. In addition, several observations suggest that RASSF10 is regulated on a post-transcriptional level.

In *fz* or *dsh* mutants, RASSF10 levels are severely reduced (Figure 3.14) and RASSF10 is stabilised by co-expression of Fz and Dsh (or Baz) in S2 cells (Figure 3.15). This indicates that RASSF10 may be prone to degradation if uncoupled from Fz/Dsh and would also explain why RASSF10 is planar polarised. In order to identify the relevant enzymes involved in regulating RASSF10 stability, one strategy might be to perform AP-MS experiments of ectopically expressed *Drosophila* RASSF10 from lysates of S2 cells treated with proteasome inhibitors.

6.3.4 Is the function of RASSF10 conserved in other species?

Besides the similar interaction network of human RASSF9 and RASSF10 and *Drosophila* RASSF10 (see 6.1) there is no substantial evidence so far that the human homologues could function in a similar way (see 1.2.2). In fact, human RASSF9 and RASSF10 do not show membrane localisation in cell culture based stainings: RASSF10 is cytoplasmic and re-localises to the spindle pole during mitosis (Hill et al., 2011). Ectopically expressed RASSF9 is also cytoplasmic and shows an enrichment in endosomes (Chen et al., 1998). However, the localisation could of course be dependent on the cell type. Interestingly, RASSF10 is primarily expressed in the brain in *Xenopus* tadpoles (Hill et al., 2011), suggesting that its expression is, like *Drosophila* RASSF10, tissue-specific and that it might be important for neurogenesis. RASSF9 is expressed in multiple tissues in mice and rats (Lee et al., 2011, Chen et al., 1998). However, as the functions of RASSF9 and RASSF10 in other species are not well understood, it is difficult to predict their conservation. In contrast, the function of RASSF8 in maintaining the integrity of cell junctions is conserved in *Drosophila* and humans (Lock et al., 2010, Langton et al., 2009, Zaessinger et al., 2015). While *Drosophila* and human RASSF8 show high sequence similarity (Langton et al., 2009), *Drosophila* RASSF10 (and RASSF9) has very limited homology with human RASSF9/10 (see 3.1) and might therefore be functionally divergent. In the absence of a detailed phylogenetic analysis of the N-terminal RASSF genes through evolution, it is not possible to conclude whether *Drosophila RASSF9* and *RASSF10* are true homologues of human *RASSF9/10*. In this thesis, I have retained the nomenclature used by Sherwood et al (Sherwood et al., 2010), however, it may be necessary to change this nomenclature based on further analysis. It

will also be interesting to investigate the function of human or mouse RASSF9 and 10 in order to relate their function to my findings on *Drosophila* RASSF10.

6.4 What is the developmental function of RASSF9?

Drosophila RASSF9 was so far an uncharacterised gene. My work showed that RASSF9 can physically interact with the same proteins as RASSF8 and RASSF10 (Figure 6.1) and tagged transgenes localise apically at the cell cortex (Figure 3.13 and Figure 4.15). The localisation of ectopic expressed RASSF9 was not, in contrast to RASSF10, dependent on the presence of Fz or Dsh (Figure 3.14), indicating that other proteins recruit RASSF9 to the membrane. Potential candidates could be its physical interaction partners ASPP (Figure 3.3) or even Baz (Figure 3.6), as both localise at the junctions (Krahn et al., 2010b, Langton et al., 2007). This could be tested in *ASPP* or *baz* loss-of-function experiments.

However, unlike *RASSF8* or *RASSF10* mutants, *RASSF9* mutants do not exhibit an obvious phenotype, making it difficult to address its biological function. The mild reduction in wing size (Figure 3.19) of *RASSF9* mutants would suggest pro-growth functions. Interestingly, mice mutant for *RASSF9* are also smaller compared to wild type (Lee et al., 2011). The findings that *RASSF9* worsens the stout bristle phenotype of *baz* or *pins* knockdowns (Figure 4.12) and *RASSF9, RASSF10* double mutants show stronger genetic interactions with ACD components compared to *RASSF10* single mutants (see 4.3), could suggest that it might be involved in ACD of SOPs. However, it is unlikely that RASSF9 would function identically to RASSF10, as expression of RASSF9 cannot rescue the bristle defects of *RASSF10* mutants (Figure 4.2 and Figure 4.3) and it is also possible that the effects caused by *RASSF9* loss are not specific for ACD of SOPs, as discussed for PP1s in 4.4. A crucial step in understanding the physiological function of RASSF9 will be to find when and where it is expressed. I generated an antibody against RASSF9. Hence, stainings across different developmental stages and tissues could be performed or alternatively an endogenous GFP-RASSF9 line could be generated using the CRISPR/Cas9 system. In addition, the *RASSF9* mutants should be carefully analysed for defects through different

developmental stages. It will be interesting to see what the specific function of *Drosophila* RASSF9 might be.

6.5 N-terminal RASSFs: similar interactions but specific functions

Although N-terminal RASSFs share several binding partners and, as discussed in 3.6, we cannot rule out redundant functions, it seems that N-terminal RASSFs act specifically in different tissues and developmental stages, defined by differences of binding partners and expression patterns. RASSF8 is, together with ASPP, recruited to the membrane in photoreceptors of the developing retina by its binding partner MAGI and RASSF8 then in turn positions Baz at the adherens junctions (Zaessinger et al., 2015). Yanxiang Zhou proposed in his thesis that ASPP/PP1 complexes could then stabilise Baz at the adherens junctions by dephosphorylation (unpublished results). In contrast, RASSF10 is specifically expressed in SOP cells and is recruited by its binding partners Fz/Dsh to one side of the cell cortex, and might then promote the planar polarisation of the Baz-aPKC-Par6 complex (perhaps by recruiting PP1, see 6.3.2). Ectopic expression of RASSF9/10 does not rescue the round wing phenotype of *RASSF8* mutants (Figure 3.22) and RASSF9 expression does not rescue the bristle defect of *RASSF10* mutants (Figure 4.2 and Figure 4.3), suggesting that the slight differences in binding partners are sufficient to separate their functions. This model is further supported by the observation that human RASSF8 localises at the tight junctions (Lock et al., 2010), while RASSF7 and RASSF10 seem to localise at the mitotic spindle (Hill et al., 2011, Recino et al., 2010). In this context, it would be interesting to test the functions the sole *C. elegans* N-terminal RASSF, K05B2.2, (Sherwood et al., 2010).

6.6 Discussion of the Spc25 project

6.6.1 The function of the ubiquitin binding of Spc25

The kinetochore component Spc25 was identified as a novel ubiquitin-binding protein with an as yet unknown ubiquitin-binding domain, however the functional relevance of the ubiquitin binding remained elusive (Zhao, 2010). The ubiquitin-binding deficient

spc25 (L109A) mutant has no obvious phenotype, but Shengkai Zhao found a synthetic interaction between *spc25 (L109A)* and temperature-sensitive alleles of Dsn1 (*dsn1-7* and *dsn1-8*), suggesting that the function of Spc25's ubiquitin binding might lie in maintaining the stability of the kinetochore. In this work several approaches were taken to gain further insight into this theory.

Firstly, I found additional genetic interactions of *spc25 (L109A)* with temperature-sensitive mutants of other kinetochore components (Figure 5.2). Interestingly, all of the affected mutants were in close proximity to Spc25 and belonged to the KMN network, formed by the Mtw1 complex, the Spc105 complex and the Ndc80 complex (Cheeseman et al., 2006). *spc25 (L109A)* increased the temperature sensitivities of alleles (besides *DSN1*) of *SPC105* as well as *NDC80* and *NUF2* of the Ndc80 complex. Strikingly, the combination of *spc25 (L109A)* with different temperature-sensitive alleles of *SPC24* resulted in lethality. By contrast, no effect was seen for temperature-sensitive mutants of the remaining Mtw1 complex (Nsl1, Mtw1, Nnf1), Ndc10 and members of the Dam1 complex (Dam1, Duo1, Ask1, Dad1). My findings support a model in which the ubiquitin system around Spc25 might act specifically within the KMN network and is important for the stability - at least of pre-destabilised - kinetochore complexes.

However, the critical evidence that the genetic interactions of *spc25 (L109A)* are caused by its ubiquitin-binding deficiency and not due to the destabilisation of kinetochore components by the L109A mutation independently of ubiquitin, still needs to be provided. Attempts of fusing two different UBDs - UIM domain or MIU domain- to *spc25 (L109A)* (or *SPC24*) failed to rescue the phenotypes of *spc105-15 spc25 (L109A)* and *spc24-1 spc25 (L109A)* double mutants (Figure 5.5 and Figure 5.6). As an alternative, catalytic domains of deubiquitylation enzymes could be fused to the temperature-sensitive alleles of *DSN1*, *SPC105* or the members of the Ndc80 complex. If the phenotypes were due to the ubiquitin-binding deficiency, this should phenocopy the effects seen for *spc25 (L109A)*.

Furthermore, Dsn1, Nsl1 and Spc105 of the KMN network were shown to be ubiquitylated (Figure 5.7) and their stability was not affected by different tags (Figure 5.8). Importantly, monoubiquitylation of Dsn1 and Spc105 was independent of proteasomal activity (Figure 5.9). All three are in immediate proximity to Spc25

(Joglekar et al., 2009) and associate with Spc24/Spc25 (Maskell et al., 2010, Hornung et al., 2010), which makes them attractive candidates for interacting with the UBD of Spc25.

As a starting point I focused on analysing the ubiquitylation of Dsn1, trying to reveal the ubiquitylation site(s) and the responsible ubiquitylation factors. If Dsn1 (or other ubiquitylated potential targets) was the ubiquitylated interactor of Spc25, ubiquitylation-deficient mutants should behave epistatic to *spc25 (L109A)*. However, the strategy of finding the region containing the relevant lysine residue(s) was inconclusive, as the four different lysine mutant groups of Dsn1 were all still ubiquitylated (Figure 5.10), suggesting that there might be a redundancy between ubiquitylation sites, or even that no specific lysine residue is required. It would be interesting to see how the ubiquitylation is affected in different lysine mutant group combinations. Furthermore, loss of none of the 11 E2 ubiquitin-conjugating enzymes in yeast affected the ubiquitylation of Dsn1, except in the case of Rad6. Rad6, together with the E3 ubiquitin ligase Ubr2, seems to be responsible for polyubiquitylation (and possibly subsequent degradation), but not monoubiquitylation of Dsn1 (Figure 5.11, Figure 5.13 and (Akiyoshi et al., 2013b)). This strongly suggests a redundancy between the E2s and thus, in order to reveal the responsible E2 enzymes for monoubiquitylation, different double mutant combinations could be tested.

At this point, the ubiquitylated interactor(s) remains unknown. Spc105 and Nsl1 will have to be analysed using the same approach as for Dsn1, with regards to their regulation of ubiquitylation. Relevant, i.e. kinetochore-associated E3(s) could be identified using *in vivo* pull-down experiments combined with mass spectrometry approaches. Although Dsn1, Nsl1 and Spc105 are plausible candidates, it is possible that Spc25 binds to a different ubiquitylated target. Further candidates could be identified in mass spectrometry experiments, comparing *in vivo* pull-downs of wild type and Spc25 (L109A) mutant proteins (or with a stronger mutant) or screening the as yet untested kinetochore components for synthetic interactions with *spc25 (L109A)*. Recently, a new centromere associated component Cnn1 (CENP-T) was identified, which can directly interact with the globular domains of Spc25/Spc24 and is, moreover, competing with Dsn1/Nsl1 for the same binding surface (Malvezzi et al., 2013). It

would be interesting to see whether Cnn1 is involved in the ubiquitin-binding activity of Spc25.

Lastly, this work aimed to further characterise the unknown UBD of Spc25. The minimal region of Spc25 required for ubiquitin binding (linker and globular domain) does not show sequence similarity to any of the known ubiquitin-binding domains and interestingly, the L109 residue that is crucial for the ubiquitin binding lies in the flexible linker region (Zhao, 2010). Moreover, Spc24 might also contribute to the ubiquitin binding. Although the crystallisation trials of a truncated Spc25-Spc24 complex and ubiquitin in collaboration with Martin Singleton were unsuccessful, I found that the affinity for the binding of the Spc25 (L109A) mutant to ubiquitin was reduced compared to wild type Spc25 - but not abolished - using the BIACORE system (Figure 5.16), which could be the reason for the not obvious phenotype. However, as the obtained K_D values were not considered reliable and as the binding was 100 times weaker for wild type Spc25 than it was previously reported by Shengkai Zhao, these measurements should be repeated and complemented with alternative methods, e.g. ITC. Based on the finding that the Spc25 (L109A) mutant quite possibly has residual ubiquitin-binding abilities, it will be important to reveal other contact sites in order to obtain a stronger allele, which might give a stronger phenotype. This could be achieved by taking several different approaches. Firstly, crystallisation trials could be repeated by fusing ubiquitin to either Spc25 or Spc24. NMR titration studies could be an alternative approach to characterise the interaction between ubiquitin and Spc25 (Spc24), as the NMR structure for the globular domain of Spc25 is already available (Wei et al., 2006). Lastly, a negative two-hybrid screen between ubiquitin and different Spc25 mutants (created randomly by PCR) could reveal residues important for the interaction. Spc25 mutants negative for the interaction with ubiquitin would then have to be tested for their ability to bind to Spc24 to dismiss the possibility that disassembly of the Spc25/Spc24 complex causes the ubiquitin-binding deficiency.

In conclusion, in this thesis several approaches were taken to further elucidate the function and mechanism of the ubiquitin binding of Spc25. However, as discussed above, the approaches taken in this thesis need to be continued in order to give satisfying answers. Together with the suggestions made above, other future experiments will be necessary to assess the role of the ubiquitin binding of Spc25. In his thesis,

Shengkai Zhao analysed defects in chromosome segregation performing a plasmid loss assay in *spc25 (L109A)* mutants and wild type cells and could not detect a difference (Zhao, 2010). However, there are more sensitive approaches to detect chromosome segregation defects. Chromosome loss assays with strains that harbour the minichromosome CFIII containing a suppressor of the *ade2-101* locus indicate segregation defects upon loss of CFIII, based on a colour change from white to red (Spencer et al., 1990). Hanna Windecker, a post-doc in Helle Ulrich's lab, found in the meantime that the *spc25 (L109A)* mutant indeed causes a mild defect in chromosome segregation using this approach (unpublished result). This strongly supports the relevance for the ubiquitin-binding ability of Spc25. One way to further characterise the chromosome segregation defect would be the live imaging of GFP-labelled chromosomes (Straight et al., 1996). Another approach to address whether the ubiquitin system based on the ubiquitin binding of Spc25 is important for the stability of the kinetochore could be to compare the composition of kinetochores in wild type versus *spc25 (L109A)* mutants. Native kinetochores can be purified from yeast cells with a minichromosome purification protocol combined with affinity purification of FLAG-tagged Dsn1 (Akiyoshi et al., 2009, Akiyoshi et al., 2010). Mass-spectrometry of the purified kinetochore complexes would then reveal whether *spc25 (L109A)* mutants show differences in the composition compared to the wild type situation. These approaches are currently being pursued by Hanna Windecker in the Ulrich lab.

6.6.2 The ubiquitin system(s) at the kinetochore

The ubiquitin system was so far mainly reported to be important for regulating the kinetochore assembly by means of ubiquitin-mediated degradation (Akiyoshi et al., 2013b, Davies and Kaplan, 2010, Honda et al., 2000, Kopski and Huffaker, 1997). In this study I provide evidence for the existence of a proteasome independent function for the ubiquitin system centred on the ubiquitin-binding activity of Spc25 and the KMN network (Spc105 complex, Mtw1 complex and Ndc80 complex).

The E3 ubiquitin ligase Ubr2, together with its adaptor Mub1, were shown to regulate the levels of Dsn1 at the kinetochore and, moreover, were acting as a control system to remove malfunctioning Dsn1 (Akiyoshi et al., 2013b). As Dsn1 was one of our potential ubiquitylated interactors of Spc25, I assessed whether the Ubr2 ubiquitin-

mediated degradation system and the Spc25 based ubiquitin system are connected and my results suggest that both systems act separately from each other.

Firstly, loss of *UBR2* function and the ubiquitin-binding deficient mutant of Spc25, *spc25 (L109A)*, both further destabilise several temperature-sensitive mutants of the KMN network (*dsn1-7*, *ndc80-1*, *nuf2-61*, *spc24-1*) (Figure 5.12). However, their effects are not epistatic, indicating that they work independently.

As mentioned above, Ubr2 (Mub1) was reported to ubiquitylate and target Dsn1 for degradation (Akiyoshi et al., 2013b). Indeed, I could confirm that polyubiquitylation of Dsn1 was dependent on the presence of Ubr2 (Figure 5.9 and Figure 5.11) and polyubiquitylation of Dsn1 seemed to target it to the proteasome (Figure 5.9). In addition, my results suggest that the ubiquitin-conjugating enzyme Rad6 is the responsible E2 for the polyubiquitylation of Dsn1, which is consistent with previous reports that Ubr2/Rad6 act together to target other substrates for degradation, such as Rpn4 (Ju et al., 2008, Wang et al., 2004) and Sml1 (Andreson et al., 2010). Interestingly, the study by Akiyoshi et al., suggests either that Rad6 is not the responsible E2, or that there might be a redundancy between the E2s targeting Dsn1, as deletion of *RAD6* failed to rescue the lethality of a mutant allele of *DSN1*, while deletion of *UBR2* (and *MUB1*) did (Akiyoshi et al., 2013b).

Importantly and in contrast, neither Ubr2 nor Rad6 affected the monoubiquitylation of Dsn1 and monoubiquitylated Dsn1 is not targeted by the proteasome (Figure 5.9 and Figure 5.11), thus further supporting the model of a proteasome independent function of the ubiquitin system. However, at this point one cannot completely rule out that Ubr2/Rad6 are not responsible for the monoubiquitylation of Dsn1, as they might act redundantly with other E2/E3s.

The presence of the two different ubiquitin pathways is further strengthened by the finding that *Δubr2* has an opposite effect on the phenotype of *spc105* temperature-sensitive alleles. While *spc25 (L109A)* worsens the phenotype, *Δubr2* slightly rescues it (Figure 5.12). Together with the finding that deletion of *UBR2* increased the levels of ubiquitylated Spc105 (Figure 5.11), this might suggest that Ubr2 could be involved in regulating Spc105 levels in a similar way to Dsn1. However, in the case of Spc105, further experiments would be necessary to validate this.

In conclusion, one could speculate that while Ubr2 guarantees the integrity of the kinetochore by regulating the levels of Dsn1 (and maybe other kinetochore proteins) and preventing assembly of malfunctioning kinetochore complexes, as suggested by the Biggin's group (Akiyoshi et al., 2013b), the ubiquitin system around Spc25 would act to stabilise already formed kinetochore complexes. As discussed in 6.6.1, further experiments will be necessary to validate the latter hypothesis. However, regardless of whether or not Dsn1, or Spc105 or Nsl1 are the ubiquitylated interactors of Spc25, the fact that the monoubiquitylation of Dsn1, Nsl1 and Spc105 are independent of the E3 ubiquitin ligase Ubr2 (Figure 5.11) and that the monoubiquitylation of Dsn1 and Spc105 are independent of proteasome activity (Figure 5.9), strongly implies proteasome-independent functions for the ubiquitin system at the kinetochore.

One striking question remains unclear: is the ubiquitin system around Spc25 conserved in other species? Human Spc25 (with or without human Spc24) did not interact with ubiquitin in the yeast two-hybrid experiment (Figure 5.17). However, the interaction could be too weak to be detected with the two-hybrid system. As an alternative, *in vitro* and *in vivo* pull-downs of human Spc25/24 with ubiquitin could be performed to assess the ubiquitin-binding ability. Interestingly, at least the ubiquitin-mediated degradation of kinetochore components as a system to regulate the assembly of kinetochore components seems to be conserved in mammalian systems (Davies and Kaplan, 2010, Honda et al., 2000).

Chapter 7 Appendix

7.1 Yeast strains

Table 7.1 - List of yeast strains used in this thesis

yHU	Name	Genotype	Source
2	DF5 alpha	*his3-Δ200, leu2-3,2-112, lys2-801, trp1-1(am), ura3-52*	(Finley et al., 1987)
3	DF5 a	*his3-Δ200, leu2-3,2-112, lys2-801, trp1-1(am), ura3-52*	(Finley et al., 1987)
4	*Δubc6,7*	DF5 *ubc6::HIS3, ubc7::HIS3*	(Mayer et al., 1998)
48	*rad6 a*	DF5 *rad6::HIS3*	(Ulrich and Jentsch, 2000)
69	*cdc34-1*	DF5 *cdc34-1*	(Goebl et al., 1988)
195	PJ69-4A	trp1-901, leu2-3,112, ura3-52, his3-200, gal4Δ, gal80Δ, LYS2::GAL1-HIS3, GAL2-ADE2, met2::GAL7-lacZ	(James et al., 1996)
198	*ubc8*	DF5 *ubc8::URA3*	(Davies et al., 2010)
338	*ubr2*	DF5 *ylr024c::HIS3MX6*	Helle Ulrich
346	*ubc13*	DF5 *ubc13::HIS3*	(Ulrich and Jentsch, 2000)
457	W303 K699	*ade2-1, ura3-1, his3-11,15, trp1-1, leu2-3,112, can1-100*	(Thomas and Rothstein, 1989)
458	W303 K700	*ade2-1, ura3-1, his3-11,15, trp1-1, leu2-3,112, can1-100*	(Thomas and Rothstein, 1989)
581	*ubc1*	DF5 *ubc1::HIS3*	(Seufert et al., 1990)
582	*ubc4*	DF5 *ubc4::HIS3*	(Seufert et al., 1990)
583	*ubc5*	DF5 *ubc5::LEU2*	(Seufert et al., 1990)
585	*ubc10*	DF5 *ubc10::LEU2*	(Davies et al., 2010)
586	*ubc11*	DF5 *ubc11::HIS3*	(Davies et al., 2010)
790	BY4741	*leu2Δ0, met15Δ0, ura3Δ0, his3Δ0*	(Brachmann et al., 1998)

	DSN1-TAP	BY4741 *DSN1-TAP::HIS3*	OPEN BIOSYSTEMS
	NNF1-TAP	BY4741 *NNF1-TAP::HIS3*	OPEN BIOSYSTEMS
	NSL1-TAP	BY4741 *NSL1-TAP::HIS3*	OPEN BIOSYSTEMS
	MTW1-TAP	BY4741 *MTW1-TAP::HIS3*	OPEN BIOSYSTEMS
	ubr2	BY4742 *ubr2::KanMX*	EUROSCARF
2260	*pdr5Δ*	DF5 *pdr5::KanMX*	(Zhao, 2010)
2376	*dsn1-7*	*ade2-1 trp1-1 can1-100 leu2-3,112 his3-11,15 ura3 ssd1*	(Nekrasov et al., 2003)
2377	*dsn1-8*	*ade2-1 trp1-1 can1-100 leu2-3,112 his3-11,15 ura3 ssd1*	(Nekrasov et al., 2003)
2493	*spc25 L109A*	*ade2-1 trp1-1 can1-100 leu2-3,112 his3-11,15 ura3 ssd1 spc25(L109A)*	(Zhao, 2010)
2494	*dsn1-8 spc25 L109A*	*ade2-1 trp1-1 can1-100 leu2-3,112 his3-11,15 ura3 ssd1 dsn1-8 spc25(L109A)*	(Zhao, 2010)
2606	YPH985 S288C	*ura3-52, lys2-801, ade2-101, trp1-Δ63, his3-Δ200, leu2-Δ1* *ura3-52, lys2-801, ade2-101, trp1-Δ63, his3-Δ200, leu2-Δ1* *CFIII (CEN3.L.YPH983) HIS3 SUP11*	(Connelly and Hieter, 1996)
2619	*ndc10-1*	*ade2-1 trp1-1 can1-100 leu2-3,112 his3-11,15 ura3 ssd1, ndc10-1*	(Nekrasov et al., 2003)
2620	*mtw1-11*	*ade2-1 trp1-1 can1-100 leu2-3,112 his3-11,15 ura3 ssd1, mtw1-11*	(Nekrasov et al., 2003)
2621	*nnf1-77*	*ade2-1 trp1-1 can1-100 leu2-3,112 his3-11,15 ura3 ssd1, nnf1-77*	(Nekrasov et al., 2003)
2622	*nsl1-6*	*ade2-1 trp1-1 can1-100 leu2-3,112 his3-11,15 ura3 ssd1, nsl1-6*	(Nekrasov et al., 2003)
2623	*nsl1-5*	*ade2-1 trp1-1 can1-100 leu2-3,112 his3-11,15 ura3 ssd1, nsl1-5*	(Nekrasov et al., 2003)
2624	*spc105-4*	*ade2-1 trp1-1 can1-100 leu2-3,112 his3-11,15 ura3 ssd1, spc105-4*	(Nekrasov et al., 2003)
2625	*spc105-15*	*ade2-1 trp1-1 can1-100 leu2-3,112 his3-11,15 ura3 ssd1, spc105-15*	(Nekrasov et al., 2003)
2626	*dam1-31*	*ade2-1 trp1-1 can1-100 leu2-3,112 his3-11,15 ura3 ssd1, dam1-31*	(Nekrasov et al., 2003)
2627	*duo1-61*	*ade2-1 trp1-1 can1-100 leu2-3,112 his3-11,15 ura3 ssd1, duo1-61*	(Nekrasov et al., 2003)
2628	*dad1-13*	*ade2-1 trp1-1 can1-100 leu2-3,112 his3-11,15 ura3 ssd1, dad1-13*	(Nekrasov et al., 2003)
2629	*ask1-22*	*ade2-1 trp1-1 can1-100 leu2-3,112 his3-11,15 ura3 ssd1, ask1-22*	(Nekrasov et al., 2003)

2630	*spc24-1*	*ade2-1 trp1-1 can1-100 leu2-3,112 his3-11,15 ura3 ssd1, spc24-1*	(Nekrasov et al., 2003)
2632	*ndc80-1*	*ade2-1 trp1-1 can1-100 leu2-3,112 his3-11,15 ura3 ssd1, ndc80-1*	(Nekrasov et al., 2003)
2633	*nuf2-61*	*ade2-1 trp1-1 can1-100 leu2-3,112 his3-11,15 ura3 ssd1, nuf2-61*	(Nekrasov et al., 2003)
2639	*DSN1-6HA*	DF5 *DSN1-6HA::klTRP1*	This study
2640	*DSN1-9myc*	DF5 *DSN1-9myc::klTRP1*	This study
2642	*ndc10-1 spc25 L109A*	W303 *ndc10-1, spc25 L109A*	This study
2644	*mtw1-11 spc25 L109A*	W303 *mtw1-11, spc25 L109A*	This study
2648	*nnf1-77 spc25 L109A*	W303 *nnf1-77, spc25 L109A*	This study
2650	*nsl1-6 spc25 L109A*	W303 *nsl1-6, spc25 L109A*	This study
2661	*nsl1-5 spc25 L109A*	W303 *nsl1-5, spc25 L109A*	This study
2663	*spc105-4 spc25 L109A*	W303 *spc105-4, spc25 L109A*	This study
2665	*spc105-15 spc25 L109A*	W303 *spc105-15, spc25 L109A*	This study
2667	*dam1-31 spc25 L109A*	W303 *dam1-31, spc25 L109A*	This study
2705	*spc24-12*	*spc24-12 ura3-52 lys2-801 ade2-101 trp1-Δ63 his3-Δ200 leu2-Δ1* (S288C)	(Le Masson et al., 2002)
2706	*spc24-13*	*spc24-13 ura3-52 lys2-801 ade2-101 trp1-Δ63 his3-Δ200 leu2-Δ1* (S288C)	(Le Masson et al., 2002)
2762	*SPC105-9myc*	DF5 *SPC105-9myc::klTRP1*	This study
2767	YPH985 *spc25 L109A*	*ura3-52, lys2-801, ade2-101, trp1-Δ63, his3-Δ200, leu2-Δ1, spc25(L109A) CFIII (CEN3.L.YPH983) HIS3 SUP11*	This study
2781	*DSN1-TAP Δubr2*	*leu2Δ0, met15Δ0 or lys2Δ0, ura3Δ0, his3Δ0, DSN1-TAP::HIS3, ubr2::KanMX*	This study
2782	*DSN1-6HA Δubr2*	DF5 *DSN1-6HA::klTRP1, ubr2::HIS3MX6*	This study
2783	*DSN1-6HA*	DF5 *DSN1-6HA::klTRP1*	This study
2784	*NSL1-TAP Δubr2*	leu2Δ0, met15Δ0 or lys2Δ0, ura3Δ0, his3Δ0, NSL1-TAP::HIS3, ubr2::KanMX	This study
2773	*duo1-61 spc25 L109A*	W303 *duo1-61, spc25 L109A*	This study
2774	*dad1-13 spc25 L109A*	W303 *dad1-13, spc25 L109A*	This study
2776	*ask1-22 spc25 L109A*	W303 *ask1-22, spc25 L109A*	This study

2778	*ndc80-1 spc25 L109A*	W303 *ndc80-1, spc25 L109A*	This study
2780	*nuf2-61 spc25 L109A*	W303 *nuf2-61, spc25 L109A*	This study
2797	*SPC105-6HA Δubr2*	DF5 *SPC105-6HA::klTRP1, ubr2::HIS3MX6*	This study
2796	*DSN1-6HA Δpdr5*	DF5 *DSN1-6HA::klTRP1, pdr5::KanMX*	This study
2849	*SPC105-HA Δpdr5*	DF5 *SPC105-6HA::klTRP1, pdr5::KanMX*	This study
2850	*SPC105-HA Δpdr5 Δubr2*	DF5 SPC105-6HA::klTRP1, pdr5::KanMX, ubr2::HIS3MX6	This study
2851	*DSN1-HA Δpdr5 Δubr2*	DF5 *DSN1-6HA::klTRP1, pdr5::KanMX, ubr2::HIS3MX6*	This study
2852	*Δubr2*	W303 *ubr2::HIS3MX6*	This study
2853	*spc25 L109A Δubr2*	W303 *spc25(L109A) ubr2::HIS3MX6*	This study
2854	*dsn1-7 Δubr2*	W303 *dsn1-7 ubr2::HIS3MX6*	This study
2856	*dsn1-8 Δubr2*	W303 *dsn1-8 ubr2::HIS3MX6*	This study
2855	*dsn1-7 spc25 L109A Δubr2*	W303 *dsn1-7 spc25(L109A) ubr2::HIS3MX6*	This study
2857	*dsn1-8 spc25 L109A Δubr2*	W303 *dsn1-8 spc25(L109A) ubr2::HIS3MX6*	This study
2858	*spc105-4 Δubr2*	W303 *spc105-4 ubr2::HIS3MX6*	This study
2860	*spc105-15 Δubr2*	W303 *spc105-15 ubr2::HIS3MX6*	This study
2859	*spc105-4 spc25 L109A Δubr2*	W303 *spc105-4 spc25(L109A) ubr2::HIS3MX6*	This study
2861	*spc105-15 spc25 L109A Δubr2*	W303 *spc105-15 spc25(L109A) ubr2::HIS3MX6*	This study
2862	*ndc80-1 Δubr2*	W303 *ndc80-1 ubr2::HIS3MX6*	This study
2863	*ndc80-1 spc25 L109A Δubr2*	W303 *ndc80-1 spc25(L109A) ubr2::HIS3MX6*	This study
2864	*nuf2-61 Δubr2*	W303 *nuf2-61 ubr2::HIS3MX6*	This study
2865	*nuf2-61 spc25 L109A Δubr2*	W303 *nuf2-61 spc25(L109A) ubr2::HIS3MX6*	This study
2866	*spc24-1 Δubr2*	W303 *spc24-1 ubr2::HIS3MX6*	This study
2995	*SPC24-3FLAG*	W303 *SPC24-3FLAG::HIS3MX6*	This study
2996	*SPC24-UIM-3FLAG*	W303 *SPC24-UIM-3FLAG::HIS3MX6*	This study
2997	*SPC24-MIU-3FLAG*	W303 *SPC24-MIU-3FLAG::HIS3MX6*	This study
2998	*SPC25-3FLAG*	W303 *SPC25-3FLAG::HIS3MX6*	This study

2999	*SPC25-UIM-3FLAG*	W303 *SPC25-UIM-3FLAG::HIS3MX6*	This study
3000	*SPC25-MIU-3FLAG*	W303 *SPC25-MIU-3FLAG::HIS3MX6*	This study
3001	*spc25 L109A SPC24-3FLAG*	W303 *spc25 (L109A), SPC24-3FLAG::HIS3MX6*	This study
3002	*spc25 L109A SPC24-UIM-3FLAG*	W303 *spc25 (L109A), SPC24-UIM-3FLAG::HIS3MX6*	This study
3003	*spc25 L109A SPC24-MIU-3FLAG*	W303 *spc25 (L109A), SPC24-MIU-3FLAG::HIS3MX6*	This study
3004	*spc25 L109A-3FLAG*	W303 *spc25 (L109A), SPC25-3FLAG::HIS3MX6*	This study
3005	*spc25 L109A -UIM-3FLAG*	W303 *spc25 (L109A), SPC25-UIM-3FLAG::HIS3MX6*	This study
3006	*spc25 L109A -MIU-3FLAG*	W303 *spc25 (L109A), SPC25-MIU-3FLAG::HIS3MX6*	This study
3007	*spc105-15 SPC24-3FLAG*	W303 *spc105-15, SPC24-3FLAG::HIS3MX6*	This study
3008	*spc105-15 SPC24-UIM-3FLAG*	W303 *spc105-15, SPC24-UIM-3FLAG::HIS3MX6*	This study
3009	*spc105-15 SPC24-MIU-3FLAG*	W303 *spc105-15, SPC24-MIU-3FLAG::HIS3MX6*	This study
3010	*spc105-15 SPC25-3FLAG*	W303 *spc105-15, SPC25-3FLAG::HIS3MX6*	This study
3011	*spc105-15 SPC25-UIM-3FLAG*	W303 *spc105-15, SPC25-UIM-3FLAG::HIS3MX6*	This study
3012	*spc105-15 SPC25-MIU-3FLAG*	W303 *spc105-15, SPC25-MIU-3FLAG::HIS3MX6*	This study
3013	*spc105-15 spc25 L109A SPC24-3FLAG*	W303 *spc105-15, spc25 L109A, SPC24-3FLAG::HIS3MX6*	This study
3014	*spc105-15 spc25 L109A SPC24-UIM-3FLAG*	W303 *spc105-15, spc25 L109A, SPC24-UIM-3FLAG::HIS3MX6*	This study
3015	*spc105-15 spc25 L109A SPC24-MIU-3FLAG*	W303 *spc105-15, spc25 L109A, SPC24-MIU-3FLAG::HIS3MX6*	This study
3016	*spc105-15 spc25 L109A-3FLAG*	W303 *spc105-15, spc25 L109A, SPC25-3FLAG::HIS3MX6*	This study
3017	*spc105-15 spc25 L109A -UIM-3FLAG*	W303 *spc105-15, spc25 L109A, SPC25-UIM-3FLAG::HIS3MX6*	This study

3018	*spc105-15 spc25 L109A -MIU-3FLAG*	W303 *spc105-15, spc25 L109A, SPC25-MIU-3FLAG::HIS3MX6*	This study
3019	*spc24-1 3FLAG*	W303 *spc24-1, SPC24-3FLAG::HIS3MX6*	This study
3020	*spc24-1 UIM-3FLAG*	W303 *spc24-1, SPC24-UIM-3FLAG::HIS3MX6*	This study
3021	*spc24-1 MIU-3FLAG*	W303 *spc24-1, SPC24-MIU-3FLAG::HIS3MX6*	This study
3022	*spc24-1 SPC25-3FLAG*	W303 *spc24-1, SPC25-3FLAG::HIS3MX6*	This study
3023	*spc24-1 SPC25-UIM-3FLAG*	W303 *spc24-1, SPC25-UIM-3FLAG::HIS3MX6*	This study
3024	*spc24-1 SPC25-MIU-3FLAG*	W303 *spc24-1, SPC25-MIU-3FLAG::HIS3MX6*	This study
3065	*DSN1_a*	DF5 *Leu2::Yip128-^{HA}DSN1_a[LEU2]*	This study
3066	*DSN1_b*	DF5 *Leu2::Yip128-^{HA}DSN1_b[LEU2]*	This study
3067	*DSN1_c*	DF5 *Leu2::Yip128-^{HA}DSN1_c[LEU2]*	This study
3068	*DSN1_d*	DF5 *Leu2::Yip128-^{HA}DSN1_d[LEU2]*	This study
3069	*DSN1_wt*	DF5 *Leu2::Yip128-^{HA}DSN1_wt[LEU2]*	This study
3075	*SPC24-MIU (A58G)-3FLAG*	W303 *SPC24-MIU (A58G)-3FLAG::HIS3MX6*	This study
3076	*SPC25 L109A SPC24-MIU (A58G)-3FLAG*	W303 *spc25(L109A), SPC24-MIU (A58G)-3FLAG::HIS3MX6*	This study
3077	*spc105-15 SPC24-MIU (A58G)-3FLAG*	W303 *spc105-15, SPC24-MIU (A58G)-3FLAG::HIS3MX6*	This study
3078	*spc105-15 spc25 L109A SPC24-MIU (A58G)-3FLAG*	W303 *spc105-15, spc25 L109A, SPC24-MIU (A58G)-3FLAG::HIS3MX6*	This study
3079	*Δubc1 DSN1-6HA*	DF5 *ubc1::HIS3, DSN1-6HA::kanMX4*	This study
3080	*Δrad6 a DSN1-6HA*	DF5 *rad6::HIS3, DSN1-6HA::kanMX4*	This study
3081	*cdc34-1 DSN1-6HA*	DF5 *cdc34-1*, *DSN1-6HA::kanMX4*	This study
3082	*Δubc4 DSN1-6HA*	DF5 *ubc4::HIS3 DSN1-6HA::kanMX4*	This study
3083	*Δubc5 DSN1-6HA*	DF5 *ubc5::LEU2 DSN1-6HA::kanMX4*	This study
3084	*Δubc6,7 DSN1-6HA*	DF5 *ubc6::HIS3, ubc7::HIS3, DSN1-6HA::kanMX4*	This study

3085	*Δubc8 DSN1-6HA*	DF5 *ubc8::URA3, DSN1-6HA::kanMX4*	This study
3086	*Δubc10 DSN1-6HA*	DF5 *ubc10::LEU2, DSN1-6HA::kanMX4*	This study
3087	*Δubc11 DSN1-6HA*	DF5 *ubc11::HIS3, DSN1-6HA::kanMX4*	This study
3088	*Δubc13 DSN1-6HA*	DF5 *ubc13::HIS3, DSN1-6HA::kanMX4*	This study
3089	*DSN1-6HA* (KAN)	DF5 *DSN1-6HA::kanMX4*	This study
3098	*spc25 L109A spc24-1 MIU-3FLAG*	W303 *spc25 L109A, spc24-1, SPC24-MIU-3FLAG::HIS3MX6*	This study

7.2 *E. coli* strains

Table 7.2 - List of *E. coli* strains used for this thesis.

Name	Use	Genotype	Source
One Shot Top10	Production of plasmids, cloning	F- *mcrA* Δ(*mrr-hsd*RMS-*mcr*BC) Φ80*lac*ZΔM15 Δ *lac*X74 *rec*A1 *ara*D139 Δ(*araleu*)7697 *gal*U *gal*K *rps*L (StrR) *end*A1 *nup*G	Life Technologies
One Shot *ccd*B Survival 2 T1^{R}	Production of plasmids with the *ccdB* gene	F- *mcr*A Δ(*mrr-hsd*RMS-*mcr*BC) Φ80*lac*ZΔM15 Δ*lac*X74 *rec*A1 *ara*Δ139 Δ(*ara-leu*)7697 *gal*U *gal*K *rps*L (Str^{R}) *end*A1 *nup*G *fhu*A::*IS2*	Life Technologies
BL21(DE3)p LysS	Protein expression	F- *omp*T *hsd*S$_{B}$(rB- mB-) *dcm gal* λ(DE3) pLysS Cm^{r}	Promega
BL21 codon^{2+}	Protein expression	F- *omp*T *hsd*S(rB- mB-) *dcm*$^{+}$ Tet^{R} *gal* (DE3) *end*A Hte	Dale Wigley

7.3 Statistics for the mechanoreceptor defect quantifications

The bristle defects of different genotypes were analysed for significant differences using a Fisher's exact test (Freeman-Halton extension) and P values are listed in Table 7.3. For genotypes that had 7 different defect groups (Figure 4.10, Figure 4.11, Figure 4.12 and Figure 4.14) group 5 bristle defects and group 6 (or over) bristle defects were treated as one group to allow the calculation of P values.

Table 7.3 - Test of significance for mechanoreceptor defects between genotypes using Fisher's exact test.

Genotype A	Genotype B	P value	
Figure 4.2			
$F10^{B221}$	*$F10^{B221}$/Df*	>0.9999	n.s.
$F10^{C321}$	*$F10^{C321}$/Df*	0.0381	*
$F9^{128}$, $F10^{B221}$	*$F9^{128}$, $F10^{B221}$ /Df*	0.0670	n.s.
ctrl F10	*$F10^{C321}$*	0.0052	**
$F10^{B221}$	*$F9^{128}$, $F10^{B221}$*	0.9198	n.s.
$F10^{B221}$	*$F10^{C321}$*	<0.0001	***
$F10^{B221}$/Df	*$F9^{128}$, $F10^{B221}$ /Df*	0.0828	n.s.
$F10^{B221}$/Df	*$F10^{C321}$/Df*	<0.0001	***
$F10^{B221}$	*males $F10^{B221}$*	0.0001	***
$F10^{C321}$	*males $F10^{C321}$*	0.8056	n.s.
$F9^{128}$, $F10^{B221}$	*males $F9^{128}$, $F10^{B221}$*	0.0011	**
$F10^{B221}$	*ubi-GFP; $F10^{B221}$*	0.0031	**
$F10^{B221}$	*ubi-GFP-F9; $F10^{B221}$*	0.1000	n.s.
ubi-GFP; $F10^{B221}$	*ubi-GFP-F9; $F10^{B221}$*	0.0047	**
ubi-GFP; $F10^{B221}$	*ubi-GFP; $F9^{128}$, $F10^{B221}$*	0.1350	n.s.
$F9^{128}$, $F10^{B221}$	*ubi-GFP; $F9^{128}$, $F10^{B221}$*	0.2757	n.s.
$F9^{128}$, $F10^{B221}$	*ubi-GFP-F9; $F9^{128}$, $F10^{B221}$*	0.1559	n.s.
ubi-GFP; $F9^{128}$, $F10^{B221}$	*ubi-GFP-F9; $F9^{128}$, $F10^{B221}$*	0.0834	n.s.
ubi-GFP-F9; $F10^{B221}$	*ubi-GFP-F9; $F9^{128}$, $F10^{B221}$*	0.0011	**
$F10^{B221}$	*$F8^{6}$, $F10^{B221}$*	0.0045	**
$F10^{B221}$	*$F8^{6}$, $F9^{128}$, $F10^{B221}$*	0.7425	n.s.
$F9^{128}$, $F10^{B221}$	*$F8^{6}$, $F9^{128}$, $F10^{B221}$*	0.4105	n.s.
Figure 4.3			
$F10^{B221}$	*$F10^{B221}$/Df*	0.0186	*
$F10^{C321}$	*$F10^{C321}$/Df*	0.1885	n.s.
$F9^{128}$, $F10^{B221}$	*$F9^{128}$, $F10^{B221}$ /Df*	0.0231	*
$F10^{B221}$	*$F9^{128}$, $F10^{B221}$*	0.0246	*
$F10^{B221}$	*$F10^{C321}$*	0.0028	**
$F10^{B221}$/Df	*$F9^{128}$, $F10^{B221}$ /Df*	0.6585	n.s.
$F10^{B221}$/Df	*$F10^{C321}$/Df*	0.0001	**
$F10^{B221}$	*males $F10^{B221}$*	0.2886	n.s.
$F10^{C321}$	*males $F10^{C321}$*	0.2687	n.s.
$F9^{128}$, $F10^{B221}$	*males $F9^{128}$, $F10^{B221}$*	0.3936	n.s.
$F10^{B221}$	*ubi-GFP; $F10^{B221}$*	0.0870	n.s.

ubi-GFP; F10^{B221}	*ubi-GFP-F9; F10^{B221}*	0.0307	*
F10^{B221}	*ubi-GFP-F9; F10^{B221}*	0.5523	n.s.
ubi-GFP; F10^{B221}	*ubi-GFP; F9^{128}, F10^{B221}*	0.0354	*
F9^{128}, F10^{B221}	*ubi-GFP; F9^{128}, F10^{B221}*	0.0648	n.s.
ubi-GFP; F9^{128}, F10^{B221}	*ubi-GFP-F9; F9^{128}, F10^{B221}*	0.0092	**
F9^{128}, F10^{B221}	*ubi-GFP-F9; F9^{128}, F10^{B221}*	0.0251	*
ubi-GFP-F9; F10^{B221}	*ubi-GFP-F9; F9^{128}, F10^{B221}*	0.0569	n.s.
F10^{B221}	*F8^{6}, F10^{B221}*	0.4626	n.s.
F10^{B221}	*F8^{6}, F9^{128}, F10^{B221}*	0.1428	n.s.
F9^{128}, F10^{B221}	*F8^{6}, F9^{128}, F10^{B221}*	<0.0001	***
Figure 4.4			
F10^{B221}	*F10^{B221}/Df*	0.0076	**
F10^{C321}	*F10^{C321}/Df*	0.0272	*
F9^{128}, F10^{B221}	*F9^{128}, F10^{B221}/Df*	<0.0001	***
F10^{B221}	*F9^{128}, F10^{B221}*	<0.0001	***
F10^{B221}	*F10^{C321}*	<0.0001	***
F10^{B221}/Df	*F9^{128}, F10^{B221}/Df*	0.0881	n.s.
F10^{B221}/Df	*F10^{C321}/Df*	0.1328	n.s.
F10^{B221}	*males F10^{B221}*	<0.0001	***
F10^{C321}	*males F10^{C321}*	0.0091	**
F9^{128}, F10^{B221}	*males F9^{128}, F10^{B221}*	>0.9999	n.s.
F10^{B221}	*ubi-GFP; F10^{B221}*	<0.0001	n.s.
ubi-GFP; F10^{B221}	*ubi-GFP-F10; F10^{B221}*	0.8330	n.s.
ubi-GFP; F10^{B221}	*ubi-GFP-F9; F10^{B221}*	0.3678	n.s.
ubi-GFP; F10^{B221}	*ubi-GFP; F9^{128}, F10^{B221}*	0.0050	**
F9^{128}, F10^{B221}	*ubi-GFP; F9^{128}, F10^{B221}*	>0.9999	n.s.
ubi-GFP; F9^{128}, F10^{B221}	*ubi-GFP-F9; F9^{128}, F10^{B221}*	0.6777	n.s.
ubi-GFP; F9^{128}, F10^{B221}	*ubi-GFP-F10; F9^{128}, F10^{B221}*	0.6777	n.s.
F8^{6}	*F8^{6}, F10^{B221}*	0.1531	n.s.
F8^{6}	*F8^{6}, F9^{128}, F10^{B221}*	0.0095	**
F10^{B221}	*F8^{6}, F10^{B221}*	<0.0001	***
F10^{B221}	*F8^{6}, F9^{128}, F10^{B221}*	<0.0001	***
F9^{128}, F10^{B221}	*F8^{6}, F9^{128}, F10^{B221}*	>0.9999	n.s.
Figure 4.10A			
F10^{B221}	*dsh^{1};; F10^{B221}*	<0.0001	***
Figure 4.10B			
F10^{B221}	*dsh^{1};; F10^{B221}*	<0.0001	***
dsh^{1}	*dsh^{1};; F10^{B221}*	<0.0001	***

dsh^{1}	*dsh*^{1};; *F10*^{B221}/+	0.5955	n.s.
dsh^{1}	*dsh*^{1};; *F9*^{128}	0.7596	n.s.
dsh^{1}	*dsh*^{1};; *F9*^{128}/+	>0.9999	n.s.
Figure 4.11			
nubG4/+; F10^{B221}	*nubG4/UAS-fz; F10*^{B221}	<0.0001	***
nubG4/+; F9^{128}, *F10*^{B221}	*nubG4/UAS-fz; F9*^{128}, *F10*^{B221}	<0.0001	***
nubG4/UAS-fz; F10^{B221}	*nubG4/UAS-fz; F9*^{128}, *F10*^{B221}	0.0018	**
nubG4/UAS-fz; F10^{B221}/+	*nubG4/UAS-fz; F9*^{128}, *F10*^{B221}/+	0.8217	n.s.
nubG4/+; F10^{B221}	*nubG4/+; F9*^{128}, *F10*^{B221}	0.2084	n.s.
nubG4/+; F10^{B221}	*nubG4/UAS-arm; F10*^{B221}	0.6931	n.s.
nubG4/+; F9^{128}, *F10*^{B221}	*nubG4/UAS-arm; F9*^{128}, *F10*^{B221}	0.7516	n.s.
nubG4/UAS-arm; F10^{B221}	*nubG4/UAS-arm; F9*^{128}, *F10*^{B221}	0.8772	n.s.
Figure 4.12			
nubG4/baz RNAi	*nubG4/baz RNAi; F9*^{128}	<0.0001	***
nubG4/baz RNAi	*nubG4/baz RNAi; F10*^{B221}	<0.0001	***
nubG4/+; F10^{B221}	*nubG4/baz RNAi; F10*^{B221}	<0.0001	***
nubG4/baz RNAi	*nubG4/baz RNAi; F9*^{128}, *F10*^{B221}	<0.0001	***
nubG4/+; F9^{128}, *F10*^{B221}	*nubG4/baz RNAi; F9*^{128}, *F10*^{B221}	<0.0001	***
nubG4/pins RNAi	*nubG4/pins RNAi; F9*^{128}	<0.0001	***
nubG4/pins RNAi	*nubG4/pins RNAi; F10*^{B221}	<0.0001	***
nubG4/+; F10^{B221}	*nubG4/pins RNAi; F10*^{B221}	<0.0001	***
nubG4/pins RNAi	*nubG4/pins RNAi; F9*^{128}, *F10*^{B221}	<0.0001	***
nubG4/+; F9^{128}, *F10*^{B221}	*nubG4/pins RNAi; F9*^{128}, *F10*^{B221}	<0.0001	***
nubG4/pins RNAi; F10^{B221}	*nubG4/pins RNAi; F9*^{128}, *F10*^{B221}	>0.9999	n.s.
Figure 4.13			
nubG4/+; F10^{B221}	*nubG4/ASPP RNAi; F10*^{B221}	0.0375	*
nubG4/+; F9^{128}, *F10*^{B221}	*nubG4/ASPP RNAi; F9*^{128}, *F10*^{B221}	0.0209	*
nubG4/ASPP RNAi; F10^{B221}	*nubG4/ASPP RNAi; F9*^{128}, *F10*^{B221}	0.1438	n.s.
Figure 4.14			
nubG4, baz RNAi/+	*flw*^{1}/+; *nubG4, baz RNAi/+*	0.0012	**
nubG4, baz RNAi/+	*nubG4, baz RNAi/+; PP1α87B*$^{87Bg-3}$/+	<0.0001	***
nubG4, baz RNAi/+	*nubG4, baz RNAi/+; PP1α96A*^{2}/+	0.0851	n.s.
nubG4, baz RNAi/+	*nubG4, baz RNAi/ASPP RNAi*	<0.0001	***
Background noise (Figure 4.2 and 4.11)			
F10^{B221}	*nubG4/+; F10*^{B221}	0.0153	*

Reference List

ABERLE, H., BAUER, A., STAPPERT, J., KISPERT, A. & KEMLER, R. 1997. beta-catenin is a target for the ubiquitin-proteasome pathway. *EMBO J,* 16**,** 3797-804.

ACAR, M., JAFAR-NEJAD, H., GIAGTZOGLOU, N., YALLAMPALLI, S., DAVID, G.*, et al.* 2006. Senseless physically interacts with proneural proteins and functions as a transcriptional co-activator. *Development,* 133**,** 1979-89.

ADAMS, M. D., CELNIKER, S. E., HOLT, R. A., EVANS, C. A., GOCAYNE, J. D.*, et al.* 2000. The Genome Sequence of Drosophila melanogaster. *Science,* 287**,** 2185-2195.

ADLER, P. N., CHARLTON, J. & LIU, J. 1998. Mutations in the cadherin superfamily member gene dachsous cause a tissue polarity phenotype by altering frizzled signaling. *Development,* 125**,** 959-68.

ADLER, P. N., CHARLTON, J. & VINSON, C. 1987. Allelic variation at the frizzled locus of Drosophila. *Developmental Genetics,* 8**,** 99-119.

ADLER, P. N., KRASNOW, R. E. & LIU, J. 1997. Tissue polarity points from cells that have higher Frizzled levels towards cells that have lower Frizzled levels. *Curr Biol,* 7**,** 940-9.

AIGOUY, B., FARHADIFAR, R., STAPLE, D. B., SAGNER, A., ROPER, J. C.*, et al.* 2010. Cell flow reorients the axis of planar polarity in the wing epithelium of Drosophila. *Cell,* 142**,** 773-86.

AKIYOSHI, B., NELSON, C. R. & BIGGINS, S. 2013a. The Aurora B Kinase Promotes Inner and Outer Kinetochore Interactions in Budding Yeast. *Genetics,* 194**,** 785-789.

AKIYOSHI, B., NELSON, C. R., DUGGAN, N., CETO, S., RANISH, J. A.*, et al.* 2013b. The Mub1/Ubr2 ubiquitin ligase complex regulates the conserved Dsn1 kinetochore protein. *PLoS Genet,* 9**,** e1003216.

AKIYOSHI, B., NELSON, C. R., RANISH, J. A. & BIGGINS, S. 2009. Analysis of Ipl1-mediated phosphorylation of the Ndc80 kinetochore protein in Saccharomyces cerevisiae. *Genetics,* 183**,** 1591-5.

AKIYOSHI, B., SARANGAPANI, K. K., POWERS, A. F., NELSON, C. R., REICHOW, S. L.*, et al.* 2010. Tension directly stabilizes reconstituted kinetochore-microtubule attachments. *Nature,* 468**,** 576-9.

AMBEGAONKAR, A. A., PAN, G., MANI, M., FENG, Y. & IRVINE, K. D. 2012. Propagation of Dachsous-Fat planar cell polarity. *Curr Biol,* 22**,** 1302-8.

ANDRESON, B. L., GUPTA, A., GEORGIEVA, B. P. & ROTHSTEIN, R. 2010. The ribonucleotide reductase inhibitor, Sml1, is sequentially phosphorylated, ubiquitylated and degraded in response to DNA damage. *Nucleic Acids Res,* 38**,** 6490-501.

ATWOOD, B. K., LOPEZ, J., WAGER-MILLER, J., MACKIE, K. & STRAIKER, A. 2011. Expression of G protein-coupled receptors and related proteins in HEK293, AtT20, BV2, and N18 cell lines as revealed by microarray analysis. *BMC Genomics,* 12**,** 14.

AXELROD, J. D. 2001. Unipolar membrane association of Dishevelled mediates Frizzled planar cell polarity signaling. *Genes Dev,* 15**,** 1182-7.

AXELROD, J. D., MATSUNO, K., ARTAVANIS-TSAKONAS, S. & PERRIMON, N. 1996. Interaction between Wingless and Notch signaling pathways mediated by dishevelled. *Science,* 271**,** 1826-32.

AXELROD, J. D., MILLER, J. R., SHULMAN, J. M., MOON, R. T. & PERRIMON, N. 1998. Differential recruitment of Dishevelled provides signaling specificity in the planar cell polarity and Wingless signaling pathways. *Genes Dev,* 12**,** 2610-22.

AXTON, J. M., DOMBRADI, V., COHEN, P. T. & GLOVER, D. M. 1990. One of the protein phosphatase 1 isoenzymes in Drosophila is essential for mitosis. *Cell,* 63**,** 33-46.

AYUKAWA, T., AKIYAMA, M., MUMMERY-WIDMER, J. L., STOEGER, T., SASAKI, J.*, et al.* 2014. Dachsous-Dependent Asymmetric Localization of Spiny-Legs Determines Planar Cell Polarity Orientation in Drosophila. *Cell Rep*.

BAENA-LOPEZ, L. A., BAONZA, A. & GARCIA-BELLIDO, A. 2005. The orientation of cell divisions determines the shape of Drosophila organs. *Curr Biol,* 15**,** 1640-4.

BASTOCK, R., STRUTT, H. & STRUTT, D. 2003. Strabismus is asymmetrically localised and binds to Prickle and Dishevelled during Drosophila planar polarity patterning. *Development,* 130**,** 3007-14.

BATE, M. & ARIAS, A. M. 1991. The embryonic origin of imaginal discs in Drosophila. *Development,* 112**,** 755-761.

BEHRENDS, C. & HARPER, J. W. 2011. Constructing and decoding unconventional ubiquitin chains. *Nat Struct Mol Biol,* 18**,** 520-8.

BELLAICHE, Y., BEAUDOIN-MASSIANI, O., STUTTEM, I. & SCHWEISGUTH, F. 2004. The planar cell polarity protein Strabismus promotes Pins anterior localization during asymmetric division of sensory organ precursor cells in Drosophila. *Development,* 131**,** 469-78.

BELLAICHE, Y., GHO, M., KALTSCHMIDT, J. A., BRAND, A. H. & SCHWEISGUTH, F. 2001a. Frizzled regulates localization of cell-fate determinants and mitotic spindle rotation during asymmetric cell division. *Nat Cell Biol,* 3**,** 50-7.

BELLAICHE, Y., RADOVIC, A., WOODS, D. F., HOUGH, C. D., PARMENTIER, M. L.*, et al.* 2001b. The Partner of Inscuteable/Discs-large complex is required to establish planar polarity during asymmetric cell division in Drosophila. *Cell,* 106**,** 355-66.

BENTON, R. & ST JOHNSTON, D. 2003a. A conserved oligomerization domain in drosophila Bazooka/PAR-3 is important for apical localization and epithelial polarity. *Curr Biol,* 13**,** 1330-4.

BENTON, R. & ST JOHNSTON, D. 2003b. Drosophila PAR-1 and 14-3-3 inhibit Bazooka/PAR-3 to establish complementary cortical domains in polarized cells. *Cell,* 115**,** 691-704.

BERGAMASCHI, D., SAMUELS, Y., JIN, B., DURAISINGHAM, S., CROOK, T.*, et al.* 2004. ASPP1 and ASPP2: Common Activators of p53 Family Members. *Molecular and Cellular Biology,* 24**,** 1341-1350.

BERGAMASCHI, D., SAMUELS, Y., O'NEIL, N. J., TRIGIANTE, G., CROOK, T.*, et al.* 2003. iASPP oncoprotein is a key inhibitor of p53 conserved from worm to human. *Nat Genet,* 33**,** 162-167.

BESSON, C., BERNARD, F., CORSON, F., ROUAULT, H., REYNAUD, E.*, et al.* 2015. Planar Cell Polarity Breaks the Symmetry of PAR Protein Distribution prior to Mitosis in Drosophila Sensory Organ Precursor Cells. *Curr Biol,* 25**,** 1104-10.

BETSCHINGER, J., MECHTLER, K. & KNOBLICH, J. A. 2003. The Par complex directs asymmetric cell division by phosphorylating the cytoskeletal protein Lgl. *Nature,* 422**,** 326-330.

BHANOT, P., BRINK, M., SAMOS, C. H., HSIEH, J. C., WANG, Y.*, et al.* 1996. A new member of the frizzled family from Drosophila functions as a Wingless receptor. *Nature,* 382**,** 225-30.

BIGGINS, S. 2013. The composition, functions, and regulation of the budding yeast kinetochore. *Genetics,* 194**,** 817-46.

BIGGINS, S., SEVERIN, F. F., BHALLA, N., SASSOON, I., HYMAN, A. A.*, et al.* 1999. The conserved protein kinase Ipl1 regulates microtubule binding to kinetochores in budding yeast. *Genes Dev,* 13**,** 532-44.

BILDER, D., SCHOBER, M. & PERRIMON, N. 2003. Integrated activity of PDZ protein complexes regulates epithelial polarity. *Nat Cell Biol,* 5**,** 53-58.

BOENS, S., SZEKER, K., VAN EYNDE, A. & BOLLEN, M. 2013. Interactor-guided dephosphorylation by protein phosphatase-1. *Methods Mol Biol,* 1053**,** 271-81.

BOSVELD, F., BONNET, I., GUIRAO, B., TLILI, S., WANG, Z.*, et al.* 2012. Mechanical control of morphogenesis by Fat/Dachsous/Four-jointed planar cell polarity pathway. *Science,* 336**,** 724-7.

BOTSTEIN, D., CHERVITZ, S. A. & CHERRY, J. M. 1997. Yeast as a model organism. *Science,* 277**,** 1259-60.

BOUTROS, M., PARICIO, N., STRUTT, D. I. & MLODZIK, M. 1998. Dishevelled activates JNK and discriminates between JNK pathways in planar polarity and wingless signaling. *Cell,* 94**,** 109-18.

BOWMAN, S. K., NEUMULLER, R. A., NOVATCHKOVA, M., DU, Q. & KNOBLICH, J. A. 2006. The Drosophila NuMA Homolog Mud regulates spindle orientation in asymmetric cell division. *Dev Cell,* 10**,** 731-42.

BRACHMANN, C. B., DAVIES, A., COST, G. J., CAPUTO, E., LI, J.*, et al.* 1998. Designer deletion strains derived from Saccharomyces cerevisiae S288C: a useful set of strains and plasmids for PCR-mediated gene disruption and other applications. *Yeast,* 14**,** 115-32.

BRITTLE, A., THOMAS, C. & STRUTT, D. 2012. Planar polarity specification through asymmetric subcellular localization of Fat and Dachsous. *Curr Biol,* 22**,** 907-14.

BRITTLE, A. L., REPISO, A., CASAL, J., LAWRENCE, P. A. & STRUTT, D. 2010. Four-jointed modulates growth and planar polarity by reducing the affinity of dachsous for fat. *Curr Biol,* 20**,** 803-10.

BROEMER, M. & MEIER, P. 2009. Ubiquitin-mediated regulation of apoptosis. *Trends Cell Biol,* 19**,** 130-40.

BUFFIN, E. & GHO, M. 2010. Laser microdissection of sensory organ precursor cells of Drosophila microchaetes. *PLoS One,* 5**,** e9285.

CALLEJA, M., RENAUD, O., USUI, K., PISTILLO, D., MORATA, G.*, et al.* 2002. How to pattern an epithelium: lessons from achaete-scute regulation on the notum of Drosophila. *Gene,* 292**,** 1-12.

CARMENA, A., MURUGASU-OEI, B., MENON, D., JIMENEZ, F. & CHIA, W. 1998. Inscuteable and numb mediate asymmetric muscle progenitor cell divisions during Drosophila myogenesis. *Genes Dev,* 12**,** 304-15.

CASAL, J., STRUHL, G. & LAWRENCE, P. A. 2002. Developmental compartments and planar polarity in Drosophila. *Curr Biol,* 12**,** 1189-98.

CAVALLO, R. A., COX, R. T., MOLINE, M. M., ROOSE, J., POLEVOY, G. A.*, et al.* 1998. Drosophila Tcf and Groucho interact to repress Wingless signalling activity. *Nature,* 395**,** 604-8.

CHAN, J. J., FLATTERS, D., RODRIGUES-LIMA, F., YAN, J., THALASSINOS, K.*, et al.* 2013. Comparative analysis of interactions of RASSF1-10. *Adv Biol Regul*.

CHEESEMAN, I. M., CHAPPIE, J. S., WILSON-KUBALEK, E. M. & DESAI, A. 2006. The conserved KMN network constitutes the core microtubule-binding site of the kinetochore. *Cell,* 127**,** 983-97.

CHEESEMAN, I. M., DRUBIN, D. G. & BARNES, G. 2002. Simple centromere, complex kinetochore: linking spindle microtubules and centromeric DNA in budding yeast. *J Cell Biol,* 157**,** 199-203.

CHEN, C. M. & STRUHL, G. 1999. Wingless transduction by the Frizzled and Frizzled2 proteins of Drosophila. *Development,* 126**,** 5441-52.

CHEN, L., JOHNSON, R. C. & MILGRAM, S. L. 1998. P-CIP1, a novel protein that interacts with the cytosolic domain of peptidylglycine alpha-amidating monooxygenase, is associated with endosomes. *J Biol Chem,* 273**,** 33524-32.

CHEN, W. S., ANTIC, D., MATIS, M., LOGAN, C. Y., POVELONES, M.*, et al.* 2008. Asymmetric homotypic interactions of the atypical cadherin flamingo mediate intercellular polarity signaling. *Cell,* 133**,** 1093-105.

CHEN, Z. J. & SUN, L. J. 2009. Nonproteolytic functions of ubiquitin in cell signaling. *Mol Cell,* 33**,** 275-86.

CHIN, M. L. & MLODZIK, M. 2013. The Drosophila selectin furrowed mediates intercellular planar cell polarity interactions via frizzled stabilization. *Dev Cell,* 26**,** 455-68.

CHO, B., PIERRE-LOUIS, G., SAGNER, A., EATON, S. & AXELROD, J. D. 2015. Clustering and Negative Feedback by Endocytosis in Planar Cell Polarity Signaling Is Modulated by Ubiquitinylation of Prickle. *PLoS Genet,* 11.

CIFERRI, C., PASQUALATO, S., SCREPANTI, E., VARETTI, G., SANTAGUIDA, S.*, et al.* 2008. Implications for kinetochore-microtubule attachment from the structure of an engineered Ndc80 complex. *Cell,* 133**,** 427-39.

CLEVERS, H. 2006. Wnt/beta-catenin signaling in development and disease. *Cell,* 127**,** 469-80.

CLEVERS, H. & NUSSE, R. 2012. Wnt/beta-catenin signaling and disease. *Cell,* 149**,** 1192-205.

CLIFFE, A., HAMADA, F. & BIENZ, M. 2003. A role of Dishevelled in relocating Axin to the plasma membrane during wingless signaling. *Curr Biol,* 13**,** 960-6.

CONG, W., HIROSE, T., HARITA, Y., YAMASHITA, A., MIZUNO, K.*, et al.* 2010. ASPP2 Regulates Epithelial Cell Polarity through the PAR Complex. *Current Biology,* 20**,** 1408-1414.

CONNELLY, C. & HIETER, P. 1996. Budding yeast SKP1 encodes an evolutionarily conserved kinetochore protein required for cell cycle progression. *Cell,* 86**,** 275-85.

COURBARD, J. R., DJIANE, A., WU, J. & MLODZIK, M. 2009. The Apical/Basal-polarity determinant Scribble cooperates with the PCP core factor Stbm/Vang and functions as one of its effectors. *Dev Biol,* 333**,** 67-77.

COUSO, J. P., BISHOP, S. A. & MARTINEZ ARIAS, A. 1994. The wingless signalling pathway and the patterning of the wing margin in Drosophila. *Development,* 120**,** 621-36.

DANCHECK, B., RAGUSA, M. J., ALLAIRE, M., NAIRN, A. C., PAGE, R.*, et al.* 2011. Molecular Investigations of the Structure and Function of the Protein Phosphatase 1:Spinophilin:Inhibitor-2 Heterotrimeric Complex. *Biochemistry,* 50**,** 1238-1246.

DANSRANJAVIN, T., WAGENLEHNER, F., GATTENLOEHNER, S., STEGER, K., WEIDNER, W.*, et al.* 2012. Epigenetic down regulation of RASSF10 and its possible clinical implication in prostate carcinoma. *The Prostate,* 72**,** 1550-1558.

DAS, G., JENNY, A., KLEIN, T. J., EATON, S. & MLODZIK, M. 2004. Diego interacts with Prickle and Strabismus/Van Gogh to localize planar cell polarity complexes. *Development,* 131**,** 4467-76.

DAVIES, A. A., NEISS, A. & ULRICH, H. D. 2010. Ubiquitylation of the 9-1-1 checkpoint clamp is independent of rad6-rad18 and DNA damage. *Cell,* 141**,** 1080-7.

DAVIES, A. E. & KAPLAN, K. B. 2010. Hsp90–Sgt1 and Skp1 target human Mis12 complexes to ensure efficient formation of kinetochore–microtubule binding sites. *The Journal of Cell Biology,* 189**,** 261-274.

DE CASTRO, E., SIGRIST, C. J., GATTIKER, A., BULLIARD, V., LANGENDIJK-GENEVAUX, P. S.*, et al.* 2006. ScanProsite: detection of PROSITE signature matches and ProRule-associated functional and structural residues in proteins. *Nucleic Acids Res,* 34**,** W362-5.

DEL VALLE RODRIGUEZ, A., DIDIANO, D. & DESPLAN, C. 2012. Power tools for gene expression and clonal analysis in Drosophila. *Nat Meth,* 9**,** 47-55.

DELUCA, J. G., GALL, W. E., CIFERRI, C., CIMINI, D., MUSACCHIO, A.*, et al.* 2006. Kinetochore microtubule dynamics and attachment stability are regulated by Hec1. *Cell,* 127**,** 969-82.

DESHAIES, R. J. & JOAZEIRO, C. A. 2009. RING domain E3 ubiquitin ligases. *Annu Rev Biochem,* 78**,** 399-434.

DIKIC, I., WAKATSUKI, S. & WALTERS, K. J. 2009. Ubiquitin-binding domains - from structures to functions. *Nat Rev Mol Cell Biol,* 10**,** 659-71.

DJIANE, A., YOGEV, S. & MLODZIK, M. 2005. The apical determinants aPKC and dPatj regulate Frizzled-dependent planar cell polarity in the Drosophila eye. *Cell,* 121**,** 621-31.

DOERFLINGER, H., VOGT, N., TORRES, I. L., MIROUSE, V., KOCH, I.*, et al.* 2010. Bazooka is required for polarisation of the Drosophila anterior-posterior axis. *Development,* 137**,** 1765-73.

DOLLAR, G. L., WEBER, U., MLODZIK, M. & SOKOL, S. Y. 2005. Regulation of Lethal giant larvae by Dishevelled. *Nature,* 437**,** 1376-1380.

ESPELIN, C. W., KAPLAN, K. B. & SORGER, P. K. 1997. Probing the architecture of a simple kinetochore using DNA-protein crosslinking. *J Cell Biol,* 139**,** 1383-96.

FALVELLA, F. S., MANENTI, G., SPINOLA, M., PIGNATIELLO, C., CONTI, B.*, et al.* 2006. Identification of RASSF8 as a candidate lung tumor suppressor gene. *Oncogene,* 25**,** 3934-3938.

FANTO, M. & MLODZIK, M. 1999. Asymmetric Notch activation specifies photoreceptors R3 and R4 and planar polarity in the Drosophila eye. *Nature,* 397**,** 523-6.

FEIGUIN, F., HANNUS, M., MLODZIK, M. & EATON, S. 2001. The ankyrin repeat protein Diego mediates Frizzled-dependent planar polarization. *Dev Cell,* 1**,** 93-101.

FIEDLER, M., MENDOZA-TOPAZ, C., RUTHERFORD, T. J., MIESZCZANEK, J. & BIENZ, M. 2011. Dishevelled interacts with the DIX domain polymerization interface of Axin to interfere with its function in down-regulating beta-catenin. *Proc Natl Acad Sci U S A,* 108**,** 1937-42.

FINLEY, D., OZKAYNAK, E. & VARSHAVSKY, A. 1987. The yeast polyubiquitin gene is essential for resistance to high temperatures, starvation, and other stresses. *Cell,* 48**,** 1035-46.

FINLEY, D., ULRICH, H. D., SOMMER, T. & KAISER, P. 2012. The ubiquitin-proteasome system of Saccharomyces cerevisiae. *Genetics,* 192**,** 319-60.

FISHER, R. D., WANG, B., ALAM, S. L., HIGGINSON, D. S., ROBINSON, H.*, et al.* 2003. Structure and ubiquitin binding of the ubiquitin-interacting motif. *J Biol Chem,* 278**,** 28976-84.

FLETCHER, G. C., LUCAS, E. P., BRAIN, R., TOURNIER, A. & THOMPSON, B. J. 2012. Positive feedback and mutual antagonism combine to polarize Crumbs in the Drosophila follicle cell epithelium. *Curr Biol,* 22**,** 1116-22.

FORMSTECHER, E., ARESTA, S., COLLURA, V., HAMBURGER, A., MEIL, A.*, et al.* 2005. Protein interaction mapping: a Drosophila case study. *Genome Res,* 15**,** 376-84.

FRANCISCO, L., WANG, W. & CHAN, C. S. 1994. Type 1 protein phosphatase acts in opposition to IpL1 protein kinase in regulating yeast chromosome segregation. *Mol Cell Biol,* 14**,** 4731-40.

FREEMAN, G. H. & HALTON, J. H. 1951. Note on an exact treatment of contingency, goodness of fit and other problems of significance. *Biometrika,* 38**,** 141-9.

FRISE, E., KNOBLICH, J. A., YOUNGER-SHEPHERD, S., JAN, L. Y. & JAN, Y. N. 1996. The Drosophila Numb protein inhibits signaling of the Notch receptor during cell-cell interaction in sensory organ lineage. *Proc Natl Acad Sci U S A,* 93**,** 11925-32.

FUNAKOSHI, M. & HOCHSTRASSER, M. 2009. Small epitope-linker modules for PCR-based C-terminal tagging in Saccharomyces cerevisiae. *Yeast,* 26**,** 185-92.

FURMAN, D. P. & BUKHARINA, T. A. 2011. Drosophila mechanoreceptors as a model for studying asymmetric cell division. *Int J Dev Biol,* 55**,** 133-41.

FURUYAMA, S. & BIGGINS, S. 2007. Centromere identity is specified by a single centromeric nucleosome in budding yeast. *Proceedings of the National Academy of Sciences,* 104**,** 14706-14711.

GAGLIARDI, M., HERNANDEZ, A., MCGOUGH, I. J. & VINCENT, J. P. 2014. Inhibitors of endocytosis prevent Wnt/Wingless signalling by reducing the level of basal beta-catenin/Armadillo. *J Cell Sci,* 127**,** 4918-26.

GAO, B., SONG, H., BISHOP, K., ELLIOT, G., GARRETT, L.*, et al.* 2011. Wnt signaling gradients establish planar cell polarity by inducing Vangl2 phosphorylation through Ror2. *Dev Cell,* 20**,** 163-76.

GESTAUT, D. R., GRACZYK, B., COOPER, J., WIDLUND, P. O., ZELTER, A.*, et al.* 2008. Phosphoregulation and depolymerization-driven movement of the Dam1 complex do not require ring formation. *Nat Cell Biol,* 10**,** 407-414.

GHO, M., BELLAICHE, Y. & SCHWEISGUTH, F. 1999. Revisiting the Drosophila microchaete lineage: a novel intrinsically asymmetric cell division generates a glial cell. *Development,* 126**,** 3573-84.

GIETZ, R. D. & SUGINO, A. 1988. New yeast-Escherichia coli shuttle vectors constructed with in vitro mutagenized yeast genes lacking six-base pair restriction sites. *Gene,* 74**,** 527-34.

GIRALDEZ, A. J. & COHEN, S. M. 2003. Wingless and Notch signaling provide cell survival cues and control cell proliferation during wing development. *Development,* 130**,** 6533-6543.

GOEBL, M. G., YOCHEM, J., JENTSCH, S., MCGRATH, J. P., VARSHAVSKY, A.*, et al.* 1988. The yeast cell cycle gene CDC34 encodes a ubiquitin-conjugating enzyme. *Science,* 241**,** 1331-5.

GOLDSTEIN, B. & MACARA, I. G. 2007. The PAR proteins: fundamental players in animal cell polarization. *Dev Cell,* 13**,** 609-22.

GOMES, J. E., CORADO, M. & SCHWEISGUTH, F. 2009. Van Gogh and Frizzled act redundantly in the Drosophila sensory organ precursor cell to orient its asymmetric division. *PLoS One,* 4**,** e4485.

GOMEZ-SKARMETA, J. L., CAMPUZANO, S. & MODOLELL, J. 2003. Half a century of neural prepatterning: the story of a few bristles and many genes. *Nat Rev Neurosci,* 4**,** 587-98.

GOODRICH, L. V. & STRUTT, D. 2011. Principles of planar polarity in animal development. *Development,* 138**,** 1877-92.

GRABBE, C., HUSNJAK, K. & DIKIC, I. 2011. The spatial and temporal organization of ubiquitin networks. *Nat Rev Mol Cell Biol,* 12**,** 295-307.

GRATZ, S. J., CUMMINGS, A. M., NGUYEN, J. N., HAMM, D. C., DONOHUE, L. K.*, et al.* 2013. Genome engineering of Drosophila with the CRISPR RNA-guided Cas9 nuclease. *Genetics,* 194**,** 1029-35.

GROS, J., SERRALBO, O. & MARCELLE, C. 2009. WNT11 acts as a directional cue to organize the elongation of early muscle fibres. *Nature,* 457**,** 589-93.

GUBB, D. & GARCIA-BELLIDO, A. 1982. A genetic analysis of the determination of cuticular polarity during development in Drosophila melanogaster. *J Embryol Exp Morphol,* 68**,** 37-57.

GUBB, D., GREEN, C., HUEN, D., COULSON, D., JOHNSON, G.*, et al.* 1999. The balance between isoforms of the prickle LIM domain protein is critical for planar polarity in Drosophila imaginal discs. *Genes Dev,* 13**,** 2315-27.

GUNAGE, R. D., REICHERT, H. & VIJAYRAGHAVAN, K. 2014. Identification of a new stem cell population that generates Drosophila flight muscles. *Elife,* 3.

GUO, C., ZHANG, X. & PFEIFER, G. P. 2011. The Tumor Suppressor RASSF1A Prevents Dephosphorylation of the Mammalian STE20-like Kinases MST1 and MST2. *Journal of Biological Chemistry,* 286**,** 6253-6261.

GUO, J., YANG, Y., YANG, Y., LINGHU, E., ZHAN, Q.*, et al.* 2015. RASSF10 suppresses colorectal cancer growth by activating P53 signaling and sensitizes colorectal cancer cell to docetaxel. *Oncotarget,* 6**,** 4202-13.

HALE, R., BRITTLE, A. L., FISHER, K. H., MONK, N. A. & STRUTT, D. 2015. Cellular interpretation of the long-range gradient of Four-jointed activity in the Drosophila wing. *Elife,* 4.

HAMADA, F., TOMOYASU, Y., TAKATSU, Y., NAKAMURA, M., NAGAI, S.*, et al.* 1999. Negative regulation of Wingless signaling by D-axin, a Drosophila homolog of axin. *Science,* 283**,** 1739-42.

HAMMOND-MARTEL, I., YU, H. & AFFAR EL, B. 2012. Roles of ubiquitin signaling in transcription regulation. *Cell Signal,* 24**,** 410-21.

HAO, H. X., XIE, Y., ZHANG, Y., CHARLAT, O., OSTER, E.*, et al.* 2012. ZNRF3 promotes Wnt receptor turnover in an R-spondin-sensitive manner. *Nature,* 485**,** 195-200.

HARRIS, T. J. & PEIFER, M. 2005. The positioning and segregation of apical cues during epithelial polarity establishment in Drosophila. *J Cell Biol,* 170**,** 813-23.

HARTENSTEIN, V. & POSAKONY, J. W. 1989. Development of adult sensilla on the wing and notum of Drosophila melanogaster. *Development,* 107**,** 389-405.

HARUMOTO, T., ITO, M., SHIMADA, Y., KOBAYASHI, T. J., UEDA, H. R.*, et al.* 2010. Atypical cadherins Dachsous and Fat control dynamics of noncentrosomal microtubules in planar cell polarity. *Dev Cell,* 19**,** 389-401.

HAURI, S., WEPF, A., VAN DROGEN, A., VARJOSALO, M., TAPON, N.*, et al.* 2013. Interaction proteome of human Hippo signaling: modular control of the co-activator YAP1. *Mol Syst Biol,* 9**,** 713.

HELPS, N. R., LUO, X., BARKER, H. M. & COHEN, P. T. 2000. NIMA-related kinase 2 (Nek2), a cell-cycle-regulated protein kinase localized to centrosomes, is complexed to protein phosphatase 1. *Biochemical Journal,* 349**,** 509-518.

HENDRICKX, A., BEULLENS, M., CEULEMANS, H., DEN ABT, T., VAN EYNDE, A.*, et al.* 2009. Docking motif-guided mapping of the interactome of protein phosphatase-1. *Chem Biol,* 16**,** 365-71.

HESSON, L., DUNWELL, T., COOPER, W., CATCHPOOLE, D., BRINI, A.*, et al.* 2009. The novel RASSF6 and RASSF10 candidate tumour suppressor genes are frequently epigenetically inactivated in childhood leukaemias. *Molecular Cancer,* 8**,** 42.

HEWAWASAM, G., SHIVARAJU, M., MATTINGLY, M., VENKATESH, S., MARTIN-BROWN, S.*, et al.* 2010. Psh1 Is an E3 Ubiquitin Ligase that Targets the Centromeric Histone Variant Cse4. *Mol Cell,* 40**,** 444-54.

HEWAWASAM, G. S. & GERTON, J. L. 2011. Cse4 gets a kiss-of-death from Psh1. *Cell Cycle,* 10**,** 566-7.

HICKE, L., SCHUBERT, H. L. & HILL, C. P. 2005. Ubiquitin-binding domains. *Nat Rev Mol Cell Biol,* 6**,** 610-621.

HILGERS, V., BUSHATI, N. & COHEN, S. M. 2010. Drosophila microRNAs 263a/b confer robustness during development by protecting nascent sense organs from apoptosis. *PLoS Biol,* 8**,** e1000396.

HILL, V. K., UNDERHILL-DAY, N., KREX, D., ROBEL, K., SANGAN, C. B.*, et al.* 2011. Epigenetic inactivation of the RASSF10 candidate tumor suppressor gene is a frequent and an early event in gliomagenesis. *Oncogene,* 30**,** 978-89.

HOCHSTRASSER, M. 1996. Ubiquitin-dependent protein degradation. *Annu Rev Genet,* 30**,** 405-39.

HOEGE, C., PFANDER, B., MOLDOVAN, G.-L., PYROWOLAKIS, G. & JENTSCH, S. 2002. RAD6-dependent DNA repair is linked to modification of PCNA by ubiquitin and SUMO. *Nature,* 419**,** 135-141.

HONDA, K., MIHARA, H., KATO, Y., YAMAGUCHI, A., TANAKA, H.*, et al.* 2000. Degradation of human Aurora2 protein kinase by the anaphase-promoting complex-ubiquitin-proteasome pathway. *Oncogene,* 19**,** 2812-9.

HONG, Y., STRONACH, B., PERRIMON, N., JAN, L. Y. & JAN, Y. N. 2001. Drosophila Stardust interacts with Crumbs to control polarity of epithelia but not neuroblasts. *Nature,* 414**,** 634-8.

HORNUNG, P., MAIER, M., ALUSHIN, G. M., LANDER, G. C., NOGALES, E.*, et al.* 2010. Molecular Architecture and Connectivity of the Budding Yeast Mtw1 Kinetochore Complex. *J Mol Biol*.

HUANG, F., DAMBLY-CHAUDIERE, C. & GHYSEN, A. 1991. The emergence of sense organs in the wing disc of Drosophila. *Development,* 111**,** 1087-95.

HURLEY, J. H., LEE, S. & PRAG, G. 2006. Ubiquitin-binding domains. *Biochem J,* 399**,** 361-72.

HURLEY, T. D., YANG, J., ZHANG, L., GOODWIN, K. D., ZOU, Q.*, et al.* 2007. Structural Basis for Regulation of Protein Phosphatase 1 by Inhibitor-2. *Journal of Biological Chemistry,* 282**,** 28874-28883.

HUSNJAK, K. & DIKIC, I. 2012. Ubiquitin-binding proteins: decoders of ubiquitin-mediated cellular functions. *Annu Rev Biochem,* 81**,** 291-322.

HUTTERER, A., BETSCHINGER, J., PETRONCZKI, M. & KNOBLICH, J. A. 2004. Sequential roles of Cdc42, Par-6, aPKC, and Lgl in the establishment of epithelial polarity during Drosophila embryogenesis. *Dev Cell,* 6**,** 845-54.

IKEDA, F. & DIKIC, I. 2008. Atypical ubiquitin chains: new molecular signals. 'Protein Modifications: Beyond the Usual Suspects' review series. *EMBO Rep,* 9**,** 536-42.

IMMERGLUCK, K., LAWRENCE, P. A. & BIENZ, M. 1990. Induction across germ layers in Drosophila mediated by a genetic cascade. *Cell,* 62**,** 261-8.

ISHIKAWA, H. O., TAKEUCHI, H., HALTIWANGER, R. S. & IRVINE, K. D. 2008. Four-jointed is a Golgi kinase that phosphorylates a subset of cadherin domains. *Science,* 321**,** 401-4.

ITOH, K., KRUPNIK, V. E. & SOKOL, S. Y. 1998. Axis determination in Xenopus involves biochemical interactions of axin, glycogen synthase kinase 3 and beta-catenin. *Curr Biol,* 8**,** 591-4.

JAFAR-NEJAD, H., ACAR, M., NOLO, R., LACIN, H., PAN, H.*, et al.* 2003. Senseless acts as a binary switch during sensory organ precursor selection. *Genes Dev,* 17**,** 2966-78.

JAFAR-NEJAD, H., TIEN, A. C., ACAR, M. & BELLEN, H. J. 2006. Senseless and Daughterless confer neuronal identity to epithelial cells in the Drosophila wing margin. *Development,* 133**,** 1683-92.

JAMES, P., HALLADAY, J. & CRAIG, E. A. 1996. Genomic libraries and a host strain designed for highly efficient two-hybrid selection in yeast. *Genetics,* 144**,** 1425-36.

JANKE, C., ORTIZ, J., LECHNER, J., SHEVCHENKO, A., MAGIERA, M. M.*, et al.* 2001. The budding yeast proteins Spc24p and Spc25p interact with Ndc80p and Nuf2p at the kinetochore and are important for kinetochore clustering and checkpoint control. *EMBO J,* 20**,** 777-91.

JARMAN, A. P. 2002. Studies of mechanosensation using the fly. *Human Molecular Genetics,* 11**,** 1215-1218.

JENNY, A., DARKEN, R. S., WILSON, P. A. & MLODZIK, M. 2003. Prickle and Strabismus form a functional complex to generate a correct axis during planar cell polarity signaling. *EMBO J,* 22**,** 4409-20.

JENNY, A., REYNOLDS-KENNEALLY, J., DAS, G., BURNETT, M. & MLODZIK, M. 2005. Diego and Prickle regulate Frizzled planar cell polarity signalling by competing for Dishevelled binding. *Nat Cell Biol,* 7**,** 691-7.

JIANG, J. & STRUHL, G. 1998. Regulation of the Hedgehog and Wingless signalling pathways by the F-box/WD40-repeat protein Slimb. *Nature,* 391**,** 493-6.

JOGLEKAR, A. P., BLOOM, K. & SALMON, E. D. 2009. In vivo protein architecture of the eukaryotic kinetochore with nanometer scale accuracy. *Curr Biol,* 19**,** 694-9.

JOHNSON, K. & WODARZ, A. 2003. A genetic hierarchy controlling cell polarity. *Nat Cell Biol,* 5**,** 12-14.

JOHNSTON, L. A. & SANDERS, A. L. 2003. Wingless promotes cell survival but constrains growth during Drosophila wing development. *Nat Cell Biol,* 5**,** 827-833.

JONES, K. H., LIU, J. & ADLER, P. N. 1996. Molecular analysis of EMS-induced frizzled mutations in Drosophila melanogaster. *Genetics,* 142**,** 205-15.

JONES, P., BINNS, D., CHANG, H. Y., FRASER, M., LI, W.*, et al.* 2014. InterProScan 5: genome-scale protein function classification. *Bioinformatics,* 30**,** 1236-40.

JU, D., WANG, L., MAO, X. & XIE, Y. 2004. Homeostatic regulation of the proteasome via an Rpn4-dependent feedback circuit. *Biochem Biophys Res Commun,* 321**,** 51-7.

JU, D., WANG, X., XU, H. & XIE, Y. 2008. Genome-wide analysis identifies MYND-domain protein Mub1 as an essential factor for Rpn4 ubiquitylation. *Mol Cell Biol,* 28**,** 1404-12.

JUSTICE, N., ROEGIERS, F., JAN, L. Y. & JAN, Y. N. 2003. Lethal giant larvae acts together with numb in notch inhibition and cell fate specification in the Drosophila adult sensory organ precursor lineage. *Curr Biol,* 13**,** 778-83.

KALLAY, L. M., MCNICKLE, A., BRENNWALD, P. J., HUBBARD, A. L. & BRAITERMAN, L. T. 2006. Scribble associates with two polarity proteins, Lgl2 and Vangl2, via distinct molecular domains. *J Cell Biochem,* 99**,** 647-64.

KEMPKENS, O., MEDINA, E., FERNANDEZ-BALLESTER, G., OZUYAMAN, S., LE BIVIC, A.*, et al.* 2006. Computer modelling in combination with in vitro studies reveals similar binding affinities of Drosophila Crumbs for the PDZ domains of Stardust and DmPar-6. *Eur J Cell Biol,* 85**,** 753-67.

KIM, S. E., HUANG, H., ZHAO, M., ZHANG, X., ZHANG, A.*, et al.* 2013. Wnt stabilization of beta-catenin reveals principles for morphogen receptor-scaffold assemblies. *Science,* 340**,** 867-70.

KIRCHNER, J., GROSS, S., BENNETT, D. & ALPHEY, L. 2007. Essential, overlapping and redundant roles of the Drosophila protein phosphatase 1 alpha and 1 beta genes. *Genetics,* 176**,** 273-81.

KISHIDA, S., YAMAMOTO, H., HINO, S., IKEDA, S., KISHIDA, M.*, et al.* 1999. DIX domains of Dvl and axin are necessary for protein interactions and their ability to regulate beta-catenin stability. *Mol Cell Biol,* 19**,** 4414-22.

KIYOMITSU, T., OBUSE, C. & YANAGIDA, M. 2007. Human Blinkin/AF15q14 is required for chromosome alignment and the mitotic checkpoint through direct interaction with Bub1 and BubR1. *Dev Cell,* 13**,** 663-76.

KLEIN, T. J., JENNY, A., DJIANE, A. & MLODZIK, M. 2006. CKIepsilon/discs overgrown promotes both Wnt-Fz/beta-catenin and Fz/PCP signaling in Drosophila. *Curr Biol,* 16**,** 1337-43.

KNOBLICH, J. A. 2008. Mechanisms of asymmetric stem cell division. *Cell,* 132**,** 583-97.

KNOP, M., SIEGERS, K., PEREIRA, G., ZACHARIAE, W., WINSOR, B.*, et al.* 1999. Epitope tagging of yeast genes using a PCR-based strategy: more tags and improved practical routines. *Yeast,* 15**,** 963-72.

KOELZER, S. & KLEIN, T. 2003. A Notch-independent function of Suppressor of Hairless during the development of the bristle sensory organ precursor cell of Drosophila. *Development,* 130**,** 1973-88.

KOO, B. K., SPIT, M., JORDENS, I., LOW, T. Y., STANGE, D. E.*, et al.* 2012. Tumour suppressor RNF43 is a stem-cell E3 ligase that induces endocytosis of Wnt receptors. *Nature,* 488**,** 665-9.

KOPEIN, D. & KATANAEV, V. L. 2009. Drosophila GoLoco-protein Pins is a target of Galpha(o)-mediated G protein-coupled receptor signaling. *Mol Biol Cell,* 20**,** 3865-77.

KOPSKI, K. M. & HUFFAKER, T. C. 1997. Suppressors of the ndc10-2 mutation: a role for the ubiquitin system in Saccharomyces cerevisiae kinetochore function. *Genetics,* 147**,** 409-20.

KRAHN, M. P., BUCKERS, J., KASTRUP, L. & WODARZ, A. 2010a. Formation of a Bazooka-Stardust complex is essential for plasma membrane polarity in epithelia. *J Cell Biol,* 190**,** 751-60.

KRAHN, M. P., EGGER-ADAM, D. & WODARZ, A. 2009. PP2A antagonizes phosphorylation of Bazooka by PAR-1 to control apical-basal polarity in dividing embryonic neuroblasts. *Dev Cell,* 16**,** 901-8.

KRAHN, M. P., KLOPFENSTEIN, D. R., FISCHER, N. & WODARZ, A. 2010b. Membrane targeting of Bazooka/PAR-3 is mediated by direct binding to phosphoinositide lipids. *Curr Biol,* 20**,** 636-42.

KRAMPS, T., PETER, O., BRUNNER, E., NELLEN, D., FROESCH, B.*, et al.* 2002. Wnt/wingless signaling requires BCL9/legless-mediated recruitment of pygopus to the nuclear beta-catenin-TCF complex. *Cell,* 109**,** 47-60.

KULATHU, Y., AKUTSU, M., BREMM, A., HOFMANN, K. & KOMANDER, D. 2009. Two-sided ubiquitin binding explains specificity of the TAB2 NZF domain. *Nat Struct Mol Biol,* 16**,** 1328-30.

LAEMMLI, U. K. 1970. Cleavage of structural proteins during the assembly of the head of bacteriophage T4. *Nature,* 227**,** 680-5.

LAMPERT, F., HORNUNG, P. & WESTERMANN, S. 2010. The Dam1 complex confers microtubule plus end-tracking activity to the Ndc80 kinetochore complex. *J Cell Biol,* 189**,** 641-9.

LANGEVIN, J., LE BORGNE, R., ROSENFELD, F., GHO, M., SCHWEISGUTH, F.*, et al.* 2005a. Lethal giant larvae controls the localization of notch-signaling regulators numb, neuralized, and Sanpodo in Drosophila sensory-organ precursor cells. *Curr Biol,* 15**,** 955-62.

LANGEVIN, J., MORGAN, M. J., SIBARITA, J. B., ARESTA, S., MURTHY, M., *et al.* 2005b. Drosophila exocyst components Sec5, Sec6, and Sec15 regulate DE-Cadherin trafficking from recycling endosomes to the plasma membrane. *Dev Cell,* 9**,** 365-76.

LANGTON, P. F., COLOMBANI, J., AERNE, B. L. & TAPON, N. 2007. Drosophila ASPP Regulates C-Terminal Src Kinase Activity. *Dev Cell,* 13**,** 773-782.

LANGTON, P. F., COLOMBANI, J., CHAN, E. H., WEPF, A., GSTAIGER, M., *et al.* 2009. The dASPP-dRASSF8 complex regulates cell-cell adhesion during Drosophila retinal morphogenesis. *Curr Biol,* 19**,** 1969-78.

LAPRISE, P. & TEPASS, U. 2011. Novel insights into epithelial polarity proteins in Drosophila. *Trends Cell Biol,* 21**,** 401-8.

LATHAM, J. A., CHOSED, R. J., WANG, S. & DENT, S. Y. 2011. Chromatin signaling to kinetochores: transregulation of Dam1 methylation by histone H2B ubiquitination. *Cell,* 146**,** 709-19.

LAWRENCE, N., DEARDEN, P., HARTLEY, D., ROOSE, J., CLEVERS, H., *et al.* 2000. dTcf antagonises Wingless signalling during the development and patterning of the wing in Drosophila. *Int J Dev Biol,* 44**,** 749-56.

LAWRENCE, P. A., BODMER, R. & VINCENT, J. P. 1995. Segmental patterning of heart precursors in Drosophila. *Development,* 121**,** 4303-8.

LE BORGNE, R. & SCHWEISGUTH, F. 2003. Unequal segregation of Neuralized biases Notch activation during asymmetric cell division. *Dev Cell,* 5**,** 139-48.

LE MASSON, I., SAVEANU, C., CHEVALIER, A., NAMANE, A., GOBIN, R., *et al.* 2002. Spc24 interacts with Mps2 and is required for chromosome segregation, but is not implicated in spindle pole body duplication. *Mol Microbiol,* 43**,** 1431-43.

LEE, C. M., YANG, P., CHEN, L. C., CHEN, C. C., WU, S. C., *et al.* 2011. A novel role of RASSF9 in maintaining epidermal homeostasis. *PLoS One,* 6**,** e17867.

LEE, S., TSAI, Y. C., MATTERA, R., SMITH, W. J., KOSTELANSKY, M. S., *et al.* 2006. Structural basis for ubiquitin recognition and autoubiquitination by Rabex-5. *Nat Struct Mol Biol,* 13**,** 264-71.

LI, V. S., NG, S. S., BOERSEMA, P. J., LOW, T. Y., KARTHAUS, W. R., *et al.* 2012. Wnt signaling through inhibition of beta-catenin degradation in an intact Axin1 complex. *Cell,* 149**,** 1245-56.

LIN, Y. Y. & GUBB, D. 2009. Molecular dissection of Drosophila Prickle isoforms distinguishes their essential and overlapping roles in planar cell polarity. *Dev Biol,* 325**,** 386-99.

LIU, C.-Y., LV, X., LI, T., XU, Y., ZHOU, X., *et al.* 2011. PP1 Cooperates with ASPP2 to Dephosphorylate and Activate TAZ. *Journal of Biological Chemistry,* 286**,** 5558-5566.

LIU, H. & NAISMITH, J. H. 2009. A simple and efficient expression and purification system using two newly constructed vectors. *Protein Expr Purif,* 63**,** 102-11.

LLANOS, S., ROYER, C., LU, M., BERGAMASCHI, D., LEE, W. H., *et al.* 2011. Inhibitory member of the apoptosis-stimulating proteins of the p53 family (iASPP) interacts with protein phosphatase 1 via a noncanonical binding motif. *J Biol Chem,* 286**,** 43039-44.

LOCK, F. E., UNDERHILL-DAY, N., DUNWELL, T., MATALLANAS, D., COOPER, W., *et al.* 2010. The RASSF8 candidate tumor suppressor inhibits

cell growth and regulates the Wnt and NF-[kappa]B signaling pathways. *Oncogene,* 29**,** 4307-4316.

LONDON, N., CETO, S., RANISH, J. A. & BIGGINS, S. 2012. Phosphoregulation of Spc105 by Mps1 and PP1 Regulates Bub1 Localization to Kinetochores. *Current biology : CB,* 22**,** 900-906.

LONGTINE, M. S., MCKENZIE, A., 3RD, DEMARINI, D. J., SHAH, N. G., WACH, A.*, et al.* 1998. Additional modules for versatile and economical PCR-based gene deletion and modification in Saccharomyces cerevisiae. *Yeast,* 14**,** 953-61.

LU, B., USUI, T., UEMURA, T., JAN, L. & JAN, Y. N. 1999. Flamingo controls the planar polarity of sensory bristles and asymmetric division of sensory organ precursors in Drosophila. *Curr Biol,* 9**,** 1247-50.

LUO, W., PETERSON, A., GARCIA, B. A., COOMBS, G., KOFAHL, B.*, et al.* 2007. Protein phosphatase 1 regulates assembly and function of the beta-catenin degradation complex. *EMBO J,* 26**,** 1511-21.

MA, D., YANG, C.-H., MCNEILL, H., SIMON, M. A. & AXELROD, J. D. 2003. Fidelity in planar cell polarity signalling. *Nature,* 421**,** 543-547.

MALVEZZI, F., LITOS, G., SCHLEIFFER, A., HEUCK, A., MECHTLER, K.*, et al.* 2013. *A structural basis for kinetochore recruitment of the Ndc80 complex via two distinct centromere receptors*.

MAO, J., WANG, J., LIU, B., PAN, W., FARR, G. H., 3RD*, et al.* 2001. Low-density lipoprotein receptor-related protein-5 binds to Axin and regulates the canonical Wnt signaling pathway. *Mol Cell,* 7**,** 801-9.

MAO, Y., TOURNIER, A. L., BATES, P. A., GALE, J. E., TAPON, N.*, et al.* 2011. Planar polarization of the atypical myosin Dachs orients cell divisions in Drosophila. *Genes Dev,* 25**,** 131-6.

MAPELLI, M. & GONZALEZ, C. 2012. On the inscrutable role of Inscuteable: structural basis and functional implications for the competitive binding of NuMA and Inscuteable to LGN. *Open Biol,* 2**,** 120102.

MARTINEZ ARIAS, A. 2003. Wnts as morphogens? The view from the wing of Drosophila. *Nat Rev Mol Cell Biol,* 4**,** 321-325.

MASKELL, D. P., HU, X. W. & SINGLETON, M. R. 2010. Molecular architecture and assembly of the yeast kinetochore MIND complex. *J Cell Biol,* 190**,** 823-34.

MATAKATSU, H. & BLAIR, S. S. 2006. Separating the adhesive and signaling functions of the Fat and Dachsous protocadherins. *Development,* 133**,** 2315-24.

MATIS, M., RUSSLER-GERMAIN, D. A., HU, Q., TOMLIN, C. J. & AXELROD, J. D. 2014. Microtubules provide directional information for core PCP function. *Elife,* 3**,** e02893.

MAYER, T. U., BRAUN, T. & JENTSCH, S. 1998. Role of the proteasome in membrane extraction of a short-lived ER-transmembrane protein. *EMBO J,* 17**,** 3251-7.

MCGILL, M. A., MCKINLEY, R. F. & HARRIS, T. J. 2009. Independent cadherin-catenin and Bazooka clusters interact to assemble adherens junctions. *J Cell Biol,* 185**,** 787-96.

MCGRATH, J. P., JENTSCH, S. & VARSHAVSKY, A. 1991. UBA 1: an essential yeast gene encoding ubiquitin-activating enzyme. *EMBO J,* 10**,** 227-36.

MCKINLEY, R. F. A., YU, C. G. & HARRIS, T. J. C. 2012. Assembly of Bazooka polarity landmarks through a multifaceted membrane-association mechanism. *Journal of Cell Science,* 125**,** 1177-1190.

MERALDI, P. & NIGG, E. A. 2001. Centrosome cohesion is regulated by a balance of kinase and phosphatase activities. *Journal of Cell Science,* 114**,** 3749-3757.

MERKEL, M., SAGNER, A., GRUBER, F. S., ETOURNAY, R., BLASSE, C.*, et al.* 2014. The balance of prickle/spiny-legs isoforms controls the amount of coupling between core and fat PCP systems. *Curr Biol,* 24**,** 2111-23.

MILÁN, M., CAMPUZANO, S. & GARCÍA-BELLIDO, A. 1996. Cell cycling and patterned cell proliferation in the wing primordium of Drosophila. *Proceedings of the National Academy of Sciences,* 93**,** 640-645.

MONTCOUQUIOL, M., RACHEL, R. A., LANFORD, P. J., COPELAND, N. G., JENKINS, N. A.*, et al.* 2003. Identification of Vangl2 and Scrb1 as planar polarity genes in mammals. *Nature,* 423**,** 173-177.

MONTPETIT, B., HAZBUN, T. R., FIELDS, S. & HIETER, P. 2006. Sumoylation of the budding yeast kinetochore protein Ndc10 is required for Ndc10 spindle localization and regulation of anaphase spindle elongation. *The Journal of Cell Biology,* 174**,** 653-663.

MORAIS-DE-SA, E., MIROUSE, V. & ST JOHNSTON, D. 2010. aPKC phosphorylation of Bazooka defines the apical/lateral border in Drosophila epithelial cells. *Cell,* 141**,** 509-23.

MORENO-MORENO, O., TORRAS-LLORT, M. & AZORIN, F. 2006. Proteolysis restricts localization of CID, the centromere-specific histone H3 variant of Drosophila, to centromeres. *Nucleic Acids Res,* 34**,** 6247-55.

MUKAI, A., YAMAMOTO-HINO, M., AWANO, W., WATANABE, W., KOMADA, M.*, et al.* 2010. Balanced ubiquitylation and deubiquitylation of Frizzled regulate cellular responsiveness to Wg/Wnt. *EMBO J,* 29**,** 2114-25.

MUKHOPADHYAY, D., ARNAOUTOV, A. & DASSO, M. 2010. The SUMO protease SENP6 is essential for inner kinetochore assembly. *J Cell Biol,* 188**,** 681-92.

MURRE, C., MCCAW, P. S., VAESSIN, H., CAUDY, M., JAN, L. Y.*, et al.* 1989. Interactions between heterologous helix-loop-helix proteins generate complexes that bind specifically to a common DNA sequence. *Cell,* 58**,** 537-44.

NARIMATSU, M., BOSE, R., PYE, M., ZHANG, L., MILLER, B.*, et al.* 2009. Regulation of planar cell polarity by Smurf ubiquitin ligases. *Cell,* 137**,** 295-307.

NEKRASOV, V. S., SMITH, M. A., PEAK-CHEW, S. & KILMARTIN, J. V. 2003. Interactions between centromere complexes in Saccharomyces cerevisiae. *Mol Biol Cell,* 14**,** 4931-46.

NEUMANN, C. J. & COHEN, S. M. 1996. A hierarchy of cross-regulation involving Notch, wingless, vestigial and cut organizes the dorsal/ventral axis of the Drosophila wing. *Development,* 122**,** 3477-3485.

NOLO, R., ABBOTT, L. A. & BELLEN, H. J. 2000. Senseless, a Zn finger transcription factor, is necessary and sufficient for sensory organ development in Drosophila. *Cell,* 102**,** 349-62.

NYBAKKEN, K., VOKES, S. A., LIN, T.-Y., MCMAHON, A. P. & PERRIMON, N. 2005. A genome-wide RNA interference screen in Drosophila melanogaster cells for new components of the Hh signaling pathway. *Nat Genet,* 37**,** 1323-1332.

OLOFSSON, J., SHARP, K. A., MATIS, M., CHO, B. & AXELROD, J. D. 2014. Prickle/spiny-legs isoforms control the polarity of the apical microtubule network in planar cell polarity. *Development,* 141**,** 2866-74.

PAI, L. M., ORSULIC, S., BEJSOVEC, A. & PEIFER, M. 1997. Negative regulation of Armadillo, a Wingless effector in Drosophila. *Development,* 124**,** 2255-66.

PATEL, N. H., SCHAFER, B., GOODMAN, C. S. & HOLMGREN, R. 1989. The role of segment polarity genes during Drosophila neurogenesis. *Genes Dev,* 3**,** 890-904.

PENENGO, L., MAPELLI, M., MURACHELLI, A. G., CONFALONIERI, S., MAGRI, L*., et al.* 2006. Crystal structure of the ubiquitin binding domains of rabex-5 reveals two modes of interaction with ubiquitin. *Cell,* 124**,** 1183-95.

PENTON, A., WODARZ, A. & NUSSE, R. 2002. A mutational analysis of dishevelled in Drosophila defines novel domains in the dishevelled protein as well as novel suppressing alleles of axin. *Genetics,* 161**,** 747-62.

PERRIMON, N. & MAHOWALD, A. P. 1987. Multiple functions of segment polarity genes in Drosophila. *Dev Biol,* 119**,** 587-600.

PETI, W., NAIRN, A. C. & PAGE, R. 2013. Structural basis for protein phosphatase 1 regulation and specificity. *FEBS J,* 280**,** 596-611.

PETRONCZKI, M. & KNOBLICH, J. A. 2001. DmPAR-6 directs epithelial polarity and asymmetric cell division of neuroblasts in Drosophila. *Nat Cell Biol,* 3**,** 43-49.

PETROVIC, A., PASQUALATO, S., DUBE, P., KRENN, V., SANTAGUIDA, S*., et al.* 2010. The MIS12 complex is a protein interaction hub for outer kinetochore assembly. *J Cell Biol,* 190**,** 835-52.

PHILLIPS, R. G. & WHITTLE, J. R. 1993. wingless expression mediates determination of peripheral nervous system elements in late stages of Drosophila wing disc development. *Development,* 118**,** 427-38.

PINSKY, B. A., KOTWALIWALE, C. V., TATSUTANI, S. Y., BREED, C. A. & BIGGINS, S. 2006a. Glc7/protein phosphatase 1 regulatory subunits can oppose the Ipl1/aurora protein kinase by redistributing Glc7. *Mol Cell Biol,* 26**,** 2648-60.

PINSKY, B. A., KUNG, C., SHOKAT, K. M. & BIGGINS, S. 2006b. The Ipl1-Aurora protein kinase activates the spindle checkpoint by creating unattached kinetochores. *Nat Cell Biol,* 8**,** 78-83.

POLESELLO, C., HUELSMANN, S., BROWN, NICHOLAS H. & TAPON, N. 2006. The Drosophila RASSF Homolog Antagonizes the Hippo Pathway. *Current Biology,* 16**,** 2459-2465.

PORT, F., CHEN, H. M., LEE, T. & BULLOCK, S. L. 2014. Optimized CRISPR/Cas tools for efficient germline and somatic genome engineering in Drosophila. *Proc Natl Acad Sci U S A,* 111**,** E2967-76.

RANJITKAR, P., PRESS, M. O., YI, X., BAKER, R., MACCOSS, M. J*., et al.* 2010. An E3 Ubiquitin Ligase Prevents Ectopic Localization of the Centromeric Histone H3 Variant via the Centromere Targeting Domain. *Mol Cell,* 40**,** 455-64.

RECINO, A., SHERWOOD, V., FLAXMAN, A., COOPER, WENDY N., LATIF, F*., et al.* 2010. Human RASSF7 regulates the microtubule cytoskeleton and is required for spindle formation, Aurora B activation and chromosomal congression during mitosis. *Biochemical Journal,* 430**,** 207-213.

REEVES, N. & POSAKONY, J. W. 2005. Genetic programs activated by proneural proteins in the developing Drosophila PNS. *Dev Cell,* 8**,** 413-25.

REITER, L. T., POTOCKI, L., CHIEN, S., GRIBSKOV, M. & BIER, E. 2001. A Systematic Analysis of Human Disease-Associated Gene Sequences In Drosophila melanogaster. *Genome Research,* 11**,** 1114-1125.

RHYU, M. S., JAN, L. Y. & JAN, Y. N. 1994. Asymmetric distribution of numb protein during division of the sensory organ precursor cell confers distinct fates to daughter cells. *Cell,* 76**,** 477-91.

RIBEIRO, P. S., JOSUE, F., WEPF, A., WEHR, M. C., RINNER, O.*, et al.* 2010. Combined functional genomic and proteomic approaches identify a PP2A complex as a negative regulator of Hippo signaling. *Mol Cell,* 39**,** 521-34.

RICHTER, A. M., PFEIFER, G. P. & DAMMANN, R. H. 2009. The RASSF proteins in cancer; from epigenetic silencing to functional characterization. *Biochimica et Biophysica Acta (BBA) - Reviews on Cancer,* 1796**,** 114-128.

RICHTER, A. M., WALESCH, S. K., WÜRL, P., TAUBERT, H. & DAMMANN, R. H. 2012. The tumor suppressor RASSF10 is upregulated upon contact inhibition and frequently epigenetically silenced in cancer. *Oncogenesis,* 1**,** e18.

RODRIGUES, N. T. L., LEKOMTSEV, S., JANANJI, S., KRISTON-VIZI, J., HICKSON, G. R. X.*, et al.* 2015. Kinetochore-localized PP1-Sds22 couples chromosome segregation to polar relaxation. *Nature,* 524**,** 489-492.

RODRIGUEZ-VICIANA, P., SABATIER, C. & MCCORMICK, F. 2004. Signaling Specificity by Ras Family GTPases Is Determined by the Full Spectrum of Effectors They Regulate. *Molecular and Cellular Biology,* 24**,** 4943-4954.

ROEGIERS, F., YOUNGER-SHEPHERD, S., JAN, L. Y. & JAN, Y. N. 2001a. Bazooka is required for localization of determinants and controlling proliferation in the sensory organ precursor cell lineage in Drosophila. *Proc Natl Acad Sci U S A,* 98**,** 14469-74.

ROEGIERS, F., YOUNGER-SHEPHERD, S., JAN, L. Y. & JAN, Y. N. 2001b. Two types of asymmetric divisions in the Drosophila sensory organ precursor cell lineage. *Nat Cell Biol,* 3**,** 58-67.

ROYER, C., KOCH, S., QIN, X., ZAK, J., BUTI, L.*, et al.* 2014. ASPP2 Links the Apical Lateral Polarity Complex to the Regulation of YAP Activity in Epithelial Cells. *PLoS ONE,* 9**,** e111384.

RULIFSON, E. J., WU, C. H. & NUSSE, R. 2000. Pathway specificity by the bifunctional receptor frizzled is determined by affinity for wingless. *Mol Cell,* 6**,** 117-26.

SAGNER, A., MERKEL, M., AIGOUY, B., GAEBEL, J., BRANKATSCHK, M.*, et al.* 2012. Establishment of global patterns of planar polarity during growth of the Drosophila wing epithelium. *Curr Biol,* 22**,** 1296-301.

SAMUELS-LEV, Y., O'CONNOR, D. J., BERGAMASCHI, D., TRIGIANTE, G., HSIEH, J.-K.*, et al.* 2001. ASPP Proteins Specifically Stimulate the Apoptotic Function of p53. *Molecular Cell,* 8**,** 781-794.

SCHAEFER, M., PETRONCZKI, M., DORNER, D., FORTE, M. & KNOBLICH, J. A. 2001. Heterotrimeric G proteins direct two modes of asymmetric cell division in the Drosophila nervous system. *Cell,* 107**,** 183-94.

SCHAGDARSURENGIN, U., RICHTER, A. M., WÖHLER, C. & DAMMANN, R. H. 2009. Frequent epigenetic inactivation of RASSF10 in thyroid cancer. *Epigenetics,* 4**,** 571-576.

SCHEEL, H. & HOFMANN, K. 2003. A novel interaction motif, SARAH, connects three classes of tumor suppressor. *Curr Biol,* 13**,** R899-900.

SCHLEIFFER, A., MAIER, M., LITOS, G., LAMPERT, F., HORNUNG, P.*, et al.* 2012. CENP-T proteins are conserved centromere receptors of the Ndc80 complex. *Nat Cell Biol,* 14**,** 604-613.

SCHWEISGUTH, F. 2015. Asymmetric cell division in the Drosophila bristle lineage: from the polarization of sensory organ precursor cells to Notch-mediated binary fate decision. *Wiley Interdiscip Rev Dev Biol,* 4**,** 299-309.

SEGALEN, M. & BELLAICHE, Y. 2009. Cell division orientation and planar cell polarity pathways. *Semin Cell Dev Biol,* 20**,** 972-7.

SEGALEN, M., JOHNSTON, C. A., MARTIN, C. A., DUMORTIER, J. G., PREHODA, K. E*., et al.* 2010. The Fz-Dsh planar cell polarity pathway induces oriented cell division via Mud/NuMA in Drosophila and zebrafish. *Dev Cell,* 19**,** 740-52.

SEUFERT, W., MCGRATH, J. P. & JENTSCH, S. 1990. UBC1 encodes a novel member of an essential subfamily of yeast ubiquitin-conjugating enzymes involved in protein degradation. *EMBO J,* 9**,** 4535-41.

SHARMA, R. P. & CHOPRA, V. L. 1976. Effect of the Wingless (wg1) mutation on wing and haltere development in Drosophila melanogaster. *Dev Biol,* 48**,** 461-5.

SHERWOOD, V., MANBODH, R., SHEPPARD, C. & CHALMERS, A. D. 2008. RASSF7 Is a Member of a New Family of RAS Association Domain–containing Proteins and Is Required for Completing Mitosis. *Molecular Biology of the Cell,* 19**,** 1772-1782.

SHERWOOD, V., RECINO, A., JEFFRIES, A., WARD, A. & CHALMERS, A. D. 2010. The N-terminal RASSF family: a new group of Ras-association-domain-containing proteins, with emerging links to cancer formation. *Biochem J,* 425**,** 303-11.

SHI, Y. 2009. Serine/Threonine Phosphatases: Mechanism through Structure. *Cell,* 139**,** 468-484.

SHIMADA, Y., USUI, T., YANAGAWA, S., TAKEICHI, M. & UEMURA, T. 2001. Asymmetric colocalization of Flamingo, a seven-pass transmembrane cadherin, and Dishevelled in planar cell polarization. *Curr Biol,* 11**,** 859-63.

SHIMADA, Y., YONEMURA, S., OHKURA, H., STRUTT, D. & UEMURA, T. 2006. Polarized transport of Frizzled along the planar microtubule arrays in Drosophila wing epithelium. *Dev Cell,* 10**,** 209-22.

SHIMIZU, N., ISHITANI, S., SATO, A., SHIBUYA, H. & ISHITANI, T. 2014. Hipk2 and PP1c cooperate to maintain Dvl protein levels required for Wnt signal transduction. *Cell Rep,* 8**,** 1391-404.

SHULMAN, J. M., PERRIMON, N. & AXELROD, J. D. 1998. Frizzled signaling and the developmental control of cell polarity. *Trends Genet,* 14**,** 452-8.

SIMOES SDE, M., BLANKENSHIP, J. T., WEITZ, O., FARRELL, D. L., TAMADA, M*., et al.* 2010. Rho-kinase directs Bazooka/Par-3 planar polarity during Drosophila axis elongation. *Dev Cell,* 19**,** 377-88.

SIMON, M. A., XU, A., ISHIKAWA, H. O. & IRVINE, K. D. 2010. Modulation of fat:dachsous binding by the cadherin domain kinase four-jointed. *Curr Biol,* 20**,** 811-7.

SIMPSON, P. 1990. Notch and the choice of cell fate in Drosophila neuroepithelium. *Trends Genet,* 6**,** 343-5.

SIMPSON, P. 2007. The stars and stripes of animal bodies: evolution of regulatory elements mediating pigment and bristle patterns in Drosophila. *Trends Genet,* 23**,** 350-8.

SINGH, J. & MLODZIK, M. 2012. Planar cell polarity signaling: coordination of cellular orientation across tissues. *Wiley Interdiscip Rev Dev Biol,* 1**,** 479-99.

SINGH, J., YANFENG, W. A., GRUMOLATO, L., AARONSON, S. A. & MLODZIK, M. 2010. Abelson family kinases regulate Frizzled planar cell polarity signaling via Dsh phosphorylation. *Genes Dev,* 24**,** 2157-68.

SKENE-ARNOLD, T. D., LUU, H. A., UHRIG, R. G., DE WEVER, V., NIMICK, M.*, et al.* 2013. Molecular mechanisms underlying the interaction of protein phosphatase-1c with ASPP proteins. *Biochem J,* 449**,** 649-59.

SOKRATOUS, K., ROACH, L. V., CHANNING, D., STRACHAN, J., LONG, J.*, et al.* 2012. Probing affinity and ubiquitin linkage selectivity of ubiquitin-binding domains using mass spectrometry. *J Am Chem Soc,* 134**,** 6416-24.

SONG, D. H., SUSSMAN, D. J. & SELDIN, D. C. 2000. Endogenous protein kinase CK2 participates in Wnt signaling in mammary epithelial cells. *J Biol Chem,* 275**,** 23790-7.

SOTILLOS, S., DIAZ-MECO, M. T., CAMINERO, E., MOSCAT, J. & CAMPUZANO, S. 2004. DaPKC-dependent phosphorylation of Crumbs is required for epithelial cell polarity in Drosophila. *J Cell Biol,* 166**,** 549-57.

SOTTOCORNOLA, R., ROYER, C., VIVES, V., TORDELLA, L., ZHONG, S.*, et al.* 2010. ASPP2 Binds Par-3 and Controls the Polarity and Proliferation of Neural Progenitors during CNS Development. *Developmental Cell,* 19**,** 126-137.

SPENCER, F., GERRING, S. L., CONNELLY, C. & HIETER, P. 1990. Mitotic chromosome transmission fidelity mutants in Saccharomyces cerevisiae. *Genetics,* 124**,** 237-49.

SRIRAM, S. M., KIM, B. Y. & KWON, Y. T. 2011. The N-end rule pathway: emerging functions and molecular principles of substrate recognition. *Nat Rev Mol Cell Biol,* 12**,** 735-747.

ST JOHNSTON, D. 2013. Using mutants, knockdowns, and transgenesis to investigate gene function in Drosophila. *Wiley Interdisciplinary Reviews: Developmental Biology,* 2**,** 587-613.

ST JOHNSTON, D. & AHRINGER, J. 2010. Cell polarity in eggs and epithelia: parallels and diversity. *Cell,* 141**,** 757-74.

STARITA, L. M., LO, R. S., ENG, J. K., VON HALLER, P. D. & FIELDS, S. 2012. Sites of ubiquitin attachment in Saccharomyces cerevisiae. *Proteomics,* 12**,** 236-40.

STOCKER, H. & GALLANT, P. 2008. Getting Started. *In:* DAHMANN, C. (ed.) *Drosophila.* Humana Press.

STOCKER, R. F. 1994. The organization of the chemosensory system in Drosophila melanogaster: a review. *Cell Tissue Res,* 275**,** 3-26.

STRAIGHT, A. F., BELMONT, A. S., ROBINETT, C. C. & MURRAY, A. W. 1996. GFP tagging of budding yeast chromosomes reveals that protein-protein interactions can mediate sister chromatid cohesion. *Curr Biol,* 6**,** 1599-608.

STRAPPS, W. R. & TOMLINSON, A. 2001. Transducing properties of Drosophila Frizzled proteins. *Development,* 128**,** 4829-35.

STRUTT, D. 2003. Frizzled signalling and cell polarisation in Drosophila and vertebrates. *Development,* 130**,** 4501-13.

STRUTT, D., JOHNSON, R., COOPER, K. & BRAY, S. 2002. Asymmetric localization of frizzled and the determination of notch-dependent cell fate in the Drosophila eye. *Curr Biol,* 12**,** 813-24.

STRUTT, D., MADDER, D., CHAUDHARY, V. & ARTYMIUK, P. J. 2012. Structure-function dissection of the frizzled receptor in Drosophila melanogaster

suggests different mechanisms of action in planar polarity and canonical Wnt signaling. *Genetics,* 192**,** 1295-313.

STRUTT, D. & STRUTT, H. 2007. Differential activities of the core planar polarity proteins during Drosophila wing patterning. *Dev Biol,* 302**,** 181-94.

STRUTT, D. & WARRINGTON, S. J. 2008. Planar polarity genes in the Drosophila wing regulate the localisation of the FH3-domain protein Multiple Wing Hairs to control the site of hair production. *Development,* 135**,** 3103-11.

STRUTT, D. I. 2001. Asymmetric localization of frizzled and the establishment of cell polarity in the Drosophila wing. *Mol Cell,* 7**,** 367-75.

STRUTT, D. I. 2002. The asymmetric subcellular localisation of components of the planar polarity pathway. *Semin Cell Dev Biol,* 13**,** 225-31.

STRUTT, H., PRICE, M. A. & STRUTT, D. 2006. Planar polarity is positively regulated by casein kinase Iepsilon in Drosophila. *Curr Biol,* 16**,** 1329-36.

STRUTT, H., SEARLE, E., THOMAS-MACARTHUR, V., BROOKFIELD, R. & STRUTT, D. 2013a. A Cul-3-BTB ubiquitylation pathway regulates junctional levels and asymmetry of core planar polarity proteins. *Development,* 140**,** 1693-702.

STRUTT, H., THOMAS-MACARTHUR, V. & STRUTT, D. 2013b. Strabismus Promotes Recruitment and Degradation of Farnesylated Prickle in Drosophila melanogaster Planar Polarity Specification. *PLoS Genet,* 9**,** e1003654.

STRUTT, H., WARRINGTON, S. J. & STRUTT, D. 2011. Dynamics of core planar polarity protein turnover and stable assembly into discrete membrane subdomains. *Dev Cell,* 20**,** 511-25.

SULLIVAN, A. & LU, X. 2007. ASPP: a new family of oncogenes and tumour suppressor genes. *British Journal of Cancer,* 96**,** 196-200.

SUN, T. Q., LU, B., FENG, J. J., REINHARD, C., JAN, Y. N.*, et al.* 2001. PAR-1 is a Dishevelled-associated kinase and a positive regulator of Wnt signalling. *Nat Cell Biol,* 3**,** 628-36.

SWANSON, K. A., KANG, R. S., STAMENOVA, S. D., HICKE, L. & RADHAKRISHNAN, I. 2003. Solution structure of Vps27 UIM-ubiquitin complex important for endosomal sorting and receptor downregulation. *EMBO J,* 22**,** 4597-606.

TAKAHASHI, S., EBIHARA, A., KAJIHO, H., KONTANI, K., NISHINA, H.*, et al.* 2011. RASSF7 negatively regulates pro-apoptotic JNK signaling by inhibiting the activity of phosphorylated-MKK7. *Cell Death and Differentiation,* 18**,** 645-655.

TAMAI, K., SEMENOV, M., KATO, Y., SPOKONY, R., LIU, C.*, et al.* 2000. LDL-receptor-related proteins in Wnt signal transduction. *Nature,* 407**,** 530-5.

TANENTZAPF, G. & TEPASS, U. 2003. Interactions between the crumbs, lethal giant larvae and bazooka pathways in epithelial polarization. *Nat Cell Biol,* 5**,** 46-52.

TAURIELLO, D. V., JORDENS, I., KIRCHNER, K., SLOOTSTRA, J. W., KRUITWAGEN, T.*, et al.* 2012. Wnt/beta-catenin signaling requires interaction of the Dishevelled DEP domain and C terminus with a discontinuous motif in Frizzled. *Proc Natl Acad Sci U S A,* 109**,** E812-20.

TAYLOR, J., ABRAMOVA, N., CHARLTON, J. & ADLER, P. N. 1998. Van Gogh: a new Drosophila tissue polarity gene. *Genetics,* 150**,** 199-210.

TEPASS, U. 2012. The apical polarity protein network in Drosophila epithelial cells: regulation of polarity, junctions, morphogenesis, cell growth, and survival. *Annu Rev Cell Dev Biol,* 28**,** 655-85.

THEISEN, H., PURCELL, J., BENNETT, M., KANSAGARA, D., SYED, A.*, et al.* 1994. dishevelled is required during wingless signaling to establish both cell polarity and cell identity. *Development,* 120**,** 347-60.

THOMAS, B. J. & ROTHSTEIN, R. 1989. Elevated recombination rates in transcriptionally active DNA. *Cell,* 56**,** 619-30.

THOMPSON, B., TOWNSLEY, F., ROSIN-ARBESFELD, R., MUSISI, H. & BIENZ, M. 2002. A new nuclear component of the Wnt signalling pathway. *Nat Cell Biol,* 4**,** 367-73.

TIAN, A. G. & DENG, W. M. 2008. Lgl and its phosphorylation by aPKC regulate oocyte polarity formation in Drosophila. *Development,* 135**,** 463-71.

TIEN, J. F., UMBREIT, N. T., GESTAUT, D. R., FRANCK, A. D., COOPER, J.*, et al.* 2010. Cooperation of the Dam1 and Ndc80 kinetochore complexes enhances microtubule coupling and is regulated by aurora B. *J Cell Biol,* 189**,** 713-23.

TOLWINSKI, N. S., WEHRLI, M., RIVES, A., ERDENIZ, N., DINARDO, S.*, et al.* 2003. Wg/Wnt signal can be transmitted through arrow/LRP5,6 and Axin independently of Zw3/Gsk3beta activity. *Dev Cell,* 4**,** 407-18.

TOOLEY, J. & STUKENBERG, P. T. 2011. The Ndc80 complex: integrating the kinetochore's many movements. *Chromosome Res,* 19**,** 377-91.

TRAWEGER, A., WIGGIN, G., TAYLOR, L., TATE, S. A., METALNIKOV, P.*, et al.* 2008. Protein phosphatase 1 regulates the phosphorylation state of the polarity scaffold Par-3. *Proc Natl Acad Sci U S A,* 105**,** 10402-7.

TREE, D. R., SHULMAN, J. M., ROUSSET, R., SCOTT, M. P., GUBB, D.*, et al.* 2002. Prickle mediates feedback amplification to generate asymmetric planar cell polarity signaling. *Cell,* 109**,** 371-81.

ULRICH, H. D. & DAVIES, A. A. 2009. In vivo detection and characterization of sumoylation targets in Saccharomyces cerevisiae. *Methods Mol Biol,* 497**,** 81-103.

ULRICH, H. D. & JENTSCH, S. 2000. Two RING finger proteins mediate cooperation between ubiquitin-conjugating enzymes in DNA repair. *EMBO J,* 19**,** 3388-97.

USUI, T., SHIMA, Y., SHIMADA, Y., HIRANO, S., BURGESS, R. W.*, et al.* 1999. Flamingo, a seven-pass transmembrane cadherin, regulates planar cell polarity under the control of Frizzled. *Cell,* 98**,** 585-95.

VAN DE WETERING, M., CAVALLO, R., DOOIJES, D., VAN BEEST, M., VAN ES, J.*, et al.* 1997. Armadillo coactivates transcription driven by the product of the Drosophila segment polarity gene dTCF. *Cell,* 88**,** 789-99.

VOLODKO, N., GORDON, M., SALLA, M., GHAZALEH, H. A. & BAKSH, S. 2014. RASSF tumor suppressor gene family: Biological functions and regulation. *FEBS Letters,* 588**,** 2671-2684.

WACH, A., BRACHAT, A., POHLMANN, R. & PHILIPPSEN, P. 1994. New heterologous modules for classical or PCR-based gene disruptions in Saccharomyces cerevisiae. *Yeast,* 10**,** 1793-808.

WAGNER, S. A., BELI, P., WEINERT, B. T., NIELSEN, M. L., COX, J.*, et al.* 2011. A proteome-wide, quantitative survey of in vivo ubiquitylation sites reveals widespread regulatory roles. *Mol Cell Proteomics,* 10**,** M111 013284.

WAKULA, P., BEULLENS, M., CEULEMANS, H., STALMANS, W. & BOLLEN, M. 2003. Degeneracy and function of the ubiquitous RVXF motif that mediates binding to protein phosphatase-1. *J Biol Chem,* 278**,** 18817-23.

WALTHER, R. F. & PICHAUD, F. 2010. Crumbs/DaPKC-dependent apical exclusion of Bazooka promotes photoreceptor polarity remodeling. *Curr Biol,* 20**,** 1065-74.

WANG, H. Y., LIU, T. & MALBON, C. C. 2006. Structure-function analysis of Frizzleds. *Cell Signal,* 18**,** 934-41.

WANG, L., MAO, X., JU, D. & XIE, Y. 2004. Rpn4 is a physiological substrate of the Ubr2 ubiquitin ligase. *J Biol Chem,* 279**,** 55218-23.

WANG, P., BAI, Y., SONG, B., WANG, Y., LIU, D*., et al.* 2011. PP1A-Mediated Dephosphorylation Positively Regulates YAP2 Activity. *PLoS ONE,* 6**,** e24288.

WASSERSCHEID, I., THOMAS, U. & KNUST, E. 2007. Isoform-specific interaction of Flamingo/Starry Night with excess Bazooka affects planar cell polarity in the Drosophila wing. *Dev Dyn,* 236**,** 1064-71.

WEHRLI, M., DOUGAN, S. T., CALDWELL, K., O'KEEFE, L., SCHWARTZ, S*., et al.* 2000. arrow encodes an LDL-receptor-related protein essential for Wingless signalling. *Nature,* 407**,** 527-30.

WEI, R. R., SCHNELL, J. R., LARSEN, N. A., SORGER, P. K., CHOU, J. J*., et al.* 2006. Structure of a central component of the yeast kinetochore: the Spc24p/Spc25p globular domain. *Structure,* 14**,** 1003-9.

WEI, R. R., SORGER, P. K. & HARRISON, S. C. 2005a. Molecular organization of the Ndc80 complex, an essential kinetochore component. *Proc Natl Acad Sci U S A,* 102**,** 5363-7.

WEI, S. Y., ESCUDERO, L. M., YU, F., CHANG, L. H., CHEN, L. Y*., et al.* 2005b. Echinoid is a component of adherens junctions that cooperates with DE-Cadherin to mediate cell adhesion. *Dev Cell,* 8**,** 493-504.

WEI, W., LI, M., WANG, J., NIE, F. & LI, L. 2012. The E3 ubiquitin ligase ITCH negatively regulates canonical Wnt signaling by targeting dishevelled protein. *Mol Cell Biol,* 32**,** 3903-12.

WEI, Z., CHEN, X., CHEN, J., WANG, W., XU, X*., et al.* 2013. RASSF10 is epigenetically silenced and functions as a tumor suppressor in gastric cancer. *Biochem Biophys Res Commun*.

WESTERMANN, S., CHEESEMAN, I. M., ANDERSON, S., YATES, J. R., DRUBIN, D. G*., et al.* 2003. Architecture of the budding yeast kinetochore reveals a conserved molecular core. *The Journal of Cell Biology,* 163**,** 215-222.

WESTERMANN, S., DRUBIN, D. G. & BARNES, G. 2007. Structures and functions of yeast kinetochore complexes. *Annu Rev Biochem,* 76**,** 563-91.

WESTERMANN, S., WANG, H.-W., AVILA-SAKAR, A., DRUBIN, D. G., NOGALES, E*., et al.* 2006. The Dam1 kinetochore ring complex moves processively on depolymerizing microtubule ends. *Nature,* 440**,** 565-569.

WIGGE, P. A. & KILMARTIN, J. V. 2001. The Ndc80p complex from Saccharomyces cerevisiae contains conserved centromere components and has a function in chromosome segregation. *J Cell Biol,* 152**,** 349-60.

WILLERT, K., BRINK, M., WODARZ, A., VARMUS, H. & NUSSE, R. 1997. Casein kinase 2 associates with and phosphorylates dishevelled. *EMBO J,* 16**,** 3089-96.

WINSTON, J. T., STRACK, P., BEER-ROMERO, P., CHU, C. Y., ELLEDGE, S. J*., et al.* 1999. The SCFβ-TRCP–ubiquitin ligase complex associates specifically with

phosphorylated destruction motifs in IκBα and β-catenin and stimulates IκBα ubiquitination in vitro. *Genes & Development,* 13**,** 270-283.

WIRTZ-PEITZ, F., NISHIMURA, T. & KNOBLICH, J. A. 2008. Linking cell cycle to asymmetric division: Aurora-A phosphorylates the Par complex to regulate Numb localization. *Cell,* 135**,** 161-73.

WODARZ, A., RAMRATH, A., GRIMM, A. & KNUST, E. 2000. Drosophila atypical protein kinase C associates with Bazooka and controls polarity of epithelia and neuroblasts. *J Cell Biol,* 150**,** 1361-74.

WOLFF, T. & RUBIN, G. M. 1998. Strabismus, a novel gene that regulates tissue polarity and cell fate decisions in Drosophila. *Development,* 125**,** 1149-59.

WONG, H. C., BOURDELAS, A., KRAUSS, A., LEE, H. J., SHAO, Y.*, et al.* 2003. Direct binding of the PDZ domain of Dishevelled to a conserved internal sequence in the C-terminal region of Frizzled. *Mol Cell,* 12**,** 1251-60.

WU, J., JENNY, A., MIRKOVIC, I. & MLODZIK, M. 2008. Frizzled-Dishevelled signaling specificity outcome can be modulated by Diego in Drosophila. *Mech Dev,* 125**,** 30-42.

WU, J., KLEIN, T. J. & MLODZIK, M. 2004. Subcellular localization of frizzled receptors, mediated by their cytoplasmic tails, regulates signaling pathway specificity. *PLoS Biol,* 2**,** E158.

WU, J. & MLODZIK, M. 2008. The frizzled extracellular domain is a ligand for Van Gogh/Stbm during nonautonomous planar cell polarity signaling. *Dev Cell,* 15**,** 462-9.

WU, J., ROMAN, A. C., CARVAJAL-GONZALEZ, J. M. & MLODZIK, M. 2013. Wg and Wnt4 provide long-range directional input to planar cell polarity orientation in Drosophila. *Nat Cell Biol,* 15**,** 1045-55.

YAICH, L., OOI, J., PARK, M., BORG, J. P., LANDRY, C.*, et al.* 1998. Functional analysis of the Numb phosphotyrosine-binding domain using site-directed mutagenesis. *J Biol Chem,* 273**,** 10381-8.

YANAGAWA, S., MATSUDA, Y., LEE, J. S., MATSUBAYASHI, H., SESE, S.*, et al.* 2002. Casein kinase I phosphorylates the Armadillo protein and induces its degradation in Drosophila. *EMBO J,* 21**,** 1733-42.

YANAGAWA, S., VAN LEEUWEN, F., WODARZ, A., KLINGENSMITH, J. & NUSSE, R. 1995. The dishevelled protein is modified by wingless signaling in Drosophila. *Genes Dev,* 9**,** 1087-97.

YANFENG, W. A., BERHANE, H., MOLA, M., SINGH, J., JENNY, A.*, et al.* 2011. Functional dissection of phosphorylation of Disheveled in Drosophila. *Dev Biol,* 360**,** 132-42.

YANFENG, W. A., TAN, C., FAGAN, R. J. & KLEIN, P. S. 2006. Phosphorylation of frizzled-3. *J Biol Chem,* 281**,** 11603-9.

YANG, C. H., AXELROD, J. D. & SIMON, M. A. 2002. Regulation of Frizzled by fat-like cadherins during planar polarity signaling in the Drosophila compound eye. *Cell,* 108**,** 675-88.

YU, F.-X. & GUAN, K.-L. 2013. The Hippo pathway: regulators and regulations. *Genes & Development,* 27**,** 355-371.

YU, X., WALTZER, L. & BIENZ, M. 1999. A new Drosophila APC homologue associated with adhesive zones of epithelial cells. *Nat Cell Biol,* 1**,** 144-51.

ZAESSINGER, S., ZHOU, Y., BRAY, S. J., TAPON, N. & DJIANE, A. 2015. Drosophila MAGI interacts with RASSF8 to regulate E-Cadherin-based adherens junctions in the developing eye. *Development,* 142**,** 1102-1112.

ZALLEN, J. A., COHEN, Y., HUDSON, A. M., COOLEY, L., WIESCHAUS, E.*, et al.* 2002. SCAR is a primary regulator of Arp2/3-dependent morphological events in Drosophila. *J Cell Biol,* 156**,** 689-701.

ZEITLINGER, J. & BOHMANN, D. 1999. Thorax closure in Drosophila: involvement of Fos and the JNK pathway. *Development,* 126**,** 3947-3956.

ZENG, X., HUANG, H., TAMAI, K., ZHANG, X., HARADA, Y.*, et al.* 2008. Initiation of Wnt signaling: control of Wnt coreceptor Lrp6 phosphorylation/activation via frizzled, dishevelled and axin functions. *Development,* 135**,** 367-75.

ZENG, X., TAMAI, K., DOBLE, B., LI, S., HUANG, H.*, et al.* 2005. A dual-kinase mechanism for Wnt co-receptor phosphorylation and activation. *Nature,* 438**,** 873-7.

ZHANG, J. & CARTHEW, R. W. 1998. Interactions between Wingless and DFz2 during Drosophila wing development. *Development,* 125**,** 3075-85.

ZHANG, L., JIA, J., WANG, B., AMANAI, K., WHARTON JR, K. A.*, et al.* 2006. Regulation of wingless signaling by the CKI family in Drosophila limb development. *Dev Biol,* 299**,** 221-237.

ZHANG, X., ZHU, J., YANG, G.-Y., WANG, Q.-J., QIAN, L.*, et al.* 2007. Dishevelled promotes axon differentiation by regulating atypical protein kinase C. *Nat Cell Biol,* 9**,** 743-754.

ZHANG, Y., WANG, Y., WEI, Y., MA, J., PENG, J.*, et al.* 2015. The tumor suppressor proteins ASPP1 and ASPP2 interact with C-Nap1 and regulate centrosome linker reassembly. *Biochem Biophys Res Commun,* 458**,** 494-500.

ZHAO, S. 2010. *Signalling Functions of Polyubiquitin Chains and Ubiquitin-binding Domains.* Doctor of Philosophy, University College London.

ZHOU, Y. 2014. *Developmental Functions of Drosophila ASPP and RASSF8.* Doctor of Philosophy, University College London.